VOLUME 107 – NO. 1/2 – JUNE 1992

ISSN 0025-3227

MARINE GEOLOGY

INTERNATIONAL JOURNAL OF MARINE GEOLOGY, GEOCHEMISTRY AND GEOPHYSICS

ELSEVIER

MARINE GEOLOGY

Scope of the journal

Marine Geology is an international medium for the publication of original studies and comprehensive reviews in the field of Marine Geology, Geochemistry and Geophysics. The editors endeavour to maintain a high scientific level and it is hoped that with its international coverage the journal will contribute to the sound development of this field.
A *letter section* is provided as a publication outlet for short papers which require *rapid* publication.

Publication schedule and subscription information – 1992

Marine Geology (ISSN 0025–3227) is published as six volumes (24 issues) a year. The subscription price for 1992 (Volumes 102–107) is Dfl. 1800 + Dfl. 186 p.h. = Dfl. 1986 (approx. US$983). The Dutch guilder price is definitive. The U.S. dollar price is subject to exchange-rate fluctuations and is given only as a guide. Subscriptions are accepted on a prepaid basis only, unless different terms have previously been agreed upon. Personal subscription rates and conditions are available upon request from the Publisher. Subscription orders can be entered only by calendar year (Jan.–Dec.) and should be sent to Elsevier Science Publishers, Journal Department, P.O. Box 211, 1000 AE Amsterdam, The Netherlands, tel. 31.20.5803642, fax 31.20.5803598, or to your usual subscription agent. Postage & handling (p.h.) charges include surface delivery, except to the following countries where air delivery via S.A.L. (Surface Air Lift) mail is ensured: Argentina, Australia, Brazil, Canada, Hong Kong, India, Israel, Japan*, Malaysia, Mexico, New Zealand, Pakistan, PR China, Singapore, South Africa, South Korea, Taiwan, Thailand and the USA. *For Japan, air delivery (S.A.L.) requires an additional charge of 25% of the normal postage and handling charge. For all other countries, airmail rates are available upon request. Claims for missing issues must be made within three months of publication (mailing) date; otherwise, such claims cannot be honoured free of charge. For further information, or a free sample copy of this or any other Elsevier Science Publishers journal, readers in the USA and Canada can contact the following address: Elsevier Science Publishing Co. Inc., Journal Information Center, 655 Avenue of the Americas, New York, NY 10010, U.S.A., tel. 212.63337502. Back issues can be ordered. For further information regarding prices etc., please contact Elsevier Science Publishers, Journal Department, P.O. Box 211, 1000 AE Amsterdam, The Netherlands, tel. 31.20.5803642, fax 31.20.5803598.

Journal Information Center

For customers in the U.S.A. and Canada wishing additional bibliographic information on this and other Elsevier journals, please contact: Elsevier Science Publishing Co. Inc., Journal Information Center, 655 Avenue of the Americas, New York, NY 10010, U.S.A., Tel: (212) 633-3750.

(continued on inside back cover)

 0025-3227/92/$05.00

This issue is printed on acid-free paper.

PRINTED IN THE NETHERLANDS

MARINE GEOLOGY

VOL. 107 (1992)

MARINE GEOLOGY

International Journal of Marine Geology, Geochemistry and Geophysics

VOL. 107 (1992)

ELSEVIER
AMSTERDAM – LONDON – NEW YORK – TOKYO

0025-3227/92/$05.00

This issue is printed on acid-free paper.

PRINTED IN THE NETHERLANDS

Marine Geology, 107 (1992) 1–7
Elsevier Science Publishers B.V., Amsterdam

Paleontological evidence for early exposure of deep oceanic crust on the Vema Fracture Zone southern wall (Atlantic Ocean, 10°45'N)

Marie-Pierre Aubry[a,b*], William A. Berggren[b], André Schaaf[a], Jean-Marie Auzende[c], Yves Lagabrielle[d] and Vassilios Mamaloukas-Frangoulis[d]

[a]*Centre de Paléontologie Stratigraphique et Paléoécologie, Université Claude Bernard, 27–43 Boulevard du 11 Novembre, 69622 Villeurbanne Cédex, France*
[b]*Woods Hole Oceanographic Institution, Woods Hole, MA 02543, USA*
[c]*IFREMER, Centre de Brest et GDR 910 "G.E.D.O.", B.P. 70, 29280 Plouzané Cédex, France*
[d]*URA 1278, Université de Bretagne occidentale et GDR 910 "G.E.D.O.", 6, Avenue Le Gorgeu, 29287 Brest Cédex, France*

(Received July 17, 1991; revision accepted January 23, 1992)

ABSTRACT

Aubry, M.-P., Berggren, W.A., Schaaf, A., Auzende, J.-M., Lagabrielle, Y. and Mamaloukas-Frangoulis, V., 1992. Paleontological evidence for early exposure of deep oceanic crust on the Vema Fracture Zone southern wall (Atlantic Ocean, 10°45'N). *Mar. Geol.*, 107: 1–7.

We present the results of a paleontological study of samples collected during the *Vemanaute* cruise on the Vema Fracture Zone southern wall where an almost complete section of oceanic crust is exposed. The three studied samples are poorly lithified yellowish calcareous sediments lying horizontally over gabbros. They contain abundant, generally well-preserved, and relatively diverse tropical late Neogene calcareous nannofloras and planktonic foraminiferal faunas, and yield a few poorly preserved radiolarians. The estimated ages are 8.8–10 Ma; 5.6–6.4 Ma (late Miocene); 4.5–4.2 Ma (early Pliocene), derived from deep-sea correlations between microfossil zonations and magnetic stratigraphy. Our results are compared to theoretical ages proposed for the crust in the surveyed area. This leads us to discuss the timing and location of mechanisms responsible for the exposure of the observed section and allows us to emphasize that early morphologies and structures may be preserved during the transform walls migration.

Introduction

The Vema Fracture Zone offsets the Mid Atlantic Ridge (MAR) by about 300 km at 10°45'N. One of the goals of the *Vemanaute* cruise to the Vema Fracture Zone was a detailed geological, petrological and structural study of a restricted area (Fig. 1), located along the southern wall of the transform, where serpentinized peridotites and amphibolites had previously been dredged. This wall constitutes the northern flank of a major, E–W trending feature, the transverse ridge, running parallel to the transform valley and culminating at a depth of less than 600 m farther west (at 44°22' W). The surveyed area is located close to the eastern tip of the transverse ridge, at 42°42'W, that is, respectively, 110 and 190 km from the western and eastern MAR axis–fracture zone intersections. Previous paleontological data obtained from samples dredged both on the flank and on the crest of the transverse ridge at 44°22'N (at about 200 km to the west of the area studied during the *Vemanaute* cruise) suggest that the uplift of this feature occurred 10 Ma ago (Bonatti and Crane, 1982; Bonatti et al., 1983).

Correspondence to: V. Mamaloukas-Frangoulis, IFREMER, Centre de Brest, B.P. 70, 29280 Plouzané Cédex, France.
*Present address: CNRS, Laboratoire de Géologie du Quaternaire, Luminy, B.P. 71, 13277 Marseille Cédex, France.

0025-3227/92/$05.00

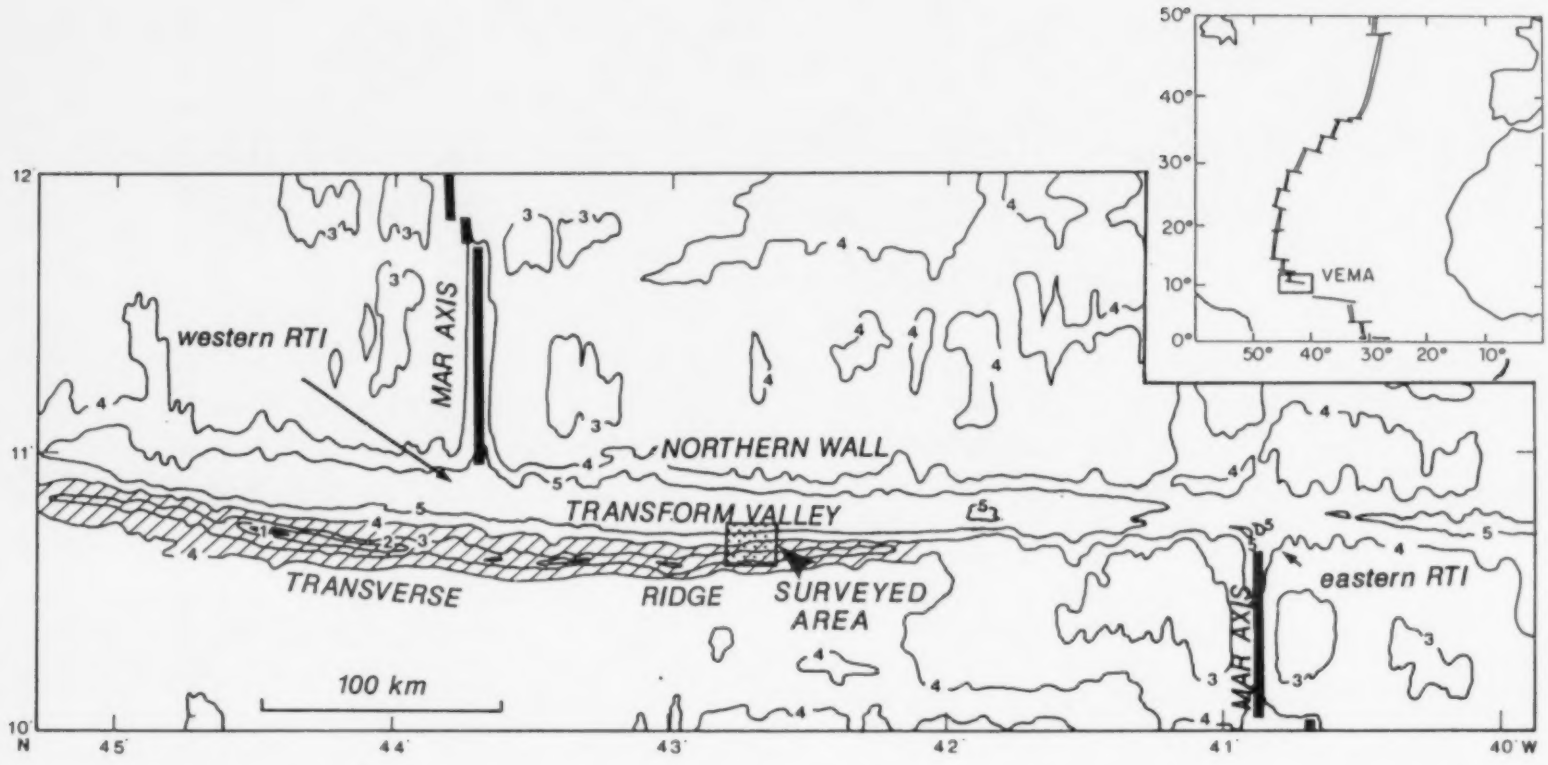

Fig. 1. A 1000-m interval chart of the Vema Fracture Zone in the North Atlantic. Dashed area emphasizes the transverse ridge. *RTI*: Ridge–Transform Intersection.

Due to lack of well-developed magnetic anomalies in this area, the age of the lithosphere in the vicinity of the Vema Fracture Zone cannot be exactly determined. Assuming a spreading rate of 16 mm/yr as proposed by Candé et al. (1988), the calculated age of the basement in the surveyed area is 11.8 Ma, whereas assuming a lower spreading rate (12 mm/yr: Van Andel et al., 1971), the predicted age should be 15.8 Ma.

Results of the dives

Two N–S transects have been conducted on the southern wall of the transform valley in the surveyed area (Fig. 2). Five dives enabled some of us to explore the entire height of the transverse ridge wall from the Vema valley floor (5150 m) to the crest of the wall (2100 and 2280 m). The section observed corresponds to an almost complete section of upper oceanic lithosphere and comprises from bottom to top: serpentinized peridotites, Fe–Ti gabbros, sheeted dykes, basalts and associated basaltic breccias (Fig. 2; Auzende et al., 1989). The contact between the basal ultramafics and the gabbros is probably tectonic along E–W trending vertical faults related to the transform activity, whereas the other contacts between the mafic layers are most probably primary. The upper gabbros are clearly intruded by isolated doleritic dykes. The average trend of the dykes within the dyke complex is N10°, parallel to the present-day spreading axis. This strongly suggests that they have been emplaced at the eastern Ridge transform intersection.

Sediment ages

At a depth of 3600 m along both transects we observed poorly lithified yellowish calcareous sediments lying horizontally over the gabbros. Samples Vema 2-7, 2-6 and 5-2 were taken during dives 2 and 5 (Fig. 2), at depths of 3690, 3670 and 3661 m, respectively. Age determination of the calcareous oozes recovered over the gabbros is based on micropaleontological analysis. Samples VE2-7, 2-6 and 5-2 are soft calcareous oceanic oozes which contain abundant, generally well-preserved, and relatively diverse tropical late Neogene calcareous nannofloras and planktonic foraminiferal faunas. In addition, they yield a few poorly preserved radiolarians. Benthic foraminifera are extremely rare, characteristic of abyssal depths and not age

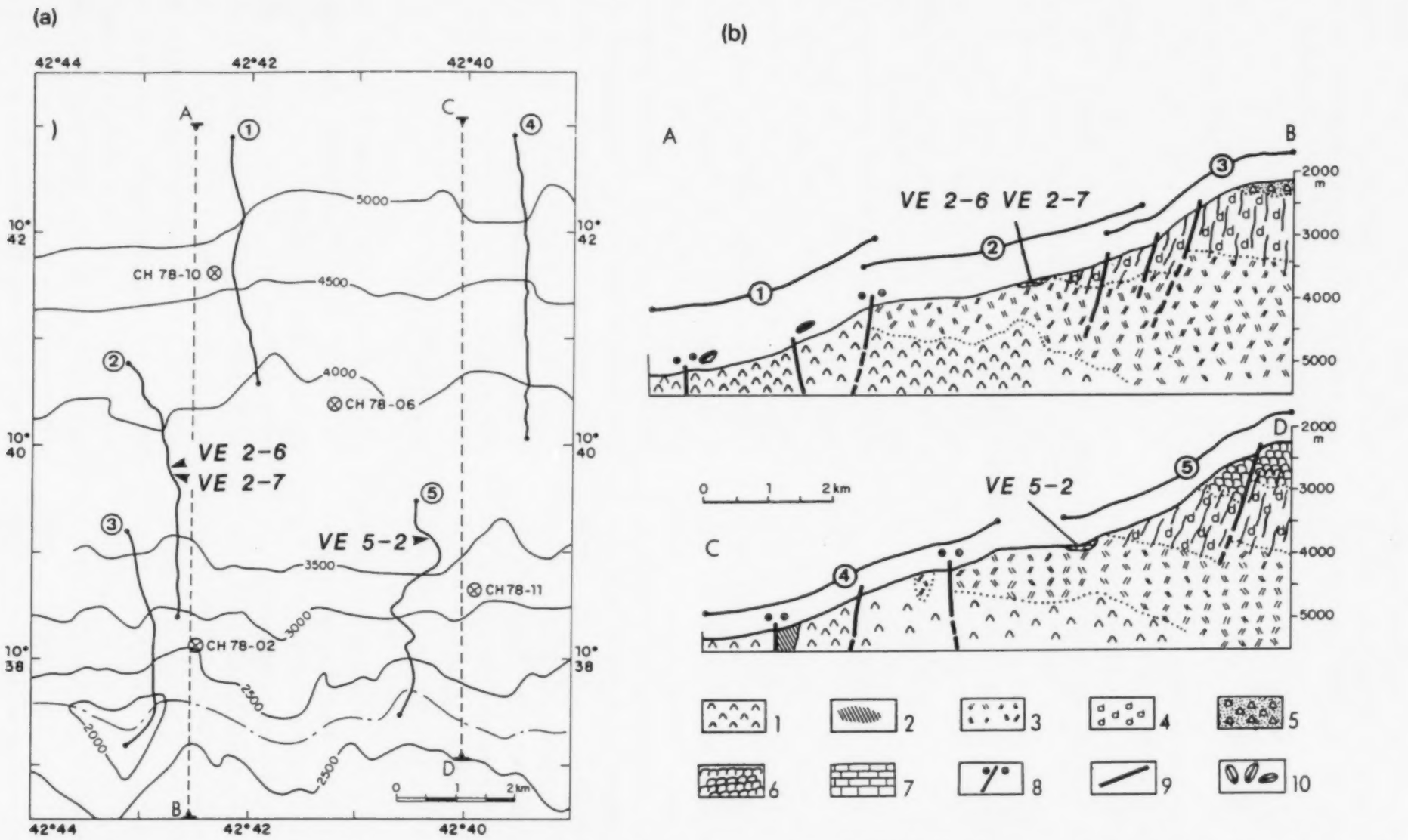

Fig. 2. (a) Bathymetric map of the study area with location of the *Nautile* dives (*1–5*), samples no. *VE2-6, VE2-7, VE5-2*, sections *A–B* and *C–D* of Fig. 2b, and dredges *CH78-10, 11, 02*. (b) Synthetic geological sections along N–S transects *A–B* and *C–D*. Note the thin sedimentary deposits preserved in both sections: samples no. *VE2-6, VE2-7* and *VE5-2*. *1* = serpentinites; *2* = amphibolites; *3* = gabbros; *4* = dykes complex; *5* = basalt pavement; *6* = pillows; *7* = indurated sediments; *8* = strike-slip faults; *9* = normal faults; and *10* = clams (from Auzende et al., 1989).

diagnostic. The estimated ages of the three samples are derived from deep-sea correlations between microfossil zonations and magnetic stratigraphy (Berggren et al., 1985).

Calcareous nannofossils

Sample VE2-7 yields a typical early late Miocene calcareous nannofossil assemblage characterized by *Discoaster hamatus* and *Catinaster calyculus* whose co-occurrence indicates the upper part of the total range Zone NN9 of Martini (1970), equivalent to subzone CN7b of Okada and Bukry (1980). Chronologically this sample is of early Late Miocene age (early Tortonian) with an estimated age between 8.8 and 10 Ma (Berggren et al., 1985).

Co-occurrence of *Discoaster quinqueramus* and various species of the genus *Amaurolithus* (i.e., *A. amplificus*, *A. primus* and *A. tricorniculatus*) in sample VE2-6 characterizes the upper part of the total range Zone NN11 (Martini, 1970), equivalent to the CN9b subzone of Okada and Bukry (1980). Thus, sample VE2-6 is of late Miocene age with an estimated age of 5.6 to 6.4 Ma.

Sample VE5-2 yields a typical early Pliocene assemblage with species of the genus *Ceratolithus* overlapping with species of the closely related genus *Amaurolithus* (Gartner and Bukry, 1975). The simultaneous occurrence of both genera indicates a biostratigraphic position restricted to the NN13–NN14 zonal interval defined by Martini (1970). The (very rare) presence of *Discoaster asymmetricus* could be regarded as indicative of Zone NN14 (Martini, 1970). However, the stratigraphic relialibility of this taxon has been questioned (Berggren et al., 1983) and it probably has no biostratigraphic significance in this case. This and the occurrence of *Ceratolithus acutus* with *C. rugosus* lead to a confident assignment of VE5-2 to the early Zone NN13 with an estimated age of 4.5 to 4.1 Ma.

Planktonic foraminifera

Sample VE2-7 is characterized, among other things, by the association of *Globigerina nepenthes*, *Globorotalia limbata* (=*Globorotalia* sp. "B" of Bolli), G. sp. "A" of Bolli, *G. lenguaensis* and *Globigerinoides extremus*. A single specimen was found of a form referable to *Paragloborotalia* cf. *siakensis*. This association suggests correlation to Zone N16 (Blow et al., 1969) despite the absence of the nominate taxon of this zone, *Neogloboquadrina acostaensis*. Chronologically, this sample is of early Late Miocene age, probably equivalent to a level near the base of paleomagnetic chron C5N (Berggren et al., 1985).

The association of *Globorotalia multicamerata*, *G. margaritae*, *G. tumida*, *Gobigerina nepenthes*, *Sphaeroidinellopsis dehiscens immatura* and *Globigerinoides conglobatus* in sample VE5-2 suggests assignment to Zone Pl1 of Berggren (1977) of the early Pliocene. This is supported by the dextrally coiled *Globorotalia limbata* and *G. pseudomiocenica*; this group exhibits a change in coiling from sinistral (below) to dextral (above) near the Miocene/Pliocene boundary in the Atlantic–Caribbean province. Chronologically, this sample is probably equivalent to the middle part of the Gilbert Chron.

The fauna in sample VE2-6 is essentially similar to that in sample VE5-2. However, the association of *Globorotalia cibaoensis*, *G. pertenuis*, dextrally coiled *G. limbata*, and *G. pseudomiocenica* and the absence of *Sphaeroidinella*, *Globigerinoides conglobatus*, *Globorotalia multicamerata* and *G. margaritae* suggest a late Miocene age, probably equivalent to paleomagnetic chron 5 or 6 (Hodell and Kennett, 1986).

Radiolarians

The stratigraphic overlap between *Lithopera bacca* and *Stichocorys delmontensis* in sample VE2-7 is indicative of an late Miocene interval between the uppermost part of the *D. pettersoni* Zone and the *D. penultima* Zone as defined and emended by Riedel and Sanfilippo (1970, 1978).

The co-occurrence of *Pterocanium prismaticum*, *Stychocorys peregrina* and *Lychnodictyum audax* suggests that sample VE5-2 belongs to the Pliocene *Spongaster pentas* Zone of Riedel and Sanfilippo (1970, 1978).

No biostratigraphically useful radiolarians were found in sample VE2-6.

Figure 3 shows the stratigraphic position of the three samples with respect to calcareous nannofos-

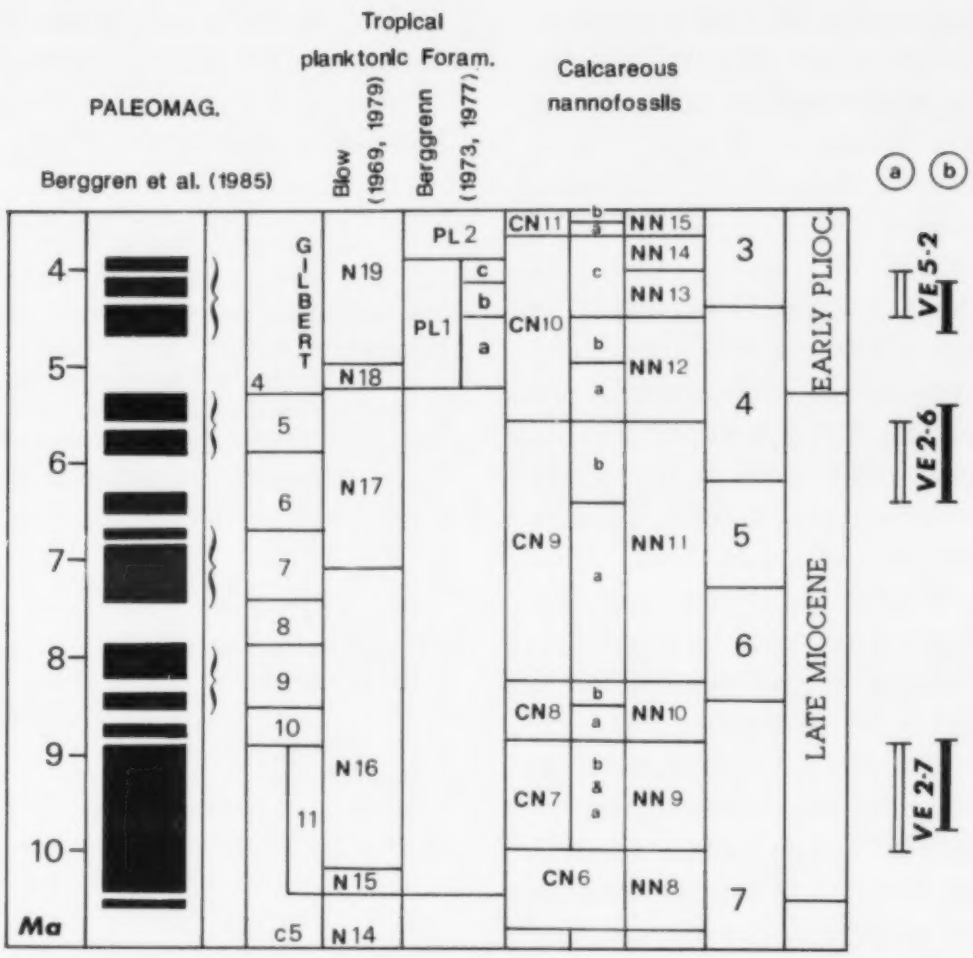

Fig. 3. Stratigraphic position and estimated ages of samples VE2-7, 2-6 and 5-2. Column "a": as deduced from the calcareous nannofossils. Column "b": as deduced from the planktonic foraminifera.

sil (column a) and planktonic foraminiferal stratigraphy (column b), and their estimated ages. There is almost exact concordance between the determinations inferred from both groups. In addition, there is no contradiction with radiolarian stratigraphy. With reference to the time scale of Berggren et al. (1985), sample VE2-7 is younger than 10 Ma and older than 8.85 Ma. The age of sample VE2-6 is between 5.6 and 6.4 Ma; that of sample VE 5-2 between 4.5 and 4.2 Ma.

Discussion and Conclusions

In situ observations of the crustal section exposed along the southern wall of the Vema transform, 190 km west of the eastern intersection, revealed that the sheeted dyke complex shows an average trend parallel to the present-day spreading axis orientation (Auzende et al., 1989; Cannat et al., 1991). This strongly suggests that the observed section of oceanic crust was created at the eastern MAR axis–Transform Fault intersection and was subsequently transported along the transform. Paleontological ages obtained here indicate that the oceanic crust that constitutes the present-day southern transform wall was subjected to tectonic processes responsible for exposure of deep crustal levels during the early Tortonian (about 10 Ma ago) or before.

Understanding the mechanisms leading to gabbro exposure and discussing the exact location where these events took place give rise to two different hypotheses.

In a first hypothesis, assuming that no changes in orientation and location of the spreading axis occured since 15–10 Ma (the theoretical age of the basement in the surveyed area) we may conclude that gabbro exposure occurred very shortly (0 to 4 m.y.) after the creation of the lithosphere and took place at the eastern MAR axis–Transform Fault intersection. In the hypothesis, the intersection domain should be the site of amagmatic stretching leading to exposure of deep crustal levels. A possible present-day equivalent of the

situation described here is the MARK area (Karson and Dick, 1983; Mével et al., 1991) where gabbros are exposed on the western corner of the eastern intersection with the MAR axis. Recent models to explain the gabbro and mantle exposures infer cyclicity of magmatism in slow- spreading ridges (Karson et al., 1987). The topography of the seafloor should result from a succession of constructional (magmatic) stages and extensional (tectonic) stages during which deep levels of the crust may be exposed (Pockalny et al., 1988).

An alternative hypothesis can be proposed taking into account an important uplift episode that affected the southern wall of the Vema Fracture Zone around 10 Ma ago, resulting in the anomalously elevated position of the transverse ridge. Whatever the reasons for this uplift are (block tilting; changes in spreading direction (Van Andel et al., 1969; Roest and Collette, 1986) local compressional regime and oscillatory spreading (Bonatti and Crane, 1982), it is possible that it resulted in the exposure of deep crustal levels of the southern wall of the fracture by faulting and related mass wasting. According to this hypothesis, the denudation of the lower crustal and mantle levels should have occurred independently from processes acting at the MAR axis transform intersection. However, it is not excluded that vertical tectonism linked to the 10 Ma event permitted the uplift of crustal and mantle rocks early exposed at the intersection domain.

Finally, results presented here show that the crustal section observed during the *Vemanaute* cruise along the southern wall of the Vema Fracture Zone has been exposed at least 10 Ma ago at the eastern ridge–transform intersection and subsequently transported along the transform wall without suffering significant deformation. This allows us to emphasize that early morphologies and structures may be preserved during the transform walls migration.

Acknowledgements

We wish to thank H. Schouten and W.B. Bryan (W.H.O.I.) and two anonymous reviewers for their comments and suggestions for improvements on an early draft of this paper. This is Woods Hole Oceanographic Institution Contribution No. 7561.

References

Auzende, J.M., Bideau, D., Bonatti, E., Cannat, M., Honnorez, J., Lagabrielle, Y., Malavieille, J., Mamaloukas-Frangoulis, V. and Mével, C., 1989. Direct observation through slow-spreading oceanic crust. Nature, 337(6209): 726–729.

Berggren, W.A., 1977. Late Neogene planktonic foraminiferal biostratigraphy of the Rio Grande Rise (South Atlantic). Mar. Micropaleontol., 2: 265–313.

Berggren, W.A., Aubry, M.-P. and Hamilton, N., 1983. Neogene magnetobiostratigraphy of Deep Sea Drilling Project Site 516 (Rio Grande Rise, South Atlantic). Init. Rep. DSDP, 72: 675–713.

Berggren, W.A., Kent, D.V. and Van Couvering, J.A., 1985. Paleogene geochronology and chronostratigraphy. In: N.J. Snelling (Editor), The Chronology of the Geological Record. Geol. Soc. London Mem., 10: 211–260.

Blow, W.H., 1969. Late middle Eocene to Recent planktonic Foraminifera stratigraphy. In: P. Brönnimann and H.H. Renz (Editors), Proc. Int. Conf. Planktonic Microfossils 1st. (Geneva, 1967.) Brill, Leiden, The Netherlands, pp. 199–421.

Bonatti, E. and Crane, K., 1982. Oscillatory spreading explanation of anomalously old uplifted crust near oceanic transforms. Nature, 300(5890): 343–345.

Bonatti, E., Sartori, R. and Boersma, A., 1983. Vertical crustal movements at the Vema Fracture Zone in the Atlantic: evidence from dredged limestones. Tectonophysics, 91: 213–232.

Candé, S.C., Labrecque, J.L. and Haxby, W.F., 1988. Plate kinematics of the South Atlantic: chron C34 to present. J. Geophys. Res., 93(B11): 13479–13492.

Cannat, M., Mamaloukas-Frangoulis, V., Auzende, J.M., Bideau, D., Bonatti, E., Honnorez, J., Lagabrielle, Y., Malavieille, J. and Mével, C., 1992. A geological cross-section of the Vema Fracture Zone transvers ridge. J. Geodyn., 13(2/4): 97–118.

Gartner, S. and Bukry, D., 1975. Morphology and phylogeny of the Coccolithophycean Family Ceratolithaceae. U.S. Geol. Surv., J. Res., 3: 451–465.

Hodell, D.A. and Kennett, J.P., 1986. Late Miocene early Pliocene stratigraphy and paleoceanography of the South Atlantic and Southwest Pacific Oceans: a synthesis. Paleoceanography, 1: 285–311.

Karson, J.A. and Dick, H.J.B., 1983. Tectonics of ridge-transform intersections at the Kane fracture zone. Mar. Geophys. Res., 6: 51–98.

Karson, J.A., Thompson, G., Humphris, S.E., Edmond, J.M., Bryan, W.B., Brown, J.R., Winters, A.T., Pockalny, R.A., Casey, J.F., Campbell, A.C., Klinkhammer, C., Palmer, M.R., Kinzler, R.J. and Sulanowska, M.M., 1987. Along axis variations in seafloor spreading in the MARK area. Nature, 328: 681–685.

Martini, E., 1970. Standard Tertiary and Quaternary calcareous nannoplankton zonation. In: A. Farinacci (Editor), Proc. II Plaktonic Conf. (Roma.) 2: 739–785

Mével, C., Cannat, M., Gente, P., Marion, E., Auzende, J.-M.

and Karson, J.A., 1991. Emplacement of deep rocks on the west Median Valley Wall of the MARK area. Tectonophysics, 190: 31–53.

Okada, H. and Bukry, D., 1980. Supplementary modification and introduction of code numbers to the low-latitude coccolith biostratigraphic zonation (Bukry, 1973; 1975). Mar. Micropaleontol., 5: 321–325.

Pockalny, R.A., Detrick, R.S. and Fox, P.J., 1988. Morphology and tectonics of the Kane Transform from Sea Beam bathymetry data. J. Geophys. Res., 93(B4): 3179–3193.

Riedel, W.R. and Sanfilippo, A., 1970. Radiolaria, Leg 4, Deep Sea Drilling Project. Init. Rep. DSDP, 4: 503–575.

Riedel, W.R. and Sanfilippo, A., 1978. Stratigraphy and evolution of tropical Cenozoic radiolarians. Micropaleontology, 24: 61–96.

Roest, W.R. and Collette, B.J., 1986. The Fifteen Twenty Fracture Zone and the North American–South American plate boundary. J. Geol. Soc., London, 143: 833–843.

Van Andel, T.H., Phillips, J.D. and Von Herzen, R.P., 1969. Rifting origin for the Vema fracture zone in the north Atlantic. Earth Planet. Sci. Lett., 5: 296–300.

Van Andel, T.H., Von Herzen, R.P. and Philips, J.D., 1971. The Vema Fracture Zone and the tectonics of transverse shear zones in oceanic crustal plates. Mar. Geophys. Res., 1: 261–283.

Marine Geology, 107 (1992) 9–33
Elsevier Science Publishers B.V., Amsterdam

Late Quaternary changes in Antarctic Bottom Water velocity inferred from sediment grain size in the northern Weddell Sea

Carol J. Pudsey

British Antarctic Survey, Natural Environment Research Council, High Cross, Madingley Road, Cambridge CB3 OET, UK

(Received April 4, 1991; revision accepted December 17, 1991)

ABSTRACT

Pudsey, C. J., 1992. Late Quaternary changes in Antarctic Bottom Water velocity inferred from sediment grain size in the northern Weddell Sea. *Mar. Geol.*, 107: 9–33.

Newly formed bottom water ($\theta \leq -0.7°C$) in the northern Weddell Sea flows E or NE at speeds up to 10-15 cm/s, with velocity decreasing towards the centre of the Weddell Gyre (preliminary results from long-term current meter moorings). Upper Quaternary sediments from this area contain a fine-grained terrigenous component (from the nepheloid layer) plus biogenic silica (mostly diatoms) with a small amount of ice-rafted debris. In cores from between 61° and 66°S and from 3300 m to 4700 m water-depth, the proportion of biogenic silica increases northwards (corresponding to increasing seasonal extent of open water vs sea-ice cover), and the proportion of silt and well-sorted fine sand in surface sediments increases with average current velocity.

Downcore, diatom-rich and diatom-poor sediments alternate on a scale of 1–3 m, and intervals with more diatoms contain a higher proportion of silt to clay. Preliminary stratigraphy suggests the cyclicity in composition and texture is related to glacial–interglacial cyclicity. During warm periods (indirectly correlated with isotope stages 1, 3, 5 etc.) biogenic silica production takes place during several months of each year, and silt and fine sand are transported by bottom currents. During glacial periods with greater sea-ice cover than at present, biogenic productivity was suppressed and no silica was preserved in the sediments: in addition, a lower proportion of terrigenous silt implies that bottom currents were weaker. At sites with a present-day average velocity of 10 cm/s, a Last Glacial Maximum average velocity of 1 cm/s or less is inferred from grain-size measurements.

Introduction

Southern Ocean deep-sea sediments contain a record of changing biological productivity, terrigenous supply from the Antarctic continent, and bottom water flow. An understanding of present-day processes can be used to interpret downcore changes in texture and composition. In the study of Quaternary sediments we may attempt to isolate the effects of glacial–interglacial cycles, neglecting longer-term changes in the shape of ocean basins. Hemipelagic sediments from an area of high accumulation rate in the northern Weddell Sea offer such an opportunity.

The deep current systems in the Southern Ocean which influence sedimentation are the Antarctic Circumpolar Current (ACC) and the generally northward flow of Antarctic Bottom Water (AABW). The ACC is forced by westerly wind stress (Nowlin and Klinck, 1986) and its eastward flow extends to the seafloor in many places: the axis of the current is close to the Antarctic Convergence (Fig. 1a). The general term AABW includes cold, dense bottom waters formed in various places around the Antarctic margin by several different processes. As much as 80% of AABW may have its source in the Weddell Sea (recent summary in Foldvik and Gammelsrød, 1988) where the deep circulation is a clockwise gyre (Deacon, 1979; Fig. 1a). Other AABW source areas include the Ross Sea, the Shackleton and Amery Ice Shelves and the Adélie Coast (Gordon, 1972). Bottom water with an Antarctic source flows north through the western Atlantic (Wright,

0025–3227/92/$05.00

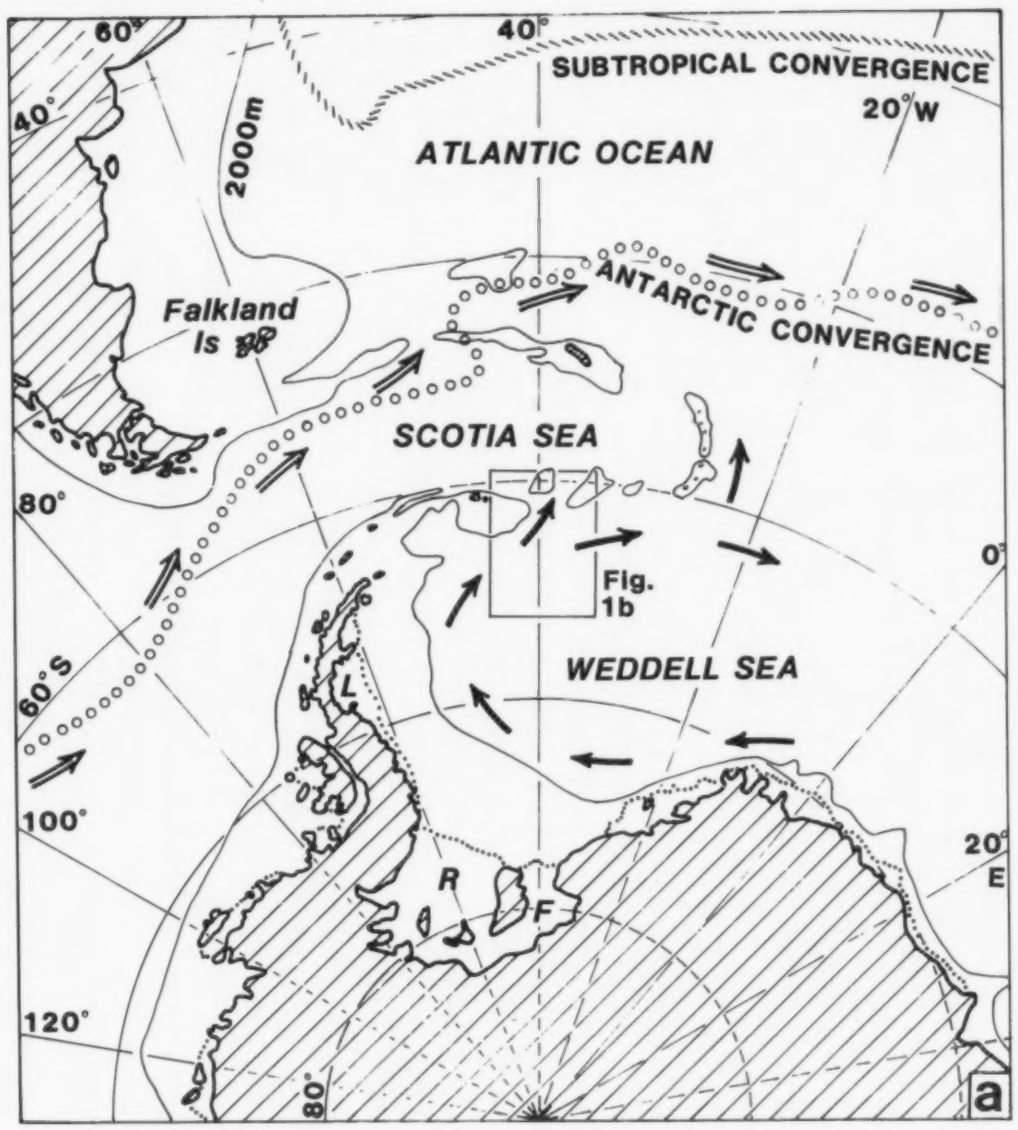

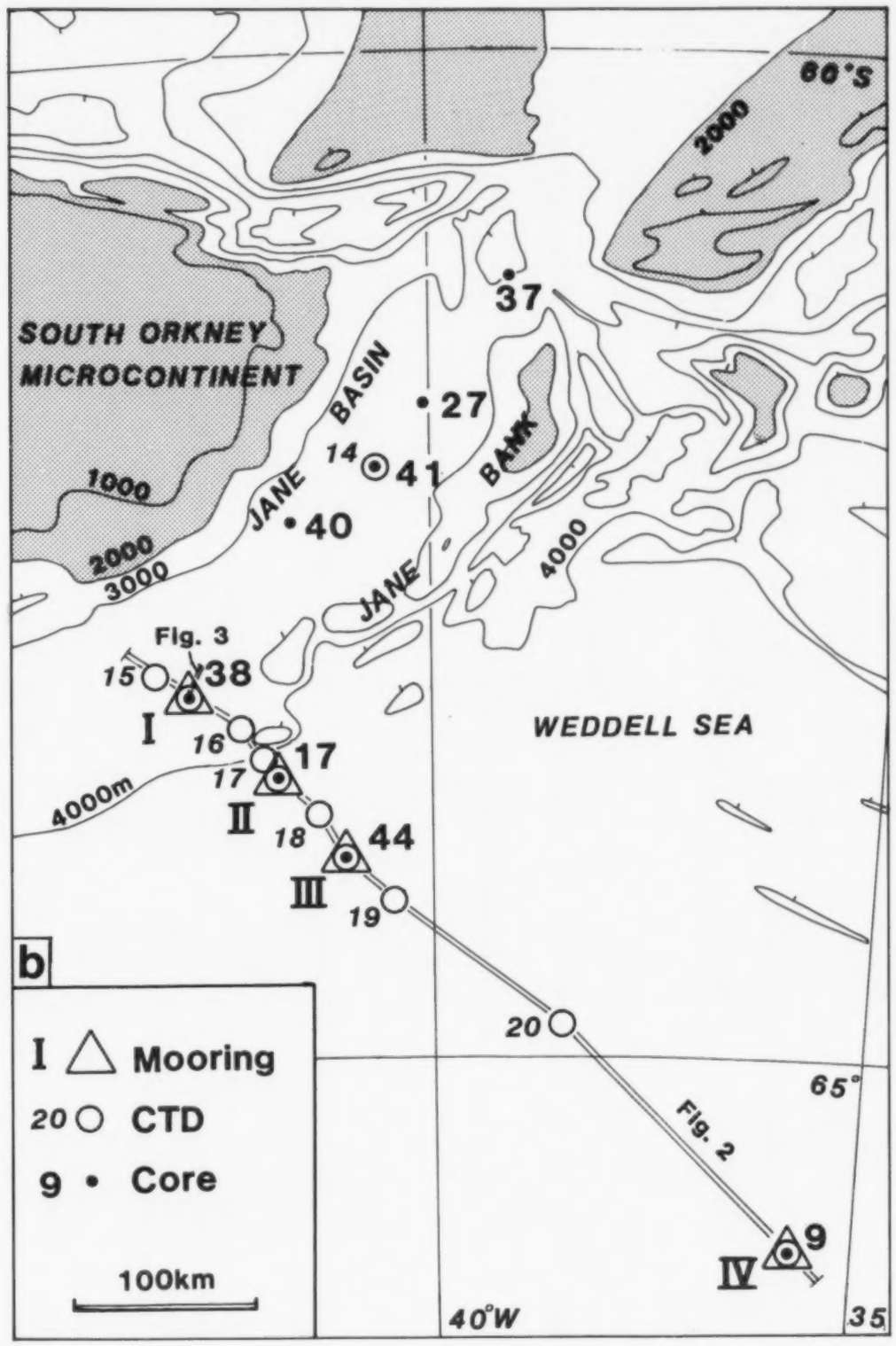

Fig. 1. (a) Location of the study area in the northern Weddell Sea (Fig. 1b). Double arrows, Antarctic Circumpolar Current; single arrows: deep circulation in Weddell Gyre. *L* = Larsen Ice Shelf, *R* = Ronne Ice Shelf; *F* = Filchner Ice Shelf; (b) Bathymetry of Jane Basin, with location of moorings, CTD stations and cores discussed in this paper. CTD 10 is at mooring site IV; CTD 11 at site III; CTD 12 at site II and CTD 13 at site I (see also Fig. 2).

1970) and has been distinguished by its temperature and salinity as far as 35°N in the subtropical North Atlantic (Amos et al., 1971; Tucholke et al., 1973); but as AABW flows away from its source it is modified by mixing with overlying water masses, which may themselves have changed during glacial-interglacial cycles. To infer changes in AABW production it is important to study the sediment record in the Weddell Sea, close to the source.

Weddell Sea Bottom Water (WSBW), the densest variety of AABW [potential temperature $\theta \leq -0.7$°C, as defined by Carmack and Foster (1975)], is thought to be formed today mostly in the southern and western Weddell Sea. The formation of dense Western Shelf Water (WSW), i.e. brine liberated during freezing of sea ice, was discussed by Gill (1973). Some WSW may mix with the ambient Warm Deep Water (WDW) at the shelf break (Foster et al., 1987; Foster and Middleton, 1979). Foldvik et al. (1985b) and Foldvik and Gammelsrød (1988) suggest that WSW formed in front of the Filchner and Ronne Ice Shelves may be supercooled during circulation below the floating ice shelves, and some meltwater added to it. The resulting Ice Shelf Water (ISW) flows downslope at about 36°W as a dense plume, and mixes below 2000 m with Warm Deep Water entering the gyre from the east (Fig. 1a), forming WSBW (Foldvik and Gammelsrød, 1988).

Although some bottom water then recirculates within the gyre (Georgi, 1981), some flows north into the Scotia Sea or beneath the ACC into the Atlantic Ocean (Gordon, 1966; Le Pichon et al., 1971; Fig. 1a). The northern Weddell Sea and southern Scotia Sea contain areas of rapid and continuous Quaternary sedimentation where the record of AABW may be studied. This paper is concerned with the area to the east and southeast of the South Orkney Microcontinent (Fig. 1b), including part of the northern Weddell Sea and Jane Basin which forms a 3500 m deep pathway for northward-flowing bottom water. I present preliminary oceanographic data from CTD (conductivity–temperature–depth) stations and long-term current meter moorings (Fig. 2), together with detailed textural and compositional data from piston and gravity cores (locations in Table 1). The moorings were laid from RRS *John Biscoe* in February 1987 and recovered by RRS *Discovery* a year later; CTD stations were occupied on both these cruises. Most of the cores were taken by RRS *Discovery* in 1988, though cores 9, 17 and 27 from the *Discovery* 1984–1985 cruise (Pudsey et al., 1988) have been re-examined.

TABLE 1

Station list for moorings, CTD stations and cores

Station		Latitude S	Longitude W	Water depth (m)
Mooring	I	63°11.0′	42°46.0′	3770
Mooring	II	63°31.0′	41°46.0′	4540
Mooring	III	63°56.5′	40°54.0′	4535
Mooring	IV	65°55.0′	35°49.5′	4730
878 CTD	010	65°54.5′	35°49.5′	4746
878 CTD	011	63°56.0′	40°53.0′	4560
878 CTD	012	63°30.5′	41°43.5′	4526
878 CTD	013	63°10.0′	42°45.5′	3788
878 CTD	014	62°04.0′	40°37.0′	3300
878 CTD	015	63°04.0′	43°08.5′	3662
878 CTD	016	63°20.0′	42°10.5′	3810
878 CTD	017	63°27.0′	41°54.0′	4760
878 CTD	018	43°42.5′	41°18.0′	4537
878 CTD	019	64°08.5′	40°24.5′	4675
878 CTD	020	64°49.5′	38°34.0′	4820
845 PC	009	65°55.0′	35°47.0′	4727
845 GC	017	63°31.0′	41°43.0′	4545
845 GC	027	61°47.0′	40°08.0′	3470
878 GC	037	61°06.5′	39°10.5′	4025
878 PC	038	63°10.0′	42°43.5′	3802
878 PC	040	62°20.0′	41°26.5′	3456
878 PC	041	62°04.0′	40°35.0′	3310
878 PC	044	63°57.0′	40°56.0′	4548

845 = 1984/85 cruise; 878 = 1987/88 cruise; PC = piston core, GC = gravity core.

The present work extends an earlier study (Pudsey et al., 1988) which reported on a core transect from the centre to the edge of the Weddell Gyre. Here it was shown that hemipelagic sediments become coarser-grained from the centre to the edge of the basin reflecting the inferred increase in bottom current velocity towards the edge. Downcore variations in grain size were also measured, and in some cores an alternation between silty and clayey mud was found. Biogenic silica is preserved only in the more silty intervals (including the core tops) of the northernmost cores. This evidence led Pudsey et al. (1988) to suggest that during glacial periods, with greater sea-ice cover than today, biological productivity was suppressed

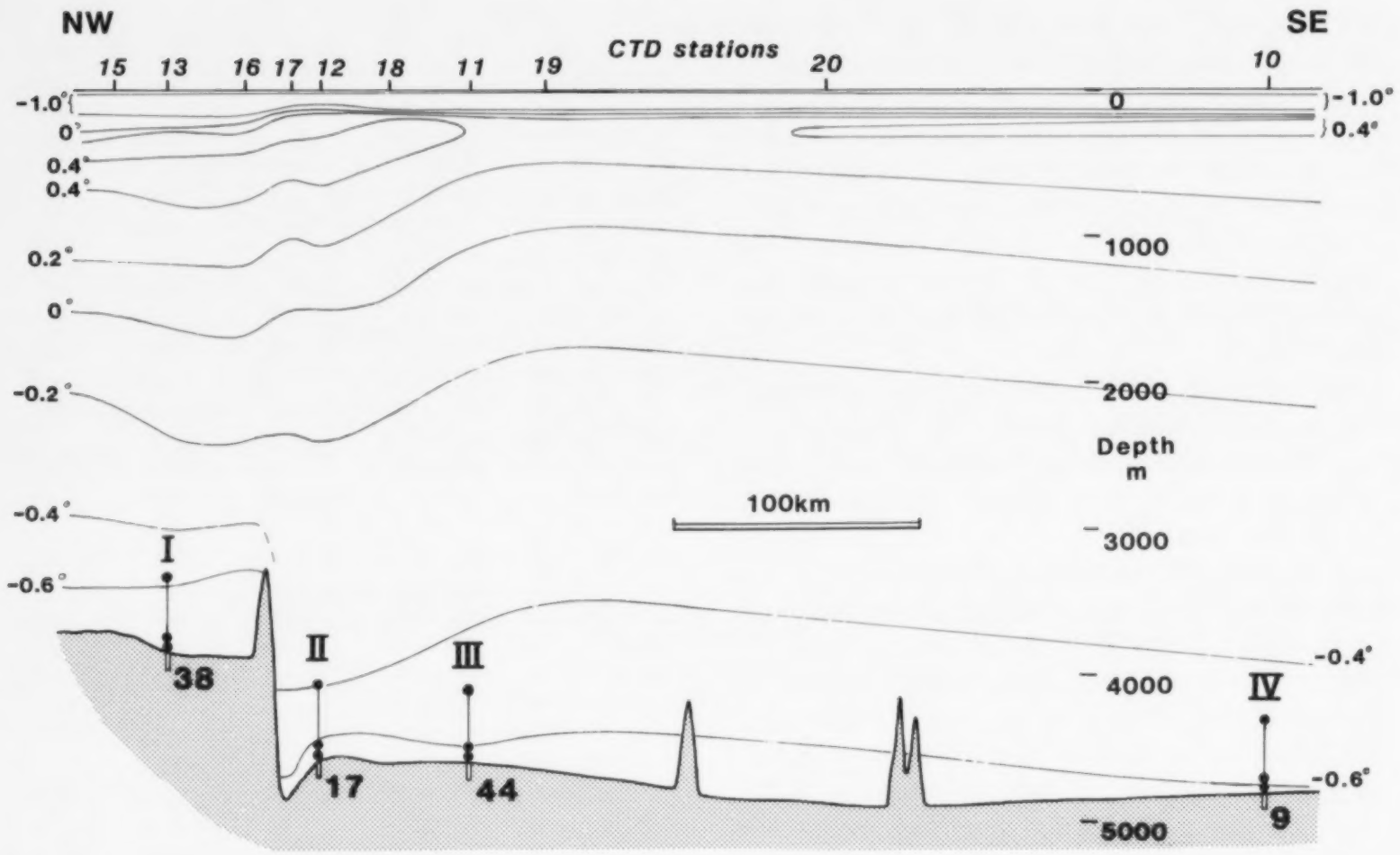

Fig. 2. Cross-section along the mooring transect showing in-situ temperature (°C) from CTD casts, positions of moorings I to IV and cores 38, 17, 44 and 9. Core length not to scale. Current meters positioned 5, 50 and 500 m above the sea bed on each mooring.

and bottom currents were weaker, transporting only the finest material in suspension. The new current meter data show that present day currents are clearly related to grain size of core-top samples; hence grain-size changes downcore can be used to make at least semi-quantitative inferences about palaeocurrent strength. Some advances have also been made in dating the cores, through magnetostratigraphy (O'Brien, 1989), biostratigraphy of the cores in Jane Basin (Jordan and Pudsey, 1992) and correlation with other cores in the southwestern Weddell Sea (Mackensen et al., 1989).

Methods

Physical oceanography

CTD

A Neil Brown CTD instrument was used with sensors for pressure, temperature, conductivity and oxygen. Casts were made to within 10 m of the bottom. Temperature was checked using a reversing thermometer triggered at the bottom of the cast: temperatures measured by reversing thermometer and CTD agreed to within 0.003°C. Salinity and oxygen were not calibrated, and in this paper it is mainly the temperature profiles which are discussed.

Current meters

Four moorings, each with current meters 5, 50 and 500 m above the seabed, were deployed from February 1987 to February 1988 (Table 2). The meters were Aanderaa RCM-5s set up to record measurements on tape once per hour. Two meters flooded and recorded no data, and in two others the tape jammed. Failures occurred in a total of six data channels in three other meters, so that no conductivity or transmissivity data were obtained. Current direction and speed were recorded for the whole deployment period on seven meters. The calibrations supplied by Aanderaa with each

TABLE 2

Parameters recorded by each current meter at moorings I–IV. Modified temperature sensors were used to measure low temperatures with improved sensitivity (Saunders and Cherriman, 1983). The data, recorded once per hour, are instantaneous measurements of temperature, conductivity, pressure and direction; speed is measured as the sum of rotor revolutions during the preceding hour. Within each box are shown the meter number (in bold type) and the number of days of good data. In meters 8250 and 3259 the tape stopped before the end of the deployment period

I	II	III	IV
6751 352 days temperature conductivity sensitive temp. direction speed	**6749** 351 days temperature sensitive temp. direction speed	**6152** 349 days pressure sensitive temp. direction speed	**3259** 316 days temperature sensitive temp. direction
8250 325 days temperature* sensitive temp. direction speed	**3257** 351 days temperature sensitive temp. direction speed	**3258** 349 days temperature sensitive temp. direction speed	**3261** Tape jammed: no data
8249 tape jammed: no data	**8248** Meter flooded; no data	**8247** 349 days temperature speed	**8246** Meter flooded: no data

*Temperature was recorded by meter 8250 for only 246 days because of intermittent sensor failures.

instrument were used to convert the recorded data to degrees and centimetres per second.

Sedimentology

Cores—general

Most core sites were selected in areas of fine-grained hemipelagic sedimentation as indicated on 3.5 kHz profiles (example in Fig. 3; see also Pudsey et al., 1988). Cores 37, 27, 41, 40 and 38 in Jane Basin constitute a latitude transect and cores 17, 44 and 9 are part of a transect from the edge to the centre of the Weddell Gyre. Core 17, very near the basin margin, is in an area of condensed sedimentation where winnowing occurs periodically. Core 9 is in the area of very slow, partly

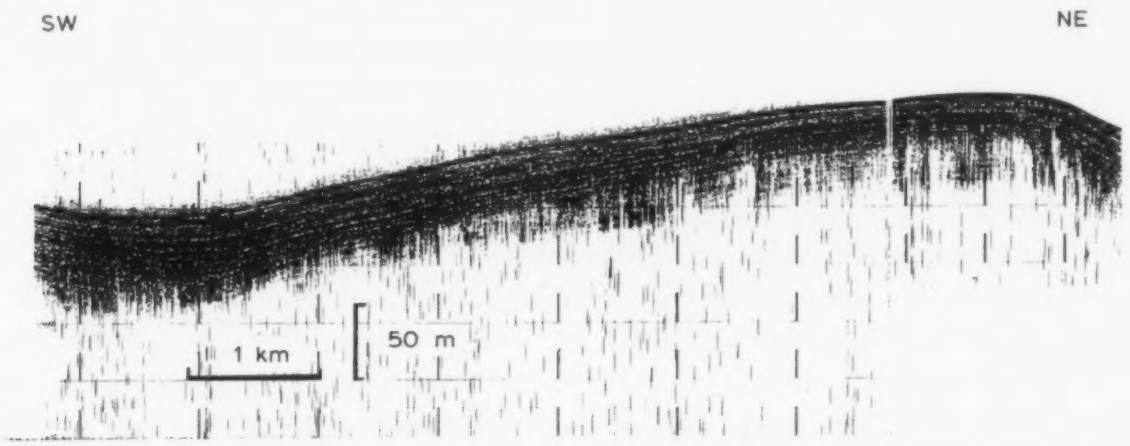

Fig. 3. 3.5 kHz profile in southern Jane Basin (location on Fig. 1b). The site of core 38 is about 2 km southwest of this profile. Parallel reflectors, lack of sediment ponding and deep sub-bottom penetration indicate hemipelagic fine-grained sediments with a low proportion of bedded silt and sand (review in Damuth, 1980).

turbiditic, sedimentation in the gyre centre (Pudsey et al., 1988). Piston or gravity cores 4 to 11 m long were recovered (Table 1); at each piston core site a trigger core 1 to 1.5 m long was also obtained. The cores were split and described on board ship. Laboratory measurements included magnetic susceptibility, silica content and grain size.

Magnetic susceptibility

A Bartington susceptibility meter with a small probe attachment was used to measure the archive half of each core at 2 cm intervals. Although detailed interpretation of the results must await further study, variations in susceptibility are useful in detecting repenetration, in correlation between trigger core and piston core top at each site, and between cores at adjacent sites (Robinson, 1990). Repeat measurements on core sections are accurate to +1 SI unit.

Silica

Almost all biogenic silica is present in the form of diatoms, with a few radiolarians, sponge spicules and silicoflagellates. The proportion of silica was measured by point-counting diatoms etc. vs terrigenous grains in smear slides. This method tends to overestimate diatoms compared with their true weight percentage (Pudsey, in prep.). This is because (a) centric diatom valves are thin discs and occupy a greater area of the slide than equant silt grains of the same weight; (b) biogenic opal is less dense than silicate minerals, and diatom valves are porous. Nevertheless this method provides a useful semiquantitative measure. Silica was measured in smear slides mainly at 20 cm intervals, with sampling density increased where necessary.

Grain size

Samples were taken at 10 cm intervals in most cores, avoiding diatom ooze layers, ash beds and the larger dropstones. Each sample of about 1 gramme was oven dried, weighed, disaggregated in 0.1% Calgon solution using an ultrasonic bath, wet-sieved to determine sand percentage and the fine fraction analysed on a Sedigraph 5000 particle size analyser. This instrument measures equivalent settling diameter (ϕ) and its output is a cumulative frequency curve from which the weight percentage within each ϕ size class can be determined. Analyses were run from 4 to 9 ϕ. Repeat analyses of samples agree to within 3% of the percentage finer than 9 ϕ. Sand percentage is accurate to within 0.5% for totals up to 10%.

Biogenic silica was not generally removed from the samples prior to grain-size analysis. Much of the sediment in this area is transported in the nepheloid layer (see Discussion) and benthic resuspension is a common process. Biogenic silica particles settling to the sea bed as components of marine snow are subject to the same current reworking processes as are terrigenous particles. There is therefore a case for measuring the size distribution of the total sediment, provided that size is measured as equivalent settling diameter. It is unlikely that biogenic silica has more than a minor effect on the size distribution because in most samples diatoms and their fragments constitute less than 20%: they have a wide size range (Fig. 4) and there is no silt mode attributable to diatoms. Samples from one interval of core 37 where diatoms form up to 24% of the sediment were leached in alkali to remove biogenic silica, and again run on the Sedigraph. The silica-free samples contain a higher proportion of silt than the untreated samples (Fig. 5), suggesting that most of the diatom fragments behave as clay-size particles (see also Calvert, 1966). The hydrodynamic equivalence of diatoms will be the subject of a future paper.

Results

Present-day water masses

A temperature cross-section southeast of the South Orkney Microcontinent is shown in Fig. 2, this is very similar to Foster and Middleton's (1979) section 100 km further southwest. In summer a mixed layer 70–100 m thick, with temperature usually just above 0°C, overlies about 200 m of Winter Water, a product of deep convection in winter (Mosby, 1934; Toole, 1981), colder than −1.5°C (Fig. 6). At the base of this layer, temperature and salinity increase to the core of Warm Deep Water at about 500 m. Below 500 m salinity

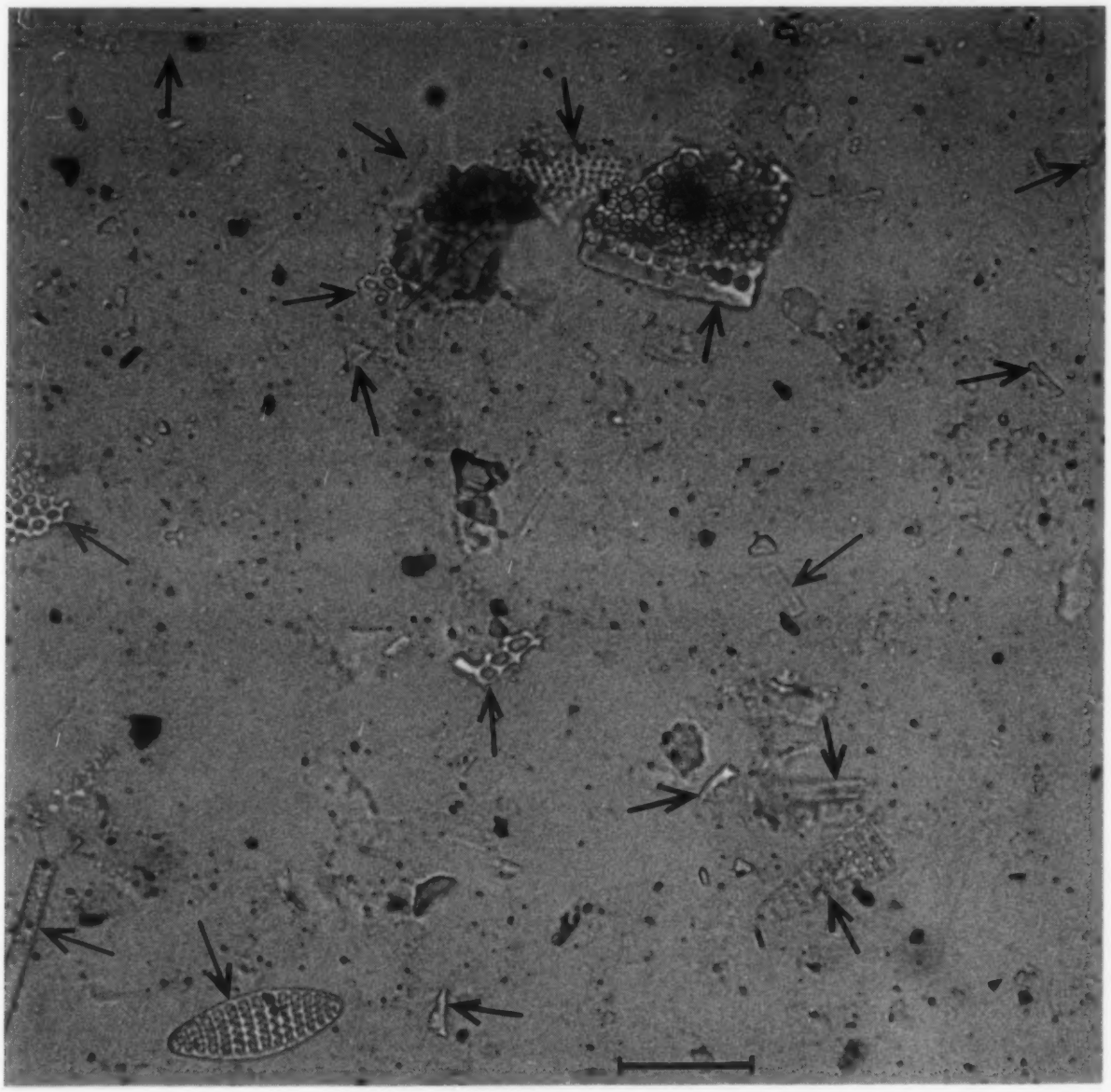

Fig. 4. Photomicrograph of diatom-bearing clayey mud showing the wide size range of particles of biogenic silica (arrowed). Scale bar is 20 μm. Core 37, 1.20 m depth.

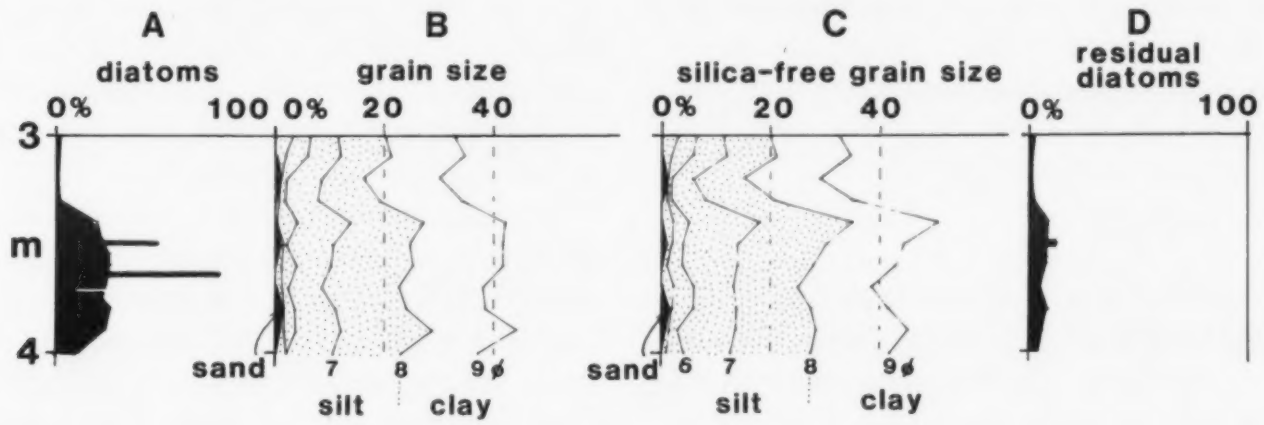

Fig. 5. The effect of biogenic silica removal on grain size distribution. (A) percent silica in the lowest metre of core 37. (B) grain size of untreated samples. The data are presented in the form of weight percentage within each ϕ interval plotted downcore. Samples were then leached with 0.5 *M* Na_2CO_3 at 85°C for 2 h. Six samples still contained about 15% diatoms, i.e. this treatment is not very effective; an additional leach of 0.5 *M* NaOH at 85°C for 2 h was used. (C) grain size of silica-free samples. Note the increased silt content from 3.4 to 4.0 m compared with B. (D) diatom percentage in leached samples. Silica removal still not complete, but a leach strong enough to dissolve all diatoms will attack clay minerals and volcanic glass as well (Hurd, 1973; DeMaster, 1981).

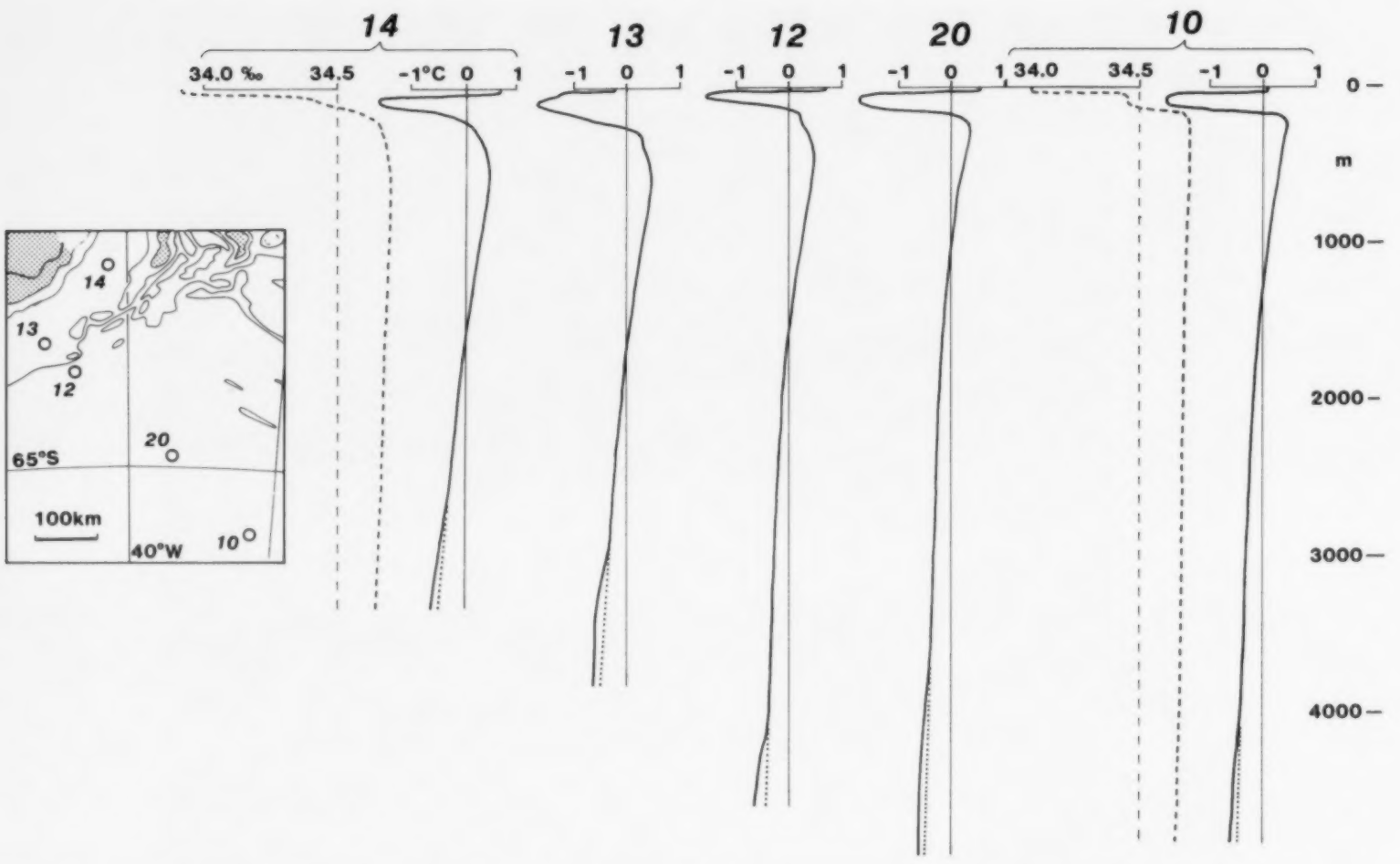

Fig. 6. In-situ temperature profiles at five CTD stations, locations on inset map (see also Fig. 2). Salinity is plotted as a dashed line for stations 10 and 14. The linear temperature change with depth in the lower half of each profile is projected downwards as a dotted line: note that a distinctly colder water mass is present at the base of each profile.

is almost constant and there is a gradual decrease in temperature to about 800 m above the seabed. A distinctly colder water mass is present in the lowest 800 m in all our temperature profiles (Fig. 6) and this is considered to be newly-formed bottom water (Carmack, 1974; Foldvik et al., 1985b). It is most distinct near the northern margin of the gyre.

Present-day currents

All the current meters recorded tidal flow, and at moorings III and IV most of the energy appears to be tidal. At the two northern moorings there was a strong E or NE flow all year. Preliminary results from each mooring are summarised from south to north and illustrated in Fig. 7. A full analysis of the current meter data is being carried out at the British Antarctic Survey and will be published separately.

Mooring IV: Flow was so slow at this site that the current meter rotor was stalled for 80% of the time. The vane can however be turned by a current too weak (< 1.5 cm/s) to spin the rotor, and semi-diurnal tidal cycles were recorded as changing directions. For seven periods of a few days each throughout the year, tidal currents reached 2–4 cm/s (Fig. 7) but for most of the year current speed was less than 1 cm/s.

Mooring III: again, the major part of near-bottom flow was tidal, but there was a slow non-tidal drift for most of the year so that the rotor was only stalled for 25% of the time, in periods of a few hours. Current speeds were typically 2–4 cm/s, with the net drift being about 1 cm/s (Fig. 7) and variable in direction throughout the year.

Mooring II: the strongest and most unidirectional flow was recorded at this site. Net drift was to the east at about 15 cm/s (Fig. 7), with speeds

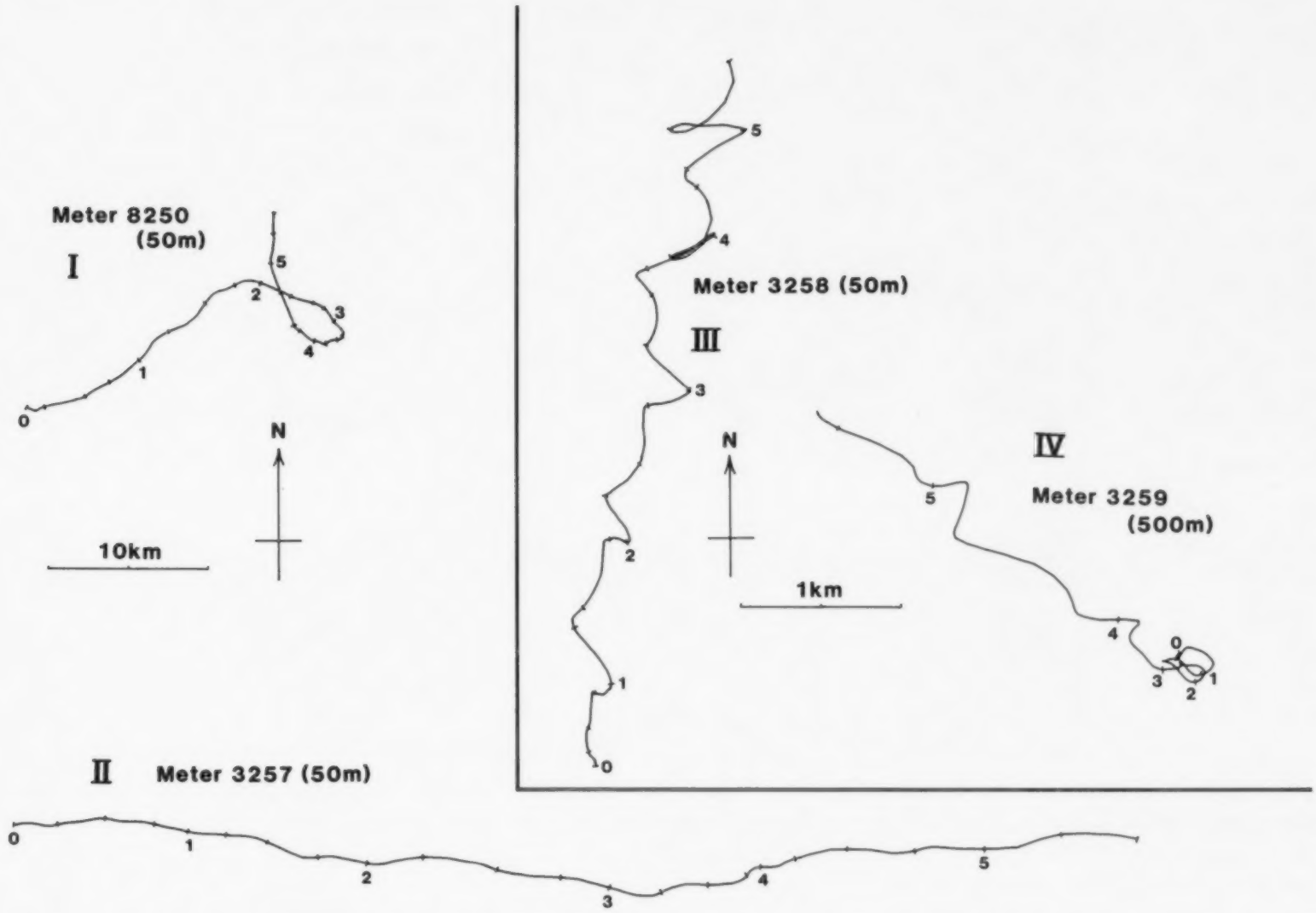

Fig. 7. Progressive vector diagrams of near-bottom currents at moorings I to IV, for the same 5½ day period. Diagrams start at 0000 (Z) on February 26th 1987, arabic numerals refer to days, intermediate time marks are at 6 hour intervals (omitted for clarity in part of IV). For meter locations see Fig. 2 and Table 2. Note that I and II are plotted on a different scale from III and IV. Numbers in parenthesis refer to height above sea bed. At mooring I, although the mean flow direction was uniform for much of the year, there were nine periods of 3–6 days each when the direction swung through 360°, recording the passage of an eddy.

of 30 cm/s attained several times during the year for periods of 1–2 days, and semi-diurnal tides with speeds up to 5 cm/s.

Mooring I: this site is similar to mooring II but with a weaker net drift, to ENE at 10 cm/s (Fig. 7). Maximum speeds were 20 cm/s. Semi-diurnal tides of up to 5 cm/s are discernible for most of the year.

Present-day sea ice

Sea ice distribution is taken from the Sea Ice Climatic Atlas (1985) supplemented by visual and radar observations during our own cruises.

The whole area of the moorings and cores is open water for about 3 months per year (Fig. 8). Over the moorings and southern cores, ice cover is intermittent or patchy for a further 1–2 months; the northern end of the coring transect may have as much as 6 months open water per year. In the northern Weddell Sea the ice edge is usually aligned NW–SE during summer, advancing northeastwards in the autumn and retreating southwestwards in the spring. In some years a tongue of old pack ice extends from the northern Antarctic Peninsula eastwards over the South Orkney area even in summer. This results from the normal clockwise surface circulation in the Weddell Sea combined with unusually strong and persistent westerly winds in the early spring.

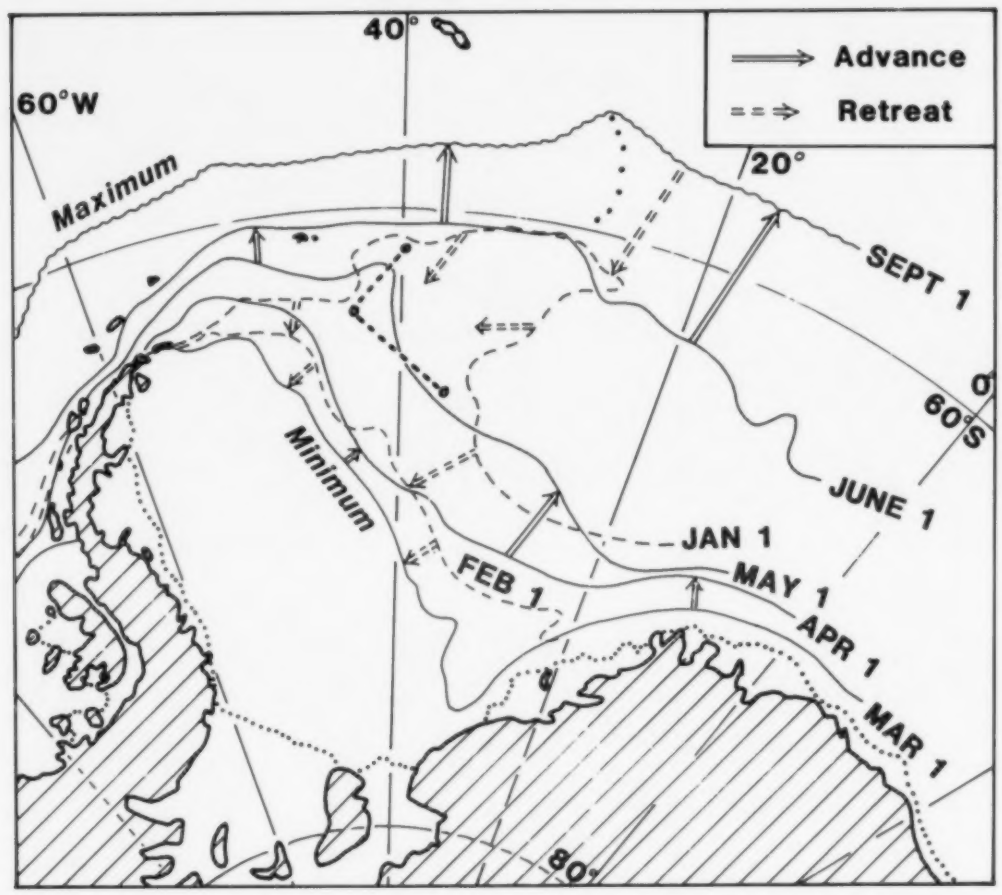

Fig. 8. Average positions over 10 years (1973–1982) of the pack ice edge in the Weddell Sea at its maximum and minimum extent (Sept.1 and March 1), and at 5 selected times during advance (solid line) and retreat (dashed line). Mooring and core transect shown by L-shaped dotted line. Source: Sea Ice Climatic Atlas, 1985.

Cores: General description

The cores consist of fine-grained terrigenous mud with a few silt laminae, dropstones and layers of altered volcanic ash (Fig. 9). Biogenic silica forms up to 20% (area percentage in smear slides; reaching 40% in core 37) of certain intervals in the northern cores, the proportion of silica generally increasing northwards towards the circum-Antarctic ooze belt (Goodell, 1973). The mud is poorly sorted and contains few sedimentary structures apart from widespread burrow mottling, though clear *Planolites* and *Chondrites* burrows occur locally. Colours include dark greyish brown (2.5Y4/2 and 1OYR4/2), greyish brown (2.5Y5/2), olive grey (5Y5/2) and dark greenish grey (5GY4/1); the more olive or green shades characterise more siliceous sediments. The lower parts of cores 41 and 44 are mainly dark grey (5Y4/1). In some intervals (e.g. base of core 9, 2.5 m in core 40), faint colour contrasts define horizontal lamination on a 1–2 cm scale. The middle of core 44 (5 to 6 m) contains several dark grey mud layers 1 to 5 cm thick with sharp bases and gradational burrowed tops.

Silt laminae up to 4 mm thick occur in cores 9 and 44, and there is a 5 cm fine sand bed near the base of core 40. The silts and sand are moderately sorted with angular grains. Ice-rafted dropstones up to 4 cm in diameter occur sparsely in most cores and are mostly sandstone or slate. Laminae and thin beds of altered volcanic ash are very common (Fig. 9). They are usually darker coloured than the surrounding mud (very dark greyish brown, 2.5Y3/2 or 10YR3/2) though some laminae of grey mud (5Y5/1) may also be altered ashes. Many ash laminae have been disrupted by bioturbation and the darker material is seen only as burrow fills. The very low sedimentation rate in core 9 has resulted in thorough mixing of any ash layers into the mud during bioturbation.

Biogenic silica occurs in intervals commonly 1–2 m thick in cores 40, 41, 27 and 37 (Fig. 9) and is present in trace amounts at the top of cores 44

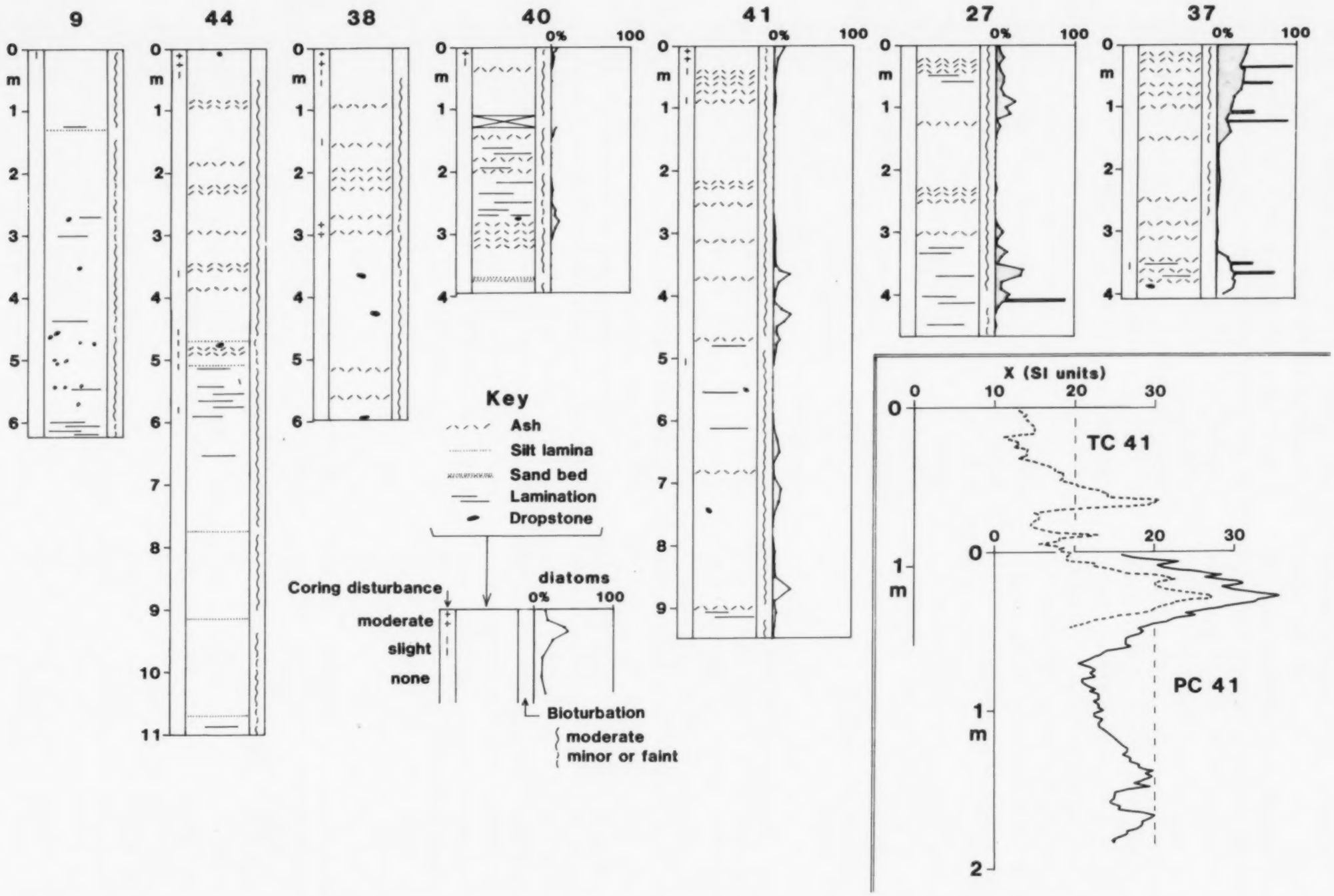

Fig. 9. Lithology and sedimentary structures of the northern Weddell Sea and Jane Basin cores. Cores consist of clayey mud except where shown otherwise (silt, ash etc.) in lithology column. There is no biogenic silica in the three southern cores except for a trace at the surface of cores 44 and 38. Trigger core and piston core data have been merged at each site: at most sites there is partial but not complete overlap between the two (see inset). Because of an operational problem, piston core 40 failed to recover a considerable thickness of surface sediment: the gap between base of trigger core and top of piston core may be more than the estimated 20 cm. Diatom percentage is area percentage in smear slides. Inset: Magnetic susceptibility (X, SI units) plotted against depth for trigger core 41 (dashed line) and the upper 2 m of piston core 41 (solid line). The broad peak of $X=37$ occurs at 1.2 m in the trigger core and 0.3 m in the piston core, and it is likely that 0.9 m of sediment is missing from the top of the piston core.

and 38. Silica is mostly in the form of diatom frustules (>95%) with a few silicoflagellates, radiolarians and sponge spicules. Diatom preservation ranges from poor to good, being better in the samples with more silica. Reworked Pliocene and Miocene diatoms are present but very uncommon. The proportion of diatoms at the sediment surface increases northeastwards, reaching 39% in the top of core 37. There is a clear downcore alternation of diatom-rich and diatom-poor intervals (Figs. 9 and 12). Each interval becomes thicker from SW to NE and the proportion of silica in the diatom-rich intervals also increases northeastwards. In cores 27 and 37 there are diatom ooze layers 1–2 cm thick which contain an unusual species assemblage in exceptionally good preservation (Jordan et al., 1991).

Grain-size analysis

Most sediments from Jane Basin and the northern Weddell Sea consist of clayey mud (Ocean Drilling Program classification: see e.g. Shipboard Scientific Party, 1988a) with 60 to 80% clay, 20 to 40% silt and 3% or less sand. In certain intervals of cores 17, 38, 40 and 41 sand forms 5–10% (rarely over 20%) and here there is generally 50–60% of clay. Sorting is poor, and few samples have a mode in the silt range (see Fig. 11). Because the sediment is mostly clay and because the silt fraction does not have a Gaussian distribution, it is considered inappropriate to represent each sample by a single parameter such as mean silt size. Instead the data are presented in the more complete form of the weight percentage within each ϕ interval plotted downcore. Silt mean is also shown for comparison with the results of other workers.

Surface sediment: cores 38, 17 and 44 were recovered from mooring sites I, II and III, respectively. Core 9, at mooring IV, failed to recover the top few centimetres of sediment, but surface samples were obtained from two adjacent sites 55 km to the SE (cores 6 and 7, Pudsey et al., 1988). There is a clear relationship between current speed and the grain size of surface sediments (Table 3). Higher current speed is reflected in a higher proportion of sand and a lower proportion of clay. In addition, the small percentage of sand in cores 9 and 44 is unsorted; the sand in core 17 is moderately sorted with a mode at about 2.7 ϕ (Fig. 10). In cores 38 and 17, the deficiency in coarse silt (4–5 ϕ: Fig. 10) may be an artifact caused by the Sedigraph stirrer's inability to keep all the coarse silt in suspension: the true size distribution is probably not bimodal, but there is abundant very fine sand.

Downcore results: Fig. 11 presents detailed grain-size data for cores 9, 44, 38, 40, 41, 27 and 37 and the results are summarised as sand: silt: clay plots, along with sediment composition, in Fig. 12. At each site the surface sediment is relatively silty and is underlain by an interval with a higher proportion of clay. Silty-clayey cycles 1–3 m thick continue to the base of each core. In the four northern cores diatoms occur in the silty intervals, but not in

TABLE 3

Summary of maximum and average current speed for each mooring, with the grain size (sand : silt : clay ratio) for the corresponding cores. Note that on mooring IV only the meter at 500 m recorded any data, and near bottom flow may have been somewhat different: however at the other sites, data from meters at 50 and 500 m are very similar

	Mooring I	Mooring II	Mooring III	Mooring IV
Height above seabed	50 m	50 m	50 m	500 m
Max speed	20 m/s	30 cm/s	5 cm/s	4cm/s
Average speed	10 cm/s	15 cm/s	1 cm/s	$\ll$1 cm/s
	Core 38	Core 17	Core 44	Core 6,7
Sand : silt : clay	13 : 28 : 59	28 : 27 : 45	1 : 33 : 66	2 : 17 : 81

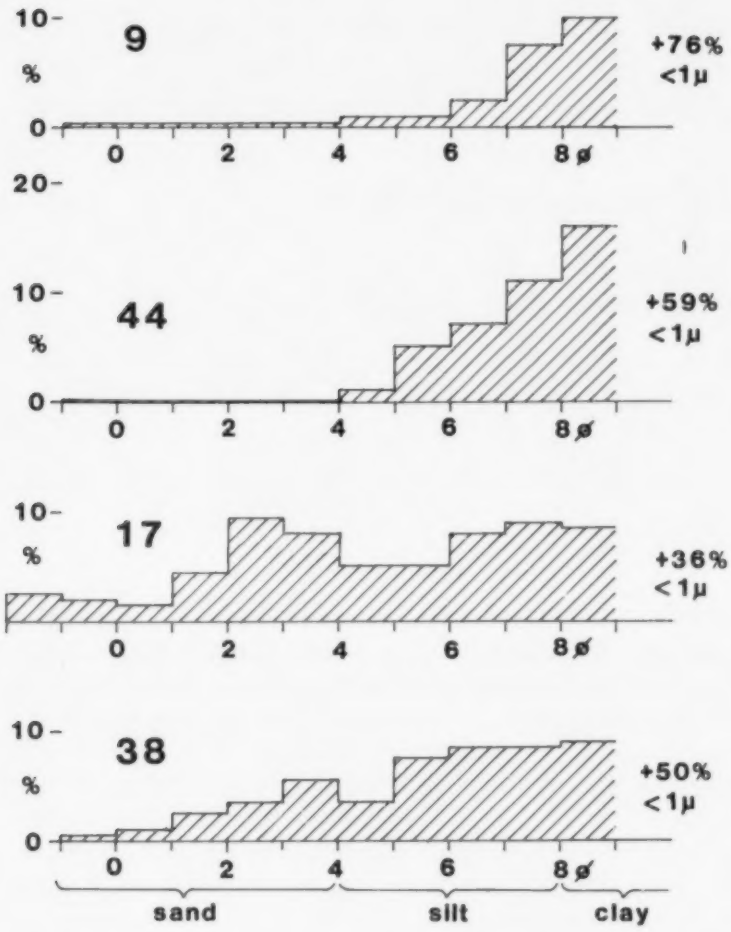

Fig. 10. Grain-size histograms for surface sediment at the mooring sites (see also Table 3). Core locations in Fig. 1b.

sufficient quantity to mask the grain-size signal: removal of biogenic silica would increase the amplitude of the silty-clayey cycles (Fig. 5).

Discussion

Sediment supply and transport

Sediment supply in a distal deep-sea setting such as described here can include pelagic input from the sea surface (biogenic silica, ice-rafted debris, volcanic ash), distal turbidites, and material transported by bottom currents. The fine grain size and lack of sorting of most of the terrigenous sediments, together with the absence of sedimentary structures except for burrow mottling and local faint lamination, imply that deposition from suspension in the nepheloid layer was the dominant process. In the next section, processes of sediment supply and transport are described in (approximately) increasing order of importance.

Turbidites

All core sites except 9 were selected to be away from areas of turbidite deposition. Core 9 lies on the abyssal plain of the Weddell Sea and contains rare silt laminae interpreted as very distal turbidites. These are also found in neighbouring cores described by Pudsey et al. (1988). Core 44, which is in an area of gently undulating topography and mainly pelagic or hemipelagic sedimentation, contains some thin (1–2 cm) dark grey mud layers at 5–6 m which are extremely fine-grained (0% sand and about 90% clay). These have sharp bases and burrowed tops and may be the products of very low-density, low-velocity turbidity currents. The sites in Jane Basin are not expected to receive turbidite sedimentation at all. This area is 1000 m above the Weddell Sea basin floor, and the South Orkney microcontinent with its very small land area and deep shelf is not an important sediment source (King and Barker, 1988). A shallow valley extends along the foot of the slope southeast of the South Orkney Microcontinent (Pudsey et al., 1988, fig. 6B): this is thought to be maintained by bottom current scour, analogous to the valley along the southwest side of the Argentine Basin (Ewing et al., 1971).

Ice-rafted debris

In the Antarctic, icebergs derived from ice shelves are observed to carry little or no sediment (Anderson et al., 1980; Drewry, 1986) and it is outlet glaciers which supply most of the debris-rich icebergs. In contrast to the Arctic, sea ice which forms over the deep Weddell Sea shelves incorporates very little suspended sediment. Aeolian dust supply to ice is also low because there is very little exposed glacial debris or rock around the Weddell Sea margins (contrast Barrett et al., 1983). Within outlet glaciers, rock debris eroded by abrasion, crushing and fracturing is comminuted during basal transport to give a complete grain-size spectrum of lithic fragments and mineral grains (Slatt and Eyles, 1981). Boulton (1978) notes that with multiple bedrock sources there may be no consistent size decrease down-glacier. Icebergs which calve and drift away continue to carry all grain sizes until the debris melts out. For the Weddell Sea sediments the proportion of poorly-

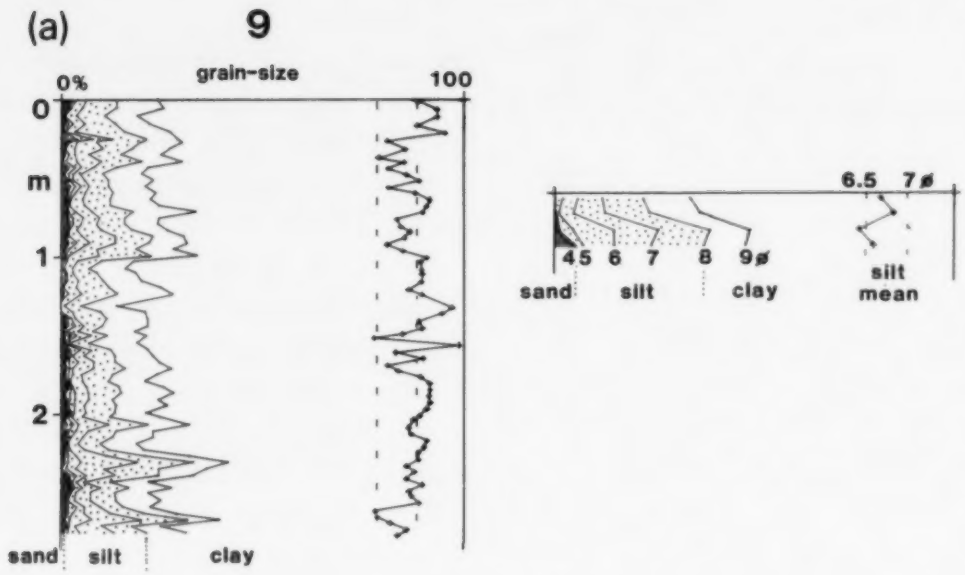

Fig. 11. Detailed grain-size data: the weight percentage within each ϕ interval is plotted downcore. Mean silt size is also shown, but this is of limited value for such clay-rich sediments. The main features of each core are as follows: Core 9–Most samples contain 1 to 2% of unsorted sand and the whole core is very fine-grained. More silty intervals occur from 0.15–0.4 m, 0.65–1.0 m, 2.0–2.15 m, 2.25–2.4 m and 2.6–2.7 m. Downcore, the weight percentage coarser than 5 ϕ (coarse silt plus sand) is constant at about 2%, except from 1–1.4 m; the greatest fluctuations occur in the size class 5–7 ϕ (medium and fine silt) which forms 2 to 15 percentage with the 7–9 ϕ interval remaining at about 8%; Core 44–Sand is almost absent and coarse silt forms 2% above 5 m, 0 to 2% below this level. There are more silty intervals from 0–0.8 m, 2.5–4.7 m, 6.3–7.4 m, 8.3–9.0 m and 9.8–10.9 m, with clayey intervals between. As in core 9 it is the weight% of medium and coarse silt which is varying the most, from 5 to 25%; Core 38–This core contains four coarse-fine cycles with the coarse intervals from 0–0.3 m, 1.3–2.3 m, 3.6–4.2 m and 4.8–5.3 m. The weight percentage of moderately sorted very fine sand varies from 0 to 48%; Core 40–There are three intervals in this core containing 5 to 10% of diatoms and these correspond to coarse-grained intervals from 0–0.4 m, 1.0–1.5 m and 2.5–3.0 m. A fourth coarse interval is present in the lowest 0.2 m. Sand and coarse silt vary from 0 to 12% and the medium plus fine silt total varies from 5 to 30%; Core 41–Four intervals of diatom-bearing silty sediment occur and each is thicker than in core 40: 0–1.0 m, 2.7–5.0 m, 6.1–7.3 m and 8.3–9.2 m. Very fine sand forms 1 to 6% of the uppermost coarse interval, but below 1.0 m the variation in sand and coarse silt percentage is not cyclic. The medium plus fine silt total varies from 5 to 11%; Core 27–Diatom-bearing sediment extends from 0–1.4 m and the silt content decreases from 38% at the core top to 21% at 1.4 m. Barren mud with about 20% silt continues down to 2.8 m; below this level diatoms form 5 to 30% and silt 25 to 30%. All size classes from very fine sand to very fine silt show some downcore cyclicity, though the variation is greatest (6 to 20%) in medium plus fine silt. Core 37–Similar to core 27, with diatom-bearing silty sediment from 0–1.6 m and 3.2 m to the base of the core. In the less diatomaceous interval in the middle, biogenic silica does not disappear completely.

sorted sand indicates the importance of ice-rafting. In cores 9, 41, 27 and 37 sand is present in small amounts (up to 3%) and its lack of sorting suggests an ice-rafted origin. These cores also probably contain a small quantity of ice-rafted silt and clay as well, but the ice-rafted debris should not mask the effects of other transport processes. Surface circulation is clockwise around the gyre, as shown by the tracks of beset ships and buoys fixed in pack ice (Limbert et al., 1989; Wadhams et al., 1989) as well as by the drift of icebergs (Swithinbank et al., 1977). Bergs derived from the margins of the Weddell Sea thus tend to stay near the western margin as they drift north, and the rate of ice-rafted debris accumulation is expected to be higher over the western shelf and slope area and Jane Basin (Fig. 1a) than towards the centre of the basin. This may help to explain the relative lack of sand in core 44. In core 9 the overall sedimentation rate is so low that ice-rafted sand, although accumulating extremely slowly, still constitutes 1–2%.

Volcanic ash

Volcanic ash has made a variable but generally small contribution to sedimentation in the Jane Basin area. For Southern Ocean cores mainly east of 20°W, Cooke and Hays (1982) emphasised the transport of ash particles by sea ice, as opposed to direct settling from the atmosphere through the

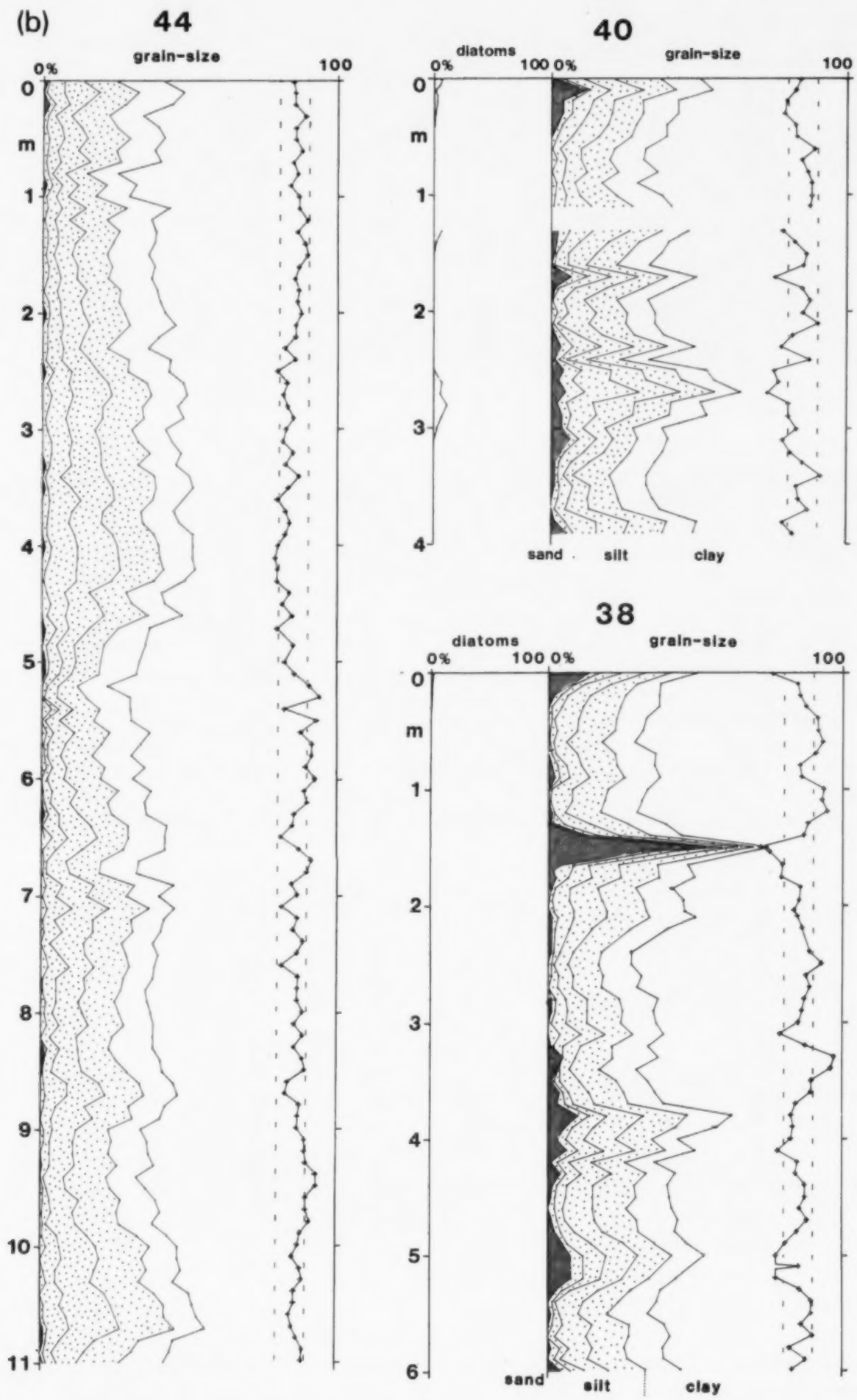
(b)
44
grain-size
0%
100
0
m
1
2
3
4
5
6
7
8
9
10
11
40
diatoms
0%
100
0%
grain-size
100
0
m
1
2
3
4
sand
silt
clay
38
diatoms
0%
100
0%
grain-size
100
0
m
1
2
3
4
5
6
sand
silt
clay

Fig. 11b.

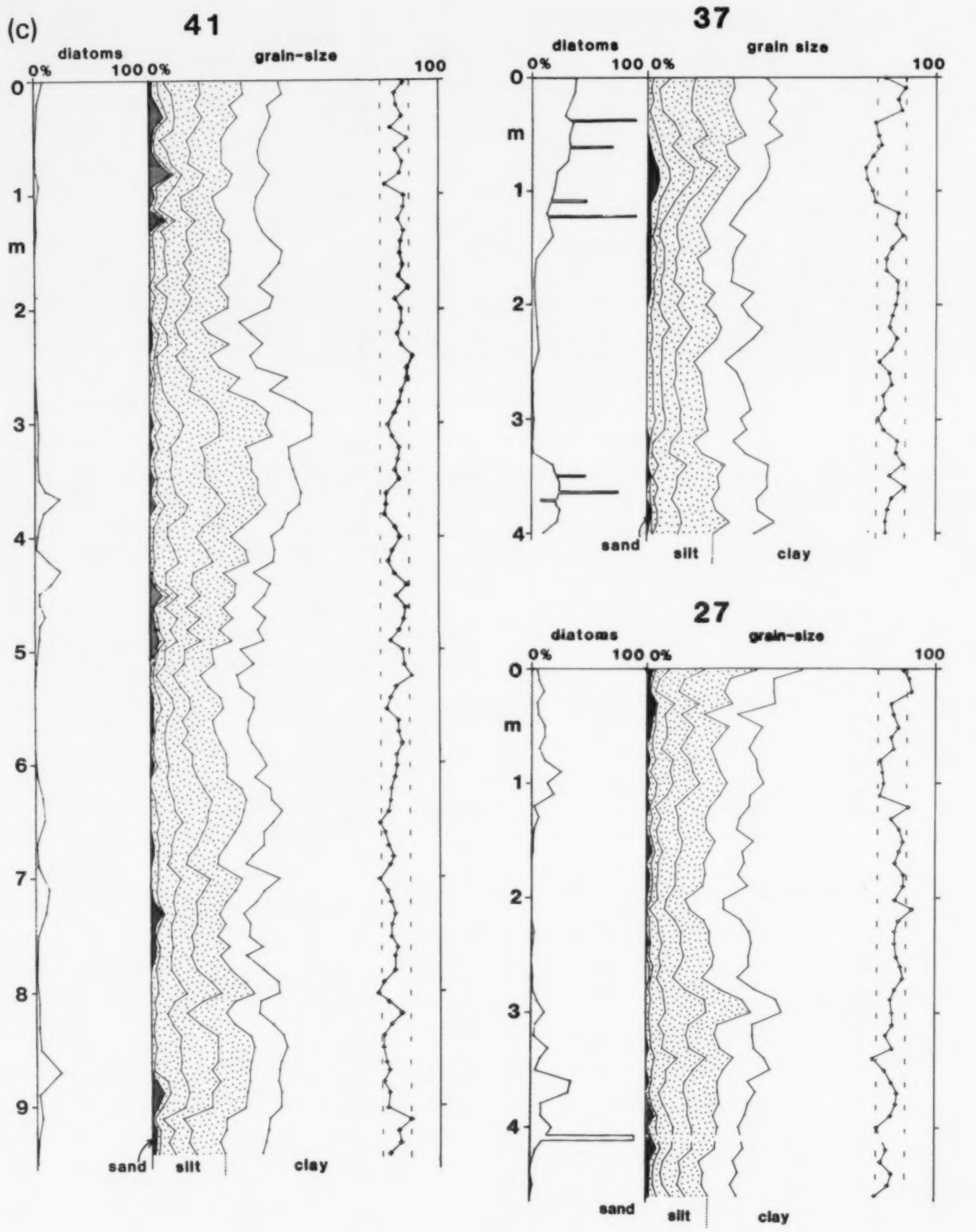

Fig. 11c.

water column. Seasonal sea ice may well have intervened between the eruption of ash and its final settling to the sea bed, but the Jane Basin cores offer no evidence for this. The occurrence of ash layers is random with respect to depth in core and silica content (Fig. 9) and it has not so far proved possible to correlate the ash layers from core to core.

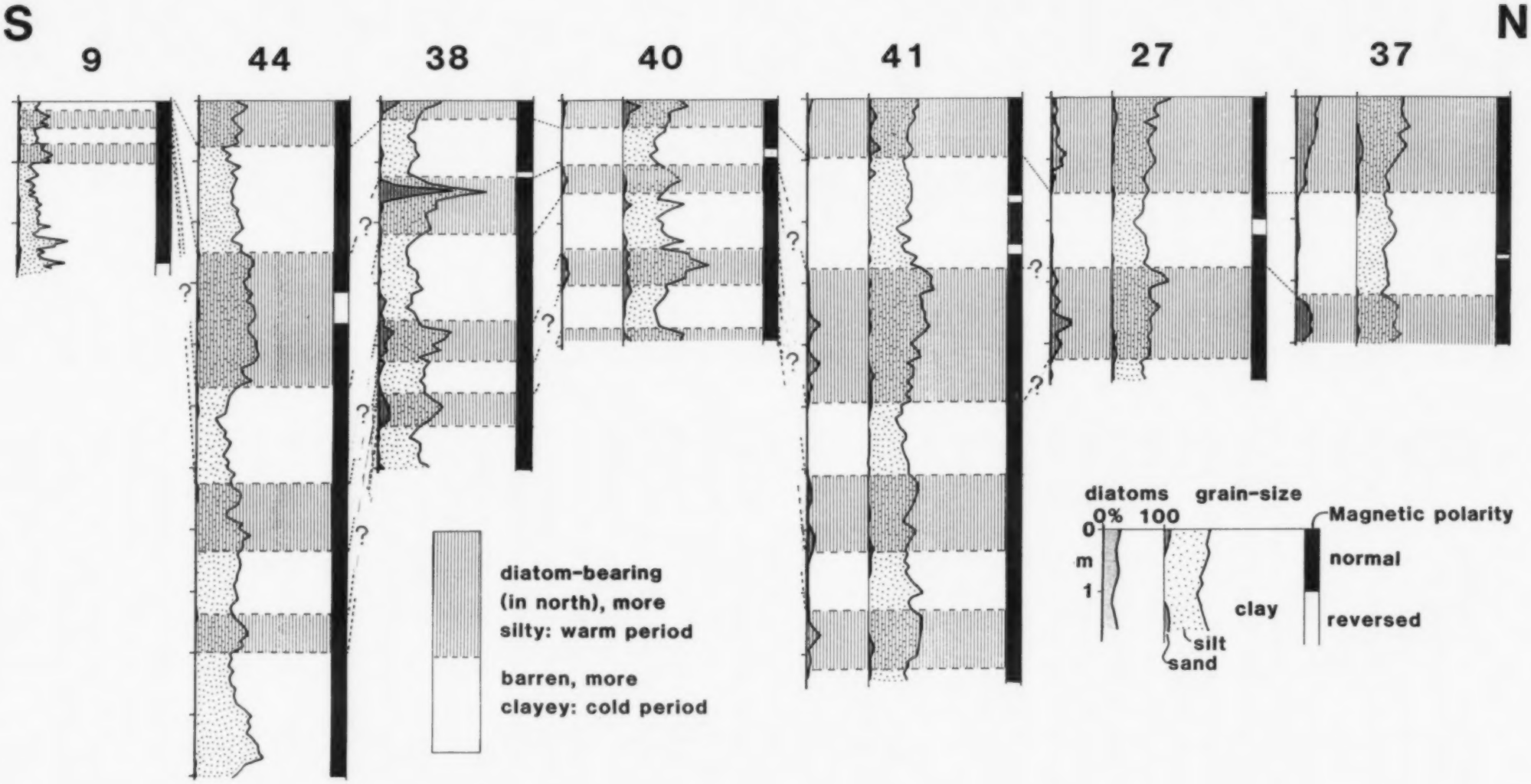

Fig. 12. Summary of grain size and silica data, with palaeomagnetic events, inferred warm/cold periods, and tentative correlation between sites.

Biogenic silica

In the surface sediments in Jane Basin the northward increase in the proportion of diatoms is related to the time extent of open water per year: 3 months at core 38, with less than 1% of diatoms at the surface, and 5–6 months at core 37, with nearly 40% (Figs. 8 and 9). The samples with fewest diatoms exhibit the poorest preservation. If there is open water for 3 months or less at a site, biogenic silica production is apparently not sufficient to survive dissolution in the water column and at the sea bed (Pokras, 1986; Burckle and Cirilli, 1987). Thus zero biogenic silica in sediments need not mean year-round sea ice cover. I interpret the barren intervals in the cores to reflect periods of increased sea-ice cover relative to today, in agreement with previous studies (Hays et al., 1976; DeFelice and Wise, 1981; Cooke and Hays, 1982). Cores 40, 41, 27 and 37 thus record evidence for several long term N–S (or NE–SW) movements of the summer sea-ice edge.

Bottom currents and the nepheloid layer

Evidence for a nepheloid layer in the Weddell Sea comes from Hollister and Elder (1969) who reported 'murky bottom water' at 26 deep-sea camera stations between 60° and 75°S and 25° and 55°W. None of the more recent oceanographic expeditions to this area has included nephelometer measurements. Sediment supply to any deep ocean basin involves a variety of mechanisms, but bottom nepheloid layers far from continental margin sources are largely maintained by resuspension of bottom sediments (McCave, 1986, and references therein). Thus in the northern Weddell Sea and Jane Basin, the size distribution of sediment in suspension is related much more closely to the strength of local currents than to the nature of sediment sources several hundred kilometres upstream. Resuspension of cohesive fine-grained sediments can be facilitated by the activities of epibenthic and burrowing organisms; resuspension events result from increased current velocity related to, for example, benthic storms (e.g. Spinrad and Zaneveld, 1982) or internal tides and waves (Dickson and McCave, 1986). Initial (upstream) sources for the Weddell Sea nepheloid layer include: (1) turbidity currents, (2) glacial meltwater and (3) pelagic input.

(1) Turbidity currents from the continental slope. Where grounded ice extends to the shelf edge, basal transport and bulldozing of sediment over the shelf edge will tend to over-steepen the upper slope, resulting in slumping and initiation of turbidity currents. Where the ice shelf is not grounded, offshore transport of sediment by shelf currents can occur locally. The southern and western Weddell Sea shelves are generally inaccessible because of pack ice, but studies in the Ross Sea, Pennell Coast and George V Coast by Dunbar et al. (1985) have documented winnowing in water depths down to 500 m with the removal of material finer than 3 ϕ (very fine sand); see also Anderson et al. (1980b). Fine-grained sediment may thus be delivered to the shelf edge and upper slope. Slope failure may occur during earthquakes or iceberg calving events (Powell, 1981; Eyles et al., 1985). As the turbidity flow wanes, material remaining in suspension can be entrained by bottom currents.

(2) Glacial meltwater carrying suspended sediment. This has been widely documented in the Arctic (review in Eyles et al., 1985) but is considered less important in the Antarctic where most of the ice is frozen to bedrock (Drewry, 1986). Drewry and Cooper (1981) demonstrated that the basal debris in an ice shelf may all melt out close to the grounding line, and noted that bottom currents may transport the fine fraction towards the open sea. The removal of fine particles in suspension was invoked by Orheim and Elverhoi (1981) to explain the coarse texture of shelf and upper slope deposits in the southern Weddell Sea. At the front of the Ronne Ice Shelf (at 3 sites near the shelf break, in 450 to 700 m water depth), Foldvik et al. (1985a,b) measured tidal currents of up to 30 cm/s and a mean NW flow of 8 cm/s; and Elverhoi and Roaldset (1983) found up to 2 g/m^3 of suspended matter in shelf waters off the Filchner Ice Shelf. It is possible therefore that silt and clay carried in suspension in Ice Shelf Water are added to the nepheloid layer in Weddell Sea Bottom Water. Future cruises are planned to investigate this mechanism further.

(3) Pelagic input from the sea surface. In the Antarctic, this is mainly biogenic silica and ice-

rafted material. Ice rafting is most important near the basin margin (see above); biogenic pelagic input occurs in open water only, being negligible beneath pack ice (Fischer et al., 1988).

It is probably reasonable to assume that a complete range of grain sizes (at least within the fine sand-silt-clay range) is available for transport within the bottom nepheloid layer in the northern Weddell Sea. Pelagic supply (ice-rafted debris and biogenic silica) and turbidites originating from ice fronts should each supply unsorted material. Without fluvial or wave reworking on the deep Antarctic continental shelf (Anderson et al., 1983) there is generally less sorting of sediment before it reaches the shelf edge than occurs at lower latitudes. Glacial–interglacial variations in supply are discussed below.

It has long been known that faster currents can carry larger sediment grains in suspension, and the relationships between flow power and sediment transport are reasonably well understood for steady flows and well-sorted non-cohesive sediments (e.g. review in Miller et al., 1977). There are however very few data relating to natural, unsteady flows and fine-grained, poorly-sorted, mixed terrigenous-biogenous cohesive sediments as found in the deep sea (McCave, 1984). Ledbetter and coworkers have used mean silt size to make inferences about present-day bottom current pathways and relative velocity changes in the Argentine Basin and Vema Channel (e.g. Ledbetter and Johnson, 1976; Ledbetter, 1979, 1984, 1986; Ledbetter and Ellwood, 1980; Blaeser and Ledbetter, 1982), but in the absence of direct current measurements, only qualitative inferences could be made. Anderson and Kurtz (1985) pointed out some of the shortcomings of using silt grain-size parameters to measure palaeospeed. For the texturally immature sediments in the Jane Basin area, the complete grain-size distribution should be considered, rather than a single parameter such as mean silt size.

Suspended sediment transport in the deep Weddell Sea is clockwise around the gyre. Assuming that all grain sizes are available, the maximum size transported and the proportion of larger grains in suspension will increase with bottom current strength. In addition, deposition of finer sediment is relatively suppressed under stronger bottom currents (McCave, 1985). The observed grain-size increase in surface sediment from the centre to the edge of the Weddell gyre (Table 3; Pudsey et al., 1988) is consistent with increasing current speed at the basin margin. Abundant fine sand and silt in some intervals of cores 38 and 40 (Fig. 11) reflects past changes in sorting and transport by bottom currents, discussed below.

Deposition

In detail, the bottom topography of the northern Weddell Sea and Jane Basin is quite complex, with areas where the deep-water pathway narrows and flow is constricted. To maintain constant volume transport, flow must speed up in these areas and slacken again downstream of them. Areas of slackening flow are where deposition from suspension will occur. In the northern Weddell Sea, deposition is lateral to (south of) the region of strongest flow; this is analogous to the Argentine Basin (Ewing et al., 1971) and to sediment drifts such as the Faro Drift (Stow et al., 1986) and the Hatton and Gardar Drifts (McCave and Tucholke, 1986).

An additional factor influencing deposition in this area may be biological productivity. The high seasonal phytoplankton production related to the receding ice edge (Smith and Nelson, 1986; Fischer et al., 1988) may enhance terrigenous deposition in the Jane Basin area, because at the end of the spring phytoplankton bloom much organic debris sinks in the form of marine snow which scavenges terrigenous grains from the nepheloid layer. Honjo (1982) has noted a similar phenomenon related to high coccolith productivity in the Panama Basin.

Glacial–interglacial variations

Time-scale

It has not been easy to date the Jane Basin and northern Weddell Sea cores with any precision. They contain no carbonate, so foraminiferal and nannofossil biostratigraphy are not available, and variations in oxygen isotope ratio cannot be used. One has to rely on siliceous biostratigraphy (where silica is present), on palaeomagnetism and on lithological correlation with other, better dated,

cores. The evidence that the sediments described here are late Quaternary in age is as follows:

(1) The 3.5 kHz profiles show thick, acoustically layered sequences in which the reflectors are parallel, without erosional unconformities or wedging-out of reflectors near the surface. There are also identifiable areas of bottom current scour, where hiatuses may be expected, but cores from these areas, such as 17 (Table 3) which contains winnowed sandy-gravelly lags, have not been used for detailed study.

(2) Diatoms, where present, belong to the *Thalassiosira lentiginosa* zone [Gersonde and Burckle, 1990; the *Coscinodiscus lentiginosus* Zone of McCollum (1975), Weaver and Gombos (1981) and Ciesielski (1983)]. This represents 0 to 0.6 Ma. A high-resolution diatom stratigraphy has been developed for the northern Jane Basin-central Scotia Sea area by Jordan and Pudsey (1992); these authors correlate the upper diatomaceous interval in cores 27 and 37 (and probably 41) with oxygen isotope stage 1, and the underlying barren and diatomaceous intervals with stages 2 and 3.

(3) In cores 27 and 37 the radiolarian *Cycladophora davisiana* exhibits downcore changes in abundance (Jordan and Pudsey, 1992) similar to those observed elsewhere in the Southern Ocean (Hays et al., 1976). The first subsurface abundance peak, correlated with the Last Glacial Maximum at 18 ka by Hays et al., occurs at 1.3 m in core 27 and 1.6 m in core 37: the base of the upper diatomaceous interval. Unfortunately the southern cores contain too few radiolarians for species counts to be made.

(4) Magnetic inclination measurements show that all cores are of normal polarity (high negative inclination), interpreted as Brunhes chron (O'Brien, 1989). Short intervals of low or positive inclination are found in all cores except 9 (Fig. 12). In core 9, of which only the Brunhes interval is discussed here, a reversal sequence extending down to the Olduvai event was measured (Pudsey et al., 1988). At ODP Site 697, near core 41, the Brunhes–Matuyama boundary was encountered at 30 mbsf and a reversed interval at 3–4.5 mbsf was interpreted as the Blake event (Shipboard Scientific Party, 1988b; O'Brien, 1989).

The data presented here are consistent with the conclusion reached by Pudsey et al. (1988) and Pudsey (1990) that diatomaceous sediments are deposited during warm stages and barren sediments during cold. If this is correct, then the reversed magnetic intervals (Fig. 12) may correspond to known events (Bleil and Gard, 1989) as follows: the event in core 44 may be the Blake event at 135 ka; the two events in core 41 may be the Lake Mungo at 30 ka and the Laschamp at about 40 ka; and the events in cores 38, 40, 27 and 37 either the Lake Mungo or the Laschamp. It is not yet certain whether warm stage 3 is reflected as a diatomaceous/silty interval in all cores or whether the second silty interval downcore is stage 5. Further high resolution magnetic inclination studies are in progress on some cores. It should be noted that even at high latitudes where magnetic inclination values are high and reversals are usually well-defined, not all brief reversed events are necessarily found in all cores (Bleil and Gard, 1989). In a core from the eastern Weddell Sea (slope terrace at 69°S, 6°W) Mackensen et al. (1989) also found that intervals of increased silica, in the form of radiolarians, correspond to oxygen isotope stages 1, 5 and 7, i.e. interglacial periods. Mackensen et al. found no reversed magnetic events in their continuous section representing 0–250 ka.

Glacial–interglacial variations in sedimentation

In each of the cores 40, 41, 27 and 37 the diatomaceous intervals, interpreted to correspond to interglacial periods, contain more silt and the barren (glacial) intervals more clay. The more southerly cores, which contain only a trace of diatoms at the surface, show a similar silty–clayey alternation which I suggest also corresponds to interglacial–glacial cycles (Fig. 12). Reasons for the occurrence of siltier sediments during warmer periods may include climatically controlled changes in: (1) sediment supply, (2) transport and/or (3) deposition in the Jane Basin area.

(1) *Sediment supply*: processes dominant on the Antarctic shelf and slope have undoubtedly changed greatly between glacial and interglacial periods, but the changes to 'upstream' supply to the nepheloid layer are not necessarily directly reflected in distal, low-energy environments. With

the advance of grounded ice to the shelf edge at glacial maximum (Stuiver et al., 1981) abundant unsorted sediment would have been supplied to the upper slope, and more (and larger?) turbidity currents been initiated. The shelf winnowing and supply of fine material to the shelf edge, described above, would not have occurred; similarly Ice Shelf Water could not have formed by the same processes as at present (see Introduction). All glacial debris therefore was supplied along a line source near the shelf break. A higher proportion of coarse debris, up to boulder size, would have reached the slope during glacial maximum; though clearly material coarser than sand size cannot be incorporated into the nepheloid layer. If Weddell Gyre circulation had been maintained during glacial maximum, i.e. bottom currents had remained the same, one would expect the same range of grain sizes to reach the northern Weddell Sea (silt and clay in the nepheloid layer, with very fine sand at the gyre margin). The volume of sediment supply might increase since less would be deposited on the shelf.

A minor contribution of sediment from ice-rafting may be discerned in cores 9, 41, 27 and 37 (see above). The proportion of poorly-sorted sand does not vary systematically down these cores.

(2) *Transport*: the presence of considerable amounts of clay throughout the cores at virtually all sites (except core 17, near Mooring II in the scour valley) implies that the northern Weddell Sea and Jane Basin have been a generally low-energy environment during the late Quaternary. Over a wider area, Ledbetter and Ciesielski (1986) found hiatuses to be rare in Brunhes age sediment in the South Atlantic sector of the Southern Ocean, consistent with bottom currents being insufficiently strong to cause erosion. The observed increase in clay content from each core top studied here to the underlying interval is unlikely to result from a change in supply (see above): if anything, *less* fine material should be supplied during glacial maximum. It is more likely that the competence of the transporting current decreased and that less silt could be carried in suspension and one may infer from the data in Figs. 11 and 12 that there have been periodic velocity changes in AABW flow in the Jane Basin area. The core top (Holocene: missing in core 9) represents a relative velocity maximum. The finer-grained interval underlying the silty core-top reflects slower bottom currents. In each of the six northern cores this finer-grained interval has a sand:silt:clay ratio of about 0:20:80, suggesting a rather uniform and low velocity over the whole area during the time represented. In fact this grain-size ratio is close to the values for surface sediment in cores 6 and 7 (Pudsey et al., 1988), near mooring IV. This implies that during the deposition of the fine-grained interval, current velocities near the gyre margin were comparable to present-day velocity near the centre, i.e. 1 cm/s or less (Table 3). Below this, grain size increases again to values comparable to the core top (in core 38, slightly coarser than the core top), suggesting currents similar to the present; and so on to the base of each core.

(3) *Deposition*: local depositional processes are unlikely to act to change sediment texture on a glacial-interglacial time scale, The shape of the basin, i.e. location of narrow areas and scour valleys, remains constant. A change in phytoplankton productivity may alter the total amount of material scavenged from the water column by marine snow, but not its size distribution.

The above considerations suggest that in the northern Weddell Sea and Jane Basin, bottom water flow was much reduced at glacial maximum relative to present interglacial conditions: flow speed near the margin of the Weddell Gyre may have been as little as one-tenth of present values. Climate-related changes in deep circulation and sediment supply and deposition are outlined in Fig. 13. One implication is that more fine sand should have been deposited in proximal areas (base of the continental slope) at glacial maximum, rather than being entrained in the nepheloid layer. However the inaccessibility of the southern and western Weddell Sea margins make it difficult to test this aspect of the model.

Regional implications

Evidence has been presented here for stronger deep circulation during interglacials, near the major source of AABW in the Weddell Sea. A number of studies further away from the AABW source, notably near the Vema Channel in the

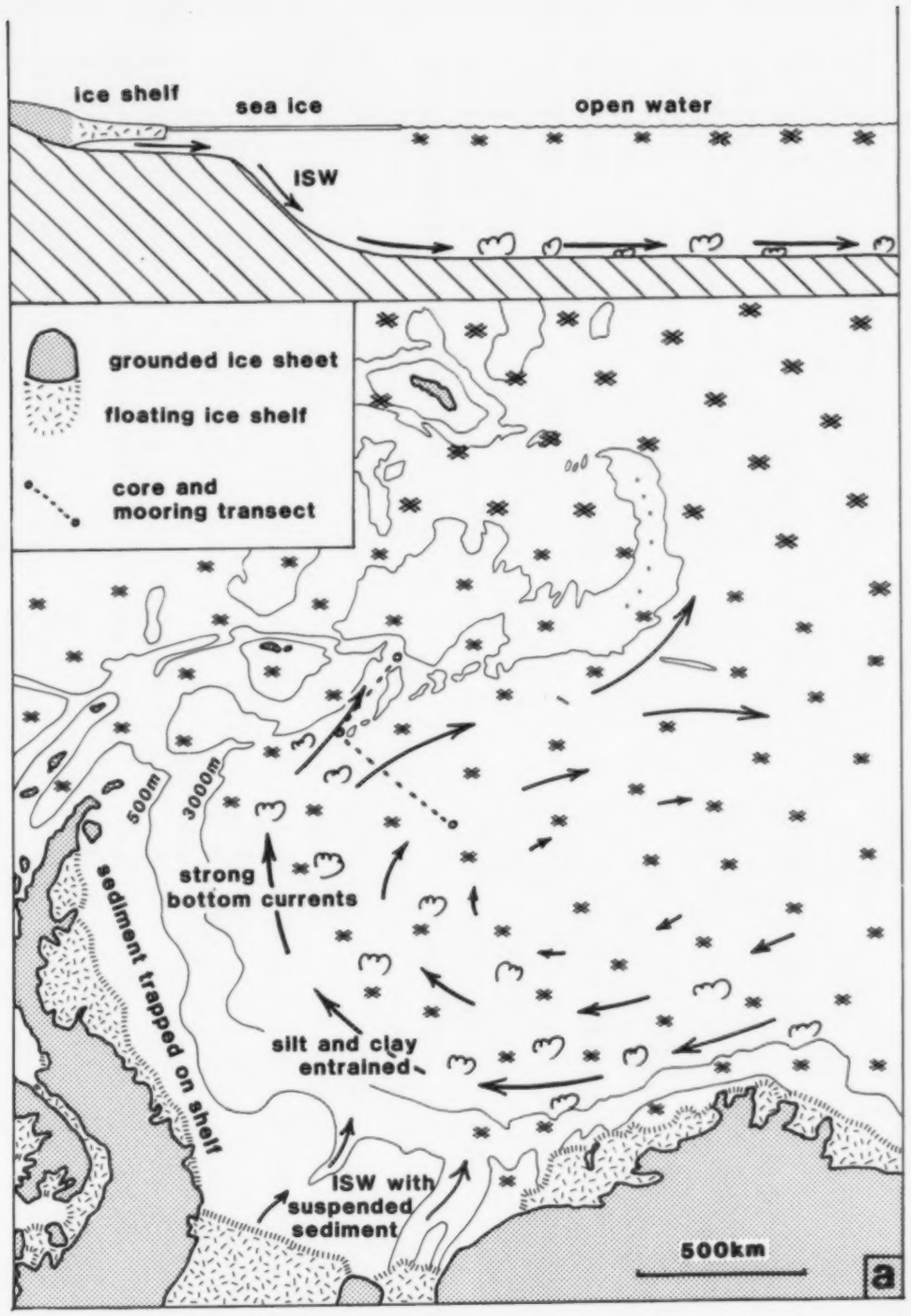

Fig. 13. (a) Deep-water circulation and sediment sources in the Weddell Sea at the present day (i.e. interglacial conditions). Within the grounded ice sheet, rock outcrops are not shown separately. The cross-section, not strictly to scale, is approximately S–N from the Ronne and Filchner Ice Shelves to Jane Basin. Seasonal diatom productivity in the area of the core/mooring transect may enhance deposition from the nepheloid layer (see text). (b) Inferred deep-water circulation and sediment sources in the Weddell Sea during glacial maximum. The ice sheet is shown grounded to the shelf edge (Stuiver et al., 1981) with a small ice cap on the South Orkney microcontinent (Sugden and Clapperton, 1977).

Argentine Basin, have also identified downcore grain-size changes in terrigenous hemipelagic sediment; but even those studies incorporating the best stratigraphic control (Ledbetter, 1984; Johnson et al., 1984) have not found a straightforward relationship between current strength and glacial/interglacial cyclicity in the Late Pleistocene. However, the deep circulation in the Argentine Basin includes water masses derived from North Atlantic Deep Water and Circumpolar Deep Water, as well as AABW (Reid et al., 1977; Georgi, 1981). In both north and south polar regions, mechanisms of deep-water production may have changed significantly between glacial and interglacial times, both in terms of the amount of water produced and of its physical and chemical characteristics (review in Corliss et al., 1986). In areas where two or more water masses from distant sources mix, one should not necessarily expect a simple relationship between deep circulation and climate. It is important to understand the sediments in the main areas of deep-water formation before attempting ocean-wide climatic interpretations.

Acknowledgements

I thank my colleagues on *Discovery* cruises 154 and 172 and *John Biscoe* cruise 10/3 for assistance in obtaining the cores, CTD and current meter data. Simon Robinson lent me a magnetic susceptibility meter and Paul O'Brien kindly made the palaeomagnetic data available prior to publication. The paper benefitted by constructive comments from John Anderson, Peter Barker, David Drewry, Ted Foster, Nick McCave and two anonymous reviewers. Margaret Riley typed the manuscript.

References

Amos, A.F., Gordon, A.L. and Schneider, E.D., 1971. Water masses and circulation patterns in the region of the Blake-Bahama Outer Ridge. Deep-Sea Res., 18: 145–165.

Anderson, J.B. and Kurtz, D.D., 1985. The use of silt grain-size parameters as a paleovelocity gauge: a critical review and case study. Geo-Mar. Lett., 5: 55–59.

Anderson, J.B., Domack, E.W. and Kurtz, D.D., 1980a. Observations of sediment-laden icebergs in Antarctic waters: implications to glacial erosion and transport. J. Glaciol., 25: 387–396.

Anderson, J.B., Kurtz, D.D., Domack, E.W. and Balshaw, K.M., 1980b. Glacial and glacial marine sediments of the Antarctic continental shelf. J. Geol., 88: 399–414.

Anderson, J.B., Brake, C., Domack, E., Myers, N. and R. Wright, 1983. Development of a polar glacial-marine sedimentation model from Antarctic Quaternary deposits and glaciological information. In: B.F. Molnia (Editor), Glacial-marine Sedimentation. Plenum. New York, pp. 233–264.

Barrett, P.J., Pyne, A.R. and Ward, B.L., 1983. Modern sedimentation in McMurdo Sound, Antarctica. In: R.L. Oliver, P.R. James and J.B. Jago (Editors), Antarctic Earth Science. Aust. Acad. Sci., Canberra, pp. 550–554.

Blaeser, C.R. and Ledbetter, M.T., 1982. Deep-sea bottom currents differentiated from texture of underlying sediment. J. Sediment Petrol., 52: 755–768.

Bleil, U. and Gard, G., 1989. Chronology and correlation of Quaternary magnetostratigraphy and nannofossil biostratigraphy in Norwegian–Greenland Sea sediments. Geol. Rundsch., 78: 1173–1187.

Boulton, G.S., 1978. Boulder shapes and grain-size distributions of debris as indicators of transport paths through a glacier and till genesis. Sedimentology, 25: 773–799.

Burckle, L.H. and Cirilli, J., 1987. Origin of diatom ooze belt in the Southern Ocean: implications for Late Quaternary paleoceanography. Micropaleontology, 33: 82–86.

Calvert, S.E., 1966. Accumulation of diatomaceous silica in the sediments of the Gulf of California. Geol. Soc. Am. Bull., 77: 569–596.

Carmack, E.C., 1974. A quantitative characterisation of water masses in the Weddell Sea during summer. Deep-Sea Res., 21: 431–442.

Carmack, E.C. and Foster, T.D., 1975. On the flow of water out of the Weddell Sea. Deep-Sea Res., 22: 711–724.

Ciesielski, P.F., 1983. The Neogene and Quaternary diatom biostratigraphy of subantarctic sediments, Deep Sea Drilling Project Leg 71. Init. Rep. DSDP, 71: 635–665.

Cooke, D.W. and Hays, J.D., 1982. Estimates of Antarctic Ocean seasonal sea-ice cover during glacial intervals. In: C. Craddock (Editor), Antarctic Geoscience. Univ. Wis. Press, pp. 1017–1025.

Corliss, B.H., Martinson, D.G. and Keffer, T., 1986. Late Quaternary deep-ocean circulation. Geol. Soc. Am. Bull., 97: 1106–1121.

Damuth, J.E., 1980. Use of high frequency (3.5–12 kHz) echograms in the study of near-bottom sedimentation processes in the deep-sea: a review. Mar. Geol., 38: 51–75.

Deacon, G.E.R., 1979. The Weddell Gyre. Deep-Sea Res., 26: 981–995.

DeFelice, D.R. and Wise, S.W., Jr., 1981. Surface lithofacies, biofacies and diatom diversity patterns as models for delineation of climatic change in the southeast Atlantic Ocean. Mar. Micropalaeontol., 6: 29–70.

DeMaster, D.J., 1981. The supply and accumulation of silica in the marine environment. Geochim. Cosmochim. Acta, 45: 1715–1732.

Dickson, R.R. and McCave, I.N., 1986. Nepheloid layers on the continental slope west of Porcupine Bank. Deep-Sea Res., 33: 791–818.

Drewry, D.J., 1986. Glacial Geologic Processes. Edward Arnold, London, 276 pp.

Drewry, D.J. and Cooper, A.P.R., 1981. Processes and models

of Antarctic glaciomarine sedimentation. Ann. Glaciol., 2: 117–122.

Dunbar, R.B., Anderson, J.B., Domack, E.W. and Jacobs, S.S., 1985. Oceanographic influences on sedimentation along the Antarctic continental shelf. In: S.S. Jacobs (Editor), Oceanology of the Antarctic Continental Shelf. Antarct. Res. Ser., 43: 291–312.

Elverhøi, A. and Roaldset, E., 1983. Glaciomarine sediments and suspended particulate matter, Weddell Sea Shelf. Antarctica. Polar Res., 1: 1–21.

Ewing, M., Eittreim, S.L., Ewing, J.I. and Le Pichon, X., 1971. Sediment transport and distribution in the Argentine Basin, 3. Nepheloid layer and processes of sedimentation. Phys. Chem. Earth, 8: 51–77.

Eyles, C.H., Eyles, N. and Miall, A.D., 1985. Models of glaciomarine sedimentation and their application to the interpretation of ancient glacial sequences. Palaeogeogr., Palaeoclimatol., Palaeoecol., 51: 15–84.

Fischer, G., Fütterer, D., Gersonde, R., Honjo, S., Ostermann, D. and Wefer, G., 1988. Seasonal variability of particle flux in the Weddell Sea and its relation to ice cover. Nature, 335: 426–428.

Foldvik, A. and Gammelsrød, T., 1988. Notes on Southern Ocean hydrography, sea-ice and bottom water formation. Palaeogeogr., Palaeoclimatol., Palaeoecol., 67: 3–17.

Foldvik, A., Gammelsrød, T., Slotsvik, N. and Tørresen, T., 1985a. Oceanographic conditions on the Weddell Sea Shelf during the German Antarctic Expedition 1979/80. Polar Res., 3: 209–226.

Foldvik, A., Gammelsrød, T. and Tørresen, T., 1985b. Physical oceanography studies in the Weddell Sea during the Norwegian Antarctic Research Expedition 1978/79. Polar Res., 3: 195–207.

Foster, T.D. and Middleton, J.H., 1979. Variability in the bottom water of the Weddell Sea. Deep-Sea Res., 26: 743–762.

Foster, T.D., Foldvik, A. and Middleton, J.H., 1987. Mixing and bottom water formation in the shelf break region of the southern Weddell Sea. Deep-Sea Res., 34: 1771–1794.

Georgi, D.T., 1981. Circulation of bottom waters in the southwestern South Atlantic. Deep-Sea Res., 28: 959–979.

Gersonde, R. and Burckle, L.H., 1990. Neogene diatom biostratigraphy of ODP Leg 113: Weddell Sea (Antarctic Ocean). Proc. ODP, Sci. Results, 113: 761–789.

Gill, A.E., 1973. Circulation and bottom water production in the Weddell Sea. Deep-Sea Res., 20: 111–140.

Goodell, H.G., 1973. The sediments. In: H.G. Goodell et al. (Editors), Marine Sediments of the Southern Oceans. Am. Geogr. Soc. Folio 17.

Gordon, A.L., 1966. Potential temperature, oxygen and circulation of bottom water in the Southern Ocean. Deep-Sea Res., 13: 1125–1138.

Gordon, A.L., 1972. Varieties and variability of Antarctic Bottom Water. Colloq. Int. CNRS, Paris, 215: 33–47.

Hays, J.D., Lozano, J.A., Shackleton, N.J. and Irving, G., 1976. Reconstruction of the Atlantic and western Indian Ocean sectors of the 18,000 B.P. Antarctic Ocean. In: R.M. Cline and J.D. Hays (Editors), Investigation of Late Quaternary Paleoceanography and Paleoclimatology. Geol. Soc. Am. Mem. 145: 337–372.

Hollister, C.D. and R.B. Elder, R.B., 1969. Contour currents in the Weddell Sea. Deep-Sea Res, 16: 99–101.

Honjo, S., 1982. Seasonality and interaction of biogenic and lithogenic particulate flux at the Panama Basin. Science, 218: 883–884.

Hurd, D.C., 1973. Interactions of biogenic opal, sediment, and seawater in the central equatorial Pacific. Geochim. Cosmochim. Acta, 37: 2257–2287.

Johnson, D.A., Ledbetter, M.T., Tappa, E. and Thunell, R., 1984. Late Tertiary/Quaternary magnetostratigraphy and biostratigraphy of Vema Channel sediments. Mar. Geol., 58: 89–100.

Jordan, R.W. and Pudsey, C.J., 1992. High-resolution diatom stratigraphy of Quaternary sediments from the Scotia Sea. Mar. Micropaleontol., 19: 201–237.

Jordan, R.W., Priddle, J., Pudsey, C.J., Barker, P.F. and Whitehouse, M.J., 1991. Unusual diatom layers in Upper Pleistocene sediments from the northern Weddell Sea. Deep-Sea Res., 38: 829–843.

King, E.C. and Barker, P.F., 1988. The margins of the South Orkney Microcontinent. J. Geol. Soc., 145: 317–331.

Ledbetter, M.T., 1979. Fluctuations of Antarctic Bottom Water velocity in the Vema Channel during the last 160,000 years. Mar. Geol., 33: 71–89.

Ledbetter, M.T., 1984. Bottom-current speed in the Vema Channel during the late Quaternary based on particle-size analysis. Mar. Geol., 58: 137–149.

Ledbetter, M.T., 1986. Bottom-current pathways in the Argentine Basin revealed by mean silt particle size. Nature, 321: 423–425.

Ledbetter, M.T. and Ciesielski, P.F., 1986. Post-Miocene disconformities and paleoceanography in the Atlantic sector of the Southern Ocean. Palaeogeogr., Palaeoclimatol., Palaeoecol., 52: 185–214.

Ledbetter, M.T. and Ellwood, B.B., 1980. Spatial and temporal changes in bottom-water velocity and direction from analysis of particle size and alignment in deep-sea sediment. Mar. Geol., 38: 245–261.

Ledbetter, M.T. and Johnson, D.A., 1976. Increased transport of Antarctic Bottom Water in the Vema Channel during the last ice age. Science, 194: 837–839.

Le Pichon, X., Eittreim, S.L. and Ludwig, W.J., 1971. Sediment transport and distribution in the Argentine Basin. 1. Antarctic Bottom Current passage through the Falkland Fracture Zone. Phys. Chem. Earth, 8: 3–28.

Limbert, D.W.S., Morrison, S.J., Sear, C.B., Wadhams, P., Rowe, M.A. and Crane, D.R., 1989. Pack-ice motion in the Weddell Sea in relation to weather systems and determination of a Weddell Sea sea-ice budget. Ann. Glaciol., 12: 104–112.

Mackensen, A., Grobe, H., Hubberten, H.-W., Spiess, V. and Fütterer, D., 1989. Stable isotope stratigraphy from the Antarctic continental margin during the last one million years. Mar. Geol., 87: 315–321.

McCave, I.N., 1984. Erosion, transport and deposition of fine-grained marine sediments. In: D.A.V. Stow and D.J.W. Piper (Editors), Fine-grained Sediments: Deep Water Processes and Facies. Spec. Publ. Geol. Soc. London, 15: 35–69.

McCave, I.N., 1985. Sedimentology and stratigraphy of box cores from the HEBBLE site on the Nova Scotian continental rise. Mar. Geol. 66: 59–89.

McCave, I.N., 1986. Local and global aspects of the bottom nepheloid layers in the world ocean. Neth. J. Sea Res., 20: 167–181.

McCave, I.N. and Tucholke, B.E., 1986. Deep current-controlled sedimentation in the western North Atlantic. In: P.R. Vogt and B.E. Tucholke (Editors), The Geology of North America, Vol. M, The Western North Atlantic Region. Geol. Soc. Am., pp. 451–468.

McCollum, D.W., 1975. Diatom stratigraphy of the Southern Ocean. Init. Rep., DSDP 28: 515–571.

Miller, M.C., McCave, I.N. and Komar, P.D., 1977. Threshold of sediment motion under undirectional currents. Sedimentology, 24: 507–527.

Mosby, H., 1934. The waters of the Atlantic Antarctic Ocean, Sci. Results Norw. Antarct. Exped. 1927–1928, 1(11): 1–131.

Nowlin, W.D., Jr. and Klinck, J.M., 1986. The physics of the Antarctic Circumpolar Current. Rev. Geophys., 24: 469–491.

O'Brien, P.D., 1989. The magnetostratigraphy of marine sediments from Jane Basin, southeast of the South Orkney Microcontinent, Antarctica. Ph.D. Thesis, Univ. Southampton, 300 pp. (Unpubl.)

Orheim, O. and Elverhøi, A., 1981. Model for submarine glacial deposition. Ann. Glaciol., 2: 123–128.

Pokras, E.M., 1986. Preservation of fossil diatoms in Atlantic sediment cores: control by supply rate. Deep-Sea Res., 33: 893–902.

Powell, R.D., 1981. A model for sedimentation by tidewater glaciers. Ann. Glaciol., 2: 129–134.

Pudsey, C.J., 1990. Grain-size and diatom content of hemipelagic sediments at Site 697, ODP Leg 113: a record of Plio-Pleistocene climate. Proc. ODP, Sci. Results, 113: 111–120.

Pudsey, C.J., in press. Calibration of a point-counting technique for estimation of biogenic silica in marine sediments. J. Sediment. Petrol., submitted.

Pudsey, C.J., Barker, P.F. and Hamilton, N., 1988. Weddell Sea abyssal sediments: a record of Antarctic Bottom Water flow. Mar. Geol., 81: 289–314.

Reid, J.L., Nowlin, Jr., W.D. and Patzert, W.C., 1977. On the characteristics and circulation of the southwest Atlantic Ocean. J. Phys. Oceanogr., 7: 62–91.

Robinson, S.G., 1990. Applications for whole-core magnetic susceptibility measurements of deep-sea sediments: ODP Leg 115 results. Proc. ODP, Sci. Results, 115: 737–771.

Saunders, P.M. and Cherriman, J.W., 1983. Abyssal temperature measurements with Aanderaa current meters. Deep-Sea Res., 30, 663–667.

Sea Ice Climatic Atlas, 1985. Vol. 1, Antarctic, Naval Oceanography Command, Asheville, North Carolina.

Shipboard Scientific Party, 1988a. Explanatory Notes. Proc. ODP, Init. Rep., 113: 13–32.

Shipboard Scientific Party, 1988b. Site 697. Proc. ODP, Init. Rep., 113: 705–774.

Slatt, R.M. and Eyles, N., 1981. Petrology of glacial sands: implications for the origin and mechanical durability of lithic fragments. Sedimentology, 28: 171–183.

Smith, W.O., Jr. and Nelson, D.M., 1986. Importance of ice edge phytoplankton production in the Southern Ocean. BioScience, 36: 251–257.

Spinrad, R. and Zaneveld, J.R.V., 1982. An analysis of the optical features of the near-bottom and bottom nepheloid layers in the area of the Scotian Rise. J. Geophys. Res., 87: 9553–9561.

Stow, D.A.V., Faugères, J.-C. and Gonthier, E., 1986. Facies distribution and textural variation in Faro Drift contourites: velocity fluctuation and drift growth. Mar. Geol., 72: 71–100.

Stuiver, M., Denton, G.H., Hughes, T.J. and Fastook, J.L., 1981. History of the marine ice sheet in West Antarctica during the last glaciation: a working hypothesis. In: G.H. Denton and T.J. Hughes (Editors), The Last Great Ice Sheets. Wiley, New York, pp. 319–436.

Sugden, D.E. and Clapperton, C.M., 1977. Maximum ice extent on island groups in the Scotia Sea, Antarctica. Quat. Res., 7: 268–282.

Swithinbank, C., McClain, P. and Little, P., 1977. Drift tracks of Antarctic icebergs. Polar Record, 18: 445–501.

Toole, J.M., 1981. Sea ice, winter convection, and the temperature minimum layer in the Southern Ocean. J. Geophys. Res., 86: 8037–8047.

Tucholke, B.E., Wright, W.R. and Hollister, C.D., 1973. Abyssal circulation over the Greater Antilles Outer Ridge. Deep-Sea Res., 20: 973–975.

Wadhams, P., Sear, C.B., Crane, D.R., Rowe, M.A., Morrison, S.J. and Limbert, D.W.S. 1989. Basin-scale ice motion and deformation in the Weddell Sea during winter. Ann. Glaciol., 12: 178–186.

Weaver, F.M. and Gombos, A.M., 1981. Southern high-latitude diatom biostratigraphy. Soc. Econ. Paleontol. Mineral., Spec. Publ., 32: 445–470.

Wright, W.R., 1970. Northward transport of Antarctic Bottom Water in the western Atlantic Ocean. Deep-Sea Res., 17: 367–371.

Marine Geology, 107 (1992) 35–50
Elsevier Science Publishers B.V., Amsterdam

Contemporary sedimentary processes in the Monterey Canyon–fan system

Cecilia M. McHugh[a,b], William B.F. Ryan[a,b] and Barbara Hecker[b]

[a]*Department of Geological Sciences of Columbia University, Palisades, NY 10946, USA*
[b]*Lamont-Doherty Geological Observatory of Columbia University, Palisades, NY 10964, USA*

(Received August 8, 1991; revision accepted January, 9, 1991)

ABSTRACT

McHugh, C.M., Ryan, W.B.F. and Hecker, B., 1992. Contemporary sedimentary processes in the Monterey Canyon–fan system. *Mar. Geol.*, 107: 35–50.

A study of the Monterey Canyon and fan was conducted to investigate contemporary sedimentary activity using a camera sled, *Alvin* dives and Sea-Beam bathymetry. Physical characteristics and plan view morphology of the walls, terraces, thalweg floor and levees of the Monterey Canyon and fan, as well as the gullied and non-gullied regions of the adjacent continental slope have been studied. The canyon floor and fan valley thalweg channel from 2900 to 3500 m exhibited properties indicative of moderate to low energy conditions (weak currents, smoothed sea-bed, deposits of disintegrated kelp, bioturbated mud substrate, fecal pellets, absence of scour). Chemosynthetic communities consisting of clams and a pogonophoran, were found in the fan valley from 3000 to 3600 m. Local areas of rockfalls and slumps from the canyon and fan valley walls were not fresh (sedimented, abundantly colonized by benthic biota). Terraces and levee crests were mud-draped and bedrock exposures on canyon walls were encrusted by benthic organisms. Freshest disturbances were found in gullies on the adjacent continental slope where bedrock was scoured clean of sediment and loose debris. A major submarine slide detached from escarpments on the lower slope, and extends across the fan. The slide surface was mud-draped, hummocky, and contained bedforms with wavelengths up to 150 m and up to 10 m relief. The survey was conducted shortly before the Loma Prieta earthquake (October 17, 1989) that caused substantial ground motion in on-shore regions of Monterey Bay. Any substantial sub-sea disturbances generated by the ensuing earthquake should be discernable from the pre-earthquake state by comparison with the deep-sea photographs and observations.

Introduction

The extent of contemporary activity within submarine canyons and deep-sea fan systems is an area of extensive research for submarine geology. The significance of currents in canyon development has been studied by many investigators (Daly, 1936; Mathews and Shepard, 1962; Heezen et al., 1964; Shepard et al., 1979). Some of these investigations were carried out on canyons that head the coast and are located on tectonically active margins such as California (Shepard et al., 1979). Submarine canyons that indent the shelf but do not extend deep into the coast have been studied on the western North Atlantic passive margin (Shepard et al., 1979). The Congo Canyon and the Fraser Seavalley whose heads penetrate deeply into their associated coastal margins, have also been studied (Mathews and Shepard, 1962; Heezen et al., 1964; Shepard et al., 1979). Evidence that seismic events such as the 1929 Grand Banks earthquake may initiate large scale turbidity currents and submarine mass-wasting were provided by Heezen and Ewing (1952), Piper et al. (1985) and Hughes-Clark (1988). Monterey Canyon is a suitable location to study contemporary erosional depositional processes because it has access to a large supply of sediment at its head. The head of Monterey Canyon is at the water front in Monterey Bay at the mouth of Elkhorn Slough. Sediment is

Correspondence to: C.M. McHugh, Department of Geological Sciences of Columbia University, Palisades, NY 10946, USA.

0025-3227/92/$05.00

transported to the head of the canyon by rivers that drain the coastal highlands, longshore wave drift and the California current system, tidally driven flows, and indirectly by the ground motion of earthquakes (Wolf, 1969; Brownlie and Taylor, 1981; Gorsline and Teng, 1989; Atwater, 1989). In the shelf and upper slope portion of the Monterey Canyon–fan system, the principal features are its tributary canyons (Fig. 1). Presently, the most important tributaries are Carmel and Soquel Canyons (Greene et al., 1988).

Recent observations raise the possibility that there are flushing episodes in the submarine canyon system coincident with tidal surges and flooding of rivers. The head of the Monterey Canyon periodically fills with sediment and the fill disappears from time to time in coincidence with seasonal floods (Gorsline and Teng, 1989). Significant sediment failure and mass-wasting is occurring in the head of the canyon and in the walls of the lower canyon (Greene et al., 1988, 1989; Eittreim et al., 1989). In this area, earthquake shocks of

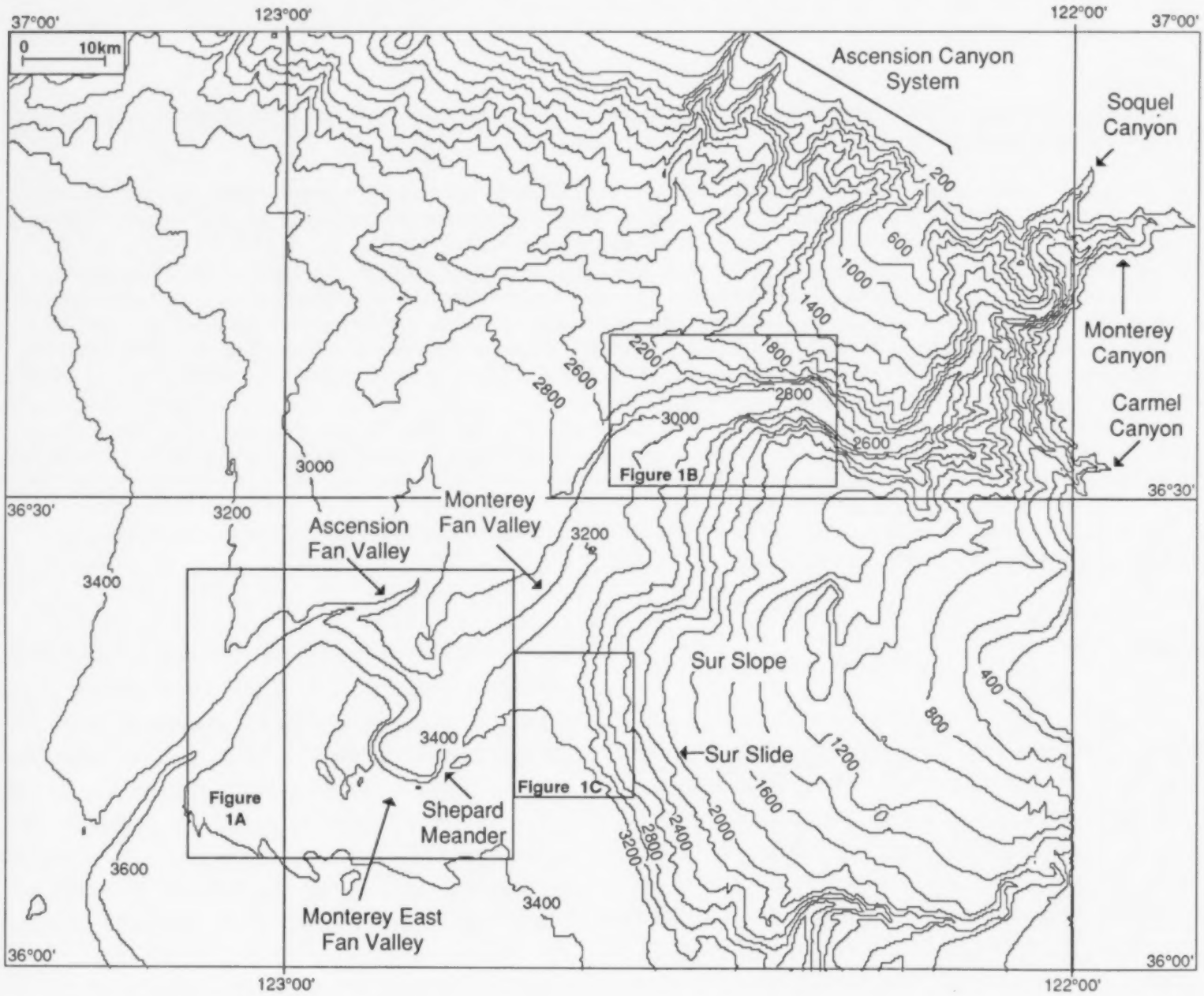

Fig. 1. Seabeam bathymetry (NOAA, 1989) showing location of surveyed regions, major canyon–fan valley systems and Sur slope and slide. Contour interval every 200 m. (A) Shepard meander and Monterey, Monterey East and Ascension Fan Valleys study area. Camera tow path, photograph, cold seep, *Alvin* dive release point and acoustic profile locations shown on the map. Contour interval every 50 m. (B) Lower Monterey Canyon–upper fan valley study area. Camera tow path, photograph and cold seep locations shown on the map. Contour interval every 50 m. (C) Surveyed region in Sur slope. Camera tow path, photograph, acoustic profile (C–C′) and camera depth profile (D–D′) locations shown on map. Contour interval every 100 m.

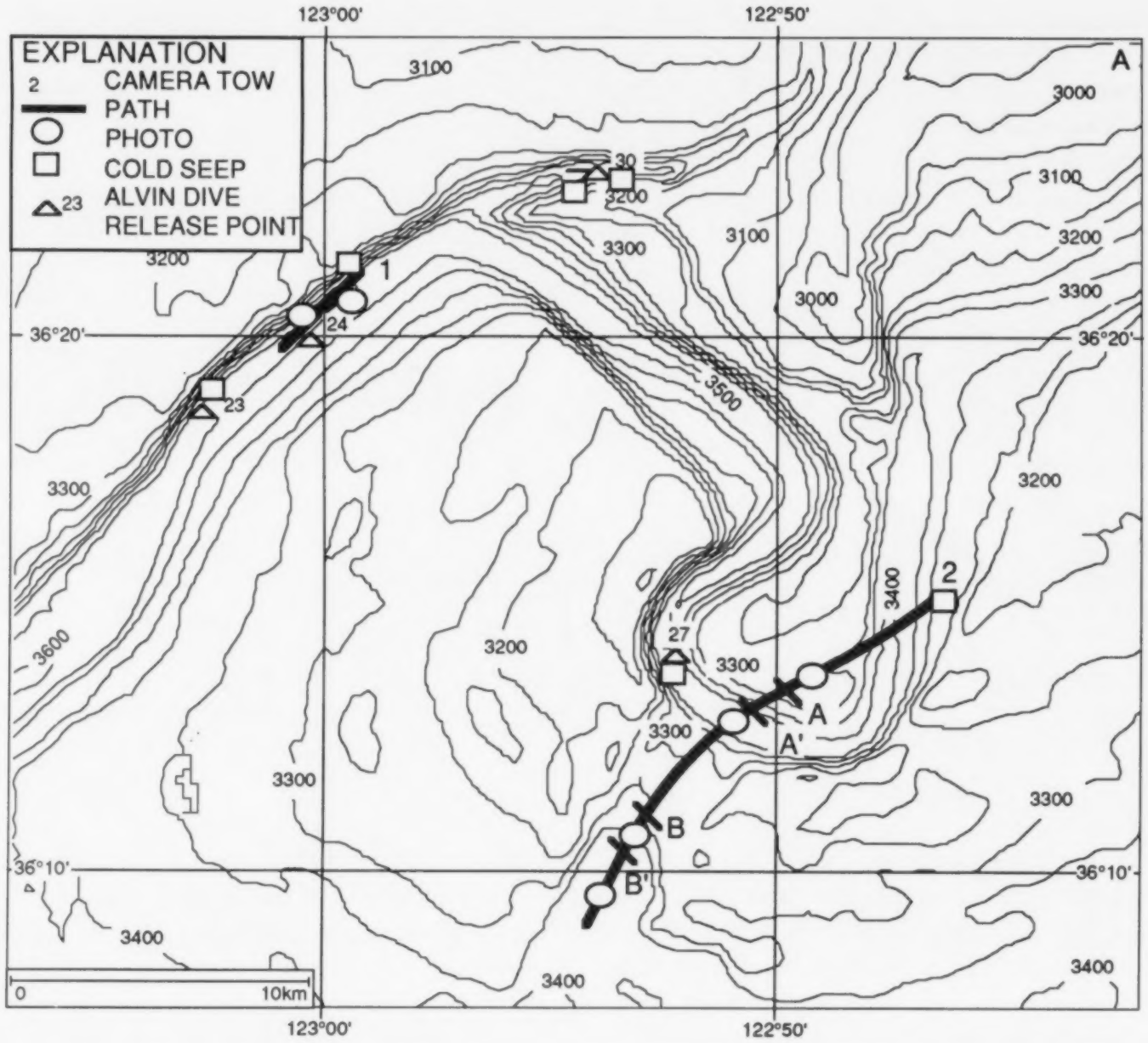

Fig. 1A.

sufficient magnitude to initiate submarine slides and liquefaction of sediments are common and the products of these disturbances contribute to fan growth.

In order to investigate the extent of canyon and fan valley activity a photographic survey was conducted from R/V *Atlantis II*. This study provides a detailed description of the Monterey Canyon and fan system as it existed in October–November 1988, before the Loma Prieta earthquake (October 1989). Photographs taken with a bottom-towed camera sled were employed to distinguish fresh disturbances at the scale of bedforms, sediment texture, microtopography and biology. Bottom towing provided near-continuous observation along extended (multi-km) transects (Figs. 1A, B and C). SeaBeam mapping was completed a few months prior to the photographic survey. Preliminary observations from the submersible dives were reported in Eittreim et al. (1989) and Embley et al. (1990).

Geologic background

The course of Monterey Canyon follows a sinuous path for 75 km through the shelf and down the slope to a depth of 3000 m, where the canyon intersects a large depositional apron known as the Monterey Fan (NOAA, 1989). The base of the continental slope near 3000 m of water depth is

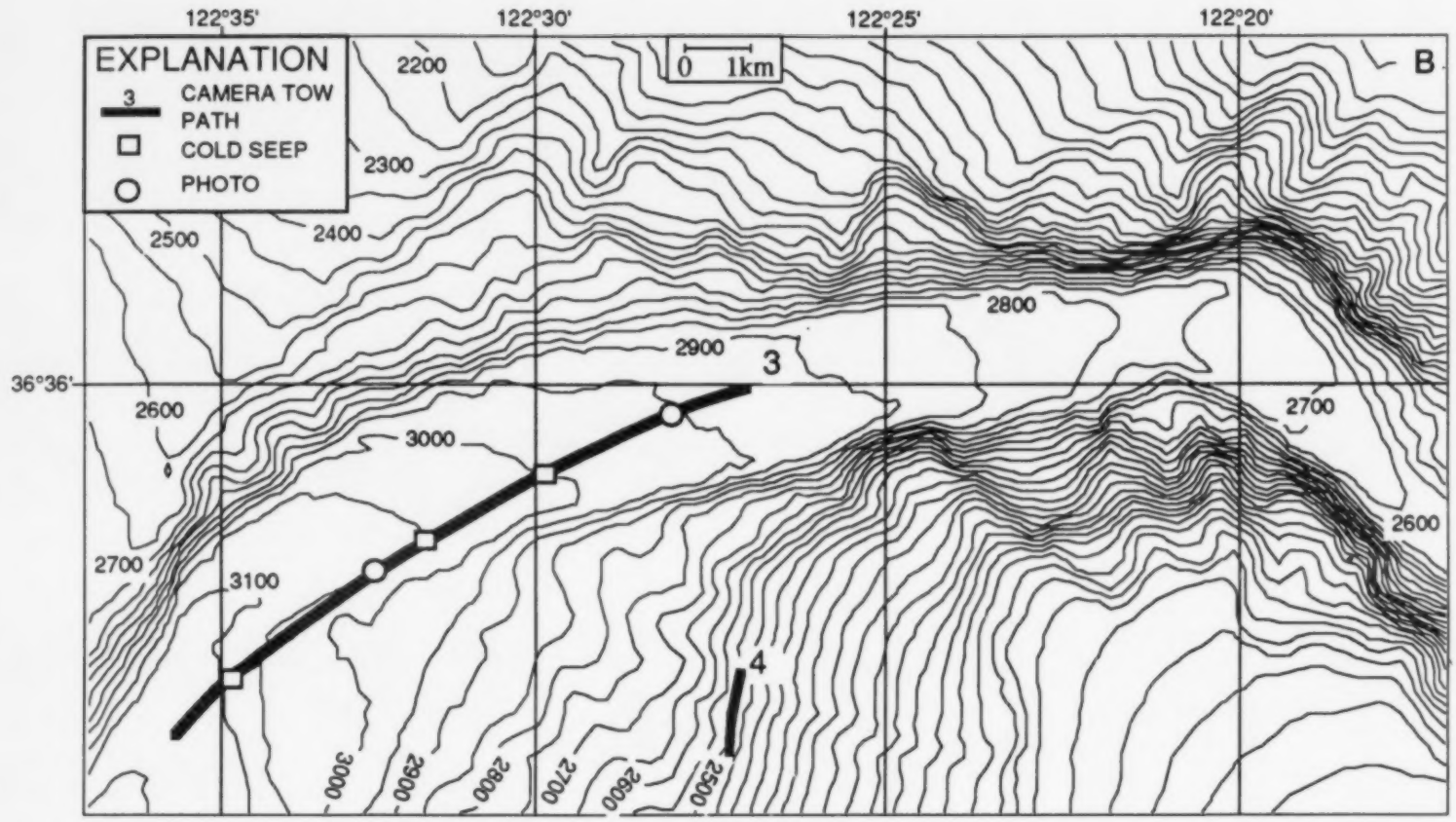

Fig. 1B.

generally accepted as the boundary between the canyon and fan settings (Shepard and Dill, 1966; Normark, 1970; Embley et al., 1990). In the shelf and slope the canyon walls are steep (more than 30°) and are incised into indurated siltstones, sandstones, limestones, granodiorites and metamorphic rocks (Martin and Emery, 1967). Below water depths of 3000 m the fan valley walls are gradual (less than 30°) and tend to be terraced. Monterey Fan continues another 400 km beyond the base of the slope to a depth of 4700 m where it merges with the abyssal plain (Normark and Gutmacher, 1989).

Although at present the major conduit of sediment to the fan is believed to be Monterey and its tributary canyons, two major canyon–fan valley systems Ascension and Monterey have provided sediment to the fan in the past (Normark, 1970; Normark et al., 1985) (Fig. 1). The Ascension Fan Valley has eleven tributary canyons, all isolated from the Monterey Canyon system (Greene et al., 1988). The fan itself is traversed by a long meandering channel, the deep water continuation of Monterey Canyon. Two striking attributes of the Monterey Fan Valley are its deep entrenchment into the fan apron and a large "horseshoe" bend between 3000 and 3500 m of water depth called the Shepard meander (Fig. 1A). Submarine fans that are predominately fine-grained (clay and silt) tend to have meandering valleys that are perched on their fan apron and confined by lateral levees (Flood et al., 1991; Feeley et al., 1990). Meanders are ubiquitous to fan valleys and typically the meander amplitude is less than a few kilometers (Damuth et al., 1983; Droz and Bellaiche, 1985; Kastens and Shor, 1985). Entrenchment has been observed on fan valleys, but its occurrence is not common (e.g. the Rhone fan valley; O'Connell, 1986). The deep entrenchment on the Monterey Fan Valley is noteworthy and its association with a large meander invites a linkage between the two phenomena. The Monterey Fan Valley is believed to be at maximum entrenchment when its relief is 300 m below the fan surface (Fig. 2).

Normark (1970) has proposed that as the result of a collapse of their common levee, the path of the Monterey Fan Valley was diverted and combined with the Ascension Fan Valley. According

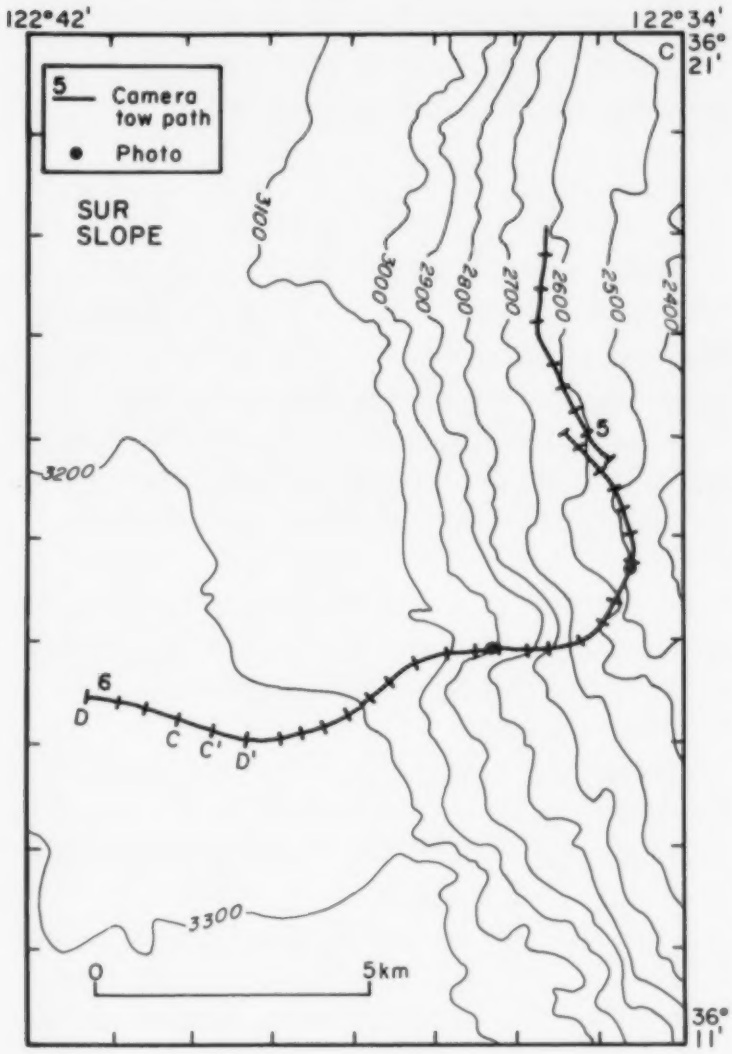

Fig. 1C.

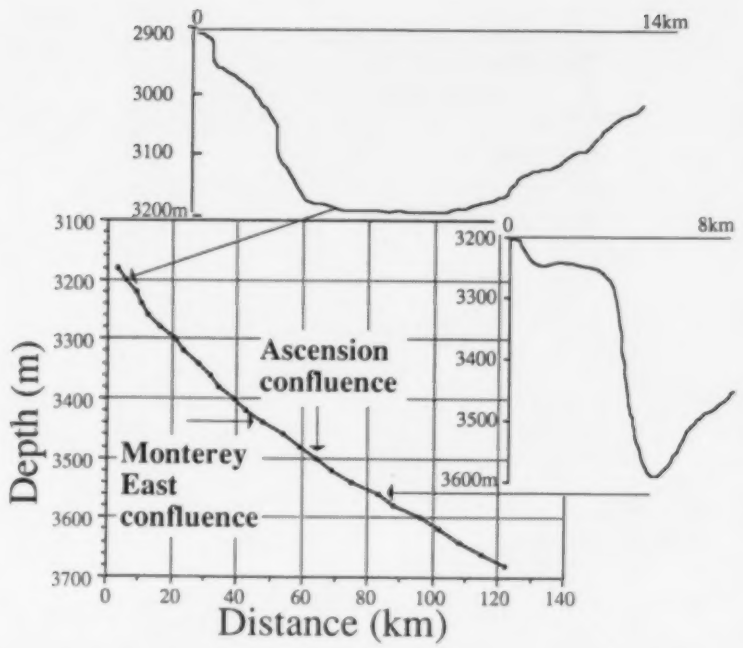

Fig. 2. Axial profile of the Monterey Fan Valley from 3180 to 3680 m of water depth. Note "V" shaped cross-section and steep walls of the Monterey Fan Valley downslope of its confluence with the Ascension Fan Valley where the channel is deeply entrenched, and the "U" shaped cross-sectional profile where the channel is not entrenched. The absence of significant knick points in the gradient profile for the Monterey Fan Valley indicates that the entrenchment has reached an equilibrium with depositional processes.

to Normark the Monterey Fan's sediment supply has been provided by both the Ascension and Monterey drainage networks. The Ascension Canyon fan system, whose present head is stranded at the edge of the shelf, became less active when its sediment supply was diminished after a sea level rise. The Monterey Canyon fan system, indents the beach, has access to a contemporary supply of sediment and remains active. Subsequent downcutting of the Monterey Fan Valley to form the entrenched channel has left the Ascension Fan Valley as a hanging tributary. Also, according to Normark, a subdued elongate depression on the Monterey Fan (called the Monterey East Fan Valley), that extends to the southwest from the convex side of the Shepard meander, is the abandoned former course of the Monterey Fan Valley. This course was abandoned after the diversion when the Monterey Fan Valley combined and fed into the lower Ascension Fan Valley.

Greene et al. (1988) has proposed an alternative hypothesis to levee collapse. Instead a series of submarine slumps may have blocked the original course of Monterey Fan Valley, thereby initiating a levee breach which in turn led to the diversion of the Monterey flow into the path of the lower Ascension Fan Valley. In both hypotheses of diversion, the post-diversion valley path is steeper than the original course. In order to achieve an equilibrium gradient, the valley is entrenched.

Methods

Data collection

The photographic coverage of the Monterey Canyon–fan system and adjacent continental slope consisted of six camera transects that covered more than 60 km of seafloor (Fig. 1A, B and C). Tracks from the bottom-towed camera sled were imprinted on the seafloor (Fig. 3A). The camera sled used for these tows (BABS) has been described by Hecker (1990). The oblique-angle pictures

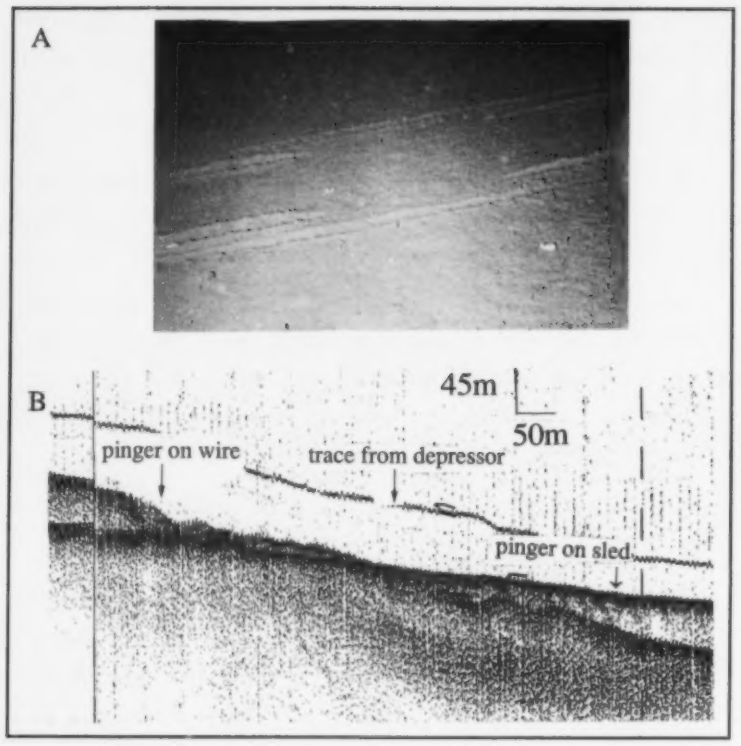

Fig. 3. (A) Sixty kilometers of camera sled tracks were imprinted on the sea-bed. Possible disturbances to the seafloor triggered by the Loma Prieta earthquake (October 17, 1989) should be noted by overprinting of the camera sled tracks. Photo courtesy of W.R. Normark. (B) Two acoustic profiles were obtained. One acoustic profile represents the bottom echo of the pinger mounted on the wire. This profile has topographic resolution. The second profile represents the direct echo to the ship made by the pinger mounted on the sled. This profile has sub-bottom penetration. Trace above the acoustic profiles is the direct echo of the pinger on the wire. Acoustic profile B–B′ showing scarp in the Monterey East Fan Valley with wrinkled bedforms on its surface up to 8 m in amplitude. Location of acoustic profile shown in Fig. 1A.

obtained enhance the ability to identify geological bedforms and bottom textures. At a 15-s exposure rate and an average towing speed of 1.2 knots a picture was taken every 8 m along the camera track. More than 6000 photos were obtained during this survey.

The on-bottom track of the towed camera sled was determined relative to the surface vessel using a combination of acoustic signal and internal on-bottom control. The internal control of the camera was provided by a pressure transducer (later converted to water depth) and the time of day to the nearest second; these were optically registered in digital format adjacent to each film frame. The acoustic signal was provided by two 12 kHz pingers transmitting at 1-s intervals. One pinger was mounted on the sled and the other on the wire (above a depressor) connecting the sled to the ship. The ship's position was determined from continuously recorded Loran-C navigation.

Data processing

Camera position was determined by calculating horizontal separation between the ship and the sled, and plotting a range circle at 1/4 h intervals along the ship's track. Within each range circle the camera depth was matched to the bathymetry and its position was plotted. The horizontal separation of the ship from the sled was computed by triangulation using the camera depth and wire out. Since the camera is mounted on a sled and we determined the sled position relative to the ship, we were also able to determine the orientation of the photographs.

Camera depth profiles were obtained by plotting the camera depths versus time; later converted to distance. The camera sled depth gives very high resolution profiles of seafloor topography. The field of view for each individual photograph is approximately 1 m at the bottom of the picture, 3 m at the top and 3 m from bottom to top, although maximum range at the top is dependent on water turbidity. The field of view for each photograph covers an area of approximately 5 m^2.

Two acoustic profiles were obtained along each tow (Fig. 3B). One acoustic profile represents the bottom echo of the pinger mounted on the wire above the depressor. Since the depressor was 20 m above the sled, this profile has less penetration, but more topographic resolution than the sled pinger trace. The depressor was approximately 100 m ahead of the sled, so geologic features on this profile are seen first. The second acoustic profile was made by the direct echo to the ship of the pinger mounted on the sled. This profile has more penetration but less topographic information since it is closer to the seafloor. Sub-bottom penetration ranges from 1 to 2 m down to 20 m (Ryan et al., 1980). The trace above the acoustic profiles is the direct echo of the pinger on the wire. Since these acoustic profiles permit geological features to be observed with high spatial resolution, these traces can be used for geologic interpretation as long as the camera remains on bottom (80% of the time).

Observations

Lower Monterey Canyon–upper Fan valley (2700 to 3100 m)

The photographic coverage of this region consisted of two camera runs (#3 and #4) that covered the thalweg and the fan's southeastern levee crest respectively. The thalweg of the lower Monterey Canyon and upper Monterey Fan is a current-smoothed and muddy environment with an abundance of traces of benthic activity (Fig. 4a). Currents have leveled benthic tracks, trails and mounds, but burrows are quite prominent. Active weak currents, are indicated by the orientation of the dorsal appendages of the populous inhabitant of this domain, the holothurian *Scotoplanes globosa*. Light back-scattering indicates that this region has high concentrations of suspended particulates (Fig. 4b). A large amount of partially decomposed algae (kelp) from the near-shore environment was concentrated in patches on the seafloor near 3100 m. A 12-m relief rocky escarpment at the base of the canyon wall attests to episodes of sediment failure and erosion. Large boulders (approximately 2 m in diameter) at the base of this escarpment were partially buried and covered with hydroids, giving the impression that this is a relatively old failure of the canyon wall (Fig. 4b).

The southeastern levee crest at 2700 m is cut by gullies of up to 20-m relief. Photographs show that presently the levees are a low energy environment stirred by faunal activity, as evidenced by numerous tracks, trails, burrows, mounds and fecal pellets. The camera traversed a large topographic depression interpreted from the bathymetry to be a collapsed valley wall.

Upper Monterey Fan Valley (3300 to 3500 m)

The photographic coverage of this area consisted of two camera runs (# 1 and # 2) that traversed the levee crests, channel walls and floors. In the region of the Shepard meander the levee crests are overlain by a thick cover of mud and appear undisturbed. Tracks, trails, mounds and burrows are quite evident suggesting that neither major episodes of erosion nor deposition have occurred recently (Fig. 5a). Particulate suspended material, as evidenced from light back-scatter, appears to be less abundant in this region relative to the canyon environment.

The thalweg at the meander bend is a "V"

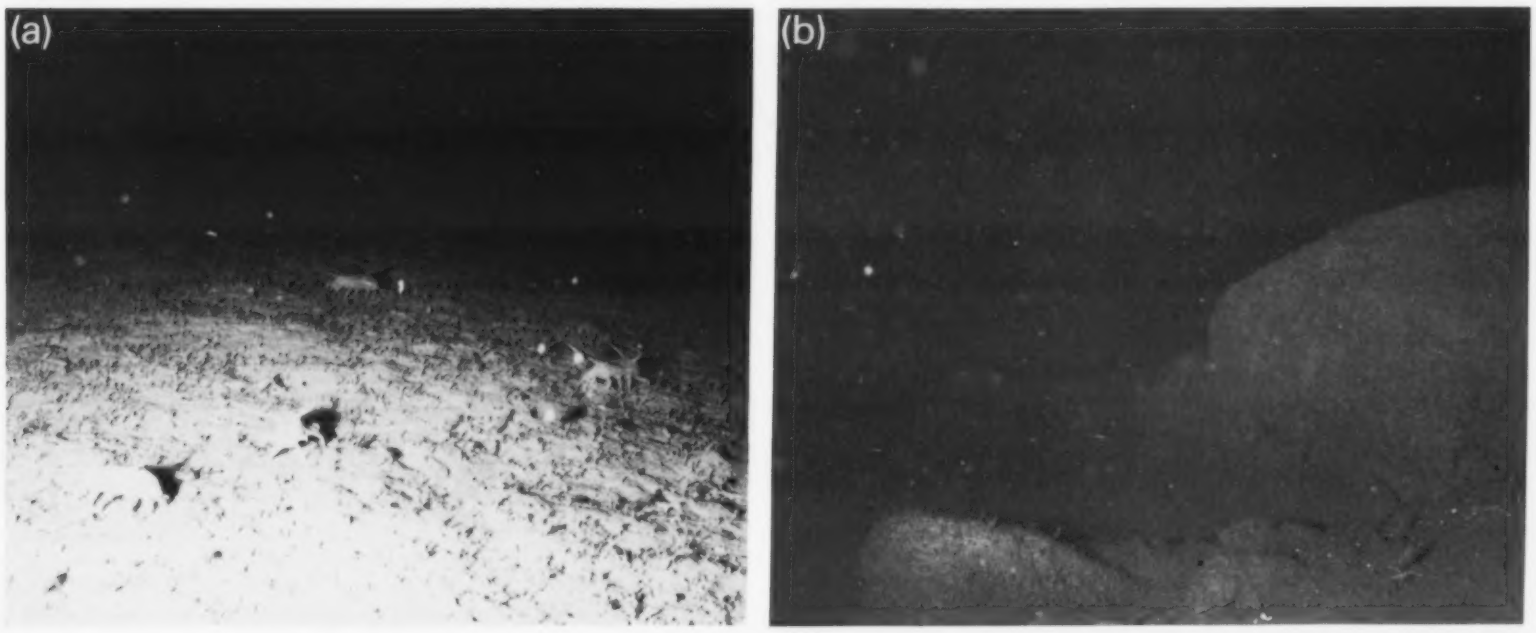

Fig. 4. Lower Monterey Canyon–upper fan valley regions. (a) Active weak currents are noted in the thalweg by the orientation of the dorsal appendages of the holothurian *Scotoplanes globosa*. The seafloor is smooth and muddy. (b) Mass-wasting in this region is not fresh. Boulders at the foot of a 12 m scarp are sedimented and covered by hydroid growths. There is a high concentration of suspended particulates.

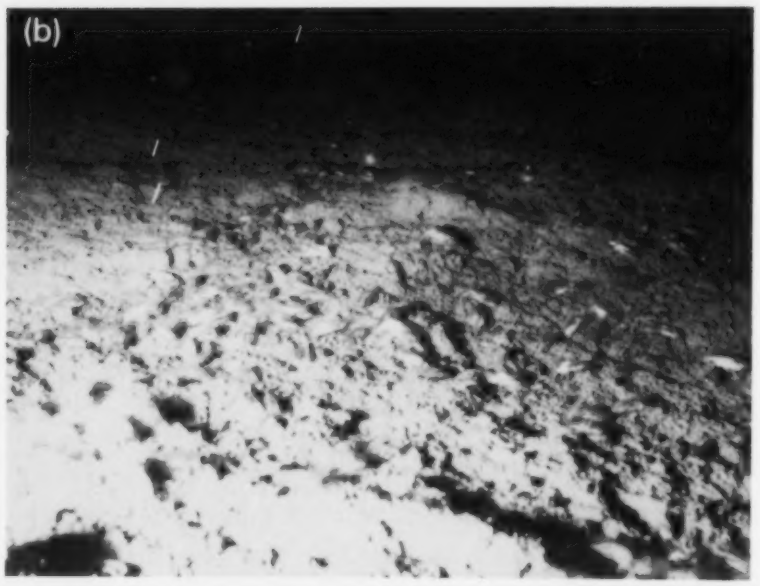

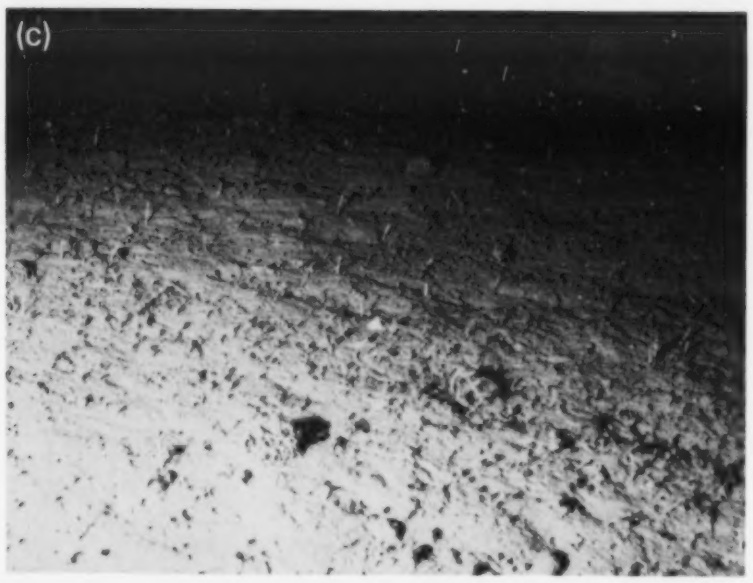

Fig. 5. Upper Monterey and Monterey East Fan Valley regions. (a) The levee crests in the region of the Shepard meander are a low energy setting. Mounds, burrows, tracks and trails give this region an undisturbed appearance where neither major episodes of erosion nor deposition have occurred recently. (b) The thalweg floor in the Shepard meander region is covered with holothurian fecal pellets and scattered with talus blocks. (c) The Monterey channel floor downslope from the confluence of the Ascension and Monterey Fan Valleys appears smooth and muddy. (d) The smooth and muddy channel floor contrast sharply with a debris apron interpreted from the bathymetry to be talus from a collapsed wall. The deposit is formed by mud, small boulders and pebbles, abundant mounding, and it is extensively colonized by sessile organism. (e) Camera approaches scarp in Monterey East Fan Valley. (f) Evidence for mass-wasting in the Monterey East Fan Valley is found in a bowl-shaped depression at the base of a scarp. Talus blocks and bedrock outcrops are revealed by sponges and anemones that are restricted to hard surfaces.

shaped notch, muddy and scattered with talus blocks. The thalweg floor has a disturbed appearance and is covered with holothurian fecal pellets giving the sediment a very rough texture (Fig. 5b). The fan valley walls are cut by numerous stepped terraces (Fig. 6). Photographs and depth profiles show that the outside wall of the meander bend is very steep, 180 m high and has bedded strata. The entrenched fan valley thalweg channel is confined by its walls and it meanders within the broader channel. The along gradient profile of the Monterey Fan Valley thalweg channel from 3180 to 3680 m, shows that the system is in equilibrium, as a result no major excavation and entrenchment are expected to occur (Fig. 2). The slope gradually diminishes from 0.3° to 0.17°.

Downslope of its confluence with the Ascension Fan Valley, the floor of the Monterey Fan Valley is smooth and muddy (Fig. 5c). A debris apron consisting of talus from a collapsed valley wall was observed on the floor of the fan valley. The camera depth profile and photographs of this region show that this deposit is 15 m in elevation and the debris consists of rounded pebbles, angular rock fragments and large boulders (Fig. 5d).

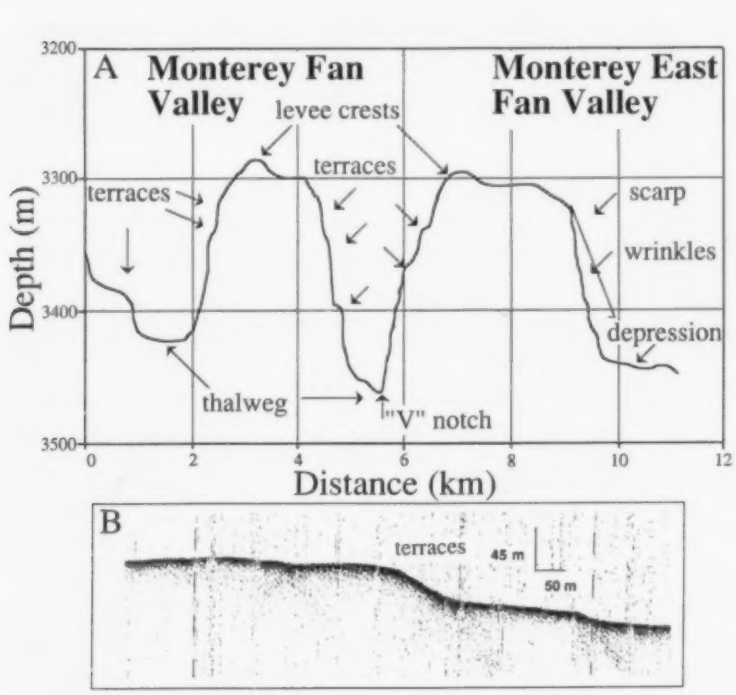

Fig. 6. Camera depth profile (run #2) along Monterey and Monterey East Fan Valleys. (A) Monterey Fan Valley terraces, broad thalweg, levee crests, "V" shaped thalweg and steep outside meander wall. In the Monterey East Fan Valley the camera descended a scarp (~100 m) with wrinkled bedforms on it surface and into a bowl shaped depression. (B) Acoustic profile A–A′ of stepped terraces: 30 and 5 m in height. Location of profile is shown in Fig. 1A.

Monterey East Fan Valley (3300 to 3500 m)

The Monterey East Fan Valley is a tranquil depositional environment characterized by a thick surficial cover of mud. The sea-bed has a generally disaggregated appearance due to the activity of benthic organisms, evidenced by abundant burrows, mounds, tracks, trails and fecal debris. Wrinkled bedforms or ridges of up to 8 m in amplitude are seen in the depth profile, acoustic profile and were photographed as the camera descended through a 100 m scarp into a bowl-shaped depression (Figs. 6A, 3b and 5e). The terrain at the base of the depression is scattered with boulders that are heavily sedimented. Sponges and anemones are found attached to large boulders and isolated patches of bedrock (Fig. 5f). The Monterey East Fan Valley contains a linear series of bowl-shaped escarpments surrounding local depressions downslope from the one crossed by the camera sled (NOAA, 1989).

Lower slope (2500 to 3200 m)

The camera depth profile of the lower slope between 2500 and 2600 m (run # 5), shows a rugged, undulating terrain of gullies that reach up to 30 m relief. The photographs show gullies and an environment characterized by a muddy seafloor disturbed by biological activity and carpeted by brittle stars (Fig. 7a).

On the lower continental slope and upper rise, between 2600 and 3200 m (run # 6), the camera crossed the detachment zone and associated debris flows of a major submarine slide. The Sur slide extends from the lower continental slope and covers more than 1000 km^2 of the fan surface (Normark and Gutmacher, 1988). Between 2600 and 3000 m the slope is sculpted with chutes that are initiated at steep amphitheatre shaped escarpments up to 100 m high. These chutes connect in a chain sequence and debouch onto hummocky and wrinkled lobate debris aprons (up to 1 km in length) on the continental rise (Fig. 8). Photographs from the floors and walls of these chutes show clean boul-

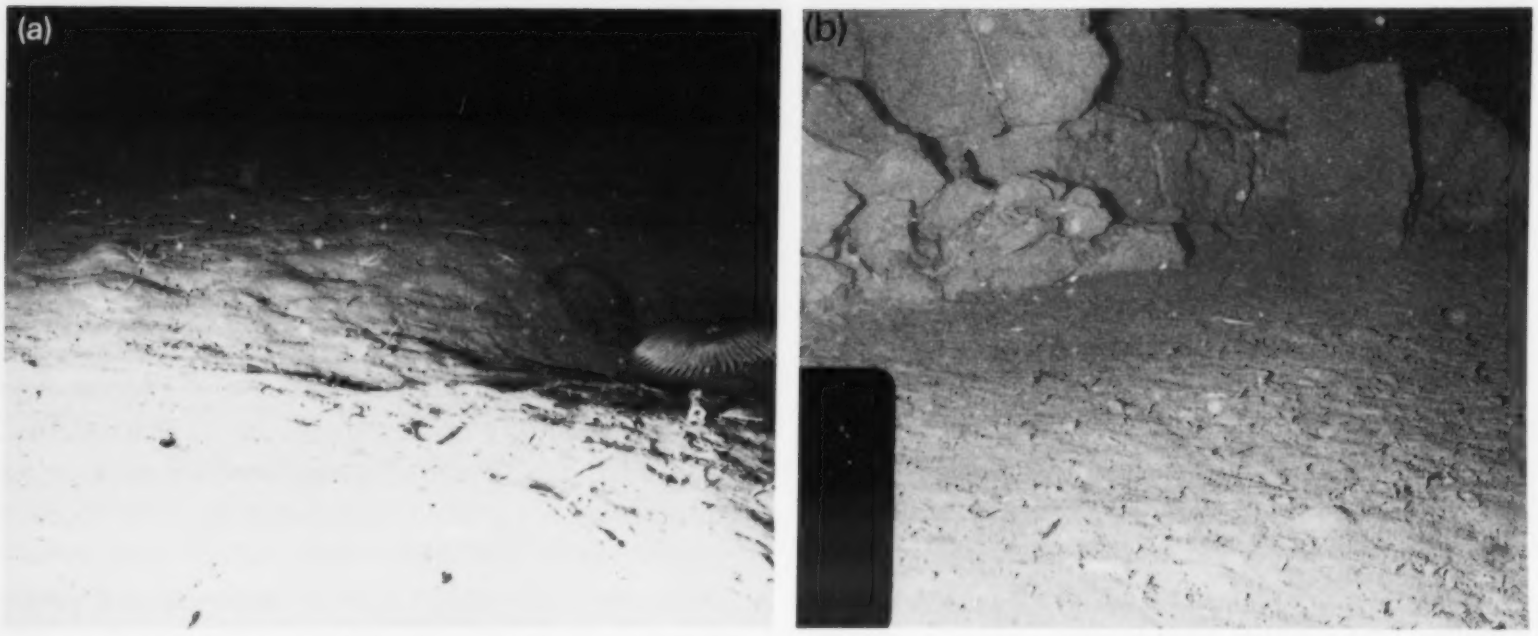

Fig. 7. Extensive mass-wasting characterizes the lower continental slope and upper rise. (a) Rugged and gullied terrain covered by mud and carpeted by brittle stars. (b) Boulders beneath scarps in the Sur slide detachment zone. Clean boulders with no sessile life or evidence of degradation reveal the freshness of mass-wasting.

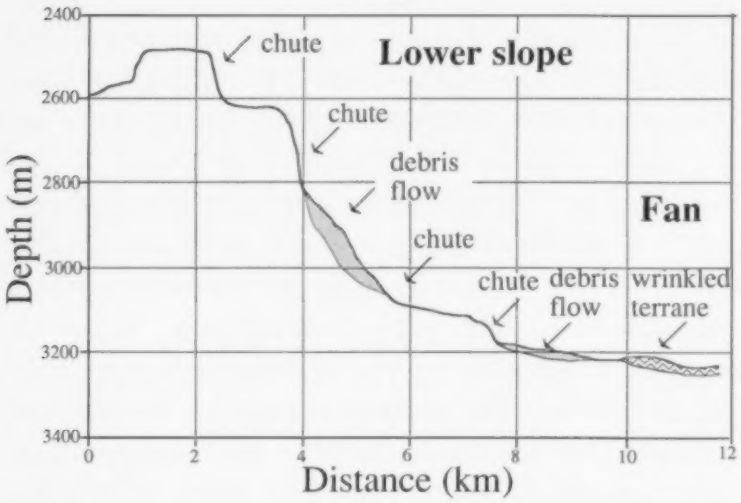

Fig. 8. Camera depth profile along the lower Sur slope and fan (run #6). The slope is sculpted by a chain sequence of gullies and chutes that terminate in lobate debris aprons. Wrinkled terrain in the fan forms part of the Sur slide surface.

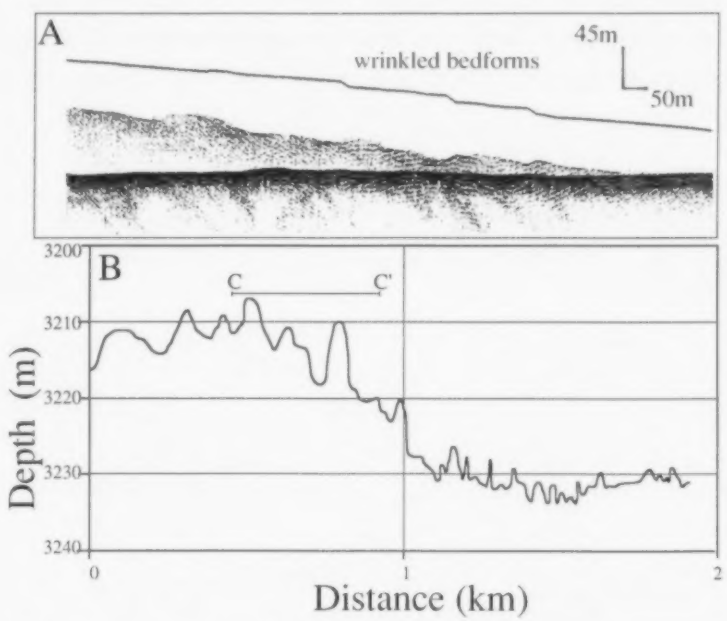

Fig. 9. Wrinkled bedforms in Sur slide region. (A) Acoustic profile of wrinkled terrain C–C'. Bedforms have wavelengths from 40 to 150 m, and can be up to 10 m in amplitude. Location of acoustic profile is shown in Figs. 1C and 9B. (B) Camera depth profile D–D' (see Fig. 1C for location) showing wrinkled terrain. Also shown is location of C–C' acoustic profile (see Fig. 9A).

ders and bedrock outcrops with no evidence of degradation or attached fauna (Fig. 7b). These charcteristics are indicative of relatively recent excavation by mass-wasting events (Hecker, 1982).

The camera crossed a wrinkled terrain at the base of the continental slope (Fig. 9). The wrinkled bedforms or ridges are on the surface of the Sur slide documented by Normark and Gutmacher (1988) and begin at a depth of 3215 m continuing for 2.5 km to a depth of 3230 m (Fig. 1c). These ridges are parallel to sub-parallel to the regional contours (NOAA, 1989). Their height ranges from 1 to 10 m, their wavelengths are from 40 to 150 m and they decrease in amplitude downslope (Fig. 9).

Chemosynthetic communities

Chemosynthetic communities were found within the Monterey and Ascension Fan Valleys (Fig. 1A and B). These findings were reported by Embley et al. (1990) and Rau et al. (1990). These communities consisted of aggregations of two clams, *Calyptogena phaseoliformis* and *Solemya* sp. and a pogonophoran (genus *Polybrachia*). The $\delta^{13}C$ values from the *Calyptogena* tissue are similar to those of other *Calyptogena* which are known to be dependent on sulfide-based chemoautotrophic symbionts (Embley et al., 1990; Rau et al., 1990). The organic/inorganic carbon measured from sediment obtained in close proximity to a clam community using Verardo et al. (1990) techniques ranged from 0.47 to 0.68% of the total weight. These values are similar to the 0 to 1.4% organic carbon measured at DSDP Leg 5 Sites 32 through 36 (Vallier, 1970). Sites 32–36 are in the general location in the Northeast Pacific Ocean as this study. Sites 35 and 36 were drilled at a similar depth (~3200 m). The organic carbon values in the Monterey Fan are low and common to the region, suggesting that the food supply for these communities is not in the sediment, but rather that it is provided by H_2S-enriched fluids possibly seeping from the walls and floor of the fan valley.

Discussion

Contemporary sedimentary and morphological features of the Monterey Canyon–fan system and adjacent slope contain two major types of erosional/depositional environments. These settings are identified by combining data on active processes and substrate texture: (1) moderate and high energy where active sedimentary processes are observed, and (2) low energy where a tranquil depositional environment with no evidence of recent disturbance is observed. Both environments have been greatly modified by mass-wasting processes.

Moderate–high energy

We interpret the Monterey Canyon upper fan valley as a moderate energy region where active sedimentation processes are occurring. The presence of contemporary sedimentary activities is revealed by: (1) visible amounts of suspended particulates, (2) currents inferred from benthic organisms, and (3) relatively fresh algal redeposition and indirectly by the smooth thalweg floor in spite of the high amount of benthic activity. There is abundant sediment in suspension, as seen from light backscatter observations, in the lower Monterey Canyon upper fan valley down to a depth of 3100 m. Everywhere else in the surveyed region suspended particle concentrations are less abundant. If suspended particulate matter is being deposited within the canyon setting, mud would carpet the sea-bed. Traces of benthic organisms as tracks, trails and mounds would be easily imprinted on the seafloor, giving the sea-bed a disturbed appearance. Yet, in the moderate energy setting the thalweg appears muddy and leveled throughout, even though there is a profusion of benthic biota. This suggests that currents may be stirring the water column and smoothing the seafloor. The flow of weak currents is also confirmed by the orientation of the dorsal appendages of the holothurian *Scotoplanes globosa*.

The heads of Monterey and Carmel Canyons come to within 8 km and a few hundred meters respectively, of extensive kelp forests (algae) found along the nearby Monterey Peninsula (C. Harrold, pers. commun., November 1988). It appears that the kelp is being reworked and transported down through the Monterey Canyon and onto the fan to a depth of 3100 m. The sediment (and entrained kelp) are being deposited as the flow exits the steeper slope and encounters the more gradual gradient of the fan setting. A high energy environment is found in the adjacent slope where extensive mass-wasting and the freshest disturbances were observed. The slope high energy environment will be discussed in the mass-wasting section.

Low energy

Sediments of the levee crests, channel floors and walls of the Monterey Fan Valley in the region of the Shepard meander, downslope from its confluence with the Ascension Fan Valley and of the Monterey East Fan Valley are muddy, generally

fine-grained and greatly disturbed by the activity of benthic organisms. We interpret these areas as a low energy, tranquil, depositional setting. There is no evidence in the photographs of active processes within the recent past except for hemipelagic sedimentation that reaches the bottom after being recycled in the water column. In addition, recent sediment is also derived from fine terrigenous particulates stirred in suspension in the canyon head, upper canyon axis and nearshore and shelf environments, that are slowly being deposited as hemipelagic sedimentation preferentially along the canyon–fan valley floor.

Although the general appearance of the sediment suggests recent low energy conditions, intermittent turbidity currents (events occurring at approximate 100 to 1000 year intervals) must continue to reach this region of the fan. Cores from the western levee of the Monterey Fan Valley downslope of its confluence with the Ascension Fan Valley show turbidity overflows with latest Pleistocene datums at 14.5 and 10.5 kyr and Holocene sediment (Brunner and Ledbetter, 1987; Normark and Gutmacher, 1989). Sediment cores taken at the intersection of Monterey and Monterey East Fan Valleys and from the axis of the Monterey East Fan Valley have sand units of Holocene age indicating that some recent turbidity overflow has occurred (Hess and Normark, 1976).

Southwest of the Shepard meander the levees are sculpted with extremely large wavelength (approximately 3 km), low relief (20 m) bedforms interpreted as megawaves (NOAA, 1989). A similar field of abyssal waves was mapped in the northwestern levee of the Monterey Fan Valley and their origin was attributed to large turbidity currents overflowing the levee (Normark et al., 1980). Comparable fields of abyssal sediment waves have been also mapped in the Magdalena fan, the Moroccan continental rise and northeastern South America (Bouma and Treadwell, 1975; Jacobi et al., 1975; Embley and Langseth, 1977).

Mass-wasting

Evidence for mass-wasting in the lower Monterey Canyon and upper-fan is seen in collapsed canyon and fan walls with development of rock-slides and debris aprons. The debris in these regions is not fresh. Bedrock exposures on canyon walls were colonized with anemones and sponges and sedimented to varying degrees. Debris from collapsed walls was also abundantly colonized and encrusted with organisms.

Photographs suggest that the Monterey East Fan Valley is not an active conduit of sediment transport from Monterey Fan Valley and that it has been modified by mass-wasting. The Scripps-MPL Deep-Tow Instrument was towed across the Monterey East Fan Valley in 1970 (Spiess and Tyce, 1973) and showed an amphitheater-shaped depression with a wrinkled terrain on its surface (Hess and Normark, 1976). These wrinkles resemble, in size and configuration, rotational slump ridges seen in Sea MARC I sonar imagery from the Western Mediterranean (O'Connell et al., 1985). They also resemble the "thumbprint" ridges seen on the Laurentian continental slope off eastern Canada near the 1929 Grand Banks Earthquake epicenter, which are attributed to the downslope movement of unstable surficial sediments (Piper et al., 1985). In the Mississippi fan arcuate ridges transverse to a debris flow direction formed when the flow was constrained by bathymetric obstacles (Kastens and Shor, 1985). In the Monterey East Fan Valley, mass-wasting has resulted in the excavation of the fill of the former valley that became cut-off during the formation of the Shepard meander. Mass-wasting was probably triggered by turbidity currents overflowing the levee, and the wrinkles in the Monterey East environment are probably pressure ridges formed by the downslope movement of unstable surficial sediment. We suggest that the loading of the megawaves in the Monterey East Fan Valley may be a triggering mechanism for the formation of the linear sequence of bowl-shaped depressions seen in the bathymetry.

Outside of the canyon fan system the slope appears to be locally transformed by mass-wasting processes. The slope between 2500 and 2700 m contains numerous gullies that may be the precursor to larger landslides and debris-flows with development of head-wall detachment cliffs. Chutes and slope canyons are formed in the lower slope from 2700 to 3100 m. The wrinkled bedforms on the

Sur slide surface near 3200 m, are most likely pressure ridges generated during the movement. We suggest that the wrinkled terrain formed due to shear stresses during debris flow emplacement as in the Mississippi Fan (Kastens and Shor, 1985).

Contemporary erosional/depositional processes in the Monterey Canyon fan valley system and adjacent slope

Our present data set indicates that the Monterey Canyon and the fan valley down to 3100 m are being modified by active sedimentary processes, while the Monterey Fan Valley downslope from 3100 m may only be affected intermittently by turbidity flows (events occurring approximately at 100 to 1000 year intervals). Monterey Canyon heads the nearshore and has access to a large mass of sediment that is transported down the canyon axis. Part of these sediments are indirectly supplied by the California climate that consists of short wet winters and long dry summers, and does not promote the growth of stabilizing vegetation (Brownlie and Taylor, 1981). Therefore, during the rainy periods there is a large amount of sediment stripping. These sediments are carried into the drainage basins and canyon axis (Gorsline and Teng, 1989). Another source of sediment for the Monterey Canyon are the strong seasonal upwellings driven by wind stress and interaction between the California current and the coastal bathymetry. The upwelling transports sediment up and down the canyon axis (Emery, 1960; Hickey, 1979). Tidally-driven flows also form part of the complex canyon circulation.

The large influx of sediment and the presence of strong currents can initiate slumping of upper canyon sediments and turbidity currents in Monterey Canyon. Turbidity flows stir sediment into suspension carrying it to the lower canyon. Similar events (strong currents, tides and turbidity currents that initiate mass-wasting) are well documented for La Jolla and Scripps Canyons also located on the California coast (Inman, 1970; Shepard and Marshall, 1973). Recent observations from Alvin indicate that the walls of the canyon are actively undergoing mass-wasting and that there are strong up and down canyon currents (Eittreim et al., 1989). If strong enough turbidity currents develop, they may flow for several days reaching further segments of the fan valley (Reynolds, 1987). These intermittent but far-reaching turbidity currents not only erode and deposit sediment in the the fan thalweg, but will also undercut the fan valley walls, triggering slumps and rockslides.

Another process that affects the thalweg area of the Monterey and Ascension Fan Valleys may be inferred from the presence of numerous seeps with their attendant chemosynthetic communities. The seeps are intermittent features, that appear to only develop on newly cut areas of the thalweg floor and walls (Embley et al., 1990). The nutrients to the seeps were not found in the sediment and appear to derive from seeping fluids. Water sources supplying nutrients to the seeps are as yet unidentified. The effects of the seeps on slope stability is uncertain, but their presence must be considered in any overview of sedimentary processes.

Earthquake induced submarine failures

Earth-shocks of the appropriate magnitude will undoubtedly contribute to mass-wasting by triggering slides, debris flows, or by initiating turbidity currents that may result from slumping and liquefaction of sediment. Earthquake-induced submarine failures in tectonically active regions as California have been well documented (Houtz, 1952; Houtz and Wellman, 1962; Menard, 1964; Coulter and Migliaccio, 1966). Normark and Gutmacher (1988), suggest that because of the young age of the Sur slide, and the relatively low sedimentation rate on the adjacent margin, the slide was probably triggered by an earthquake. The October 17, 1989, magnitude 7.1 Loma Prieta earthquake, was located in the Santa Cruz Mountains approximately 50 km from the head of Monterey Canyon. As a result of the earthquake, liquefaction of sediments destroyed buildings and other structures near the head of Monterey Canyon. The liquefaction of sediments and fresh slump scarps (3 to 6 m high and up to 100 m long) were linked to the earthquake, up to a depth of 12 m and on the upper south wall of Monterey Canyon (Greene et al., 1991). Further off-shore disturbances generated by the earthquake should

be distinguishable from pre-earthquake seafloor conditions by comparison with the deep sea photographs and by observation of camera sled tracks imprinted on the seafloor.

Conclusions

The photographic survey provided evidence of active processes in the lower Monterey Canyon–upper fan valley axes, where currents have smoothed the thalweg and deposited sediment and disintegrated kelp from the nearshore environment. The fan valley levee crests and channel walls and floor are low energy, tranquil depositional environments with a thick cover of mud that is stirred by benthic faunal activities. The fan walls in the region of the Shepard meander are primarily erosional and carved by stepped terraces. Wall outcrops are bedded and colonized by benthic organisms. The upper Monterey Fan Valley gradient is in equilibrium and no further major excavation is expected. Mass-wasting processes, such as slumps and rock-slides, erode the canyon and fan walls depositing sediment on the floors. Talus found in these regions does not appear fresh: it is sedimented and abundantly colonized and encrusted by benthic organisms. Locally, seeps control the establishment of specialized benthic communities along the lower canyon and fan valley, however seep-controlled erosion or cementation has not been noted. The Monterey East Fan Valley has been modified by mass-wasting processes; photographs suggest it is an abandoned environment, covered by mud and greatly disturbed by benthic organisms.

The adjacent Sur slope is interpreted as a high energy environment that has been recently modified by mass-wasting processes. Photographs of the floors and walls of larger gullies and chutes show the freshness of mass-wasting (bedrock outcrops and talus devoid of sediment and attached organisms). Slope failures cause landslides and debris-flows with wrinkled terrains. Such sediment displacement causes scouring and development of headwall cliffs, larger gullies, chutes and slope canyons. Earthquakes of the appropriate magnitude will generate disturbances and contribute to the observed mass-wasting. If the ground motion generated by the Loma Prieta earthquake indirectly caused seafloor disturbances in the Monterey Canyon and fan regions, it should be noted by comparing with pre-earthquake (1988) observations.

Acknowledgments

We gratefully acknowledge the personnel of the *Atlantis II* for their support of the camera survey. We are grateful to Robert W. Embley from NOAA for providing us with the ship time to do the camera survey. We also thank the other scientific personnel who participated on the cruise and contributed to the results presented in this paper, including Angela Barone, H. Gary Greene, Stephen L. Eittreim and W.R. Normark. We thank Paul Grim from NOAA for providing field maps and gridded bathymetry at a time when a later and more comprehensive survey data was classified and unavailable for use. We thank Robert Embley, Stephen Eittreim, William Normark and Gary Greene for providing maps and photographs. We are thankful to Dave Verardo for conducting the organic carbon analyses. We are grateful to B. Charlotte Schreiber for extensive discussions and reviewing of the manuscript. Kim Kastens, Jim Hayes, Stephen Eittreim and Nicholas Christie-Blick provided helpful reviews. The research has been supported by N.S.F. grants OCE 88-17563 and OCE 84-12241. This is LDGO contribution no. 4904.

References

Atwater, T., 1989. Plate tectonic history of the northeast Pacific and western North America. In: E.L. Winterer, D.M. Hussong and R.W. Decker (Editors), The Eastern Pacific Ocean and Hawaii. (The Geology of North America, N.) Geol. Soc. Am., Boulder, Colo., pp. 21–71.

Bouma, A.H. and Treadwell, T.K., 1975. Deep-sea dune-like features. Mar. Geol., 19: M53–M59.

Brownlie, W.R. and Taylor, B.D., 1981. Sediment management for southern California mountains, coastal plains, and shoreline; Part C—Coastal sediment delivery by major rivers in southern California. Pasadena, Calif. Inst. Technol., EQL Rep., 17C, 314 pp.

Brunner, C.A. and Ledbetter, M.T., 1987. Sedimentological and micropaleontological detection of turbidite muds in hemipelagic sequences: an example from the late Pleistocene

levee of Monterey Fan, central California continental margin. Mar. Micropaleontol., 12: 223–239.

Coulter, H.W. and Migliaccio, R.R., 1966. Effects of the earthquake of March 27, 1964 at Valdez, Alaska. U.S. Geol. Surv. Prof. Pap. 542-C.

Daly, R.A., 1936. Origin of submarine canyons. Am. J. Sci., Ser. 5, 31: 401–420.

Damuth, J.E., Kolla, V., Flood, R.D., Kowsmann, R.O., Monteiro, M.C., Gorini, M.A., Palma, J.J.C. and Belderson, R.H., 1983. Distributary channel meandering and bifurcation patterns on Amazon deep-sea fan as revealed by long-range side-scan sonar (GLORIA). Geology, 11: 94–98.

Droz, L. and Bellaiche, G., 1985. Rhone deep-sea fan: Morphostructure and growth pattern. Am. Assoc. Pet. Geol. Bull., 69: 460–479.

Eittreim, S.L., Embley, R.W., Normark, W.R., Greene, H.G., McHugh, C.M. and Ryan, W.B.F., 1989. Observations in Monterey Canyon and Fan Valley using the submersible ALVIN and a photographic sled. U.S. Geol. Surv. Open-File Rep., 89-291, 16 pp.

Embley, R.W. and Langseth, M.G., 1977. Sedimentation processes on the continental rise of northeastern South America. Mar. Geol., 25: 279–297.

Embley, R.W, Eittreim, S.L., McHugh, C.H., Normark, W.R., Rau, G.H., Hecker, B., DeBevoise, A.E., Greene, H.G., Ryan, W.B.F., Harrold, C. and Baxter, C., 1990. Geological setting of chemosynthetic communities in the Monterey Fan Valley system. Deep-Sea Res., 37(11): 1651–1667.

Emery, K.O., 1960. The Sea off Southern California. Wiley, New York, 366 pp.

Feeley, M.H., More, T.C., Jr., Loutit, T.S. and Bryant, W.R., 1990. Sequence stratigraphy of Mississippi Fan related to oxygen isotope sea level index. Am. Assoc. Pet. Geol. Bull., 74(4): 407–424.

Flood, R.D., Manley, P.L., Kowsmann, R.O., Appi, C.J. and Pirmez, C., 1991. Recent growth of the Amazon deep-sea Fan. In: P. Weimer and M.H. Link (Editors), Seismic Facies and Sedimentary Processes of Modern and Ancient Submarine Fans. (Frontiers in Sedimentary Geology.) Springer, New York.

Gorsline, D.S. and Teng, S.Y., 1989. The California Borderland. In: E.L. Winterer, D.M. Hussong and R.W. Decker (Editors), The Eastern Pacific Ocean and Hawaii. (The Geology of North America, N.) Geol. Soc. Am., Boulder, Colo., pp. 471–487.

Greene, H.G., Stubblefield W.L. and Theberge, A.E., Jr., 1988. Geology of the Monterey submarine canyon system and adjacent areas offshore central California: Results of NOAA SeaBeam Survey, Descriptive Report for the Surveyor Cruise. U.S.G.S. Open-File Rep., 89-221, 33 pp.

Greene, H.G., McHugh, C.M. and Ryan, W.B.F., 1989. Mass-wasting—A major modifying process in Monterey Canyon System. Eos, Trans. Am. Geophys. Union, 70(43): 1348.

Greene, H.G., Gardner-Taggart, J., Ledbetter, M.T., Barminski, R., Chase, T.E., Hicks, K.R. and Baxter, C., 1991. Offshore and onshore liquefaction at Moss Landing spit, central California—Result of the October 17, 1989, Loma Prieta earthquake. Geology, 19: 945–949.

Hecker, B., 1982. Possible benthic fauna and slope instability relationships. In: S. Saxov and J.K. Nieuwenhuis (Editors), Marine Slides and Other Mass Movements. Plenum, New York, pp. 335–347.

Hecker, B., 1990. Variation in megafaunal assemblages on the continental margin south of New England. Deep-Sea Res., 37: 37–57.

Heezen, B.C. and Ewing, M., 1952. Turbidity currents, submarine slumps and the 1929 Grand Banks turbidity current. Am. J. Sci., 250: 849–873.

Heezen, B.C., Menzies, R.J., Schneider, E.D. Ewing, W.M. and Granelli, N.C.L., 1964. Congo submarine canyon. Am. Assoc. Pet. Geol. Bull., 48: 1126–1149.

Hess, G.R. and Normark, W.R., 1976. Holocene sedimentation history of the major fan valleys of Monterey Fan. Mar. Geol., 22: 233–251.

Hickey, B.M., 1979. The California current system—Hypotheses and facts. Progr. Oceanogr., 8: 19–279.

Houtz, R., 1952. The 1953 Suva earthquake and tsunami. Bull. Seism. Soc. Am., 52: 1–12.

Houtz, R. and Wellman, H.W., 1962. Turbidity current at Kadavu Passage. Geol. Mag., 99: 52–62.

Hughes-Clarke, J.E., 1988. The geological record of the 1929 "Grand Banks" earthquake and its relevance to deep-sea clastic sedimentation. Ph.D. Thesis, Dalhousie Univ., 171 pp., (Unpubl.).

Inman, D.L., 1970. Strong currents in submarine canyons. Eos, Trans. Am. Geophys. Union, 51(4): 319.

Jacobi, R.D., Rabinowitz, P.D. and Embley, R.W., 1975. Sediment waves on the Moroccan continental rise. Mar. Geol., 19: M61–M67.

Kastens, K.A. and Shor, A.N.1985. Depositional processes of a meandering channel on Mississippi Fan. Am. Assoc. Pet. Geol. Bull., 69: 190–202.

Martin, B.D. and Emery, K.O., 1967. Geology of Monterey Canyon, California. Am. Assoc. Pet. Geol. Bull., 51(11): 2281–2304.

Mathews, W.H. and Shepard, F.P., 1962. Sedimentation of Fraser River delta, British Columbia. Am. Assoc. Pet. Geol. Bull., 46: 1416–1438.

Menard, H.W., 1964. Marine Geology of the Pacific. McGraw-Hill, New York, 271 pp.

National Ocean Service, NOAA, 1989. Bathymetric Map: Monterey Canyon M137 and Shepard meander M139. U.S. Dep. Commer., Washington, D.C.

Normark, W.R., 1970. Channel piracy on Monterey deep-sea fan. Deep-Sea Res., 17: 837–846.

Normark, W.R. and Gutmacher, C.E., 1988. Sur submarine slide, Monterey Fan, central California. Sedimentology, 35: 629–647.

Normark, W.R. and Gutmacher, C.E., 1989. Major submarine fans of the California continental rise. In: E.L. Winterer, D.M. Hussong and R.W. Decker (Editors), The Eastern Pacific Ocean and Hawaii. (The Geology of North America, N.) Geol. Soc. Am., Boulder, Colo., pp. 372–382.

Normark, W.R., Hess, G.R., Stow, D.A.V. and Bowen, A.J., 1980. Sediment waves on the Monterey Fan levee: a preliminary physical interpretation. Mar. Geol., 37: 1–18.

Normark, W.R., Gutmacher, C.E., Chase, T.E. and Wilde, P., 1985. Monterey Fan, Pacific Ocean. In: A.H. Bouma, N.E. Barnes and W.R. Normark (Editors), Submarine Fans and Related Turbidite Systems. Springer, New York, pp. 79–86.

O'Connell, S., 1986. Anatomy of modern submarine depositional and distributary systems. Ph.D. Thesis, Columbia Univ., New York, 313 pp., (Unpubl.).

O'Connell, S., Alonso, B., Kastens, K.A., Maldonado A., Malinverno, A. Nelson, C.H., Palanques, A. and Ryan, W.B.F., 1985. Morphology and downslope sediment displacement in a deep-sea valley, the Valencia Valley (Northwestern Mediterranean). Geo-Mar. Lett., 5: 149–156.

Piper, D.J.W., Shor, A.N., Farre, J.A., O'Connell, S. and Jacobi, R., 1985. Sediment slides and turbidity currents on the Laurentian Fan: Sidescan sonar investigation near the epicenter of the 1929 Grand Banks earthquake. Geology, 13: 538–541.

Rau, G.H., McHugh, C.M., Harrold, C., Baxter, C., Hecker, B. and Embley, R.W., 1990. $\delta^{13}C$, $\delta^{15}C$, and $\delta^{18}O$ of *Calyptogena phaseoliformis* (bivalve mollusc) from the Ascension Fan Valley near Monterey, California. Deep-Sea Res., 37 (11): 1669–1676.

Reynolds, S., 1987. A recent turbidity current event, Hueneme Fan, California Reconstruction of flow properties. Am. Assoc. Pet. Geol. Bull., 71: 452–463.

Ryan W.B.F., Blechschmidt, G. and Thompson, P.R., 1980. Appendix E, Technical Aspects. In: B. Hecker, G. Blechschmidt and P. Gibson (Editors), Epifaunal Zonation and Community Structure in Three Mid- and North Atlantic Canyons. (Canyon Assessment Study) U.S. Dep. of the Interior Bur. of Land Management, Washington, D.C., pp. E1–E23.

Shepard, F.P. and Dill, R.F., 1966. Submarine Canyons and Other Sea Valleys. Rand McNally, Chicago, 381 pp.

Shepard, F.P. and Marshall, N.F., 1973. Storm-generated current in La Jolla Submarine Canyon, California. Mar. Geol., 15: M19–M24.

Shepard, F.P., Marshall, N.F., McLoughlin, P.A. and Sullivan, G.G. 1979. Currents in Submarine Canyons and other Sea Valleys. Am. Assoc. Pet. Geol., Tulsa, Okla., 173 pp.

Spiess, F.N. and Tyce, R.C., 1973. Marine physical laboratory deep-tow instrumentation system. Mar. Phys. Lab. Scripps Inst. Oceanogr., SIO Ref. 73-4, 37 pp.

Vallier, T.L., 1970. Carbon carbonate results. In: D.A. McManus, R.E. Burns, O. Weser, T. Vallier, C.V. von der Borch, R.K. Olsson, R.M. Goll and E.D. Milow (Editors), Init. Rep. DSDP, V: 431–441.

Verardo, D.J., Froelich, P.N. and McIntyre, A., 1990. Determination of organic carbon and nitrogen in marine sediments using the Carlo Erba NA-1500 analyzer. Deep-Sea Res., 37 (1): 157–165.

Wolf, S.C., 1969. Coastal currents and mass transport of surface sediments over the shelf regions of Monterey Bay, California. Mar. Geol., 8: 321–336.

Marine Geology, 107 (1992) 51–60
Elsevier Science Publishers B.V., Amsterdam

Siliciclastic-to-carbonate transition on the inner shelf embayment, southwest Florida

Roger J. Sussko[a] and Richard A. Davis, Jr.[b]

[a]*International Technology Corporation, Box 7809, Edison, NJ 08818, USA*
[b]*Department of Geology, University of South Florida, Tampa, FL 33620, USA*

(Received October 2, 1991; revision accepted December 20, 1991)

ABSTRACT

Sussko, R.J. and Davis, R.A., Jr., 1992. Siliciclastic-to-carbonate transition on the inner shelf embayment, southwest Florida. *Mar. Geol.*, 107: 51–60.

The inner shelf embayment adjacent to southwest Florida is a low energy system which displays a distinct and demonstrable transition from dominantly siliciclastic sediments in the north to virtually pure biogenic carbonates in the south. Sediment sources are littoral transport from the north, autochthonous biogenic debris, a modest input from land-derived runoff and a small amount from reworking of older strata.

Siliciclastic sediments are well-sorted, fine quartz sand and terrigenous and biogenic mud which is concentrated along the coast of the southern half of the 90 km coast where it accumulates from adjacent terrigenous sources. Biogenic carbonate ranges from mud to gravel in size and is dominated by sand and gravel. The transition zone between the siliciclastic and carbonate sediments covers only about 10 km and trends NNW–SSE with a south-extending lobe of siliciclastic material along the coast.

This detailed documentation of regional change in sediment texture and composition along with the geographic distribution provides data for application to the stratigraphic record. Such siliciclastic–carbonate transitions are quite important for example in the Cambro-Ordovician of the Upper Mississippi Valley and the Cretaceous of Central Texas.

Introduction

The stratigraphic record contains numerous examples of mixed siliclastic and carbonate composition that represent a variety of geologic ages. Examples include the Cambro-Ordovician of the Upper Mississippi Valley (Ostrom, 1964; Davis, 1966; Dott and Byers, 1981), the Mississippian of the central craton (Wescott, 1982) and the Cretaceous of Central Texas (Bebout and Loucks, 1977; Inden and Moore, 1983). Recent symposia and special volumes have been devoted to this topic (e.g. Doyle and Roberts, 1987).

Modern shelf environments display this mixture and transition from one type to the other throughout various, mostly low-latitude, parts of the globe. Prominent examples are the southern Gulf of Mexico and Yucatan shelf, the northwest shelf of Australia, and the Great Barrier Reef shelf system (Scholle et al., 1983). Another commonly cited example, but heretofore undocumented in detail, is the southwest shelf embayment of Florida. This report summarizes the sedimentology of this inner shelf system with special attention given to the transition from siliciclastic to carbonate sediment provinces.

The southwest Florida shelf environment is similar to what most authors envision for shallow epeiric seas (e.g. Irwin, 1965; Heckel, 1972). For this reason, it provides analog information for modeling the depositional systems of mixed siliciclastic–carbonate environments in ancient shallow seas.

Correspondence to: R.A. Davis, Jr., Department of Geology, University of South Florida, Tampa, FL 33620, USA.

0025-3227/92/$05.00

General setting

The southwest Florida inner shelf embayment as considered here, extends from Cape Romano in the north to Cape Sable in the south, a distance along the coast of approximately 120 km (Fig. 1). This shelf embayment is bounded on the north by a coastal barrier island system, landward by the Ten Thousand Islands–Big Cypress Swamp–Everglades system of south Florida, and by Florida Bay on the south. The outer limit is here considered to be the 10 m isobath which averages 42 km from the coast (Fig. 1).

This inner shelf embayment is a gently sloping, low-energy, open marine environment with an average gradient of about 1:2500. Local relief on the shelf floor is low; typically only a few decimeters where exposed limestone surfaces are irregular. The adjacent coastal area consists of mangrove islands and swamps which are dissected by numerous creeks and streams. Small shell beaches are present on exposed islands. The only extensive and well developed beach system is the multiple cuspate foreland complex which comprises the Cape Sable area (Fig. 1). Other significant coastal sand accumulations are in the vicinity of Cape Romano where beaches and subtidal shoals are prominent.

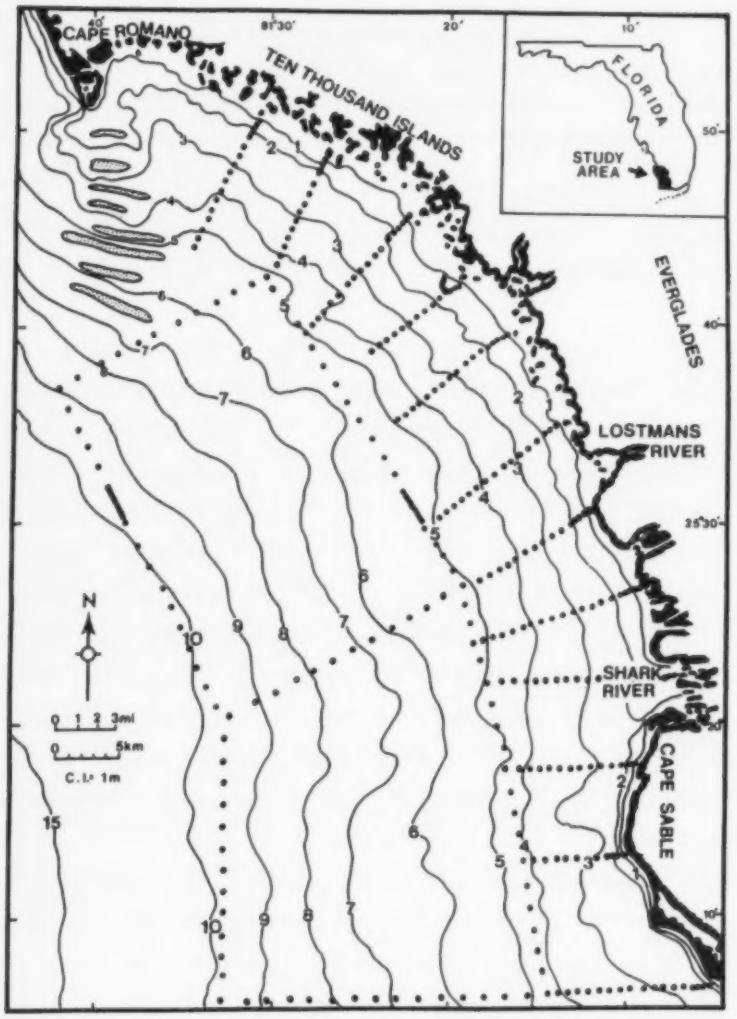

Fig. 1. Location map of inner shelf off southwestern Florida showing bathymetry. Sediment sample locations shown by heavy dots

General geology

The area is located in the Florida Peninsula sedimentary province of the Gulf of Mexico Basin. This province is characterized by a broad, low-relief plateau with steep margins and is dominated by carbonates and evaporites (Enos and Perkins, 1977). Unconsolidated sediments in the inner shelf of the southwest portion of this plateau are underlain by the Pleistocene Miami Formation and the Pliocene Tamiami Formation. Both units are interpreted as having accumulated in a shallow, low-energy, carbonate shelf environment (Enos and Perkins, 1977). Stratigraphic information from high-resolution seismic data indicates that the unconsolidated sediments on this platform are resting on an eroded karstic sequence (Holmes, 1985) of Miocene–Pleistocene age which dips gently to the south (Enos and Perkins, 1977).

According to Enos and Perkins (1977), the Miami Limestone is absent along the coast and throughout the northern half of the study area. In these areas the Tamiami Formation underlies the Holocene sequence. In the study area the Tamiami is a grayish-white to tan, fossiliferous, quartzitic grainstone.

The Ten Thousand Islands area has formed during the past 3000 years as the result of late Holocene progradation of oyster reef and mangrove islands after an initial transgressive Holocene sequence (Parkinson, 1989). Stratigraphic data on the central coastal area show a generally transgressive sequence capped by late Holocene mangrove peats and muds (Scholl, 1964). The Cape Sable area is a series of Holocene prograding cuspate forelands composed of biogenic skeletal sands and fine gravels (Roberts et al., 1977). These take the form of coastal barriers with shallow lagoons on

the landward side which contain abundant and extensive algal mat accumulations (Gebelin, 1977).

Holocene sea level history

Most data indicate that sea level has been rising throughout south Florida for nearly 7000 years (Scholl et al., 1969; Shier, 1969). It is estimated that up until 3000 years before present, sea level was rising about 25 cm/century and since that time it has slowed to about 4 cm/century (Wanless, 1982).

There have been numerous reports documenting upbuilding and progradation of the coast during this slowly rising sea level. Scholl and Stuiver (1967) determined that the rate of sediment accumulation kept up with the sea level rise during the later part of the Holocene transgression. Shier (1969) found that vermetid reefs have vertically accreted about 3 meters during the past 3000 years in the Ten Thousand Islands area. Parkinson's (1989) recent work is in general agreement and also shows substantial simultaneous seaward progradation. In the area of Cape Sable the shoreline has prograded about 8 km during the Holocene (Enos and Perkins, 1977). All of this vertical aggradation and progradation must have taken place during the slowly rising seal level of the past 3000 years. Rates of rise prior to that time did not permit establishment and stabilization of mangrove communities (Spackman et al., 1964) which were present as evidenced by the peats.

Enos and Perkins (1977) determined that about 4500 years ago flooding of Florida Bay began where the bedrock floor is about 10 m below present-day sea level. This corresponds to the outer limit of the study area. Radiocarbon dating of peats taken from below the Cape Romano shoals at 7.9 m and 4.9 m below present sea level give dates of 6470 RCYBP and 5730 RCYBP respectively (Klay, 1989). This indicates that either flooding took place much earlier in the north or that one of the interpretations is incorrect. It should be noted that the submergence curve for this area lacks control after about 1000 yr B.P. Approximate present sea level could have been attained any time in the interim.

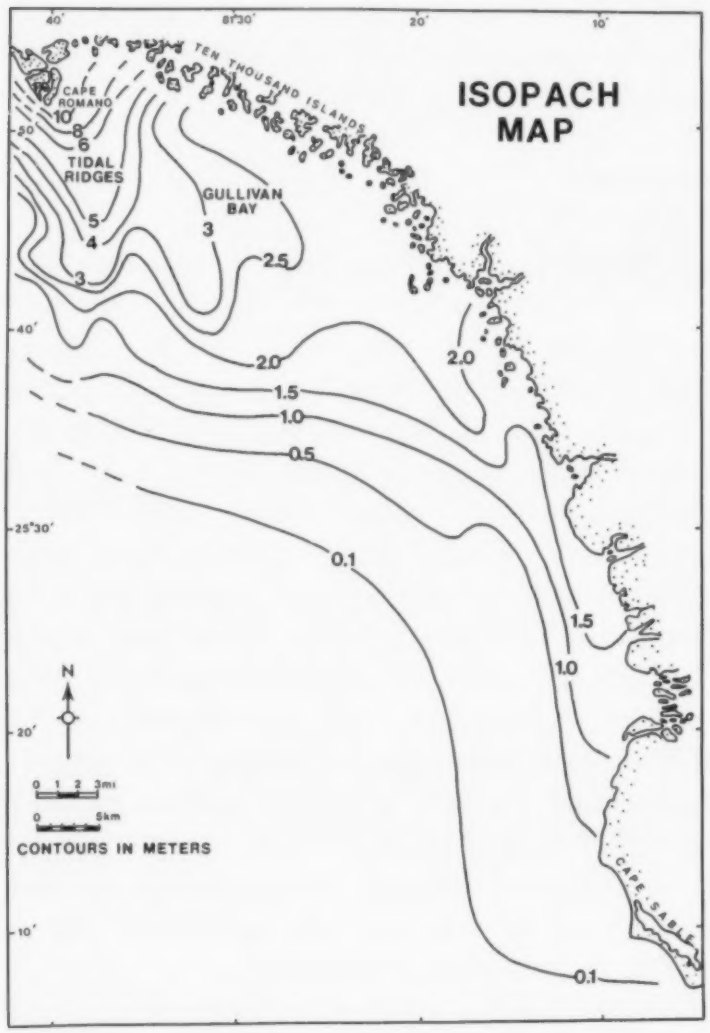

Fig. 2. Isopach map of Holocene sediments in the southwest Florida shelf embayment. This map is based on 58 vibracores, handheld cores and observations by divers.

Holocene stratigraphy

The distribution of Holocene sediments across the southwest shelf embayment shows a distinct trend from relatively thick muddy and shelly sands in the north (Fig. 2) to a discontinuous shelly pavement over the Pleistocene limestone in the south. Thickest sequences are associated with the tidal sand ridges south of Cape Romano. There is a thinning into Gullivan Bay but at least 2 m of Holocene sediment is present offshore of the Ten Thousand Islands. A coastal lobe of at least 1 m in thickness extends down to Cape Sable but beyond about 5 km in the offshore direction the Holocene is nearly absent throughout the southern two-thirds of the study area (Fig. 2).

Processes

This inner shelf system is one of the lowest energy open marine shelf systems in the world. Mean

annual wave height at the coast is 10–15 cm (Tanner, 1960) with offshore wave heights near 50 cm (U.S. Naval Weather Command, 1975). Fetch is quite limited from all but the southwest, however, most relatively large waves which enter the west Florida shelf come from the north as the result of passage of cold fronts during the winter. Hurricanes enter the Gulf with irregularity but may provide severe wave conditions from the southwest and west (Tanner, 1961; Perlmutter, 1978).

Tides are microtidal along the coast although they are among the highest on the Florida Gulf; spring range is up to 1.3 m in the north and decreases to about 0.4 m near Cape Sable. Because of the very low wave energy, this is a tide-dominated coast except at Cape Sable (Davis, 1989). Tidal currents on the open shelf have been monitored as part of this study. Low current velocities and wave influence in the shallow water provided inconclusive data on time–velocity patterns. Maximum velocity was 17 cm/s at one meter above the bed in a depth of 3 m, some 5 km from the coast in the central part of the study area. The northern area has stronger tidal currents with values over 30 cm/s between the Cape Romano shoals and the coast (Jewell, 1987).

Runoff from adjacent land areas via the numerous short rivers that drain southwest Florida (Fig. 1) varies in both space and time. This area experiences a marked seasonal precipitation cycle with most of the moisture coming between late June through late September. There is almost no rainfall during the spring and only a modest amount associated with frontal passages in the winter. A hurricane could bring several tens of centimeters of precipitation in a few days. The result is that both runoff and tidal action transports fine sediments from the land and coastal areas to the inner shelf. In the Ten Thousand Islands area the rivers do not reach the open marine environment and most of the sediment is trapped in this dense mangrove island complex. In the southern two-thirds of the area, the rivers empty directly on the open coast (Fig. 1).

Previous investigations

Holmes and Evans (1963) investigated the surface sediment of the Gullivan Bay area. They found that organic debris was relatively high and that it was provided by the mangrove swamps and related vegetated paralic environments. They also found a general relationship between grain size and physical energy in the Ten Thousand Islands with quartz sand and shell debris concentrated in tidal channels and organic debris in the protected areas. There is a general increase in grain size away from the shore and an increase in shell content to the south and west of Cape Romano to a depth of 3 m, the seaward limit of their sampling (Holmes and Evans, 1963). The Cape Romano shoals display a predictable surface sediment pattern with fine, well-sorted quartz sand on the ridges and muddy, shelly, poorly sorted quartz sand in the troughs (Jewell, 1987).

Taft and Harbaugh (1964) studied sediments from the Ten Thousand Islands area and the Whitewater Bay area adjacent to Cape Sable (Fig. 1). They noted the change in relative abundance between quartz and carbonate from north to south. Roberts et al. (1977) found small amounts of quartz in the Cape Sable area.

Sediments

In order to properly document the location and nature of the siliciclastic to carbonate transition on the inner shelf in this area, a systematic sampling plan was established. The open marine area extending from the southeast side of Gullivan Bay to Cape Sable was subdivided into 12 sub-equal transects, each of which extended normal to the local coastal trend. Surface grab samples were taken at each designated site. Sampling was at 0.5 km intervals for the first 5 samples then at 1 km intervals to the 5 m isobath. Three of these transects were extended at 2 km intervals to the 10 m isobath and a coastal parallel transect was sampled at both the 5 m and 10 m isobath with a spacing of 2 km (Fig. 1). After preliminary analysis, two closely spaced partial transects were sampled at 0.5 km intervals along the shore-parallel lines in the transition zone.

This provided a total of 312 sample locations. Sediment was collected from all but a few locations in the southwest portion of the study area where scattered shells rest directly on limestone bedrock

and grab samples could not be obtained. These conditions were confirmed by diver observations. Each sample was analyzed for its gravel, sand and mud weight fractions by wet seiving, drying and weighing. Carbonate content was determined for each sample by burning off $CaCO_3$ with dilute HCl. Weight percent organic content was also determined for 145 of the samples by heating samples in a furnace to 480°C.

Texture

Gravel

The northern end of the study area has low amounts of gravel; generally less than 10%. South of this zone nearly all samples contained more than 25% gravel with the trend of increasing gravel being essentially perpendicular to the coast (Fig. 3).

Except for a few scattered fragments of quartzitic packstone limestone, all of the gravel particles are biogenic and are produced at or near their place of accumulation. Whole shells, articulated shells and those freshly broken in combination with the low energy conditions support this generalization. The pocket of relatively high gravel content (>10%) in the northern end of the area (Fig. 3) is due to winnowing of fines and the formation of shell lags as tidal currents move across the Cape Romano shoals.

The southern half of the area is rather uniform with about 25% gravel throughout (Fig. 3). There is no discernable trend within this portion of the area either alongshore or offshore.

Sand

North of approximately latitude 25°35', sediments are greater than 90% sand except for a small area on the inner shoreface and on the coast at the Ten Thousand Islands (Fig. 4). The vast

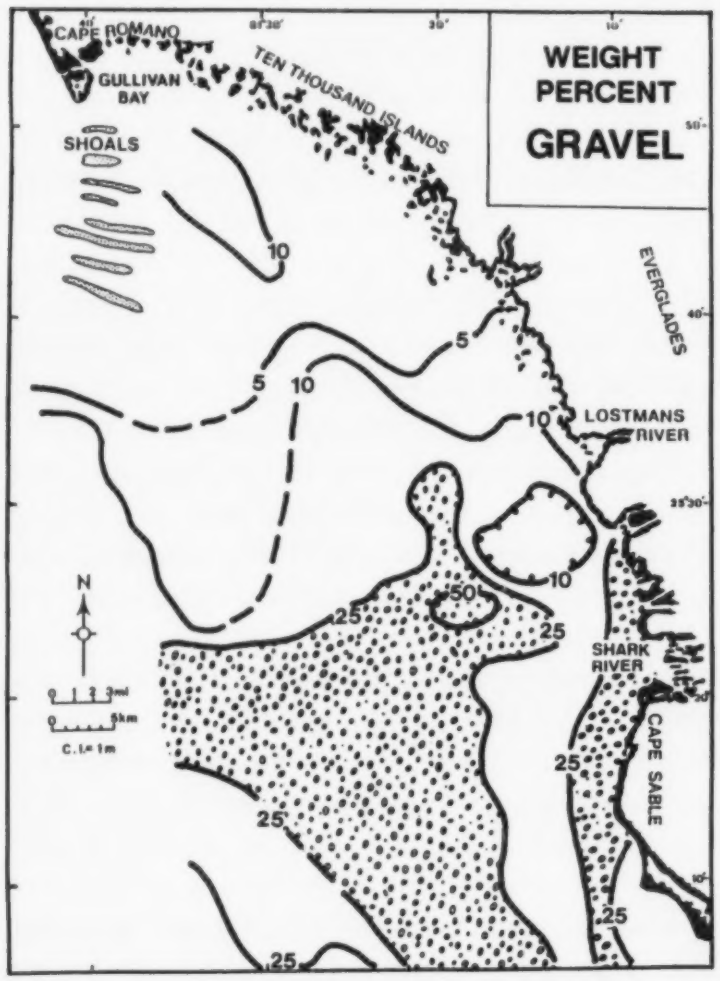

Fig. 3. Distribution of gravel size fraction in surface sediments. Areas of >25 percent are shown by the pattern.

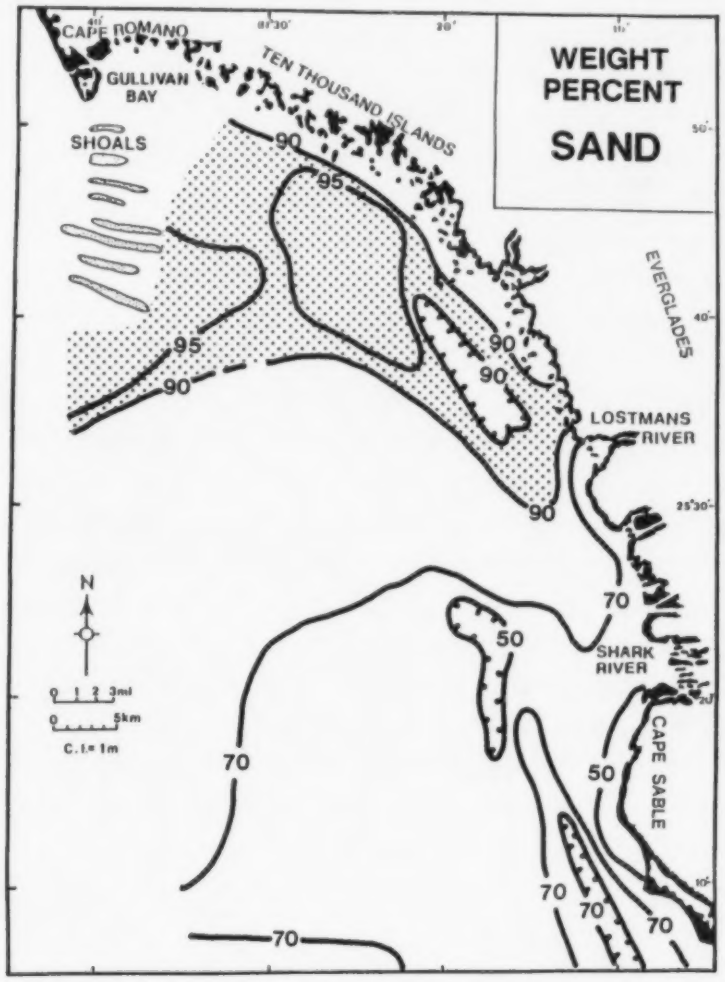

Fig. 4. Distribution of sand size fraction in surface sediments. Areas of >90 percent are shown by the pattern.

majority of the sand in the northern half of the area is very fine- to fine-grained with the exception of some local coarse patches of broken shell.

Nearly the entire study area is covered with sediments having over 50% sand with most being over 70% (Fig. 4). Both zones of less than 50% sand are essentially coast-parallel and are near Cape Sable.

The grain size of the sand fraction increases from fine to coarse from north to south. This change correlates with the change in composition from quartz to shell. The reasons for this increase are (1) not enough fine-grained quartz sand is transported south due to the overall low energy of the shelf and coast and (2) the occurrence of carbonate producing organisms increases toward the south.

Mud

The overall percentage of mud in the study area is quite low. The greatest concentration is along the coast and the abundance decreases sharply offshore (Fig. 5). Greatest concentrations are 10% mud in the northern coastal area with a band having up to 30% extending south from Lostmans River. Most of the southern coastal area contains 20% mud. Overall, the mud content offshore is low; about 5% or less. There is a noticeable increase in offshore mud in the southern part of the shelf, possibly due to the increase in abundance of carbonate mud-producing algae such as *Penicillus* and *Udotea*.

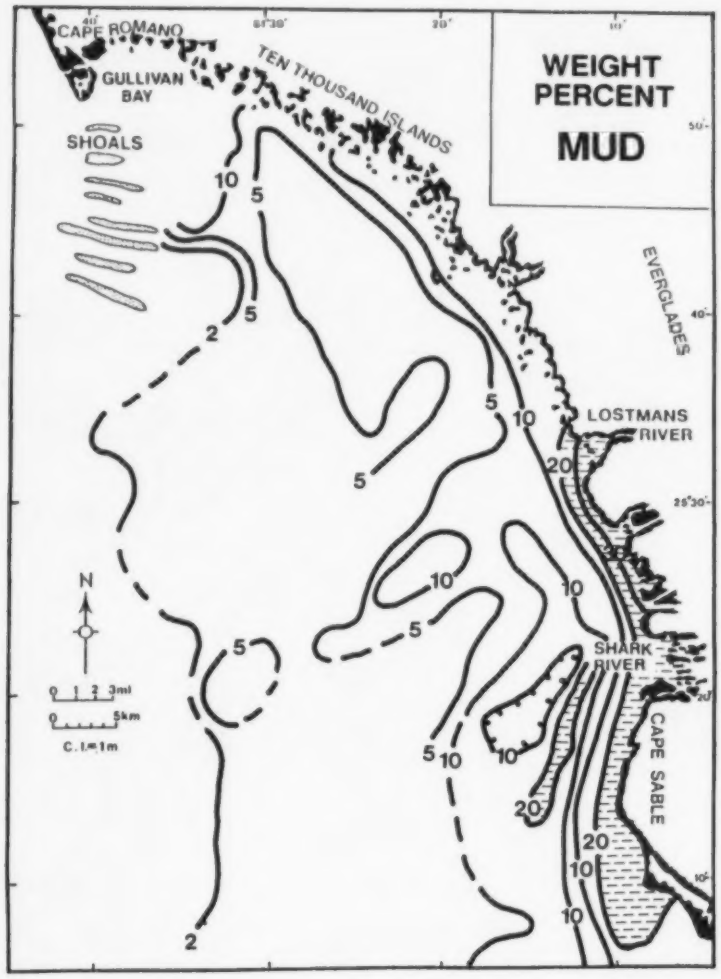

Fig. 5. Distribution of mud size fraction in surface sediments. Areas of >20 percent are shown by the pattern.

Textural patterns

Gravel is biogenic and is typically autochthonous. Few shells or shell fragments showed evidence of significant transport. The pattern of distribution of this constituent of the sediments is therefore a reflection of the distribution of the other two sediment modes, both of which are transported into and throughout this shelf environment.

Perlmutter (1982) found that currents produced by tides or waves under normal conditions were not strong enough to transport most of the quartz sand in the Ten Thousand Islands area. This is in agreement with observations made by Jewell (1987) near the Cape Romano shoals and with those made in this study. The net flood dominance of tidal currents during the passage of cold fronts does, however, result in the flushing of sediments through the shoals at Cape Romano into Gullivan Bay. The main physical processes that are capable of transporting significant amounts of sediment in this area are therefore, the currents associated with winter frontal passage or hurricanes.

The formation of the lobe of sand which extends to Cape Sable (Fig. 4) is probably due to the currents produced by winter frontal systems, which travel from the northwest to the southeast. The winds associated with these systems produce waves and longshore currents along the coast beyond the shadowing effect of Cape Romano.

A southerly extending lobe of mud (Fig. 5) is more or less similar in distribution to the sand lobe but its origin is somewhat different. Although mud is most abundant along the shoreline, there is a much greater concentration of mud in the southern half of the coast than in the north. This

results from the combination of coastal geomorphology and both biological and physical processes. In the northern half of the area the coast is dominated by a complex of coastal mangrove islands with numerous tidal channels that separate the rivers and their discharge from the open marine shelf. In the southern half of the coast in question the rivers discharge directly into the open marine environment. The mangrove–tidal channel complex on the north is characterized by abundant oyster and vermitid reefs (Shier, 1969; Parkinson, 1989). Both of these communities, but especially the oysters, take large volumes of suspended mud from the water column during the feeding process and produce large quantities of pelleted mud as a result. In addition, much fine sediment is physically trapped by oyster reefs, mangrove prop root systems and other obstructions as it moves from land into this coastal complex. The net effect is a large reduction in the amount of fine sediment that is transported to the open marine environment.

This phenomenon is less significant in the southern half of the coastal area because rivers empty directly into the open marine environment and there are fewer reefs to capture suspended fine sediment. The result is a different coastal mud pattern in each area and the difference is only partially related to marine coastal energy. The lobe of mud that extends across most of Cape Sable (Fig. 5) is the result of the northerly frontal-driven currents that move north to south in the winter.

Composition

Three main compositional groups of minerals comprise the sediments on the inner shelf off southwest Florida: (1) biogenic carbonate, both aragonite and calcite, (2) quartz and (3) clay minerals. Organic debris is also a minor but important constituent and siliceous diatoms are probably present based on previous studies (Perlmutter, 1982). Composition was determined by considering all gravel as carbonate; lithic fragments are rare. Sand was assumed to be all carbonate and quartz. It was treated with acid to remove carbonates and the relative abundance of carbonate and quartz was determined. Mud was heated to remove the organic debris and was then acidized to remove carbonate. The remainder was not analyzed for its quartz and clay mineral ratio.

Quartz

As expected, the quartz and carbonate contents of the surface sediments show a generally reciprocal relationship with quartz being the dominant fraction in the north and carbonate being dominant in the south (compare Figs. 6 and 7). Quartz was present in every sample analyzed but was $<2\%$ in the southwest corner of the study area (Fig. 6).

Nearly all of the quartz enters this shelf area via longshore transport along the barrier system to the north. A minor and undetermined amount is contributed by reworking of Pleistocene and Pliocene limestones (Enos and Perkins, 1977). Some mud-sized quartz may enter as runoff from the adjacent land including the coastal mangrove communities. All of the observed quartz in the study area is fine sand ($2–3\phi$).

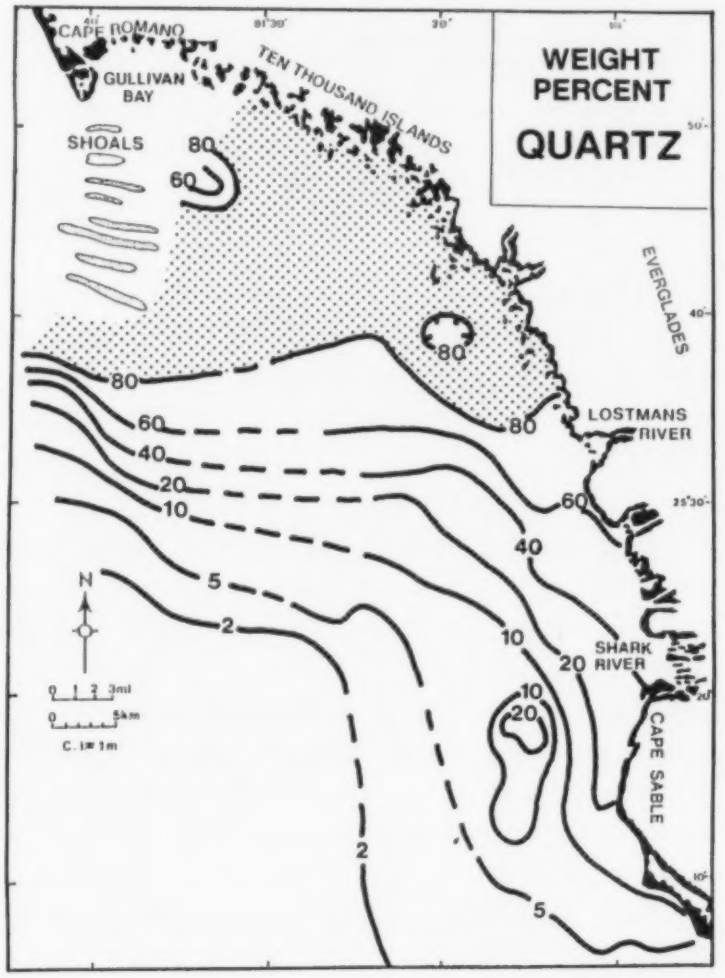

Fig. 6. Distribution of quartz fraction in surface sediments. Areas of >80 percent are shown by the pattern.

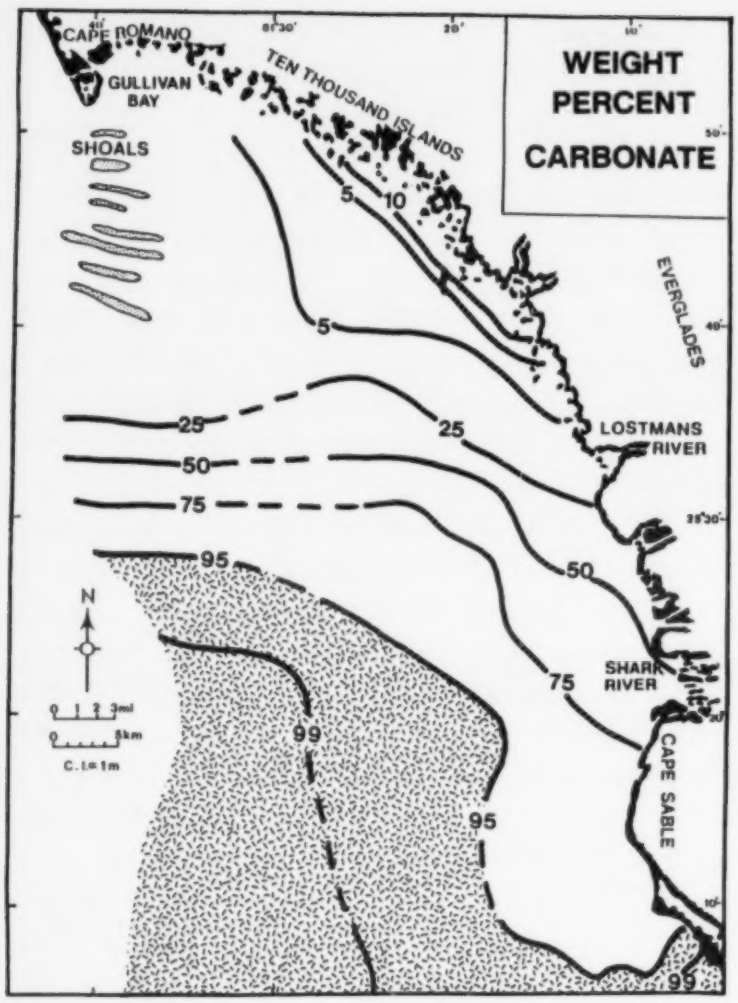

Fig. 7. Distribution of carbonate fraction in surface sediments. Areas of >95 percent are shown by the pattern.

Carbonate

The gravel sized carbonate is dominated by mollusk shells; primarily bivalves and gastropods. By far the most prevalent taxon is the bivalve *Chione*. Also commonly present are barnacles (*Balanus*), bivalve families Lucinidae, Semelidae and Arcidae, gastropods (*Turritella exoleta* and *Vermetus)*, oysters (*Crassostrea virginica*, *Ostrea*, and *Plicatula*), scaphopods (*Dentalium*) and the clams *Mercenaria* and *Tagelus*.

Carbonate-producing algae are common south of about latitude 25°30' but are rare to the north, probably due to a combination of water temperature, suspended sediment and bottom stability. The major taxon is *Halimeda*, which is mainly a producer of fine gravel and sand-sized sediment. The other carbonate producing algae are *Udotea* and *Penicillus*, which yield mud-sized carbonate particles. Sand-sized carbonate is also abundant and is comprised of broken pieces of the above taxa as well as foraminifera.

Organic material

The overall weight percentage of organic matter in the sediments is very low. Highest values are along the coast and range from 0.5 to 2.0% by weight (Fig. 8). This distribution closely parallels the highest concentrations of mud (Fig. 5). A distinct difference between the northern and southern coastal areas is shown. Another area of relatively high organic content is on the south end of Gullivan Bay at the north end of the study area, also showing a close parallel with the total mud (cf. Figs. 5 and 8).

If only the mud fraction is considered, the organic content shows a remarkably constant pattern throughout the inner shelf area. Essentially all samples, regardless of overall mud content, showed 4–6% organic matter in the mud. This suggests that the organic matter is being carried

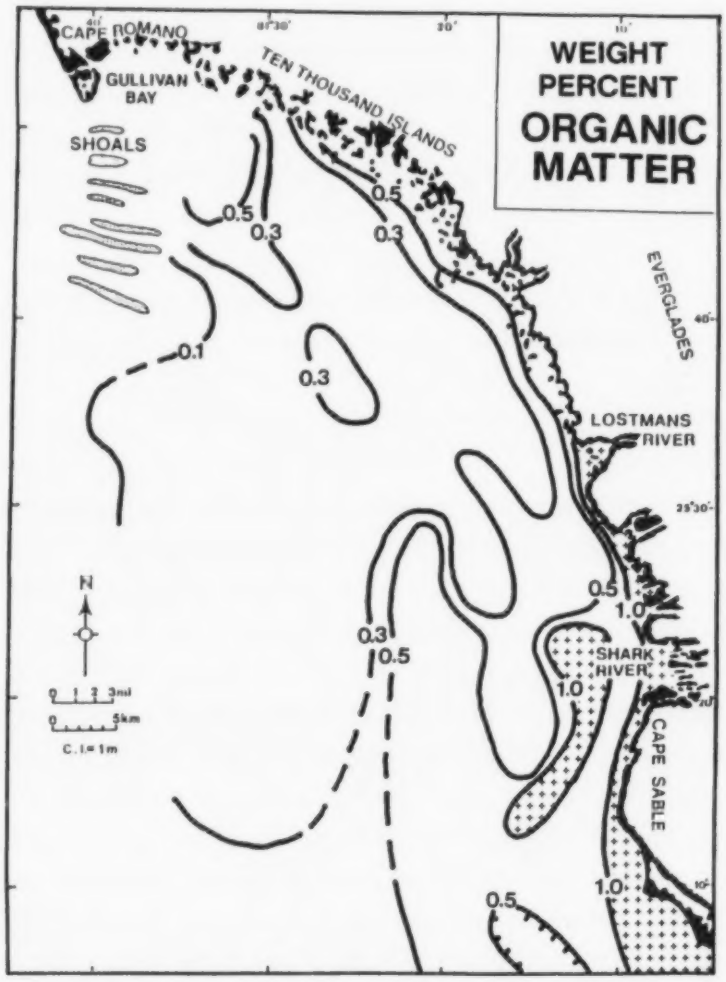

Fig. 8. Distribution of total weight percent organic matter. Areas of >1 percent are shown by the pattern.

into the marine environment with the mud, and that it is moving through the study area with the mud, rather than being produced by the benthic community on the shelf.

Distribution

The most important and obvious trend in composition of surface sediments in this area is the change from quartz-dominated to nearly pure carbonate from north to south. This zone of transition is only a few kilometers wide and has a NW–SE trend just north of latitude 25°31' (Figs. 6 and 7). Along the coast this transition occurs much farther south due to a lobe of quartz sand and mud that has been transported almost to Cape Sable.

The overall patterns result from a general absence of quartz in the southern area. Mud is restricted to the low energy coast where it is received from the mainland and biogenic shell is produced throughout the inner shelf.

Summary

Although the southwest Florida shelf area has long been known as an area where shelly quartz sand gives way to pure biogenic sand, this study provides the first systematic and detailed documentation of that transition. The transition is rather abrupt over only a few kilometers (Fig. 9) due to the slow encroachment of quartz sand from the north.

Along the adjacent shoreline there is quite a different textural and compositional pattern. Abundant terrigenous sand is carried, presumably by longshore currents, almost to Cape Sable. This is overprinted by the abundance of mud along the coast (Fig. 9); a modest amount on the north and more than twice that on the south. The great difference is due to coastal morphology and biological processes interacting with suspended sediments.

These data provide important information on one of the best modern analogs for ancient epeiric, mixed-composition shelf seas. They will be helpful in constructing actualistic stratigraphic models and can provide three-dimensional information on sediment facies for such models.

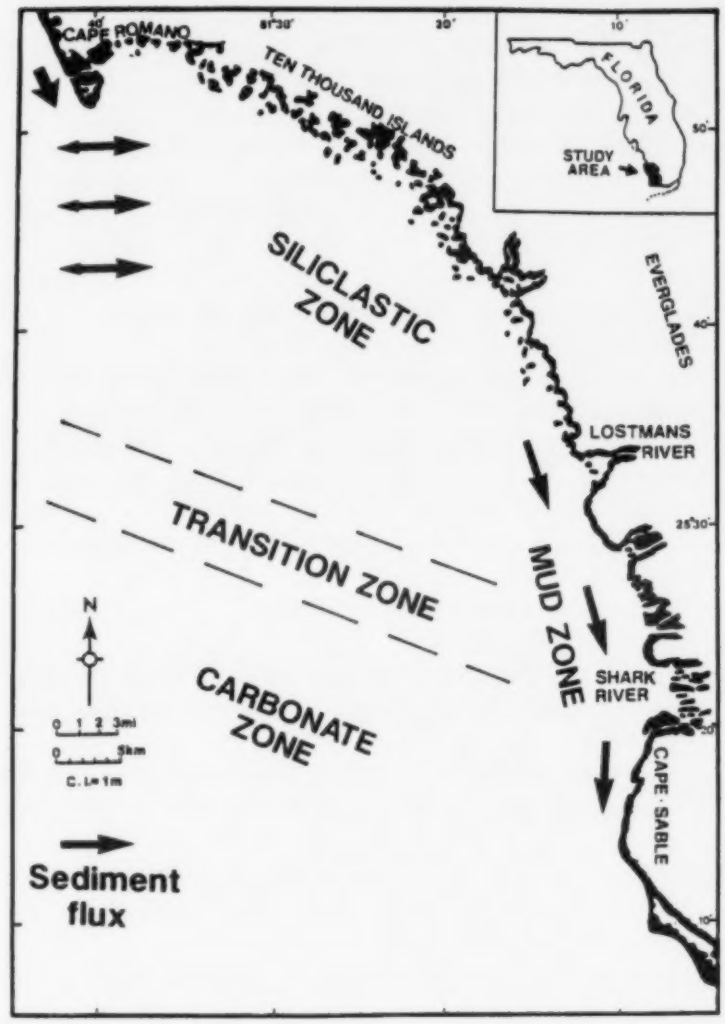

Fig. 9. Generalized summary map of the surface sediments of the southwest Florida shelf embayment showing major sediment flux paths and surface sediment facies patterns.

Acknowledgements

This paper was written and compiled by Davis from the masters thesis of Sussko. Financial support for the project came primarily from the Gulf Coast Section-SEPM and the Department of Geology at the University of South Florida. Ship time for the offshore sampling was provided by a grant from the Florida Institute of Oceanography. Special gratitude is expressed to the numerous geology students at USF who helped in the field.

References

Bebout, D.G. and Loucks, R.G. (Editors), 1977. Cretaceous carbonates of Texas and Mexico. Univ. Texas, Bur. Econ Geol., Rep. 89.

Davis, R.A., Jr., 1966. Willow River Dolomite; Ordovician analog to modern algal stromatolite environments. J. Geol., 74: 908–923.

Davis, R.A., Jr., 1989. Morphodynamics of the west Florida barrier system: the delicate balance between wave- and tide-

domination. In: W.J.M. van der Linden, S.A.P.L. Cloetingh, J.P.K. Kaasschieter et al. (Editors), Coastal Lowlands: Geology and Geotechnology. Proc. Symp. KNGMG. (The Hague, May 23–27, 1987.) Kluwer, Dordrecht, pp. 225–235.

Dott, R.H., Jr. and Byers, C.W., 1981. SEPM research conference on modern shelf and ancient cratonic sedimentation—The orthoquartzite-carbonate suite revisited. J. Sediment. Petrol., 51: 329–347.

Doyle, L. and Roberts, H.H. (Editors), 1987. Carbonate–Clastic Transitions. (Developments in Sedimentology, 42.) Elsevier, Amsterdam, 304 pp.

Enos, P. and Perkins, R.D., 1977. Quaternary sedimentation in South Florida. Geol. Soc. Am. Mem., 147, 198 pp.

Gebelin, C.D., 1977. Dynamics of Recent Carbonate Sedimentation and Ecology, Cape Sable, Florida. Brill, Leiden, The Netherlands, 120 pp.

Heckel, P.W., 1972. Recognition of ancient shallow marine environments. In: J.K. Rigby and W.K. Hamblin (Editors), Recognition of Ancient Sedimentary Environments. SEPM Spec. Publ., 16: 226–286.

Holmes, C.W., 1985. Accretion of the South Florida Platform, Late Quaternary Development. Am. Assoc. Pet. Geol. Bull., 69: 149–160.

Holmes, C.W. and Evans, R.G., 1963. Sedimentology of Gullivan Bay and vicinity, Florida. Sedimentology, 2: 189–206.

Inden, R.F. and Moore, C.H., 1983. Beach environment. In: P.A. Scholle, D.G. Bebout and C.H. Moore (Editors), Carbonate Depositional Environments. Am. Assoc. Pet. Geol. Mem., 33: 212–265.

Irwin, M.L., 1965. General theory of epeiric clear water sedimentation. Am. Assoc. Pet. Geol. Bull., 49: 445–459.

Jewell, P., 1987. Morphodynamics of tidal sand ridges, southwest Florida shelf. M.S. Thesis, Univ. South Florida, Tampa, (Unpubl.).

Klay, J.M., 1989. Stratigraphy of tidal sand ridges, southwest Florida shelf. M.S. Thesis, Univ. South Florida, Tampa, (Unpubl.).

Ostrom, M.E., 1964. Pre-Cincinnatian Paleozoic cyclic sediments in the Upper Mississippi valley. In: Symposium on Cyclic Sedimentation. Kansas Geol. Surv. Bull., 69(2): 381–398.

Parkinson, R.W., 1989. Decelerating Holocene sea-level rise and its influence on southwest Florida coastal evolution: a transgressive/regressive stratigraphy. J. Sediment. Petrol., 59: 973–996.

Perlmutter, M.A., 1978. Storm produced layering in the bays, lagoons, and channels of southwest Florida. Geol. Soc. Am., Abstracts Programs, 10: 470.

Perlmutter, M.S., 1982. The recognition and reconstruction of storm sedimentation in the nearshore, southwest Florida. Ph.D. Dissert., Univ. Miami.

Roberts, H.H., Whelan, R. and Smith, W.G., 1977. Holocene sedimentation at Cape Sable, South Florida. Sediment. Geol., 18: 25–60.

Scholl, D.W., 1964. Recent sedimentary record in mangrove swamps and rise in sea level over the southwestern Florida coast. Mar. Geol., 1: 344–366.

Scholl, D.W. and Stuiver, M., 1967. Recent submergence of southern Florida: a comparison with adjacent coasts and other eustatic data. Geol. Soc. Am., 78: 437–454.

Scholl, D.W., Craighead, F.C. and Stuiver, M., 1969. Florida submergence curve revisited: its relation to sedimentation rates. Science, 163: 562–564.

Scholle, P.A., Bebout, D.G. and Moore, C.H. (Editors), 1983. Carbonate Depositional Environments. Am. Assoc. Pet. Geol. Mem., 33, 708 pp.

Shier, D.E., 1969. Vermetid reefs and coastal development in the Ten Thousand Islands, southwest Florida. Geol. Soc. Am. Bull., 80: 485–508.

Spackman, W., Scholl, D.W. and Taft, W.H., 1964. Environments of coal formation in southern Florida. Geol. Soc. Am. Guidebook for Annu. Meet., Univ. Miami Press, 67 pp.

Taft, W.H. and Harbaugh, J.W., 1964. Modern carbonate sediments of southern Florida, Bahamas, and Espiritu Santo Island. Stanford Univ. Publ., 8, 133 pp.

Tanner, W.F., 1960. Florida coastal classification. Trans. Gulf Coast Assoc. Geol. Soc., 10: 259–266.

Tanner, W.F., 1961. Mainland beach changes due to Hurricane Donna. J. Geophys. Res., 66: 2265–2266.

U.S. Naval Weather Command, 1975. Summary of synoptic meteorological observations, eastern Gulf of Mexico.

Wanless, H.R., 1982. Editorial: Seal level is rising—so what? J. Sediment. Petrol., 52: 1051–1054.

Wescott, W.A., 1982. Depositional setting and history of the Tar Springs Sandstone (Upper Mississippian), southern Illinois. J. Sediment. Petrol., 52: 353–366.

Marine Geology, 107 (1992): 61–79
Elsevier Science Publishers B.V., Amsterdam

Quaternary sequence stratigraphy of the Brisbane River delta, Moreton Bay, Australia

Kenneth G. Evans[a], Andrew W. Stephens[b] and Graham G. Shorten[a]

[a]*School of Geology, Queensland University of Technology, 2 George Street, Brisbane, Qld 4000, Australia*

[b]*Queensland Department of Resource Industries, Mary Street, Brisbane, Qld 4000, Australia*

(Received May 15, 1991; revision accepted January 20, 1992)

ABSTRACT

Evans, K.G., Stephens, A.W. and Shorten, G.G., 1992. Quarternary sequence stratigraphy of the Brisbane River Delta, Moreton Bay, Australia. *Mar. Geol.*, 107: 61–79.

The Quarternary geological history of the Brisbane River delta front and prodelta was interpreted using seismic stratigraphic and sequence stratigraphic principles. During the last major glacial sea level episode, the floor of the bay was exposed and eroded by stream channels. In the subsequent postglacial marine transgression, the palaeochannels of the Brisbane and Pine Rivers were backfilled with mud. Sea level continued rising until about 6500 years ago and a highstand has persisted since then. During the Quarternary, sediment deposition in Moreton Bay was controlled by sea-level fluctuations, channel migration, and palaeotopography. There were at least four depositional episodes prior to the last glacial period, plus the present postglacial episode. Periods of low sea level occurred between highstands and the sea bed exposed and eroded. Eight major *seismic reflectors* were recognised and six *seismic sequences* defined. The seismic sequences represent five highstand systems tracts and one transgressive systems tract. The relationships between eustacy and system tract type were applied to glacio-eustatic sea-level curves to determine relative ages of sequences in Moreton Bay. The application of sequence stratigraphy to high frequency sea-level fluctuations was demonstrated. The stratigraphic system established within the context of sequence stratigraphy will provide a reference for future work within the region.

Introduction

Moreton Bay is fed by four rivers and several small creeks and streams. The bay is 80 km long and is open to the ocean at four locations (Southport, Jumpinpin, South Passage, and North Entrance). It is a narrow passageway, 5 km wide, in the south, and a broad expanse of water, 35 km wide, in the north enclosed by dune-island barriers on the east and the mainland on the west.

The Brisbane River enters Moreton Bay in the northwest. The influx of sediments from the river to the bay has caused an offshore delta front and prodelta to develop over an area of about 300 km^2. Together, the delta front and prodelta of the Brisbane River form the seabed of Moreton Bay from St. Helena Island in the south, Mud Island in the east, to Bramble Bay in the northwest. In Bramble Bay the prodelta merges with the Pine River delta subaqueous plain. The seabed resulting from this development comprises a planar submarine surface over the study area (Fig.1). The prodelta of the Brisbane River is asymmetrical about the mouth of the river. It has an elongate surficial distribution extending to the north (Jones and Stephens, 1981).

Pleistocene erosional surfaces of compact weathered clay developed during low sea-level periods. These surfaces and submarine sediment zones were recognised from coring and seismic profiling programmes within in the bay (Hekel et al., 1976; Jones et al., 1978; Searle et al., 1986).

The present day shoreline of northern Moreton

Correspondence to: K.G. Evans, Environment Section, Energy Division, Department of Resource Industries, G.P.O. Box 194, Brisbane, Qld 4001, Australia.

0025-3227/92/$05.00

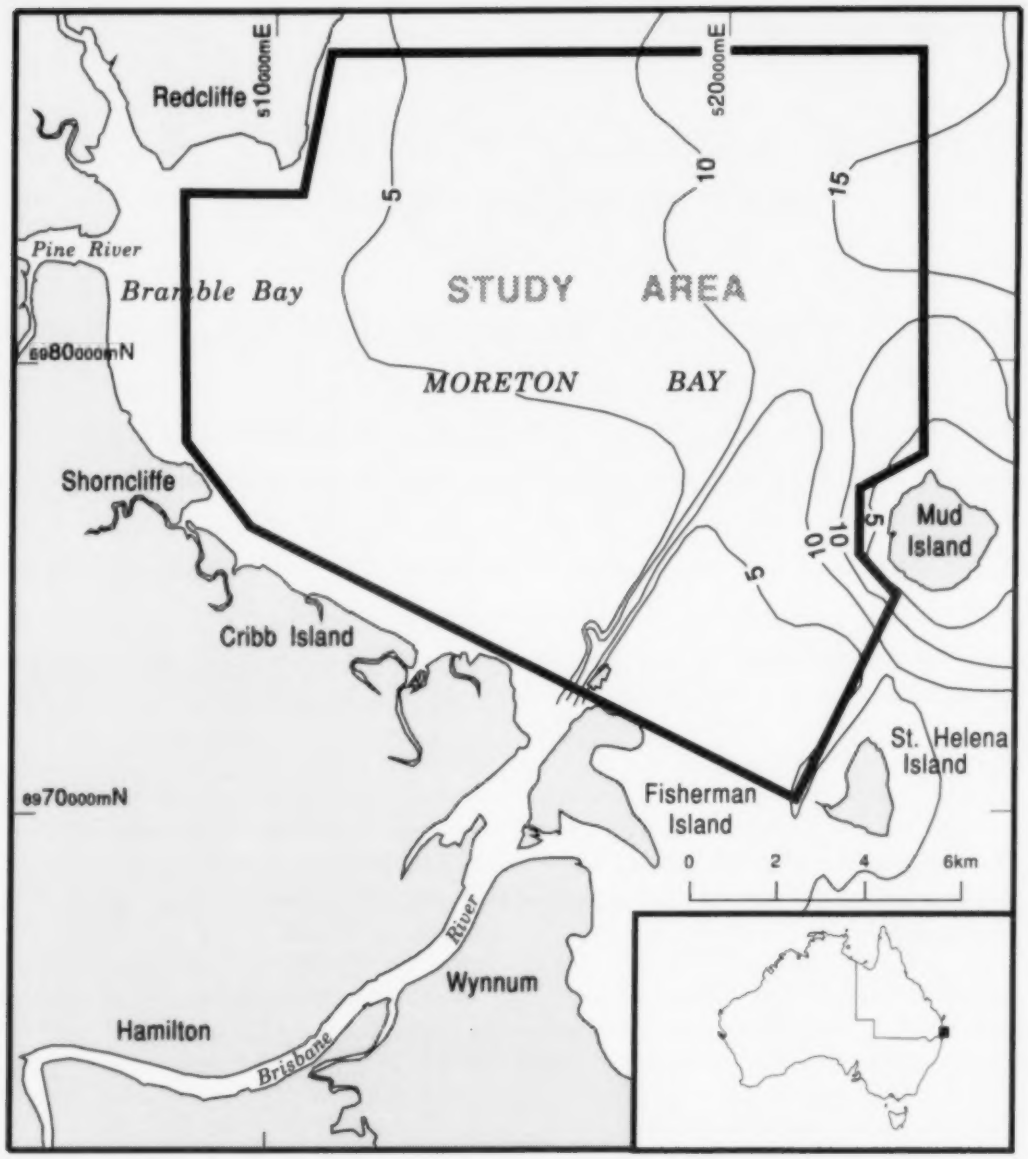

Fig.1. Map showing the location of the study area. Bathymetric contours are shown in metres.

Bay has prograded decreasing the area of the bay since the end of the postglacial marine transgression 6000 yr B.P. (Hekel et al., 1979).

Jones and Stephens (1981) considered that sea level fluctuations "... exerted a major influence on the type and location of sedimentary facies". They defined five Holocene depositional environments which resulted from the relatively constant sea level of the last 6500 years. These environments are: delta front, with deposits consisting of sand and muddy sand at the mouth of the Brisbane and Pine Rivers; prodelta, with deposits which are mainly mud and extend to the west along the front of the present western shoreline of the bay to the north of the Brisbane River mouth; coral reef, fringing bay islands; tidal deltas at the North Entrance and South Passage; and a zone of minimal deposition in the central part of the bay.

The objectives of this investigation were to:

(1) Determine the sequence stratigraphy of the Brisbane River delta front and prodelta using seismic stratigraphic principles.

(2) Interpret the Quaternary sedimentary history of the study area.

(3) To assess the application of sequence stratigraphy to high frequency sea-level fluctuations.

Geological setting

The Moreton Bay region has five main structural elements. These are the Palaeozoic South and North D'Aguilar Blocks, the Mesozoic Nambour and Ipswich Basins, and the Cainozoic Petrie Basin. The Palaeozoic basement consists of the Bunya Phyllite and the Neranleigh–Fernvale Beds of the Devonian–Carboniferous South D'Aguilar

Block, and the Rocksberg Greenstone of the Carboniferous–Permian North D'Aguilar Block (Grimes et al., 1986). Unconformably overlying the basement metamorphics are units of the Ipswich Basin consisting of shales, conglomerates and volcanics.

The larger part of northern Moreton Bay is underlain by the Triassic–Jurassic Woogaroo Subgroup and the Landsborough Sandstone. These units of the Nambour Basin crop out along much of the upland areas of the mainland shore of the study area. In the southwest they are unconformably overlain by the sediments and volcanics of the Tertiary Petrie Formation which crop out over most of the Redcliffe Peninsula. This formation also crops out along upland edges of the Brisbane River delta subaerial plain and St. Helena Island (Jones et al., 1978; Grimes et al., 1986).

The remainder of the area is covered by Quaternary sediments which have been deposited in a variety of environments including fluvial, estuarine, and marine (Hekel et al., 1976; Jones et al., 1978; Jones and Stephens, 1981; Grimes et al., 1986; Searle et al., 1986; Jones and Holmes, 1986).

Onshore to the southwest of the study area the Brisbane River is restricted to a river gorge by Palaeozoic metamorphics. The gorge opens out and marginal slopes of the bay shore have developed on the less resistant Mesozoic and Tertiary sediments. Moreton Bay itself has been cut in to the relatively soft rocks of the Petrie and Nambour Basins and partially infilled with Quaternary sediments. Moreton Bay has been impounded on the east by the Quarternary dune-island barriers, North Stradbroke Island and Moreton Island. These islands are drowned island barriers lying across the continental shelf and anchored by Mesozoic erosional highs (Stephens, 1982; Kelly and Baker, 1984).

Methods

Seismic data were collected during April 1990 and July 1990 using a Uniboom system consisting of a sound source, receiver, and graphic recorder. Figure 2 shows the location of the seismic lines completed during this investigation and lines completed during earlier investigations. Data were collected at a tow speed of about 4 knots (7.5 km/h) with the boomer firing at 0.5 s intervals. Vibrocores of soft sediments were taken at 10 offshore locations (Fig.3). The corer was driven by a pneumatic vibrator powered by an on-board air compressor. The depth of penetration was limited to the length of the 50 mm diameter aluminium core tube (6 m) and the stiffness of the sediments. Coordinates of each seismic fix and vibrocore location in this investigation were determined using two theodolites mounted on offshore navigation beacon platforms. Position fixes were recorded at approximately two minute intervals.

The Department of Resource Industries, Queensland, made available data that were collected during previous investigations in the area. These data included: all CSP records from the Boondall investigation interpreted by Searle et al. (1986) (Fig.2); CSP records from surveys conducted in northern Moreton Bay in 1974 and 1975 (Fig.2); and drillhole data from within the project area (Fig.3) (Hekel et al., 1976; Jones and Hekel, 1979).

The majority of data were reduced using manual methods. Major reflectors interpreted using data gathered during this investigation were correlated with the 1986 offshore Boondall and 1975 Moreton Bay data. The reduced levels [Australian Height Datum (AHD)] of the seabed and the selected reflector surfaces were determined. Two-way times were converted to depth using a seismic velocity through the soft sediment and water column of 1500 m/s (Searle et al., 1986). Calculations using limited data from drillhole 76/3 and 76/4 (Fig.3) give a seismic velocity of 1400 to 1500 m/s. The depth to each reflector and the sea bed was manually scaled at each fix from all available records. Tide and slant path corrections were applied to all seismic data.

Seismic stratigraphy

This investigation produced high quality CSP data which could be correlated with existing data to give an extensive coverage of the study area. Eight major reflectors were recognised and appear to be present on a regional basis. These reflectors are seismic sequence and seismic unit boundaries.

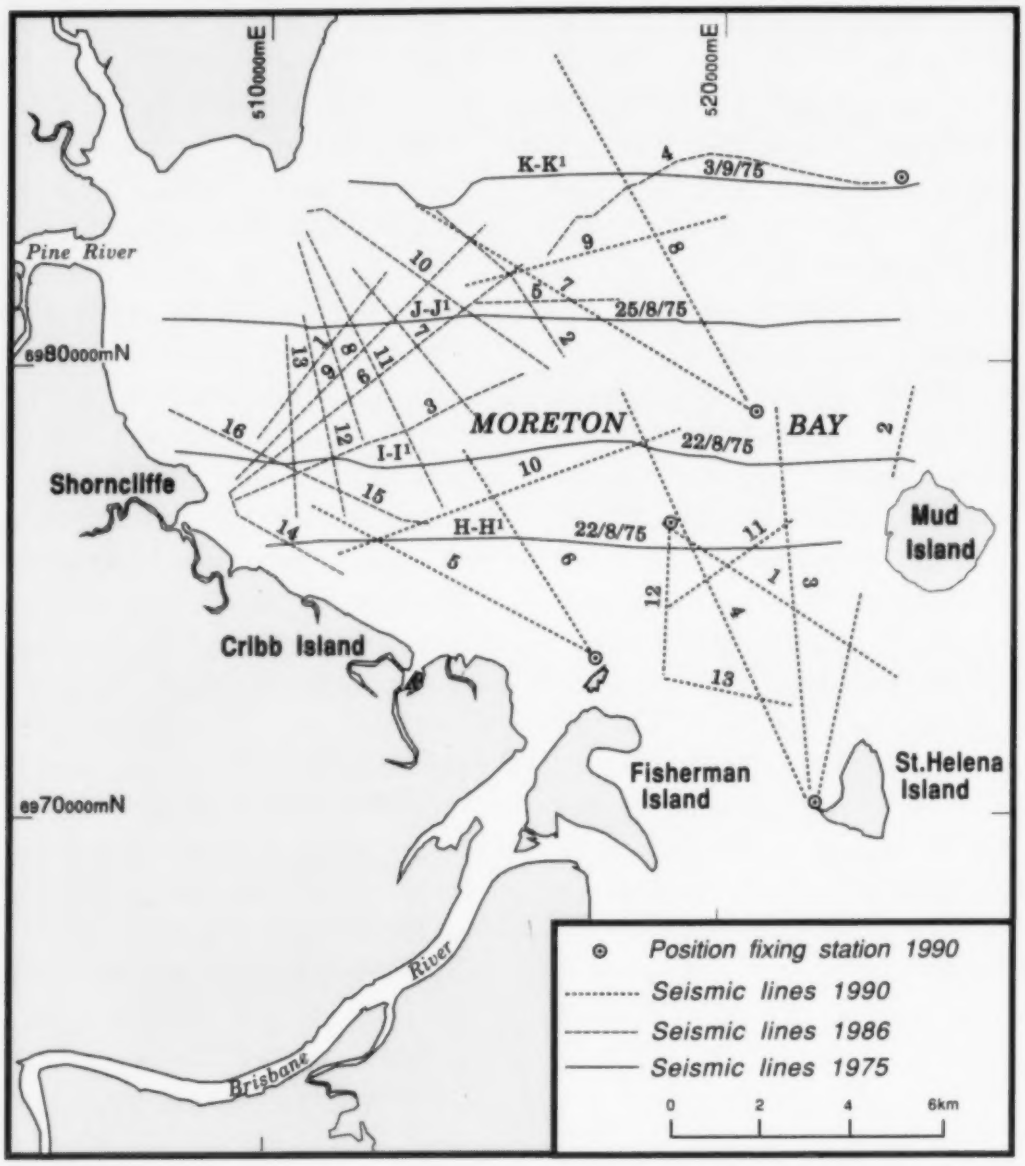

Fig.2. Location of seismic reflection lines within the study area.

The reflectors and the seabed define the boundaries of six seismic sequences, of which two have been further divided into five seismic units (Fig.4). Characteristics of seismic sequences are described in Table 1 and their signature can be seen in Figs.5, 6 and 7. Inferred ages of sequences are given in Table 2.

Interstitial gas

The presence of interstitial gas in postglacial sediments made interpretation of some lines difficult (Figs.5, 6 and 7). All seismic lines show areas where the seismic signature is opaque (Fig.5). A similar signature has been recognised elsewhere in Moreton Bay and the effect is thought to have been caused by the presence of interstitial methane gas that is biogenic in origin (Searle et al., 1986; Evans, 1991). The gas indicates that organic matter has been deposited during floods, under anaerobic conditions in fluvio–estuarine environments. Because of the opaque nature of the gas signature, it was necessary to interpolate the continuity of lower reflectors through the gas.

Seismic basement (sequences B — units Bf and Bw)

The deepest reflector (B1) is the bedrock surface. Quaternary sediments overly the contact between the Mesozoic Nambour and Cainozoic Petrie Basins. The boundary between the Mesozoic Nambour Basin and Cainozoic Petrie Basin could not be determined on the seismic sections. Reflector B1 represents the surface of the Tertiary Petrie

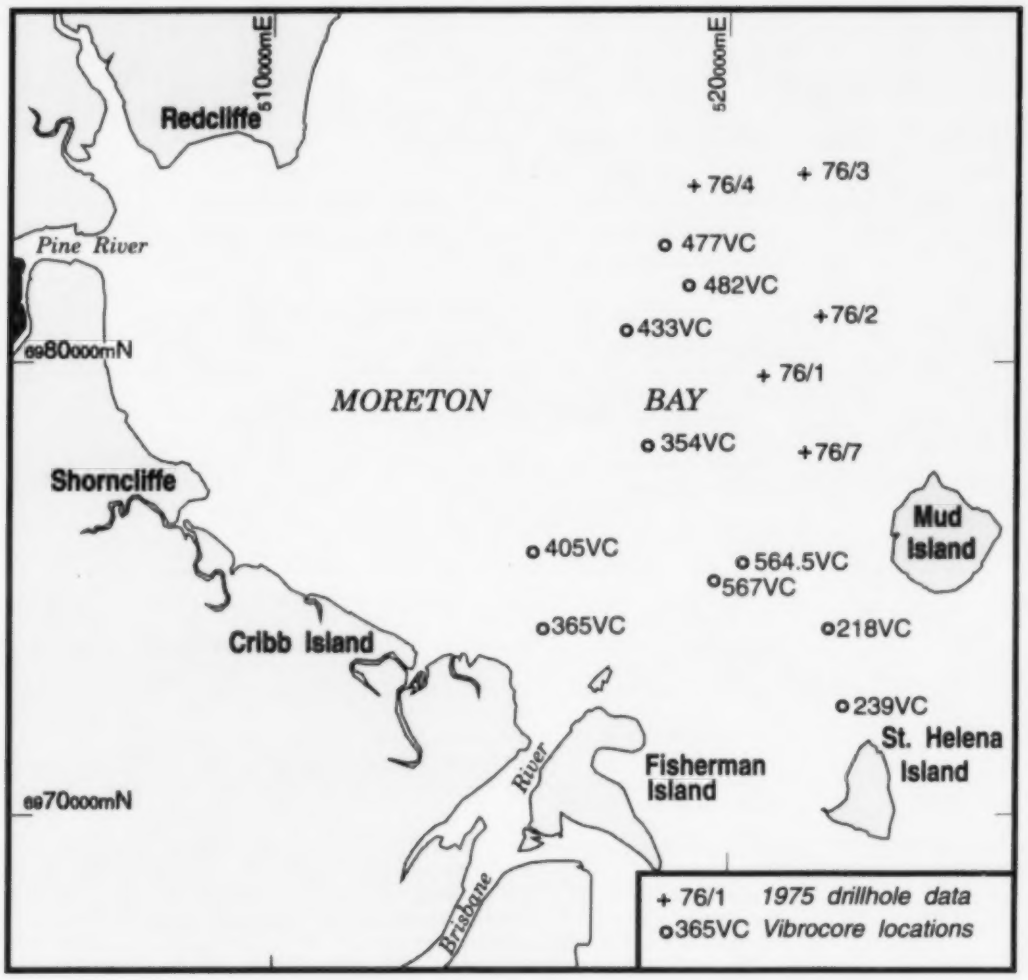

Fig.3. Vibrocore and drillhole locations within the study area.

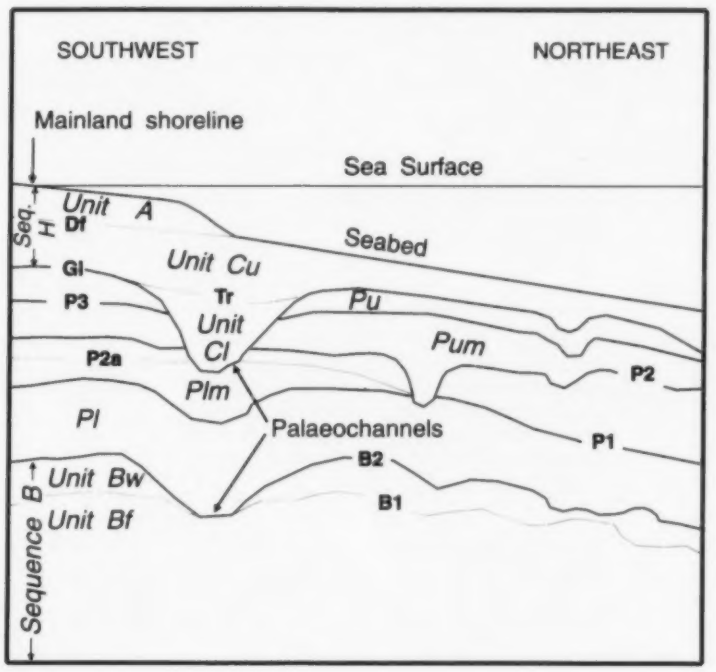

Fig.4. Schematic cross section showing the seismic sequences within the study area.

TABLE 1

Characteristics of seismic sequences in study area

Seismic Sequence	Seismic Unit	Maximum Thickness (m)	Location & Morphology	Internal Structure	Relationship	Interpretation
H	*A*	5	Laterally continuous proximal to Brisbane River mouth	Semi-transparent, weak, chaotic and hummocky.	Overlies sequence *Cu* between reflector Df and seabed.	Highstand prodgrading delta front dark grey, fine to medium, muddy sand to sand.
	Cu	11	Present over most of the area as sheet with thickest sections in palaeochannels. Upper surface forms the seabed distal from present shoreline.	Semi-transparent, opaque, turbid, sub-parallel, downlap onto reflector Tr and toplap onto upper surface.	Overlies sequence *Cl* in palaeochannels and sequence *Pu* elsewhere and is bounded at upper surface by the seabed distal from and reflector Df proximal to the present shoreline.	Highstand prodelta soft grey mud.
	Cl	15	Confined to palaeochannels incised in sequence *Pu*. Concavo-convex lenticular geometry at confluence of Pine and Brisbane River palaeochannels (Fig. 8). Upper surface does not exceed -4m at any place (Fig. 9).	Semi-transparent, opaque, turbid, well layered, distinct clinoform pattern, complex, wavy, divergent. Onlaps channel walls and toplaps or truncates at reflector Tr.	Infills palaeochannels incised in sequence *Pu* and underlies reflector Tr.	Transgressive fluvio-estuarine, grey, soft mud and muddy sand.
Pu		10	Thickest in palaeochannels and laterally extensive but seldom thicker than 5m over palaeo-interfluves. Upper surface subaerially exposed and eroded.	Semi-transparent, wavy, diverging toward base and onlapping channal walls. Even sub-parallel, chaotic, diffuse over interfluves.	Overlies sequence *Pum* between reflectors P3 and Gl.	Firm to stiff oxidised, mottled brown, green-grey and olive grey-green mud and muddy sand. Highstand prodelta and bay muds and transgressive channel fill.
Pum		15	Extends over most of the area. Thickest sections in palaeochannel fill areas. Irregularly drapes and mimics underlying topography. Upper surface subaerially exposed and eroded.	Semi-transparent, well layered, sub-parallel to parallel, diffuse.	Overlies sequence *Plm* between reflectors P2 and P3.	Similar to sequence *Plm*.
Plm		15	Extends over most of the area with thickest sheet sections in buried interfluves of palaeochannels. Irregularly, drapes and mimics underlying topography. Upper surface subaerially exposed, eroded and channelled.	Semi-transparent, strong, regular, parallel, well layered, sigmoidal, downlapping. Erosional truncation and internal erosion surfaces (reflector P2a, Fig. 7).	Overlies sequence *Pl* between reflectors P1 and P2.	Highstand marine prodelta mud overlying transgressive fluvio-estuarine channel fill.
Pl		15	Extends over most of the area as sheet and sinuous channel fill of variable thickness. Upper surface displays numerous erosion channels.	Parallel to sub-parallel, weak overlying chaotic, semi-transparent in topographic lows and channels.	Overlies bedrock sequences between reflectors B2 and P1.	Highstand marine prodelta mud, several episodes of subaerial exposure and desiccation, overlying transgressive fluvio-estuarine sand and gravel.
B	*Bw*	10	Irregular coverage over most of the area. Gullied and irregular upper surface.	Highly irregular, hummocky, discontinuous	Overlies acoustic basement. Between reflectors B1 and B2.	Weathered sediments and volcanics.
	Bf	unknown	Irregular coverage over most of the area.	Semi-transparent short weak, opaque.	Acoustic basement. Upper surface reflector B1.	Fresh sediments and volcanics.

Note. For relative ages see Table 2.

TABLE 2

Summary of relative ages of offshore seismic sequences and units

Age	Date (years B.P.)	Seismic sequence	Seismic unit
Holocene	0		
"stillstand"		*H*	*A*
	6,500		*Cu*
Postglacial	6,500		*Cl*
transgression	18,000		
Glacial	18,000		?
sea-level low	28,000		
Pre-glacial	28,000	*Pu*	
Pleistocene	138,000		
	170,000	*Pum*	
	240,000		
	318,000	*Plm*	
	340,000		
	>340,000	*Pl*	
Tertiary/		*B*	*Bw*
Mesozoic			*Bf*

Formation in the south and the surface of Triassic–Jurassic Woogaroo Subgroup or Landsborough Sandstone (seismic unit *Bf*) in the north. Engineering investigations (Coffey and Hollingsworth, 1966, 1972) indicate a deeply weathered surface on these units. It is thought that reflector B1 may be the base of the weathering profile (seismic unit *Bw*) and that the overlying reflector B2 is the surface of the weathering profile. The irregular nature of the reflector B2 indicates an erosional surface. Where B2 is not present, it is possible that the weathered overburden has been removed by erosion.

Pleistocene Pre-Glacial sequences

Four Pleistocene Pre-Glacial sequences were recognised, *Pl* (lower), *Plm* (lower middle), *Pum* (upper middle) and *Pu* (upper). The reflector at the base of the Pleistocene Pre-Glacial sequences is B2 — the weathered bedrock surface. Similar Pre-Glacial sequences have been recognised on the North Queensland shelf. Pleistocene reflectors representing erosional surfaces were recognised beneath the Glacial unconformity (Searle et al., 1981). Elsewhere, four acoustic facies have been identified in the Gulf of Patras, Greece (Chronis et al., 1991). In Ventura mainland shelf sediments, California, four Pre-Glacial Pleistocene formations have been recognised (Dahlen et al., 1990). In the Northern Tyrrhenian Sea five Late Pleistocene transgressive sequences have been recognized (Chiocci et al., 1991) but these have not been correlated with individual transgressions on available global sea-level curves.

Between fixes 468 and 477 (Fig.7) sequence *Pl* has upper weak reflectors generally parallel to reflector P1. These overly a weak, chaotic semi-transparent section filling topographic lows and channels. This probably results from coarse sediments deposited in fluvial and fluvio–estuarine conditions. Onshore, sand and gravel has been intersected in drillholes at a similar level in sediment units interpreted as having been deposited in fluvial and fluvio–estuarine environments (Evans, 1990).

The overlying weak, parallel reflectors result from deposition of fine sediments under marine conditions. The reflectors may have lost their strongly laminated character as a result of several episodes of subaerial exposure and desiccation (D.E. Searle, pers. commun., 1990).

Reflector P2a represents either an internal erosion surface or an hiatus in deposition within sequence Plm (Figs.6 and 7). Between fix 474 and fix 481 (Fig.7) reflector P2a is clearly seen. Near fix 478 the reflector truncates underlying reflectors, indicating erosion. Immediately overlying this surface is a sigmoidal pattern downlapping to the north onto the erosional surface. This indicates a progradation of sediments from the south. Near fix 475, reflector P2a becomes horizontal and parallels underlying and overlying sediments. Between the time the layer of sediment immediately below P2a was deposited in this area and the layer of sediment immediately above reflector P2a was deposited, the sediments in the prograding unit to the south were deposited. Therefore at fix 475 and to the north there was an hiatus in deposition on the P2a surface. There is no indication of the length of this hiatus and it may have resulted from relatively short term channel shifting. Reflector P2a may represent a transgressive surface developed as the shoreline transgressed during a sea-

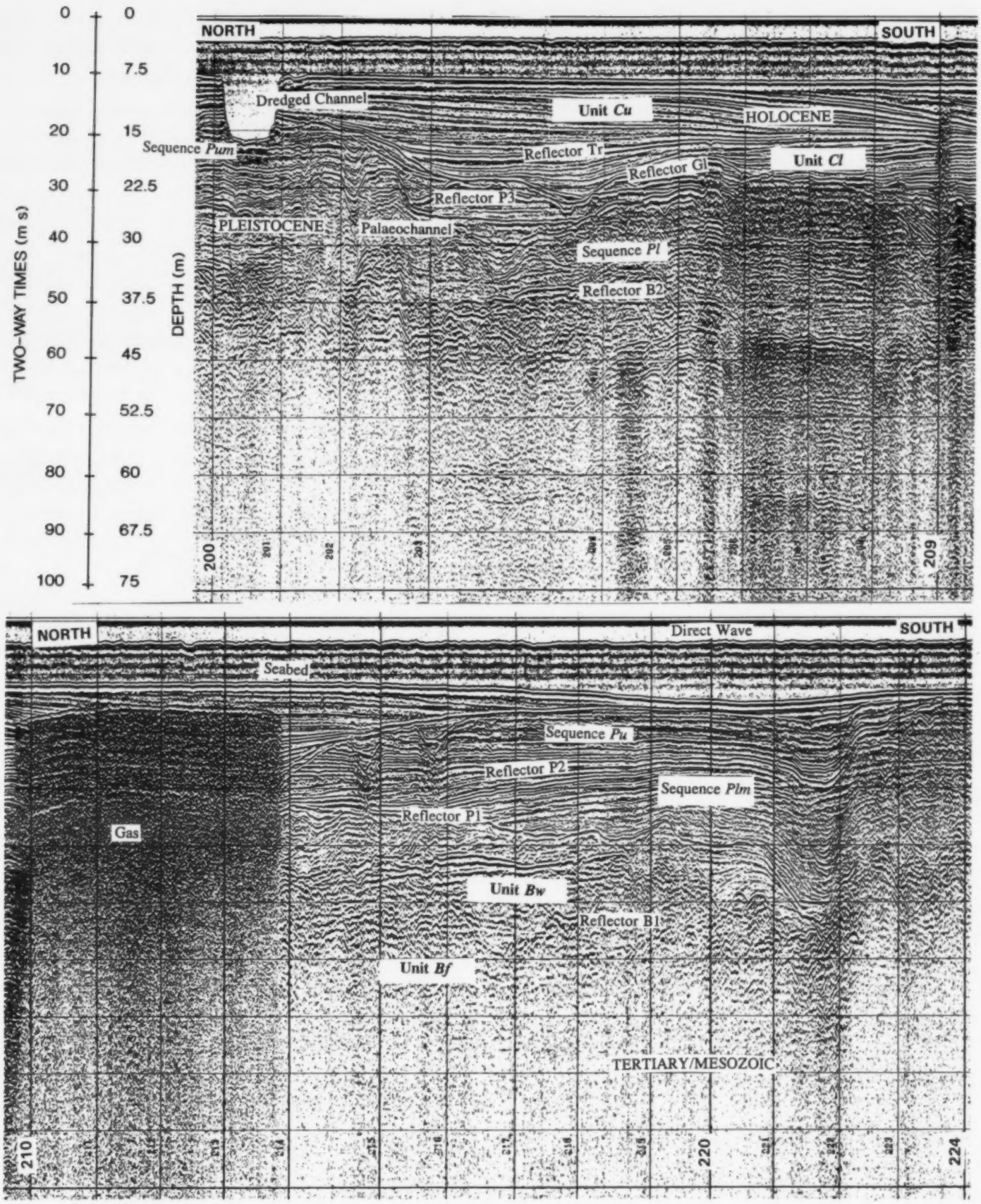

Fig.5. Interpreted profile of seismic reflection line 1, 1990, across the Brisbane River palaeochannel. The relationship of sequences is shown in Fig.4 and Table 2.

level rise. Its genesis can be compared with that of Postglacial reflector Tr and reflector T described by McMaster (1984) in his discussion of the Narragansett Bay system in Eastern U.S.A.

Draped reflectors in palaeochannels in sequence *Pum* may represent mud which has been compacted and de-watered. This is supported by drill data of Searle et al. (1986). The more diffuse

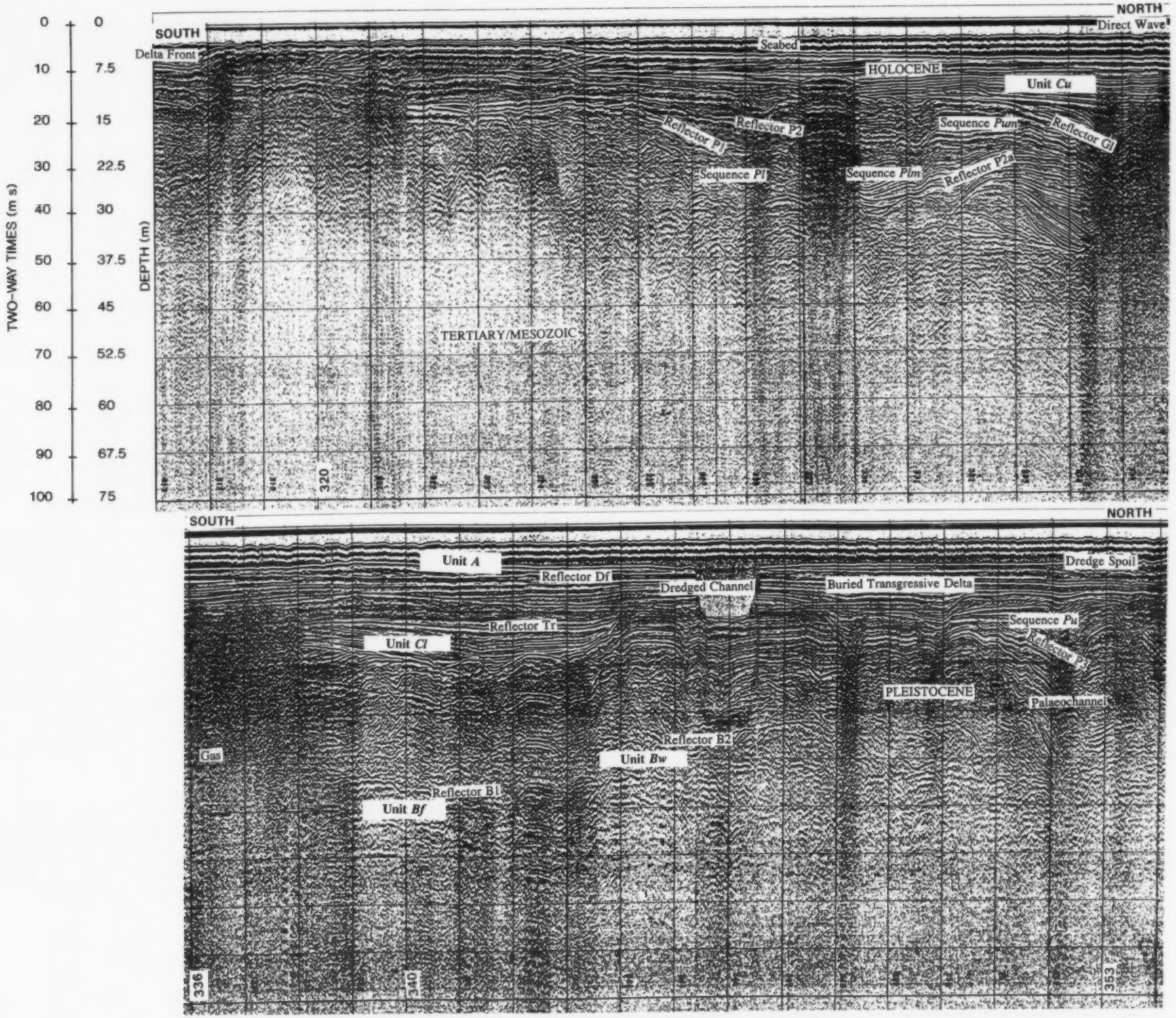

Fig.6. Interpreted profile of seismic reflection line 4, 1990. The relationship of sequences is shown in Fig.4 and Table 2.

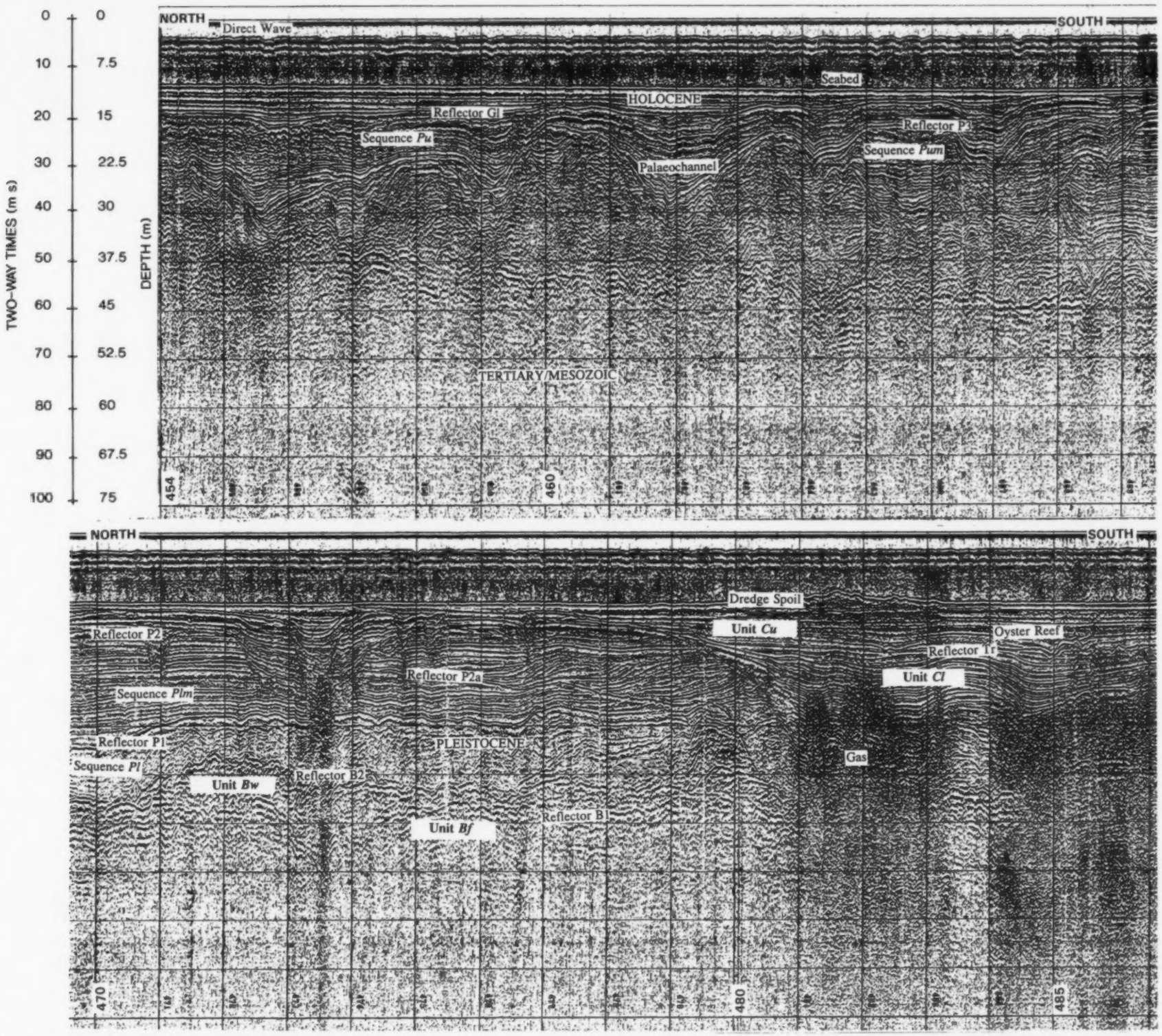

Fig.7. Interpreted profile of seismic line 8, 1990, in the vicinity of the confluence of the palaeo-Brisbane and Pine Rivers. The relationship of sequences is shown in Fig.4 and Table 2.

structures may represent coarser muddy sand, deposited in higher energy environments such as fluvial conditions. Over the interfluves, sequence *Pum* has a character very similar to sequence *Plm* and may have been deposited in a similar environment.

Reflector Gl

Reflector Gl represents the surface that was subaerially exposed and weathered during the Glacial low sea-level episode, 18 000 yr B.P., when sea level was at a glacio-eustatic minimum (Searle et al., 1986). A similar reflector has been recognised globally by numerous researchers (e.g. Searle et al., 1981, 1986; Searle, 1983; McMaster, 1984; Knebel and Scanlon, 1985; Chronis et al., 1991). The reflector has a strong, irregular and continuous character. Palaeochannels of the Brisbane and Pine Rivers have been incised in the surface. The Brisbane River palaeochannel is deeper than 40 m in some places. However, in most places the exact depth of the channels cannot be determined because reflector Gl is obscured by gas.

In many places reflector Gl truncates lower sequences and their respective bounding reflectors. Elsewhere, the surface appears channelled but Gl does not truncate lower sequences. Instead, the record shows nested channels where younger sediments have compacted and conformed with older topography (see Fig.7).

Figure 8 is a structural contour map of this Pleistocene surface. The offshore seismic data have been combined with onshore drillhole data (Evans, 1990) to give a regional indication of the surface morphology.

Postglacial sequence H (comprising seismic units A, Cu and Cl)

Three Postglacial seismic units (*A*, *Cu* and *Cl*) were recognised. The upper surface of these units is the seabed and the lower surface is reflector Gl. These units together, form seismic sequence *H*. Similar units are present in the Halifax Basin, North Queensland (Johnson and Searle, 1984) and in the Gulf of Patras, Greece (Chronis et al., 1991).

Toplap and truncation at the upper surface of the unit *Cl* indicate both an hiatus in deposition and erosion, possibly by submarine currents.

Reflector Tr defines the upper surface of unit *Cl*. It is strong and regular within the palaeochannel margins. This reflector truncates the upper internal reflectors of *Cl*, and although quite distinguishable on CSP records, cannot be recognised as a boundary in drillholes. Tr may represent a transgressive unconformity that has been developed by higher energy shoreline activity during rising sea level and correlates genetically with Green Island Reef reflector D (Searle et al., 1981) and Narragansett Bay System reflector T (McMaster, 1984). This surface grades steadily upward toward the present day shoreline (Fig.9).

Between fix 350 and fix 354 (Fig.6) there is a sub-unit which has short internal reflectors dipping steeply toward the south. This appears to be a transgressive delta front deposited on the older surface at the shallow channel margin in a higher energy environment and may indicate a slowing in the rate of sea-level rise.

At fix 485 (Fig.7) an irregularity in reflector Tr was observed. At these locations as well as on line 7 and line J–J′ there is a mound about 3 m high and about 100 m wide. This mound was intersected by vibrocore 433VC. The vibrocorer could not penetrate more than 4.2 m below the seabed. The base of the core tube was filled with disarticulated and broken shell material including mud oysters and mussels. The mounds are thought to be biohermal "oyster reefs" built up from shell deposits. Shell samples (radiocarbon laboratory sample number WK-1831) from vibrocore 433VC have a ^{14}C age of 2990 ± 61 yr [450 ± 35 yr has been subtracted to correct for reservoir effects (Gillespie, 1982)]. This suggests a minimum rate of deposition of the overlying unit, *Cu*, in the area of the bioherm as about 1.4 m/1000 yr.

In Fig.5 the internal reflectors of unit *Cu* become divergent within the Brisbane River palaeochannel margins and downlap onto the surface represented by reflector Tr. At the upper surface in this area the reflectors appear to toplap. This feature may represent a relative stillstand of sea level. The seismic structure indicates that the sediment source in this area is from the northwest and that the sink is toward the southeast.

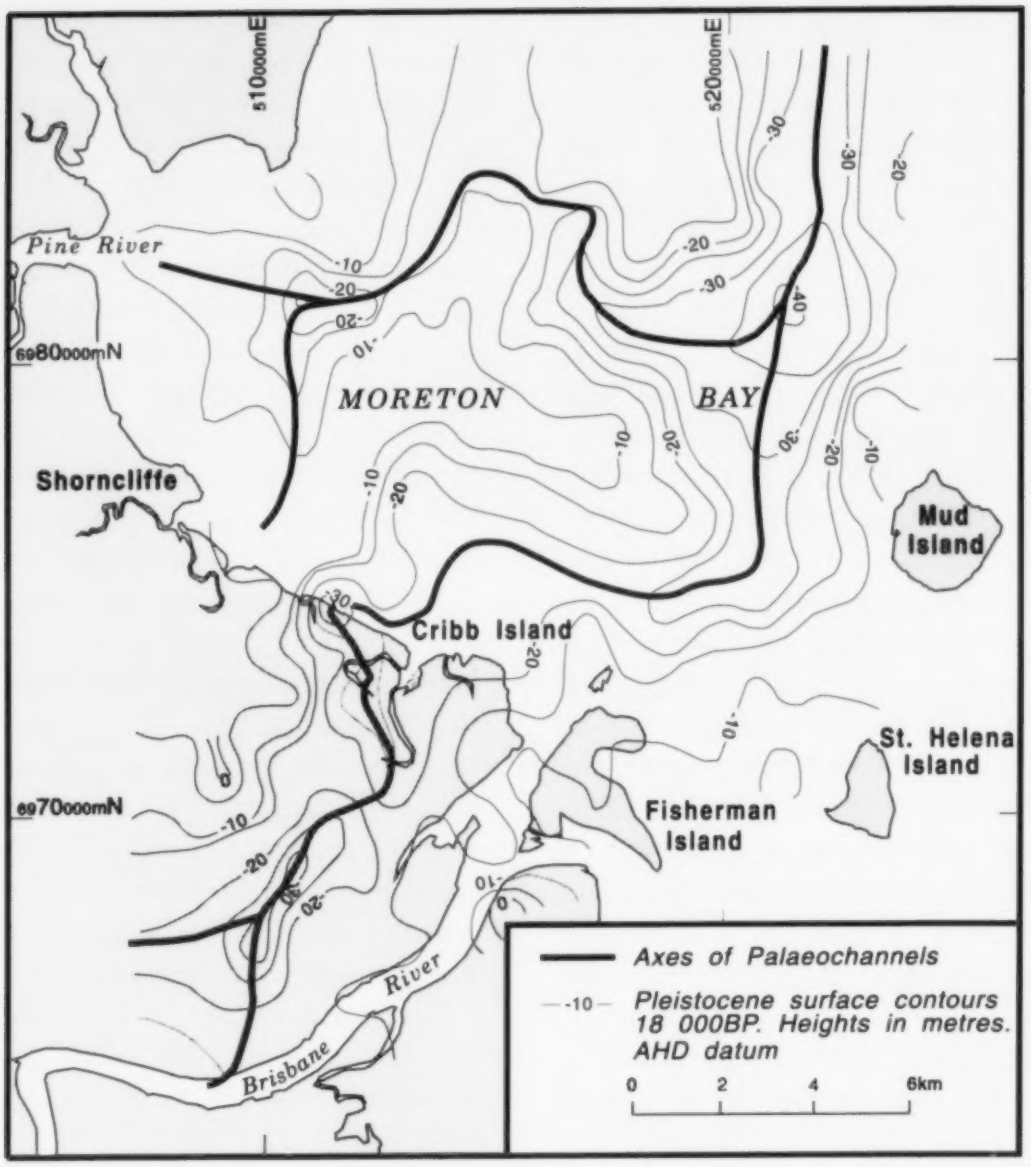

Fig.8. Structural contour map of the Pleistocene surface exposed during the last glacial low sea-level episode about 18 000 yr B.P.

Morphology and deposition of correlative sequences described in areas outside the East Coast of Australia, are in places affected by local tectonism.

Sequence stratigraphy

The distribution of seismic sequences is complex as a result of the variety of depositional environments controlled by sea-level fluctuations.

Sequence stratigraphic principles are applied to systems controlled by high frequency sea-level fluctuations resulting in sequence thicknesses of about 15 m. This method was used in interpretation of Quaternary sedimentary environments of the Mississippi delta (Boyd et al., 1989). In the Mississippi delta a type 1 sequence was recognised overlying a type 1 sequence boundary. The type 1 sequence boundary was considered to correlate with the erosional unconformity developed during the Last Glacial sea-level low. It was argued that the method may not be suitable for global correlation of sequences and their driving mechanisms.

The seismic sequences are defined in terms of sequence stratigraphy using definitions outlined by Van Wagoner et al. (1988). Units *A* and *Cu* make up a highstand systems tract (HST). Unit *Cl* is part of the transgressive systems tract (TST). The HST and TST correlate with those defined in the Townsville area, North Queensland (Harris et al., 1990). Reflectors Tr and Df are parasequence boundaries. Interstitial gas has obscured the record in the base of many channels and the lower surface of unit *Cl* is not visible in channels. Thus the

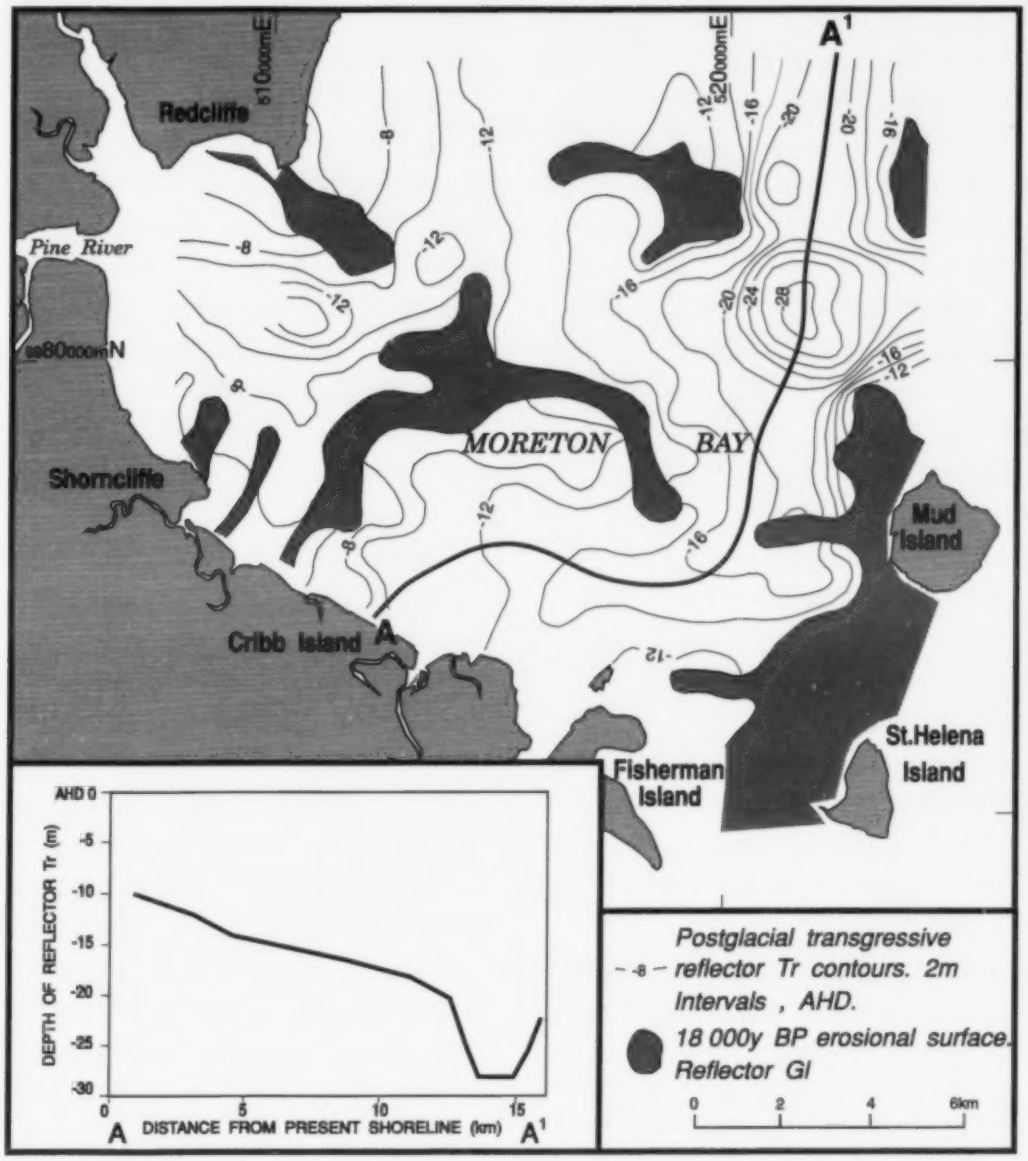

Fig.9. Contours on the surface of transgressive seismic unit *Cl*. This figure illustrates the infilling of palaeotopographic lows by estuarine muds during the most recent sea-level transgression. Section *A–A'* represents the grade of the upper surface of unit *Cl* represented by reflector Tr along *A–A'*.

leading edge transgressive surface cannot be seen. The gas also prevents delineation of fluvio–estuarine deposits within incised valleys. The Postglacial units together form a shore proximal portion of a type 1 sequence similar to that recognised by Boyd et al. (1989). The reflector Gl (Fig.7) represents the offshore subaerial Pleistocene surface of the Last Glacial period and is a type 1 sequence boundary and correlates with the type 1 sequence boundary recognised in the Mississippi delta (Boyd et al., 1989). Lowstand systems tracts (LST) are not present as any existing LSTs would be seaward of the shelf break.

Four HSTs are delineated in the Pleistocene seismic sequences deposited prior to the last Glacial period. Each of the seismic sequences: *Pl*, *Plm*, *Pum* and *Pu*, comprises a separate HST. Their respective lower bounding reflectors: B2, P1, P2 and P3 are type 1 sequence boundaries.

Seismic sequence *Plm* has an internal subsequence which is a TST. This internal subsequence has reflector P2a (a parasequence boundary) as its upper surface and reflector P1 (a type 1 sequence boundary) as its lower surface.

Different phases of eustatic rise and fall are responsible for variations in types of systems tract (Posamentier et al., 1988). The relationship between eustacy and systems tracts are, in part, as follows. A TST is deposited during rapid eustatic rise. A HST results from deposition during the final part of sea-level rise, a stillstand and the initial subsequent sea-level fall. The type 1

sequence boundary indicates a substantial relative sea-level fall. These eustatic relationships can be applied to the seismic sequences of the Brisbane River delta front and prodelta.

By applying the eustatic relationships to a glacio-eustatic sea-level curve (Fig.10) the relative ages of the seismic sequences can be estimated according to the principles of superposition (Table 2). This allows the Quaternary geological history to be interpreted.

Quaternary geological history

The Quaternary marine geological history of the Brisbane River delta front and prodelta has been controlled by sea-level rise and fall, palaeotopography and channel migration.

Through successive sea-level fluctuations the same depositional environments have existed and sediments of similar lithology have been deposited.

Pre-Glacial Pleistocene history (> 18 000 yr B.P.)

At the commencement of the Pleistocene, sediments of the Mesozoic Nambour Basin and sediments and volcanics of the Cainozoic Petrie Basin covered the study area. The seismic stratigraphy indicates that the surface (reflectors B1 and B2, Figs.5, 6 and 7) was channelled and irregular.

The glacio-eustatic sea-level curve (Chappell, 1983) indicates three major high sea-level episodes and two major sea-level lows occurred between 340 000 yr B.P. and 18 000 yr B.P. (see Fig.10). Onshore sequence stratigraphic analysis (Evans, 1990) indicates that soft sediments deposited in delta top environments have a low potential for total preservation during major sea-level fluctuations. Partial preservation has also occurred in the Gulf of Patras, Greece, where only prodelta muds are preserved below the Glacial unconformity (Chronis et al., 1991).

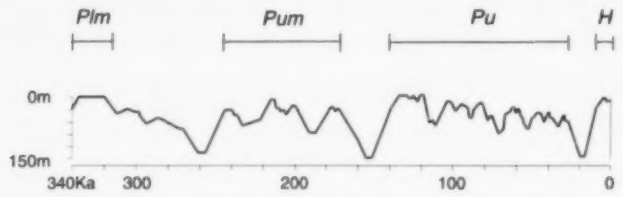

Fig.10. A glacio-eustatic sea-level curve for the last 340 000 years (after Chappell, 1983). The curve can be used to give an indication of the sea-level cycles which have affected Moreton Bay. Seismic sequences have been added to the curve.

The lower bounding reflectors (P1, P2 and P3) of seismic sequences *Plm*, *Pum* and *Pu* are considered to represent erosional surfaces formed during episodes of low sea level. The seismic sequences represent sediment deposition during high sea-level periods. Using the principle of superposition, the high sea-level periods shown in Fig.10 have been correlated with deposition of sequences *Plm*, *Pum*, and *Pu* and inferred relative ages have been assigned (Table 2).

Sediments deposited prior to 340 000 yr B.P. are represented by the poorly preserved sequence *Pl*. Sediments were deposited during marine transgressions and sea-level highstands and then removed during low stands. This sequence may represent more than one depositional episode.

The excellent detail of sequence *Plm* in seismic records, the lateral continuity and thickness in palaeo-interfluves suggests that this is the best preserved sequence. In many places the sequence has a seismic character similar to the upper sequences being deposited today. It follows that this sequence was deposited toward the end of the Pleistocene during a period of highstand deposition. This may have been the high sea-level episode which occurred from 340 000 yr B.P. to 318 000 yr B.P.

Prior to 340 000 yr B.P. there was a marine transgression. During this time the lower part of sequence *Plm* was deposited probably as estuarine mud. As sea level rose the locus of deposition moved shoreward along the existing palaeochannels incised in the surface represented by reflector Pl. A trailing edge transgressive surface (reflector P2a, Fig.7) was developed. At 340 000 yr B.P. the upper part of sequence *Plm* was deposited as prograding sandy delta front and muddy prodelta deposits. At this stage this shoreline was probably close to the embayment's bedrock margin (e.g. like the 6000 year shoreline described by Hekel et al., 1979). The limit of landward inundation by the sea was controlled by Palaeozoic and Triassic outcrop to the west of the present day shoreline. From 340 000 to 318 000 yr B.P. the shoreline probably continued to regress eastward.

When sea level began to fall again at about 318 000 yr B.P. the upper sections of sequence *Plm* were eroded and palaeochannels were formed. The sea level continued to fall until about 260 000 yr B.P. when it reached a glacio-eustatic minimum. The sea level did not rise to a glacio-eustatic maximum again until about 220 000 yr B.P. During this time the subaqueous plain was exposed and palaeochannels developed. The interfluves of these channels (Fig.7) were exposed for about 100 000 years.

During the high sea-level episode from 240 000 yr B.P. until 170 000 yr B.P. sediments were deposited (represented by *Pum*). The sea levels during this highstand were slightly less than the previous highstand. This period was punctuated by minor periods of sea-level lows, and the sea level was at its maximum for only about 2000 years. Only a thin layer of sediment was deposited over interfluves distal from the present day shoreline (Fig.7).

Between 170 000 yr B.P. and 138 000 yr B.P., the sea level had fallen to a glacio-eustaic minimum and then risen again to a level slightly higher than the present day. From 140 000 yr B.P. to about 120 000 yr B.P. the sea level was approximately 4–6 m higher than present with some minor fluctuations (Marshall and Thom, 1976). During this time sequence *Pu* was deposited. In the north of the study area, thick mud units were deposited in palaeochannels. Offshore, only a thin layer of mud, no greater than about 3 m thick, was deposited on the palaeo-interfluves. From 119 000 to 28 000 yr B.P. the sea level fell gradually. This period was also punctuated by minor sea level fluctuations, but the sea level did not rise sufficiently to cover the interfluves until the present highstand about 6500 yr B.P. The distal interfluves were exposed from about 117 000 yr B.P. to 6500 yr B.P.

Nearshore areas of deposition were restricted by the position of bedrock highs. Sequences were less extensive, more drainage channels existed, and therefore there was less preservation after erosive episodes. Offshore, on the eastern extremity of the study area, sequence deposition was more extensive. The main erosive channels were the palaeochannels of the Brisbane and Pine Rivers. These rivers seem to have occupied the same channels during several cycles of sea-level fluctuation. This has resulted in greater preservation of the sequences in interfluves.

During the Pre-Glacial period many palaeodrainage channels were occupied and re-occupied during successive low sea-level episodes. These channels were then backfilled during marine transgressions. In the upper sequences, nested channels have developed where successive sea-level falls have been less.

From 28 000 yr B.P. to about 18 000 yr B.P. sea level fell steadily. Much of the Brisbane River delta was eroded during the 10 000 years over which sea level fell, until it reached the Glacial sea level minimum. The palaeo-subaqueous delta plain became exposed and up to 30 m of sediment was removed as wide river valleys were formed by the Brisbane and Pine Rivers. The Brisbane River meandered its way across the exposed broad plain (the surface represented by reflector Gl). The Pine River at this time was a tributary of the Brisbane River and flowed into it about 15 km west of its present day mouth (stage A, Fig.11).

While exposed, the Pleistocene surface was oxidised and became over consolidated as a result of removal of overlying sediments and the water column.

Postglacial transgression history

As the sea level rose the palaeochannels were infilled by unit *Cl* comprising dark grey mud. By the end of the Pleistocene, 10 000 yr B.P., the confluence of the Pine and Brisbane River was a broad estuary. Sea level was about 30 m less than it is today (Thom and Roy, 1985). The mouths of the rivers were separated by a linear shoreline about 5 km long running nearly parallel to the present day shoreline (Fig.11, Stage B). A transgressive surface (reflector Tr) at the top of unit *Cl* had commenced to develop and the locus of deposition was moving shoreward along the palaeochannels.

By 9000 yr B.P. the Brisbane River was a broad estuary up to 5 km wide extending across the study area (Stage C, Fig.11). Unit *Cl* was being deposited as estuarine mud as sea level was still rising. Sea level was at about −20 m AHD and the rate of sea inundation of Moreton Bay was increasing. At the commencement of the Holocene the areal

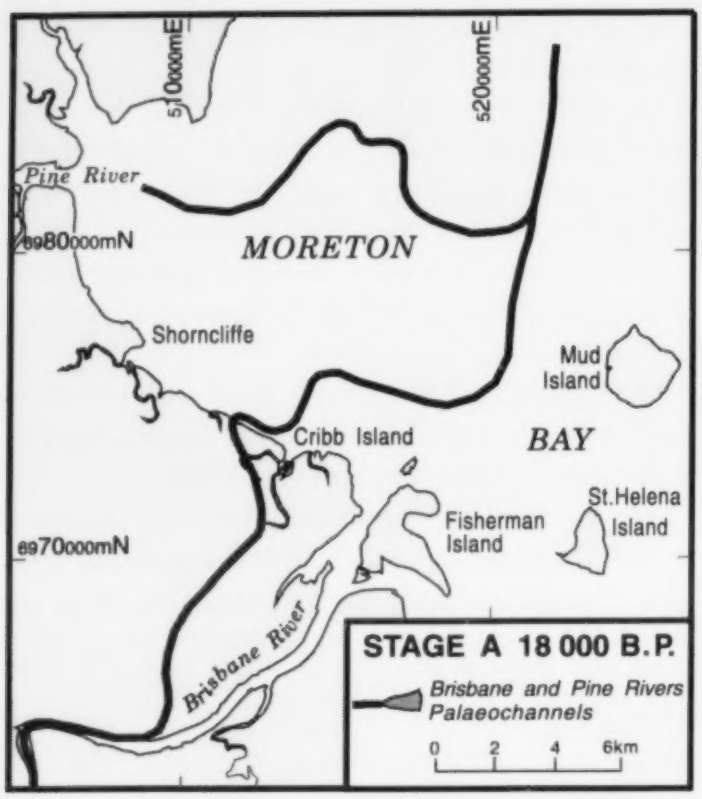

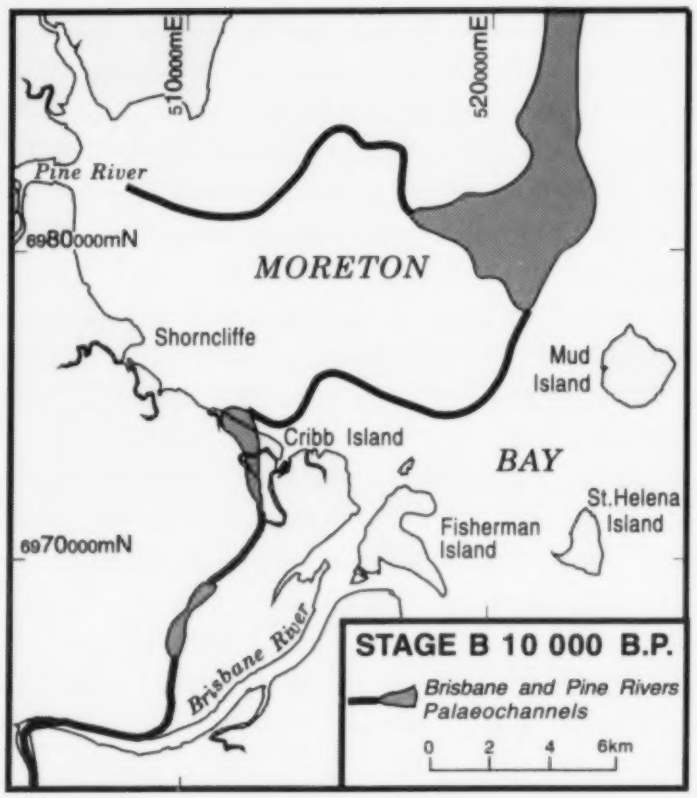

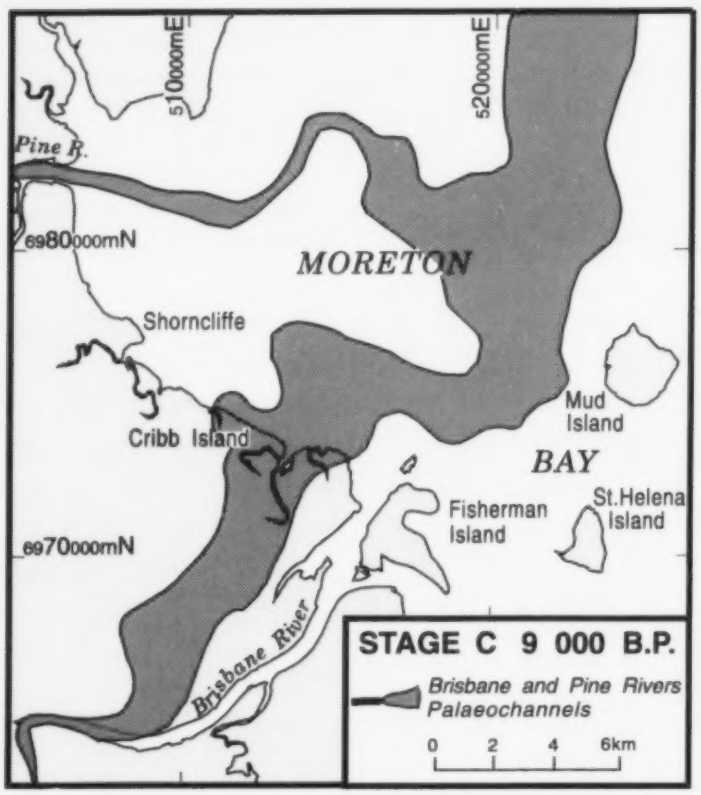

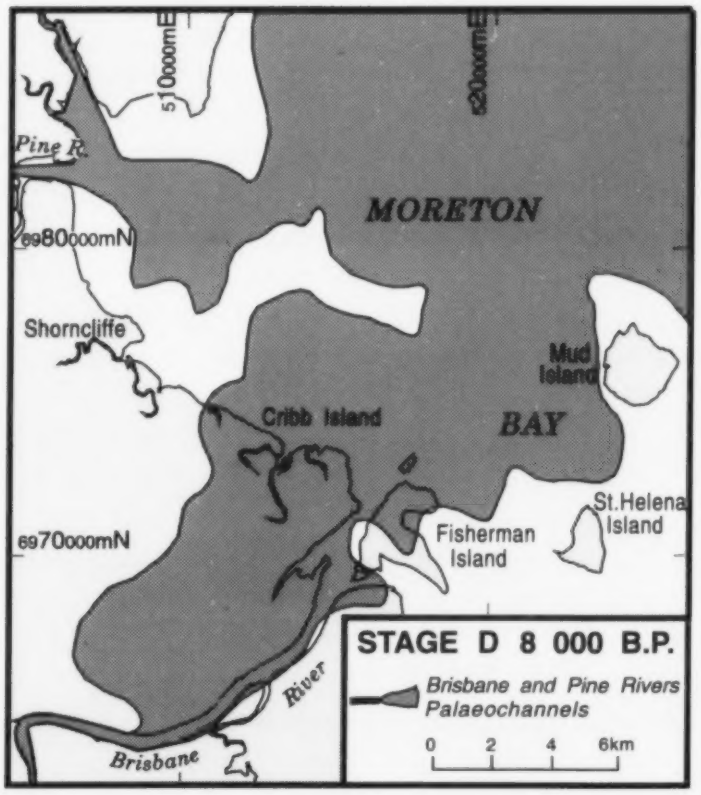

Fig.11. Four stages of inundations of the palaeo-plain by the sea since the most recent transgression commenced about 18 000 yr B.P. The increased rate of inundation toward the later stages of the transgression is illustrated by the expanded areal coverage of sea water which occurred between 9000 yr B.P. and 8000 yr B.P.

extent of water was restricted to about 1/8 of the study area (Stage B, Fig.11). The areal extent of water had increased to 7/8 of the study area by 8000 yr B.P. (Stage D, Fig. 11). The northeast portion of the study area was a small open bay. Both the Brisbane and Pine Rivers were irregular inlets with entrances to the bay between Pleistocene promontories.

Sea level continued to rise and the shoreline transgressed west and the locus of deposition continued to move westward along the palaeochannels. As the water surface area increased, wave energy increased and this may have reworked the sediments at the surface of unit *Cl*. This may explain why reflector Tr truncates some parts of *Cl*. Further offshore there was a hiatus in deposition because the locus of deposition was now further inshore and sediments were not reaching the distant areas.

Figure 9 shows a depression in the surface of unit *Cl* at the confluence of the palaeo-Brisbane and Pine Rivers. The rate of change of basin volume expansion with sea inundation increased rapidly due to the palaeo-topography. A scour hole, possibly as deep as 40 m, formed in the Pleistocene surface at the confluence of the rivers. This created a relatively large basin to be filled by transgressive sediments. The constant rate of sediment supply could not keep pace with the rapid expansion of the basin volume and the depression developed. Figure 9 shows that the transgressive upper surface of unit *Cl* has an even grade except near the depression at the confluence of the rivers about 14 km offshore.

Holocene "stillstand" history

When sea level stopped rising about 6500 years ago, a sea level highstand commenced. At this time the subaqueous plain had an irregular surface. It consisted of drowned river valleys that had broad planar surfaces of mud onlapping the margins of subaqueously exposed Pleistocene interfluves (Fig.9).

The locus of deposition commenced to move offshore again and unit *Cu* was deposited over unit *Cl* and the exposed interfluves. The fine mud of unit *Cu* has blanketed the subaqueous plain forming a broad prodelta with a planar surface. Unit *A* was the last unit to be deposited and represents the fluvial delta front at the mouth of the Brisbane River prodgrading over Cu.

The modern Brisbane River delta is fluvially dominated near the mouth of the Brisbane River and wave dominated to the northwest of the river mouth. The wave domination is expressed by the linear shoreline developed from Serpentine Creek to Shorncliffe.

Offshore, the delta front is fluvially dominated. The delta front sands have a lobate shape with an irregular seaward edge. The remainder of the study area is covered by fine prodelta mud. The mud is too fine to be deposited in the nearshore higher energy fluvial regime and has been spread across the study area by tidal currents and wave action. It has been deposited in the low energy environment of the open bay. In the northeast extremity of the study area some Pre-Glacial Pleistocene substrate is near the surface and has been covered by only a very thin veneer of prodelta mud. Figure 12 shows the surficial distribution of seismic units in the study area.

Conclusions

Eight major *reflectors* were recognised and are present on a regional basis in Moreton Bay. Reflectors B2, P1, P2, P3 and Gl are considered to be type 1 sequence boundaries, and reflectors Tr and Df are parasequence boundaries. Reflectors and the seabed define the boundaries of six *seismic sequences* (*B*, *Pl*, *Plm*, *Pum*, *Pu* and *H*). Sequences *Pl*, *Plm*, *Pum*, *Pu* and unit *Cu* plus unit *A* represent five highstand systems tracts (HST) and unit *Cl* represents a transgressive systems tract (TST).

Relative ages of depositional episodes in Moreton Bay were determined from glacio-eustatic sea-level curves by applying the relationships between eustacy and system tract type. The highest Pre-Glacial Pleistocene sequence (*Pu*) in the stratigraphic column was assumed to have formed during the high sea-level episode prior to the Last Glacial period. The ages of preceding high sea-level episodes were then applied to preceding sequences.

The sediments of the subaqueous plain result from five major episodes of deposition controlled by sea-level fluctuations, channel migration and palaeotopography. Pre-Glacial episodes are represented by seismic sequences: *Pl*, *Plm*, *Pum* and *Pu*. The Postglacial episode is represented by sequence *H*. Evidence of periods of Pleistocene glaciation are preserved as erosional surfaces in the sediment record.

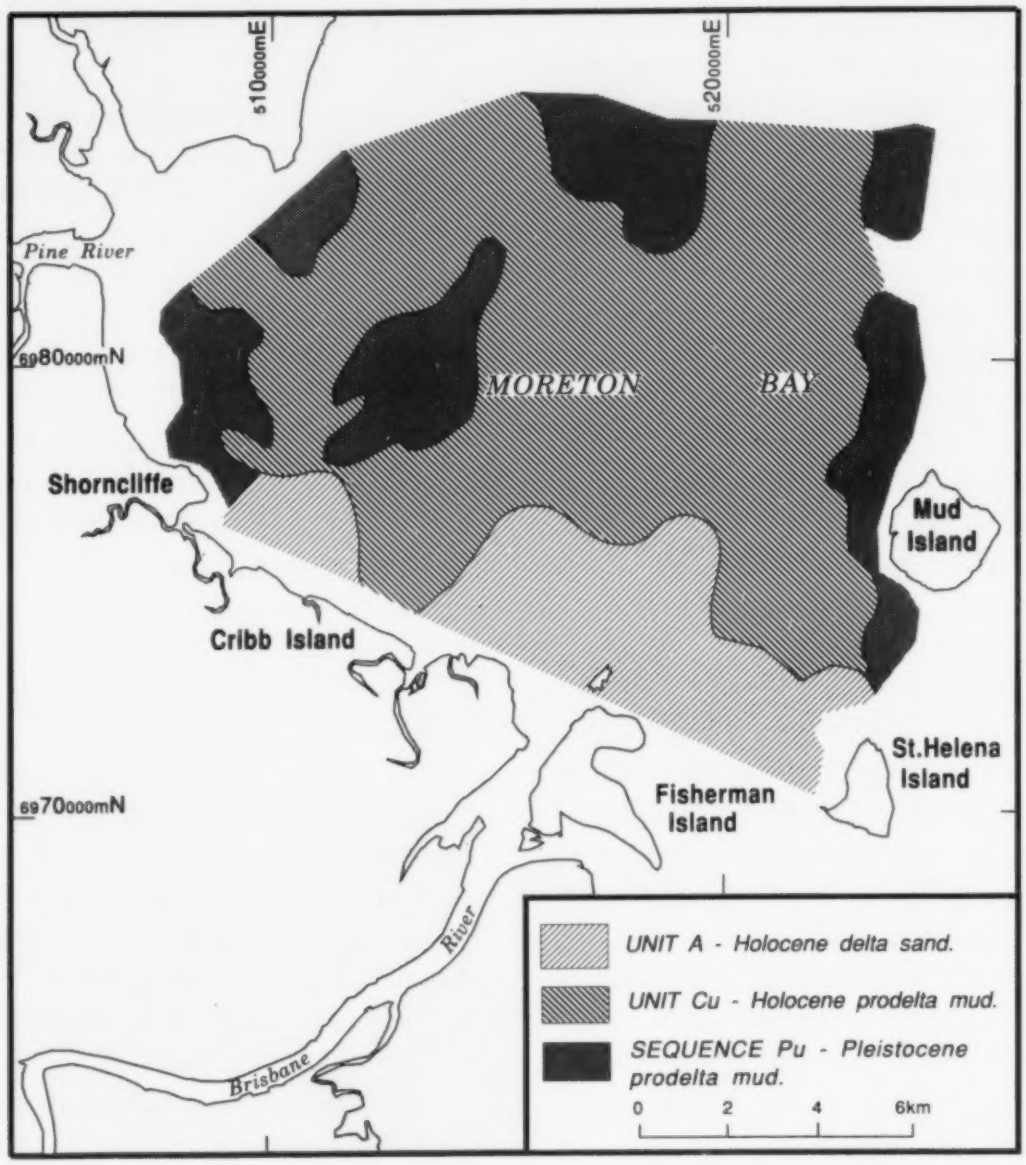

Fig.12. The surficial distribution of submarine seismic units.

Seismic units *Bf* and *Bw* comprise fresh and weathered rock respectively, and represent a basement of Mesozoic Nambour Basin and Tertiary Petrie Basin rocks.

Characteristics of older seismic sequences of the Brisbane River delta front and prodelta are repeated above in younger seismic sequences. A study of the present depositional systems episode gives an indication of the geomorphology and lithology of older sequences and the energy regimes in which they were deposited. The principle of uniformitarianism can be applied to describe the Quaternary stratigraphy of the Brisbane River delta.

The sequence stratigraphic method can be applied to sediment packages deposited in the late Quaternary as a result of high frequency sea-level fluctuations. Four separate sequences below the Postglacial were recognized, defined, and assigned inferred ages. These sequences cannot be correlated globally in the same manner as lower order cycles/sequences, that have been defined chronostratigraphically and biostratigraphically. However, limited global correlation is possible since a highstand systems tract has been recognized above a Pleistocene surface in many mid to low latitude sites.

Acknowledgments

Thank you to R. Coe (Department of Resource Industries) for his extensive technical support and field assistance with coring and seismic profiling under difficult circumstances. Thank you to D.E. Searle (Department of Resource Industries) for his

review of and comments on the manuscript. Thanks are also due to M. Jones, K. Holmes and M. Livingstone (Department of Resource Industries) for various assistance including editing, discussions, assistance with computer software and geophysical technical support. Appreciation is expressed to R. Evans, L. Donald, M. Sieters, A. James and K. Van Noord for assistance with field surveying. KGE undertook this study with assistance of a bursary from AGL Petroleum and logistic support from the Queensland Department of Resource Industries. The generous assistance of these organisations is greatfully acknowledged.

References

Boyd, R., Suter, J. and Penland, S., 1989. Relation of sequence stratigraphy to modern sedimentary environments. Geology, 17: 926–929.

Chappell, J., 1983. A revised sea level record for the last 300 000 years from Papua New Guinea. Search, 14: 99–101.

Chiocci, F.L., Orlando, L. and Tortora, P., 1991. Small-scale seismic stratigraphic and palaeogeographical evolution of the continental shelf facing the SE Elba Island (Northern Tyrrhenian Sea, Italy). J. Sediment. Petrol., 61: 506–526.

Chronis, G., Piper, D.J.W. and Anagnostou, C., 1991. Late Quaternary evolution of the Gulf of Patras, Greece: Tectonism, deltaic sedimentation and sea-level change. Mar. Geol., 97: 191–209.

Coffey and Hollingsworth, 1966. Report on general soil investigation for Serpentine Project. Brisbane City Council Serpentine Project, Job No. 1578 B.

Coffey and Hollingsworth, 1972. Report on subsurface investigation, stage 1. Commonwealth Department of Works Brisbane Airport Development.

Dahlen, M.Z., Osborne, R.H. and Gorsline, D.S., 1990. Late Quaternary history of the Ventura mainland shelf, California. Mar. Geol., 94: 317–340.

Evans, K.G., 1990. Quaternary stratigraphy of the Brisbane River delta. BAppSc (Hons) Thesis, School Appl. Geol., Queensl. Univ. Technol. (Unpubl.).

Evans, K.G., 1991. Biogenic gas in deltaic sediments, Moreton Bay, Queensland. Explor. Geophys., 22: 509–514.

Gillespie, R., 1982. Radiocarbon Users' Handbook. Macquarie Univ., North Ryde, NSW, Quat. Res. Unit Occasional Publ. 1.

Grimes, K.G., Cranfield, L.C., Donchak, P.J.T., Hutton, L.J. and Jones, M.R., 1986. Brisbane Sheet 9543. Australia 1 : 100 000 Geol. Ser., Dep. Mines, Brisbane, 1st edition.

Harris, P.T., Davies, P.J. and Marshall, J.F., 1990. Late Quaternary sedimentation on the Great Barrier Reef continental shelf and slope east of Townsville, Australia. Mar. Geol., 94: 55–77.

Hekel, H., Jones, M. and Searle, D.E., 1976. Relict sediments in Moreton Bay. Queensl. Gov. Min. J., 77: 36–45.

Hekel, H., Ward, W.T., Jones, M. and Searle, D.E., 1979. Geological development of northern Moreton Bay. In: A. Bailey and N.C. Stevens (Editors), Northern Moreton Bay Symposium. R. Soc. Queensl., Brisbane, pp. 7–18.

Johnson, D.P. and Searle, D.E., 1984. Post-glacial seismic stratigraphy, central Great Barrier Reef, Australia. Sedimentology, 31: 335–352.

Jones, M. and Hekel, H., 1979. Preliminary results of submarine drilling in central Moreton Bay. Queensl. Gov. Min. J., 80: 226–33.

Jones, M., Hekel, H. and Searle, D.E., 1978. Late Quaternary sedimentation in Moreton Bay. Univ. Queensl. Pap. Dep. Geol., 8(2): 6–17.

Jones, M.R. and Holmes, K.H., 1986. Depositional environments on the Boondall–Nudgee Beach coastal plain, southeast Queensland. Queensl. Dep. Mines Record 1986/52 (Unpubl.).

Jones, M.R. and Stephens, A.W., 1981. Quaternary geological framework and resource potential of Moreton Bay. In: G.W. Hofmann (Editor), 1981 Field Conference, Brisbane–Ipswich Area. Geol. Soc. Aust., Queensl. Division, pp.17–23.

Kelly, R.A. and Baker, J., 1984. Geological development of North and South Stradbroke Islands and surrounds. In: R.J. Coleman, J. Covacevich and P. Davie (Editors), Focus on Stradbroke: New Information on North Stradbroke Island and Surrounding Areas, 1974–1984. Boolarong Publ., Brisbane, pp.156–166.

Knebel, H.J. and Scanlon, K.M., 1985. Sedimentary framework of Penobscot Bay, Maine. Mar. Geol., 65: 305–324.

Marshall, J.D. and Thom, B.G., 1976. The sea level in the last interglacial. Nature, 263: 120–121.

McMaster, R.L., 1984. Holocene stratigraphy and depositional history of the Narragansett Bay System, Rhode Island, U.S.A. Sedimentology, 31: 777–792.

Posamentier, H.W., Jervey, M.T. and Vail, P.R., 1988. Eustatic controls on clastic deposition I — conceptual framework. In: Sea-Level Changes: An Integrated Approach. SEPM Spec. Publ., 42: 109–124.

Searle, D.E., 1983. Late Quaternary regional controls on the development of the Great Barrier Reef: geophysical evidence. Bur. Miner. Resour. J. Aust. Geol. Geophys., 8: 267–276.

Searle, D.E., Harvey, N., Hopley, D. and Johnson, D.P. 1981. Significance of results of shallow seismic research in the Great Barrier Reef province between 16°10′S and 20°05′S. In: Proc. of the Fourth Int. Coral Reef Symp. (Manila.). 1, pp.531–539.

Searle, D.E., Holmes, K.H. and Stephens, A.W., 1986. Boondall Project: Report on geological and geophysical investigations. Geol. Surv. Queensl. Record 1986/8 (Unpubl.).

Stephens, A.W., 1982. Quaternary coastal sediments of southeast Queensland. Geol. Jahrb., Reihe D, 56: 37–47.

Thom, B.G. and Roy, P.S., 1985. Relative sea level and coastal sedimentation in southeast Australia in the Holocene. J. Sediment. Petrol., 55(2): 257–264.

Van Wagoner, J.C., Posamentier, H.W., Mitchum, R.M., Vail, P.R., Sarge, J.F., Loutit, T.S. and Hardenbol, J., 1988. An overview of the fundamentals of sequence stratigraphy and key definitions. In: Sea-Level Changes: An Integrated Approach. SEPM Spec. Publ., 42: 39–45.

Marine Geology, 107 (1992) 81–101
Elsevier Science Publishers B.V., Amsterdam

Paraglacial barrier–lagoon development in the Late Pleistocene Baltic Ice Lake, southwestern Baltic

Jørn Bo Jensen[a] and Ole Stecher[b]

[a]*Geological Survey of Denmark, Thoravej 8, 2400 Copenhagen NW, Denmark*
[b]*The National Museum, Frederiksholms Kanal 12, 1220 Copenhagen K, Denmark*

(Received September 6, 1991; revision accepted February 17, 1992)

ABSTRACT

Jensen, J.B. and Stecher, O., 1992. Paraglacial barrier–lagoon development in the Late Pleistocene Baltic Ice Lake, southwestern Baltic. *Mar. Geol.*, 107: 81–101.

Marine geological investigations including shallow seismic, sedimentological and stratigraphical studies were carried out in Fakse Bay, southwestern Baltic. Seismic sequence analytical methods were used, supplemented by detailed lithological descriptions, pollen analysis and ^{14}C dating of core material. Detailed correlations between sediment facies units and seismic sequences resulted in the establishment of four depositional sequences: I. Glacial related deposits, II. lagoon/pond and freshwater coastal deposits, III. Lake-bog–lake deposits, and IV. Marine, (sub)littoral deposits. Most attention has been paid to Sequences II and III, showing the development of a transgressive freshwater barrier beach ridge and a following regression.

Pollen spectra indicate Allerød and Younger Dryas Chronozone ages (11,500–10,000 ^{14}C yrs B.P.) for the development of a sheltered lagoon/pond basin behind the transgressive freshwater barrier beach ridge. The freshwater coastal deposits are interpreted as the southwesternmost marginal deposits of the Baltic Ice Lake and represent the transgression maximum. This transgression maximum reached a level of about 13 m below the present sea level. The final drainage of the Baltic Ice Lake resulted in the development of a sheltered basin behind the former beach ridge. A fluctuating groundwater level here favoured the deposition of alternating lake gyttja and bog peat deposits in the central part of the basin. Pollen analysis and ^{14}C dating reveal that the lake deposits correspond to high groundwater levels associated with the Ancylus Lake (9000 yrs B.P.) and the Littorina Sea (7000 yrs B.P.) transgressions, while the bog sediments represent the low water stands in the early Holocene.

Introduction

At middle and high latitudes it is common to find recent beach barriers consisting of coarse clastics (Carter and Orford, 1984; Forbes and Taylor, 1987; Carter et al., 1989; Duffy et al., 1989). Sources are large amounts of coarse grained, glacial deposits that are available for coastal erosion and deposition in paraglacial coastal deposits (Forbes and Taylor, 1987). In these areas, a number of coastal development studies have been carried out in the last decade, to a great extent focusing on transgressive systems. The investigations mostly deal with the surficial morphology, using historical maps and airphotos supplemented by monitoring of variuos morphological and lithological parameters (Shaw and Forbes, 1987). In certain cases additional investigations are carried out for example coring, pollen analysis and ^{14}C dating (Shaw and Forbes, 1987; Carter et al., 1989; Duffy et al., 1989). Recently, also shallow seismic studies have occasionally been included (McCann and Kostaschuck, 1987; Shaw and Forbes, 1990; Shaw et al., 1990). In some areas Late Pleistocene isostatically uplifted coastal sequences have been investigated as well (Nielsen et al., 1988; Bowman et al., 1989; Svensson, 1989). These provide the possibility of making detailed sedimentological and morphological investigations of the fossil environments.

The present study goes a step further, as the

Correspondence to: J.B. Jensen, Geological Survey of Denmark, Ministry of the Environment, Thoravej 8, 2400 Copenhagen NW, Denmark.

0025-3227/92/$05.00

depositional sequence analysis method is applied to shallow-seismic data and detailed lithological core data in describing a paraglacial coastal barrier system created in connection with the Late Pleistocene and Early Holocene development of the Baltic Sea.

Setting

The study area is located in Fakse Bay, southeastern Denmark. The bay belongs to the western part of the Baltic Sea (Fig. 1). The water depth at the study site is 12–17 m.

The pre-Quaternary deposits in the investigation area, consist of Upper Cretaceous chalk and Lower Tertiary limestone (Baartman and Christensen, 1975). Along the Fakse Bay coast line the Cretaceous chalck is exposed in the famous Møns Cliff section (Hintze, 1937) and the Cretaceous–Tertiary boundary in the Stevns Cliff section (Surlyk, 1980).

The Pleistocene deposits mainly consist of glacial till and lacustrine deposits as well as interglacial marine deposits (Petersen and Konradi, 1974; Berthelsen et al., 1977; Hyde, 1986). Investigations of the glacial deposits (Berthelsen et al., 1977; Aber, 1980, 1982) show that the Main Weichselian Advance (20,000 yrs B.P.) (Houmark-Nielsen, 1987) was responsible for large-scale glaciotectonic deformation. The later Belt Sea Readvance (15,000 yrs B.P.) caused drumlinisation and glaciotectonic deformation.

The Baltic Basin has experienced a complicated sequence of shore level displacements since the last Weichselian deglaciation about 13,000 yrs B.P. (Lundquist, 1986). The isostatic compensation in connection with the deglaciation was followed by the marginal fore-bulge collapse. In combination with the eustatically raised sea level, it resulted in two separate dammings, succeeded by drainage and establishment of marine environments (Fig. 2) (Eronen, 1983). The Baltic Ice Lake was drained approximately 10,500 yrs B.P. and the Ancylus Lake was drained approximately 9300 yrs B.P. (Björck, 1987). After the drainage of the Ancylus Lake, a marine environment was established in the central part of the Baltic Basin. Finally at approximately 7000 yrs B.P. the Littorina Sea transgression followed, in the westernmost part drowning the highest coastlines of the Baltic Ice Lake and the Ancylus Lake, leaving them below present day sea level (Fig. 2).

Methods

Data collection

Two separate shallow-seismic cruises were carried out, each followed by sampling. The sediment sampling included vibrocoring, gravity coring, grab sampling and test suction dredging.

The first shallow-seismic lines on an E–W oriented grid (1982) were used for a preliminary interpretation. These formed the basis for a later and more detailed survey with NW–SE oriented lines (1987). Positioning was done using a Syledis precision navigation system, giving an accuracy better than 10 m. With high frequency echosounding equipment (Elac 30 kHz) water depths were recorded to be presented as point data on a computer map. Contouring was done manually. The complete seismic system consisted of an ORE subbottom profiler (3.5 kHz), an EG&G Uniboom (0.8–16 kHz) boomer system and EDO Western side-scan sonar (100 kHz). This shallow seismic information was collected concurrently and the filtered echoes were recorded on analog tape and printed on paper by graphic recorders (EPC and KLEIN).

During interpretation the ORE subbottom profiler recordings turned out to be most useful for the present study. This is due to the shallow water conditions in the survey area. The favourable configuration of the sediments allowed a penetration of 10–30 m with high resolution subbottom information (0.3 m vertical resolution).

All seismic profiles are provided with thicknesses in metres for conceptual ease. Thicknesses were calculated using an assumed velocity of 1.7 km/s. This is an approximate medium velocity in sediment, whereas actual velocity may vary from 1.5 km/s (velocity of sound in water) to 2.0 km/s (Tirant, 1979). The calculated thicknesses represent medium estimates observed to make the best fit to thickness estimates obtained from vibrocore data.

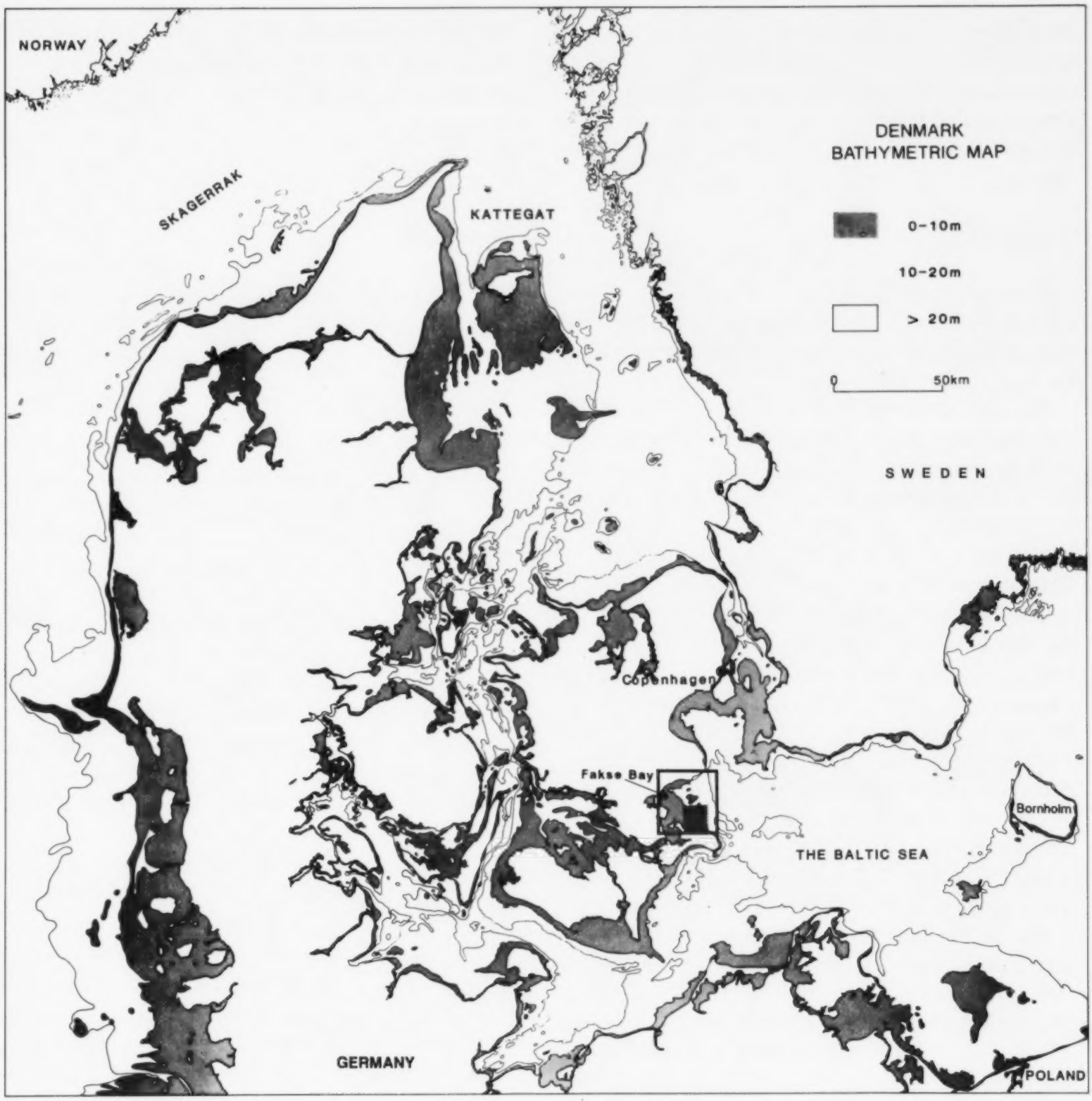

Fig. 1. Bathymetric map of the "Danish domestic waters". The Fakse Bay study area is framed and the detailed study area is marked with a black square.

Seismic interpretation

The principles of seismic stratigraphy (Vail et al., 1977; Vail, 1987) are used in the interpretation of the shallow seismic registrations. The first step in the seismic sequence analysis normaly is to interpret depositional sequences and system tracts (Van Wagoner et al., 1987, 1988) on seismic sections by identifying discontinuities on the basis of reflector terminations. The next step is to make a seismic facies analysis of reflector configuration patterns within each sequence. This is the description and geological interpretation of seismic reflection parameters, including reflection configuration,

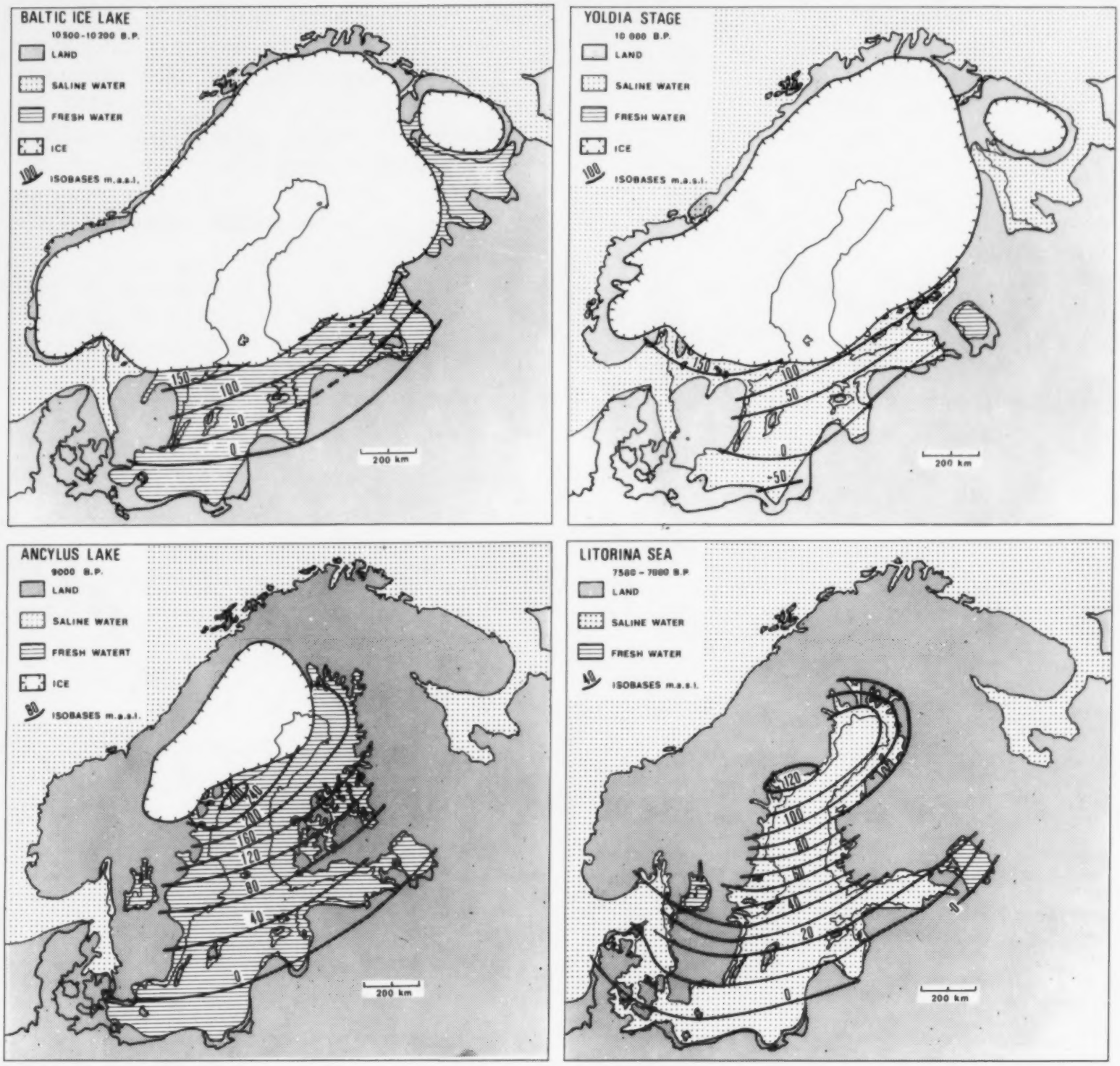

Fig. 2. Late Pleistocene and Early Holocene Baltic Basin stages. From Eronen (1983).

continuity and external form. Finally the geological interpretation is made in terms of environmental setting, depositional processes and estimates of lithology.

The shallow-seismic data collected from Fakse Bay show a combination of glacial deposits and coastal lacustrine and marine deposits. These can be divided into sequences following the original definition (Vail et al., 1977), although often it is not possible to satisfy all conditions of the more recent definition (Posamentier and Vail, 1988; Posamentier et al., 1988), as the water-deposited layers and glacial deposits do not constitute complete system tracts. Nor can they necessarily be divided in parasequences or related to eustatic sea-level changes. On the contrary, the established shallow seismic sequences are noncyclic, often non-marine, high-frequency sequences, and they may be related to local water-level changes of a duration in the order of 0.002 Ma or less. Nevertheless,

sequence analysis ensures a consistent interpretation of the seismic records. Furthermore, it provides a good background for the interpretation of lithological and biostratigraphical data and contributes to the interpretation of the environment and determination of local water-level changes.

Lithological information

Lithological information on surficial sediment layers has been obtained from visual description of grab samples, gravity cores and suction dredge subsamples (Wentworth, 1922). Detailed vertical lithofacies logs were derived from the vibrocore material, following Eyles et al. (1983).

Pollen analysis

Samples for pollen analysis were taken as isolated samples, covering as great a time span as possible. The analyses were performed by Else Kolstrup (Samples 0132, 0137, 2111, 2121 and 2122) and Bent Odgaard (Samples 0131, 0133, 0134, 0135, 0136, 2161, 2162 and 2163), who made preliminary interpretations of the data. The authors are responsible for the interpretations given in this paper.

The pollen samples (Fig. 10) were prepared using standard techniques in general following the description in Faegri and Iversen (1975).

The pollen percentages are based on the sum of trees, scrubs, herbs and grasses.

Radiocarbon dating

A number of peat samples were collected, dried and stored in plastic bags. Four samples were selected for radiocarbon dating at the laboratory of the The National Museum and Danish Geological Survey. The samples were treated with 0.3 *N* HCl to ensure complete removal of carbonate species, followed by rinsing in distilled water and drying. Clearly observed bubbling took place when samples K-5532 and K-5531 were subjected to the acid treatment suggesting the presence of carbonate species in these samples. A small subsample of each sample was collected for later determination of δ^{13}C-values. The δ^{13}C-values were measured by gas-source mass spectrometry at the Geophysical Institute, Copenhagen University, in order to correct the ^{14}C-values for isotopic fractionation relative to a terrestrial value of -25.0‰ PDB. The measured δ^{13}C-values ranged from -25.9 to -29.5‰ PDB. These values are typical of freshwater peat samples and indicate that no marine shells or other significant marine components have contributed to the CO_2 gas.

The dating results are presented in ^{14}C years prior to A.D. 1950 and are based on the recommended half-life of 5568 years. Errors quoted are ± 1 standard deviation.

Results

The seismic investigations in Fakse Bay (Fig. 1) have revealed coastal deposits at various stratigraphic levels (Jensen, 1992). This paper presents results from a detailed study area in the southernmost part of the bay (Fig. 3).

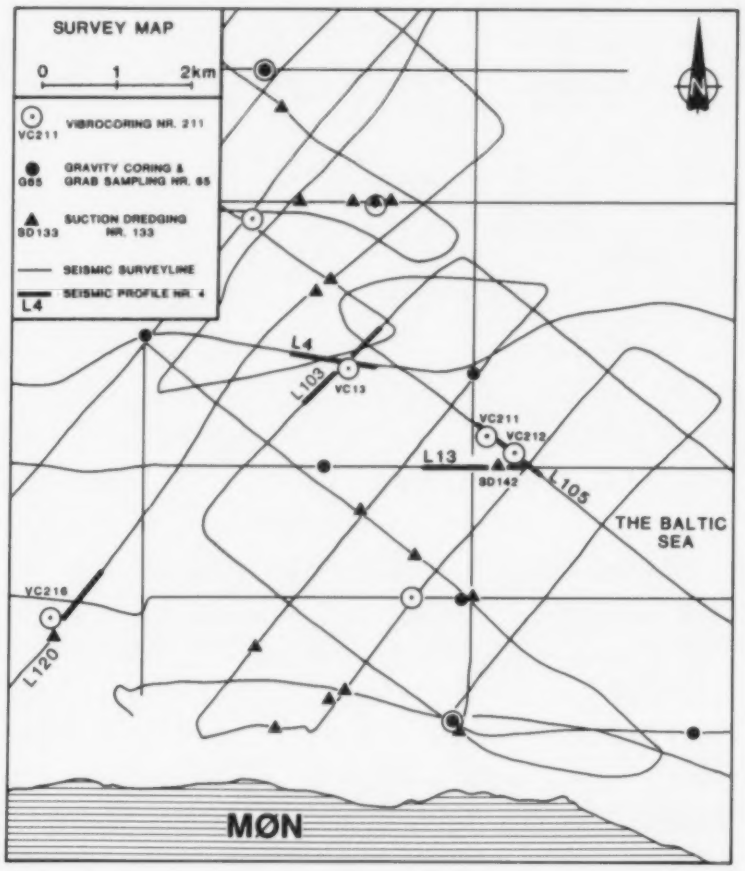

Fig. 3. Survey map showing sampling locations, survey lines and illustrated sections in the detailed study area.

Glacial surface topography

In the investigation area, all the late- and post-glacial deposits are reworked sediments. The source is the glacial landscape, developed in connection with the retreat of the Baltic Ice (Houmark-Nielsen, 1987). Therefore, it is not possible to reestablish the original glacial surface topography. However, by stripping of Late Pleistocene and Holocene stratified drift deposits, it is possible to reconstruct a modified topography of the surface left over by the melting Weichselian icecap. The resulting map (Fig. 4) shows the seismic depth to the base of the lowermost stratified units interpreted as subaqueous deposits of Late Pleistocene or Holocene age. This map shows that the underlying topography of the area basically consists of SE–NW oriented, elongated ridges, cut by narrow valleys.

The glacial surface topography, follows features in the Cretaceous chalk subsurface found at a level about 20 m below present sea level. This subsurface is cut by fault zones, leading to development of elongated valleys. Furthermore, glaciotectonic investigations at the nearby island of Møn (Berthelsen et al., 1977; Aber, 1980; Hyde, 1986) demonstrate that the dominating glacial morphological elements in the region consist of SE–NW oriented glacial floe thrusts, created by the Main Weichselian Advance (20,000 yrs B.P.). Finally the last Belt Sea Readvance (15,000 yrs B.P.) induced drumlin formation on the previous landscape in a SE–NW direction.

Thus the glacial morphological pattern can be recognized, even though the area has been exposed to heavy erosion in connection with the Late Pleistocene and Holocene transgression phases.

Seafloor topography

By comparing the glacial surface topography (Fig. 4) with the recent bathymetry (Fig. 5), it is possible to recognize the morphological elements created by Late Pleistocene and Holocene processes.

The bathymetric map reveals that the glacial

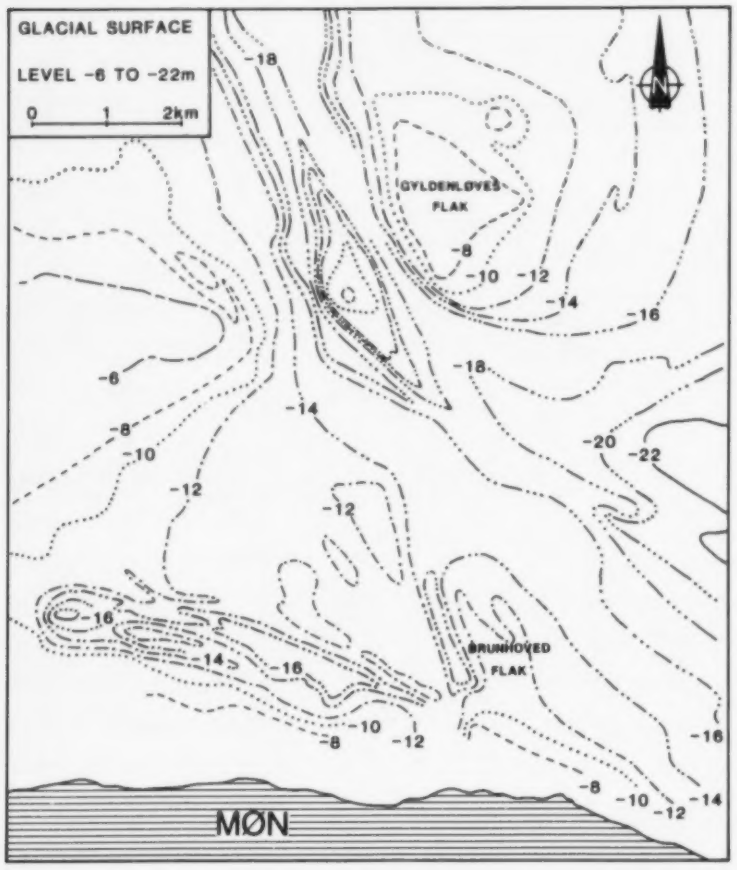

Fig. 4. Glacial surface topography in the detailed investigation area. The glacial surface is defined as the uppermost surface of glacial diamicton.

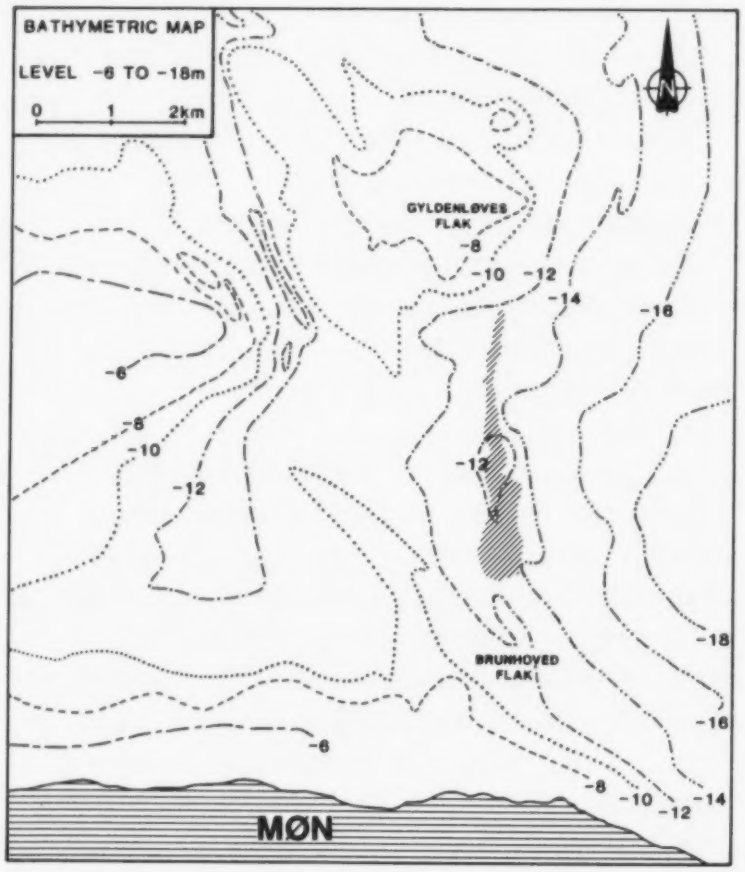

Fig. 5. Bathymetric map in the detailed investigation area. The hatched zone marks the position of a drowned barrier beach ridge, linking Brunhoved Flak and Gyldenløves Flak.

surface is leveled out, as the glacial valleys for the most part are filled with postglacial sediments. On the other hand, some positive morphological elements also appear. This is shown by the −10 m depth contour pattern revealing two elongated ridges. From analysis of seismic data, supplemented by determination of shell material and ^{14}C dating (Jensen and Petersen, 1992) these are interpreted to be spit platform and spit deposits formed during the Littorina Transgression.

However, the focus of this paper is on deposits connected to an elongated ridge represented by the −12 m depth contour (Fig. 5). The reason for the only partial appearance, is caused by the selected contour interval of 2 m, as the ridge appears to be partly eroded leaving the top level between −12 and −13 m.

Shallow seismic stratigraphy

A threedimensional reconstruction of the physiographic development of the area can be made using the dense seismic survey grid. To illustrate the seismic pattern a number of subbottom profiles (Fig. 3) have been selected. The purpose is to present a combined visualization of the three-dimensional structure, the boundaries and the internal reflection configuration of the individual seismic sequences (Fig. 6).

The lithological composition is documented by a number of vibrocores (Fig. 7).

The Quaternary seismic sequence stratigraphy compiled in Fakse Bay reveals a number of local depocenters, created in connection with deglaciation and the subsequent isostatic and eustatic competition.

Four Quaternary seismic sequences can be recognized in the area. These sequences overly Cretaceous sedimentary bedrock, which is described in more detail below.

Bedrock (Cretaceous limestone)

The bedrock at the base of the Quaternary sequences is recognized either as acoustic basement at an average subbottom depth of 15–20 m with deep valley cuts and a lack of penetration (Fig. 6), or as an angular unconformity truncating deformed stratified deposits.

The bedrock consists of Cretaceous limestone (Fig. 7, VC13) the dominant pre-Quaternary surface deposit in the southeastern part of Denmark (Baartman and Christensen, 1975).

Sequence I. Glacially related deposits

This sequence (Fig. 6) is bounded by an upper erosional truncation and a lower bounding surface, which is locally concordant but generally difficult to determine because of an internal chaotic to subparallel configuration. The internal reflection configuration is commonly chaotic in the lower part of the sequence, while in the upper part it has a tendency to have a more subparallel character.

The sequence is composed of glacial deposits consisting of till and outwash sediments deposited without much horizontal continuity (Fig. 7, VC13 and VC212). The till units are often well consolidated [matrix supported, massive (Dmm)], preloaded, thin benches (0–2 m in thickness) consisting of clay, silt and sand with contents of pebbles, cobbles and boulders. In a few cases they are rich in chalk and flint. In contrast, the valleys in the bedrock are filled by a 5 to 10 m thick unit mainly consisting of unconsolidated (not preloaded) clayey diamict with a minor content of coarse clastic material. The outwash deposits consist of sand with a fluctuating content of granules, pebbles and cobbles often dominated by chalk and flint.

Thus, in general the glacial deposits appear as thin (0–5 m) units leveling the bedrock topography, in certain cases by filling up 5 to 10 m deep valleys.

Sequence II. Lagoon/pond and freshwater coastal deposits

Typically, this sequence consists of a proximal barrier part and a landward distal lagoon part, as there is presumed little sediment supply from the landward side (Fig. 6). The upper bounding surface is truncational in the proximal eastern part, while the distal western part shows concordance to erosional truncation. The lower bounding surface is concordant to distal onlap. The proximal internal configuration shows characteristic oblique, tangential, landward prograding clinoforms. These are downlapping internal sedimentation surfaces

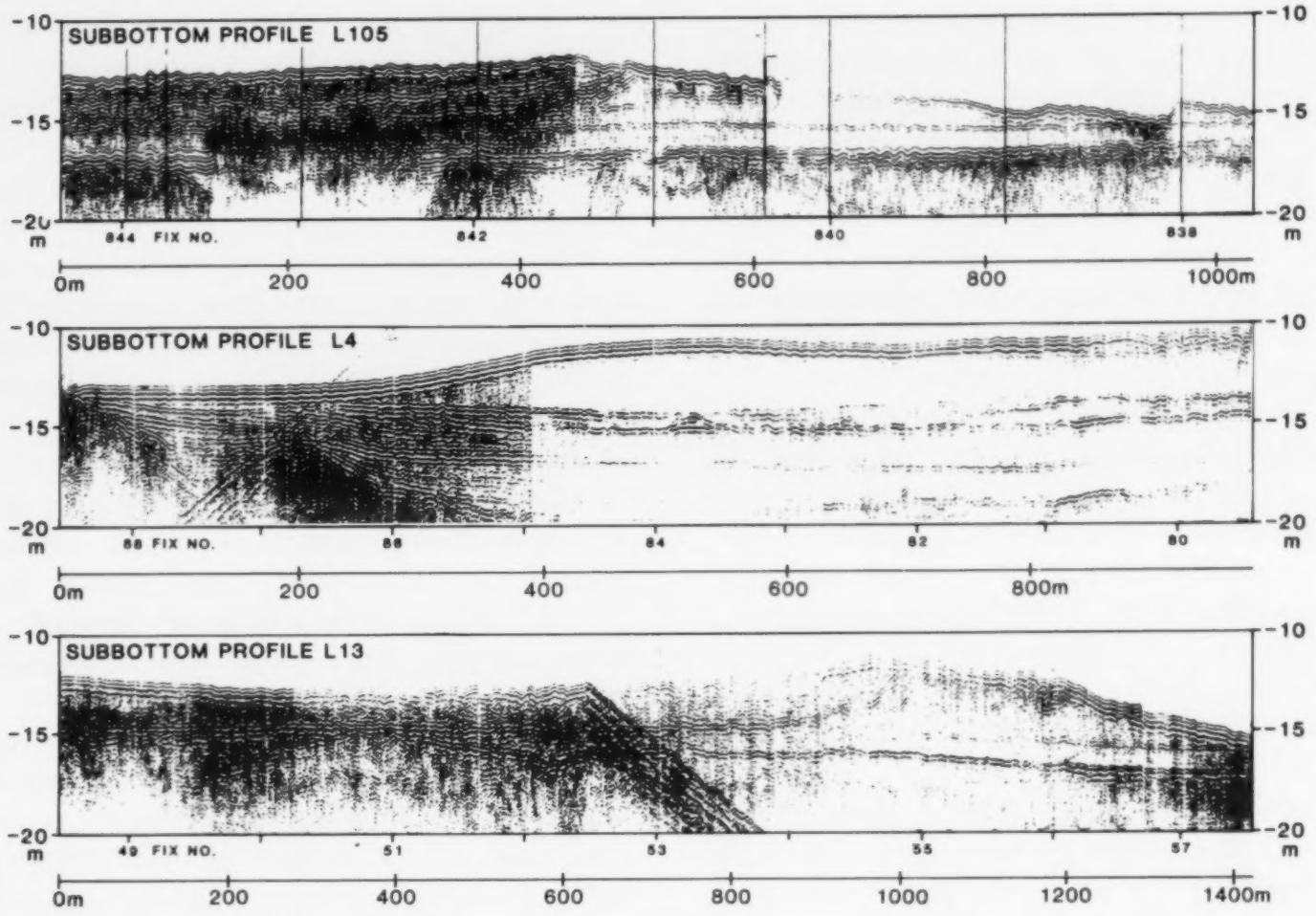
SUBBOTTOM PROFILE L105
-10
-15
-20 m
844 FIX NO.
842
840
838
0m
200
400
600
800
1000m
SUBBOTTOM PROFILE L4
88 FIX NO.
86
84
82
80
800m
SUBBOTTOM PROFILE L13
49 FIX NO.
51
53
55
57
1200
1400m

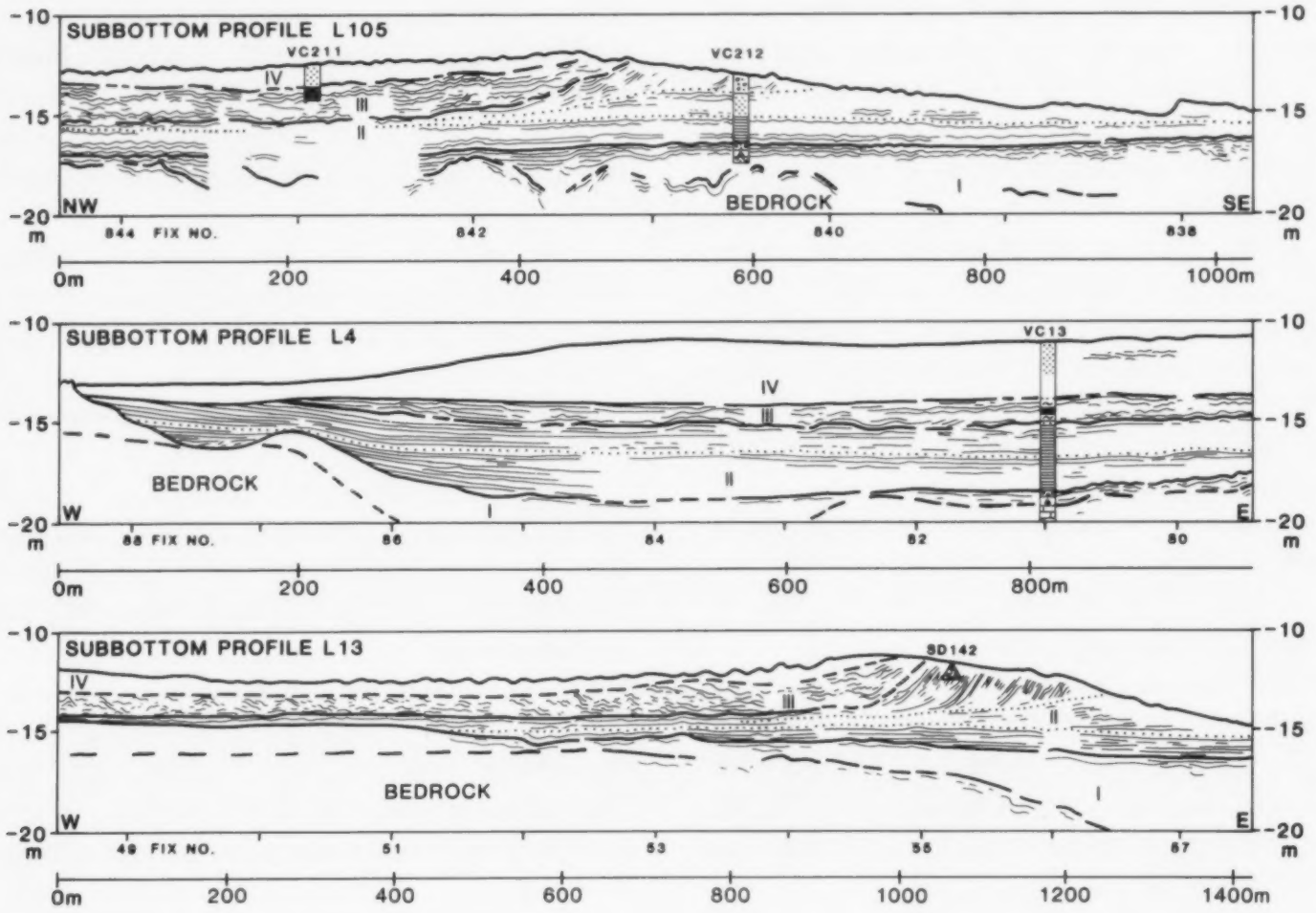
SUBBOTTOM PROFILE L105
VC211
VC212
IV
III
II
I
NW
SE
BEDROCK
SUBBOTTOM PROFILE L4
VC13
BEDROCK
W
E
SUBBOTTOM PROFILE L13
SD142
BEDROCK

revealing a retrogradational parasequence set. As a rule the correlative surfaces continue in the distal part parallel to the continuous, parallel, even-to-wavy reflection configurations, partly following the underlying topography. The internal lowermost correlative distal flooding surface shows minor, presumably subaquatic erosion, as can be recognized by erosional truncation, evident on Fig. 8 (L103). This figure shows a seismic profile in the dip direction of the erosive flooding surface, thus revealing the unconformity, while the profile in the strike direction (Fig. 6) only reveals a high amplitute concordant reflector. The retrogradational framework of the parasequences leads to erosion of the proximal part of the lowermost parasequence, leaving only the distal part preserved.

The internal configuration pattern of sequence II, described above, resulted in a combined basin-fill and wedge external geometry. The proximal landward prograding clinoform part of sequence II contains about 2 m of coarsening-upward medium to coarse sand (Fig. 7, VC212 and Fig. 6, SD142) with variable pebble content. The sedimentary structures are massive to planar cross bedding. The distal part can be divided lithologically into two major parasequences. The lowermost is bounded at the top by the prominent lowermost internal flooding surface referred to above. It consists of 0–5 m of very homogeneous clayey-silt with horizontal millimetre-thick lamination (Fl), interrupted by just a few sand laminae (Fig. 7, VC13 and VC212). Only on freshly split, non-oxidized, core surfaces the lamination can be recognized visually as a distinct variation in colour from light grey to grey. The uppermost distal part of the sequence consists of 1–2 m of clayey silt with a horizontal millimetre thick lamination, similar to the lowermost parasequence. The clay-silt laminae are disrupted by a number of 0.01–0.02 m thick layers of massive fine sand. The lowermost sand layer is quite prominent, probably marking the minor erosional discordance between the lowermost two parasequences, while the uppermost and most prominent sand layer marks the erosional discordance between sequences II and III. The distal clayey-silt deposits contain freshwater molluscs (*Anodonta*) and, in fresh cuts, scattered imprints of water mosses can be seen. The imprints disappear together with the lamination as a consequence of oxidation of sulfides present in the sediment. Vertical post-depositional in-situ root tubes ascribed to water-lily plants have been observed as well. The proximal part of this wedge-shaped sequence can be seen clearly as a ridge on the bathymetric map (Fig. 5).

Sequence II is interpreted as a transgressive coastal sequence consisting of coarse sand and pebble barrier beach ridge deposits closely connected to the former and contemporary back-barrier lagoon/pond deposits. In the most distal

Fig. 6. Shallow seismic profiles (ORE 3.5 kHz) and interpreted seismic sequences. Locations of the seismic profiles and samples are shown in Fig. 3. Uppermost three profiles show original seismic records L105, L4 and L13. Lowermost three profiles show interpreted seismic profiles L105, L4 and L13. The reflection pattern is interpreted using thick solid lines for sequence boundaries (unconformities and their correlative conformities), dotted lines for parasequence boundaries (flooding surfaces and their correlative surfaces) and thin solid lines for internal reflection pattern. Above bedrock (Cretaceous limestone) four seismic sequences are recognized:

(I) Upper erosional- and lower partly concordant bounding surfaces, with a chaotic to subparallel internal reflection pattern. Glacially related deposits.

(II) The sequence shows an upper bounding surface characterized by erosional truncation in the southeastern most part and concordance or erosional truncation in the northwesternmost part, while the lower bounding surface is concordant or onlap. The internal configuration consists of prograding clinoforms and parallel even to wavy reflectors. The sequence is divided by a retrogradational parasequences set. The external shape is basin fill to wedge shaped. Lagoon/pond and freshwater coastal deposits is the proposed interpretation.

(III) Upper bounding surface erosional and lower bounding surface onlap to concordant, with a subparallel, wavy to hummocky, clinoform, internal reflection pattern. The sequence is restricted to the Lagoon/pond basin, interpreted as lake–bog–lake deposits.

(IV) Upper bounding surface concordant to erosional and lower bounding surface mostly concordant, with a reflection-free to subparallel internal reflection pattern. Lens shaped deposits in connection to marine spit platforms (Jensen and Petersen, 1992) points to marine, near shore to shore deposits.

Sample positions and general lithological compositions of vibrocorings (*VC*) and suction dredging samples (*SD*) are indicated (Legend as Fig. 7).

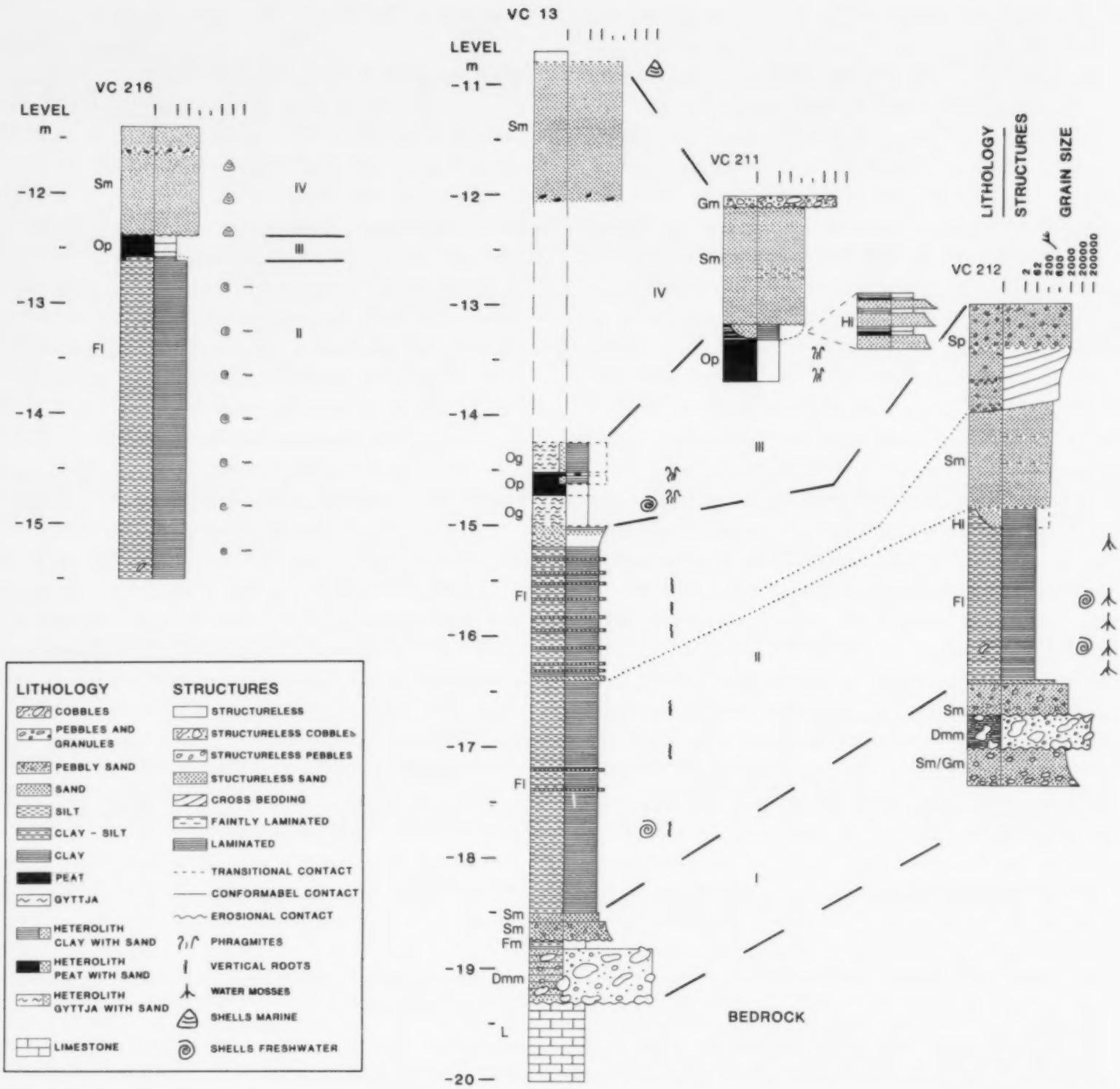

Fig. 7. Core logs showing lithology and sedimentological structures described in the vibrocores (VC). Locations are shown in Fig. 3. The interpreted correlation between lithofacies and seismic reflection pattern is also presented. Seismic sequence boundaries are marked by thick dashed lines, parasequence boundaries are marked by dotted lines and sequence numbers (*I–IV*) are indicated. Lithofacies are presented in a modified version of Eyles et al. (1983): *L* = limestone, Cretaceous; *Dmm* = matrix supported, massive, diamict; *Gm* = massive, gravel; *Sm* = massive, sand; *Sp*, planar crossbedded, sand; *Fl* = fine laminated, sand, silt, mud; *Fm* = massive, mud, silt; *Hl* = laminated, heterolithic, sand, silt, mud; *Op*, organic, peat; and *Og* = organic, gyttja. The bedrock foundation consists of Cretaceous limestone, over-layered by glacially related sediments of sequence I.

Sequence II shows a coarse grained barrier and a fine grained lagoon part, separated by parasequence boundaries. The sequence is interpreted as lagoon/pond and freshwater coastal deposits.

Sequence III consists of layered gyttja–peat–gyttja and is restricted to the lagoon/pond basin, indicating later development of a lake–bog–lake sequence.

Sequence IV is composed of fine–medium sand containing marine shell material. The sequence is interpreted as nearshore marine deposits.

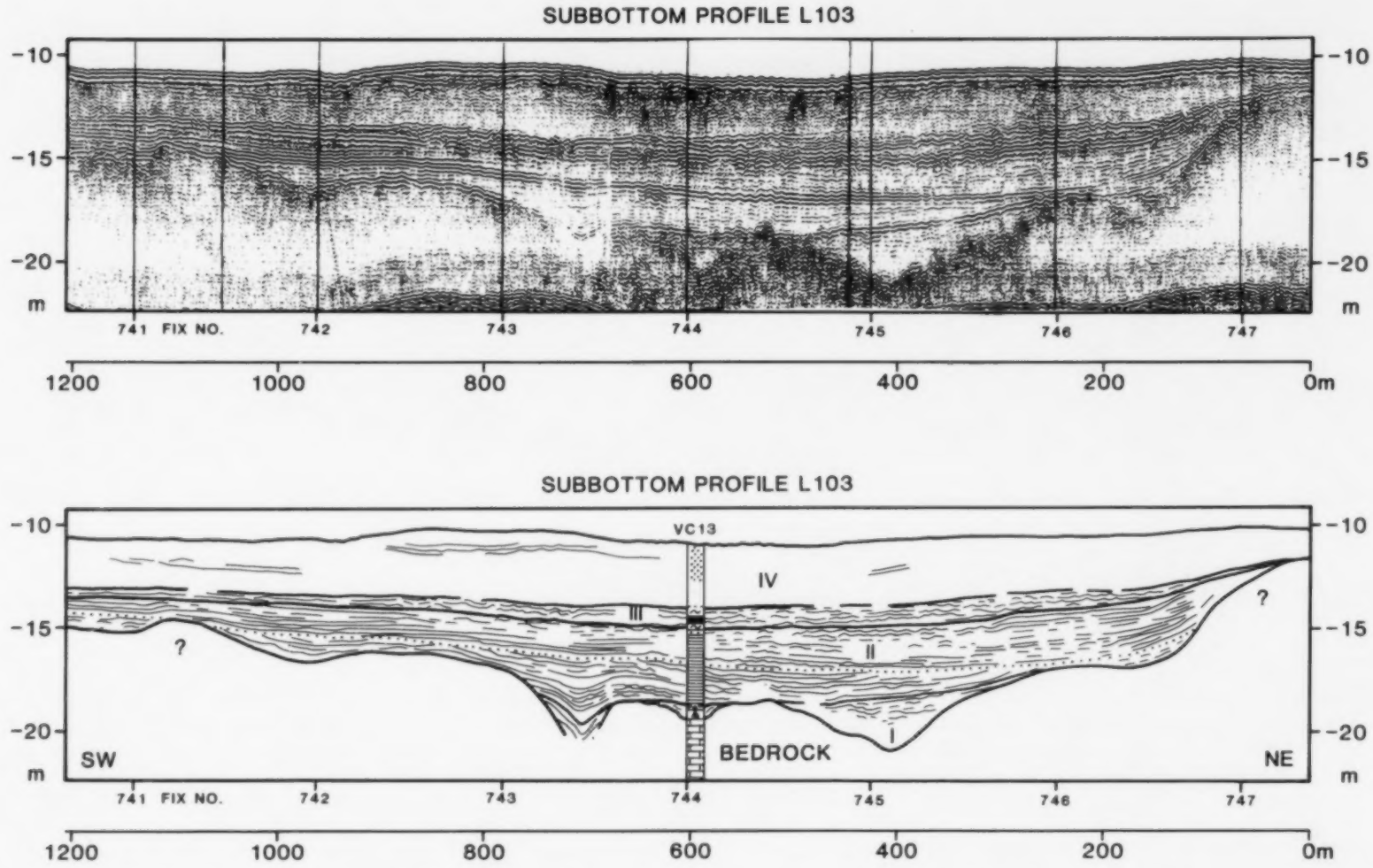

Fig. 8. Shallow seismic profile (ORE 3.5 kHz) and interpreted seismic sequences. Original seismic record L103 at top with interpretation below. The signatures and seismic reflection pattern are in general as described in Fig. 6. In this case a slightly different reflection pattern appears in sequence II, as the lowermost correlative distal flooding surface (parasequence boundary) shows a minor erosional truncation. This can apparently be seen in profile L103 because of the profile is in the dip direction of the flooding surface, whereas profiles in the strike direction (Fig. 6) show only a distinct concordant reflector.

and semi-enclosed part of the lagoon or pond, sequence II cannot be subdivided into parasequences. The internal configuration is parallel and shows a continuous parallel wavy reflection configuration, partly following the underlying topography (Fig. 9, L120). The lithology consist of fine laminated clayey silt (Fl), lacking interbedded sand layers (Fig. 7, VC216).

Sequence III. Lake–bog–lake deposits

The distribution of sequence III is limited to the lagoon/pond basin bounded by the glacial landscape and the barrier beach ridge of sequence II.

The upper bounding surface of sequence III is formed by erosional truncation. The lower unconformity is characterised by onlap on the barrier beach ridge while its correlative conformity is continuing concordant into the lagoon/pond basin (Figs. 6, 8 and 9). The internal configuration is subparallel, wavy to hummocky clinoforms. The external form is sheet drape to basin fill, as the sequence shows a very homogeneous thickness of approximately 1 m in the central part of the basin, but thins out and disappears against the rim of the basin.

The lithology of this sequence is characterised by deposits with a high organic content (Fig. 7, VC13). In the central part of the basin the sequence can be divided into 3 lithological units. The lowest consists of about 0.3 m of massive gyttja (Og) and contains frequently abundant freshwater shells (*Bithynia tentaculata*, *Planorbis planorbis*, *P. contortus*, *P. complanatus*, *P. vortex*, *Ancylus fluviatilis*, *Valvata pisinalis*, *V. cristata*, *Potamopyrgus jenkinsi*, *Lymnaea perger*, *Sphaerium corneum*, *Acroloxus lacustris*). The intermediate unit consists of

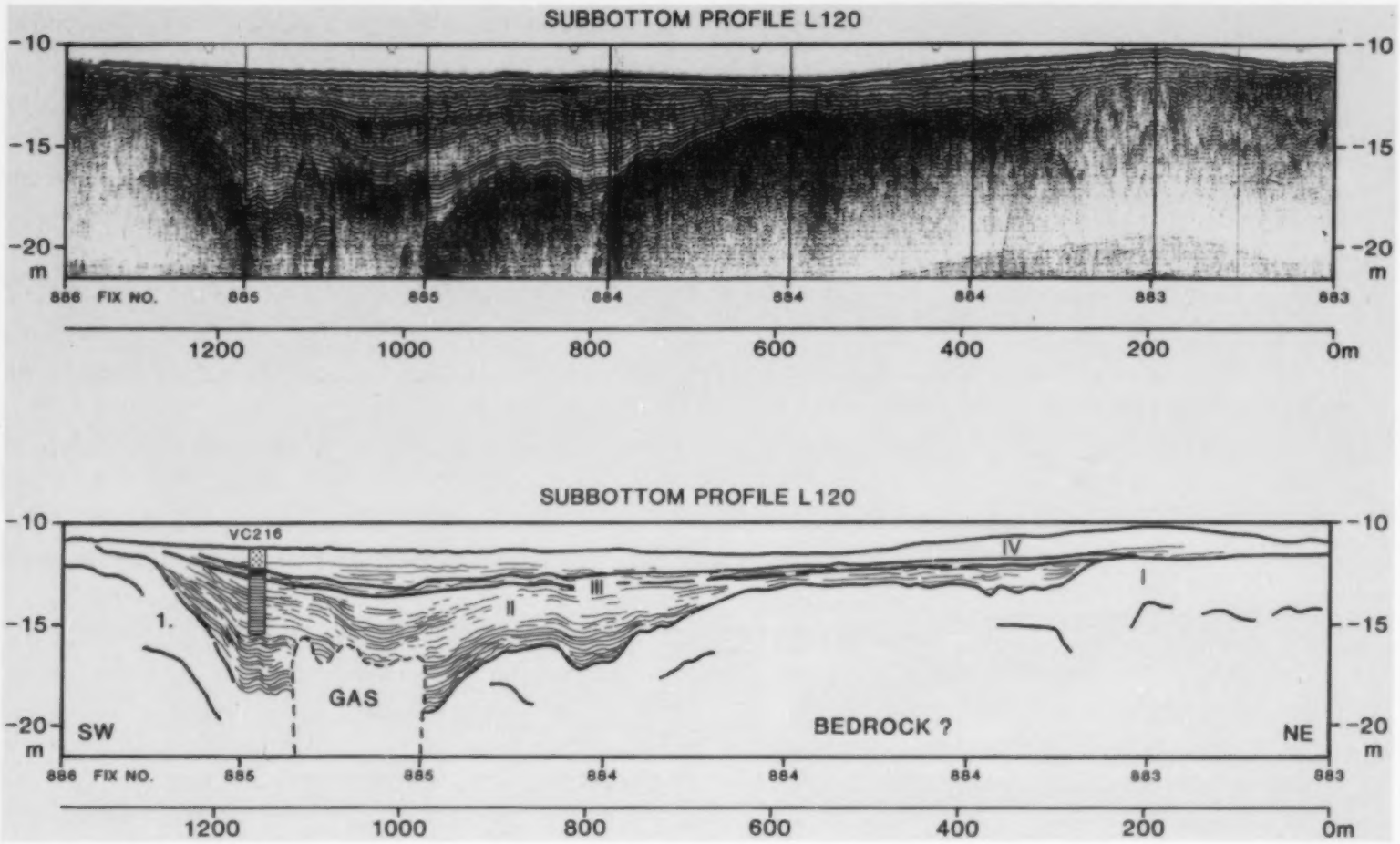

Fig. 9. Shallow seismic profile (ORE 3.5 kHz) and interpreted seismic sequences. Upper panel shows original seismic record L120 and lower panel shows interpretation. The signatures and the seismic reflection pattern are in general as described in Fig. 6. The profile is situated in the most landward part of the lagoon/pond basin, showing no visible parasequence division of sequence II.

0.2 m of partly layered peat (Op) mainly composed of reed and other lake plants. The uppermost 0.3 m of sequence III consists of layers of gyttja, containing plant remains and seeds, with interlaminated millimetre thin layers of fine sand. Partial core recovery of the sequence, landward of the barrier ridge (Fig. 7, VC211), shows the existence of about 0.4 m of a coherent, autochtonous and massive peat (Op) largely forming the uppermost half of the sequence. The peat consists mainly of reed and other lake plants. The uppermost 0.10–0.15 m of sequence III constitutes a transitional zone to sequence IV, consisting of millimetre to centimetre thick laminae of alternating fine-grained sand, lake marl and plant remains (Fig. 7, VC211).

In the most landward part of the lagoon/pond (Fig. 7, VC216) no erosive lithological boundary has been observed between sequences II and III. The boundary between the fine laminated clayey-silt deposits of sequence II and the peat deposits of sequence III is transitional, consisting of a few centimetres of laminated clay with a high content of organic material (Fl).

The seismic data combined with the lithological observations from the cores strongly suggest that sequence III consists of organic deposits in the abandoned former lagoon/pond basin. In the central part a freshwater lake developed, before a temporary drying out resulted in overgrowth. Renewed lake formation was probably caused by a rise in groundwater level. In the marginal part of the lake basin close to the former barrier beach ridge, growth presumably existed during the entire period only interrupted by lake deposits in the transition zone to sequence IV. The most distal part of the lagoon/pond area shows no hiatus between sequence II and III and the preserved part of sequence III shows an overgrowth of the basin immediately after the deposition of sequence II, not revealing any sign of lag deposits.

Sequence IV. Marine, (sub)littoral deposits

The uppermost sequence covers large parts of the survey area, and is typically developed as lenses behind sequence II ridges (Fig. 6) or as independent ridges (mounds) at the seafloor (Jensen and Petersen, 1992).

The sequence is mainly seismically transparent with some indication of parallel to subparallel reflections. The internal configuration gives the impression that the upper bounding surface is either concordant or shows truncation and the lower bounding surface is mostly concordant.

Vibrocoring in the sequence (Fig. 7, VC13, VC211, VC216) shows that sequence IV consists of fine, medium and coarse sand containing tests of marine molluscs including *Cardium edule*, *Mytilus edulis* and *Littorina littorea*.

Sequence IV consists of nearshore deposits. They are related to a number of marine spit platform and beach ridge deposits described elswhere (Jensen and Petersen, 1992).

Pollen data and ^{14}C dating

The pollen diagram (Fig. 10) is composed of 13 isolated pollen samples collected from 4 vibrocores (Fig. 7). The samples were taken from lithological units forming seismic sequences II and III. For stratigraphical purposes the results are compared with those from existing detailed continuous pollen diagrams (Iversen, 1973; Kolstrup and Buchardt, 1982; Ising, 1989).

The freshwater clayey-silt deposits in sequence II have a very low organic content typical of late glacial deposits. The pollen spectrum confirms this by showing relatively high percentages of *Artemisia* and *Gymnocarpium* as well as *Pinus* and *Betula*. Finally, the lack of *Corylus* indicates that the deposits must be at least older than 9500 yrs B.P. as the proportion of *Corylus* in this area increased markedly after that time (Mikkelsen, 1949; Iversen, 1973).

It is noteworthy that correlations can be made to detailed continuous pollen diagrams made from Late Glacial lake deposits (Torreberga ancient lake) in the southwesternmost part of Skåne, Sweden (Ising, 1989) and (Grænge ancient lake) in the western most part of Lolland, Denmark (Kolstrup and Buchardt, 1982).

The Toreberga ancient lake site was close to the shore of a bay in the Kattegat Sea north of the assumed Baltic Ice Lake threshold, but apart from the salinity difference the depositional environment was similar to the Fakse Bay locality.

At the Torreberga ancient lake site the later part of the Allerød was characterized by high percentages of *Pinus* (40–60%), *Cyperaceae* (10–20%) and low *Betula* values (10–15%), a tendency that can be recognized in the three lowermost samples (2122, 2121 and 0137) in sequence II.

For the latest part of Allerød a very high value of *Juniperus* existed (around 25%), *Pinus* receded to about 30% and *Betula* and *Salix* existed in moderately high values. Exactly this combination can be seen in sample 0136. Sample 0135 consisting of sand indicates the transitional border zone between sequence II and III in coring VC13 (Fig. 7). This sample can possibly be correlated to the upper part of Younger Dryas at Torreberga, characterized by decreasing *Juniperus* values (5–10%), *Cyperaceae* values of about 15%, *Poaceae* and *Artemisia* values of 5–10%.

In core VC216 (Fig. 7) there seems to be no major hiatus between the sequence II clay-silt deposits, the transitional clay-gyttja and the sequence III peat deposits. The pollen analyses (samples 2163 and 2162) confirm this, showing a good correlation to the Younger Dryas–Preboreal transition zone in Torreberga. This zone is characterized by a sudden increase of *Juniperus*, *Poaceae* and *Filipendula* and a decrease in *Pinus* to values below those found for *Betula*. The uppermost sample (2161) is believed to be of Preboreal age deposited after immigration of *Pinus* and before immigration of *Corylus*, which in the survey area means the time span 9700–9500 yrs B.P. (Iversen, 1973). This is in agreement with ^{14}C date K-5648 (Table 1) sampled in VC216 in the interval between the pollen samples 2162 and 2161 (at depth of 1250 cm).

The Grænge ancient lake locality was placed more inland and shows consistently more *Betula* and less *Pinus*. In spite of this the general trend is comparable, especialy the high percentages of *Juni-*

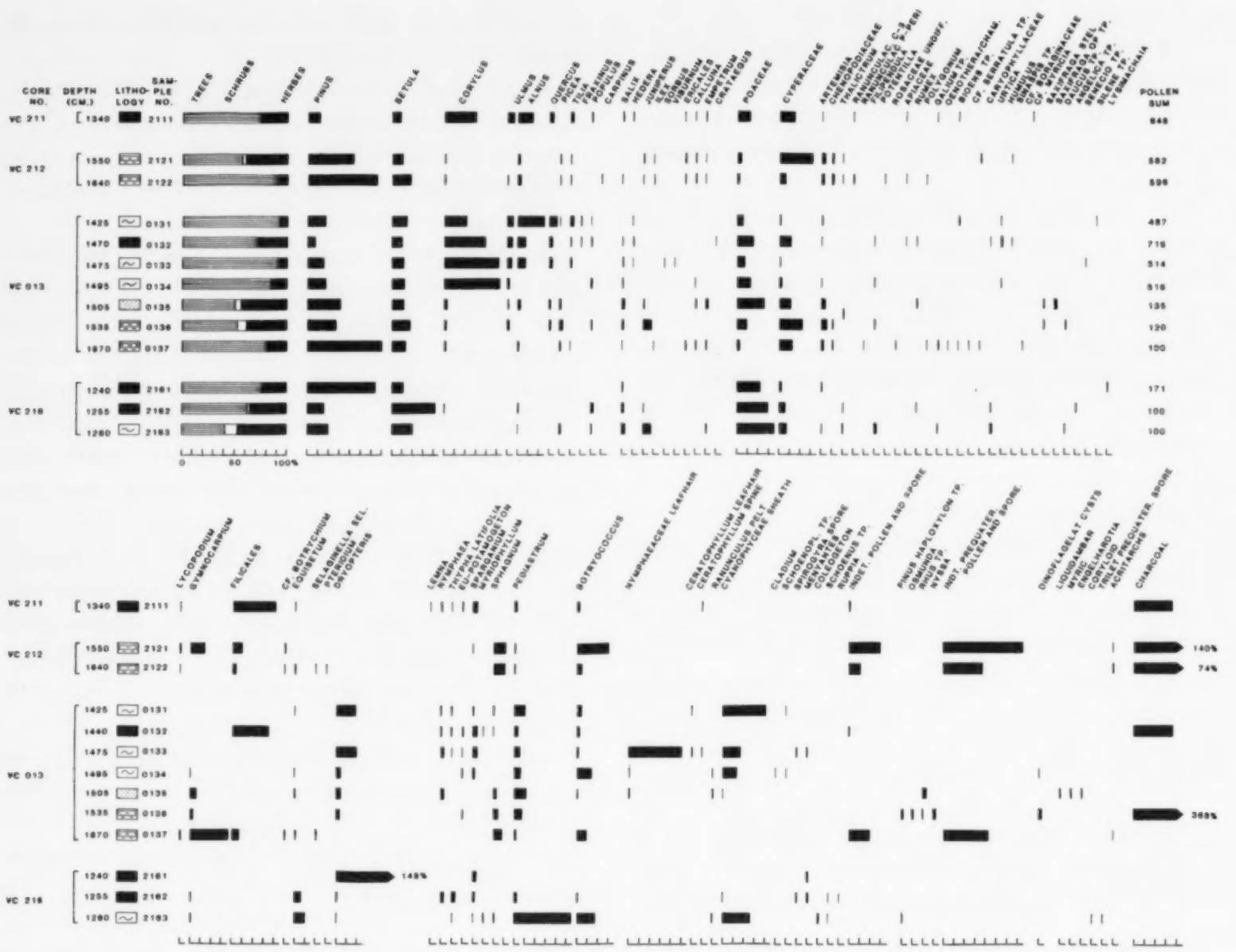

Fig. 10. Pollen percentage diagram composed of 13 single pollen samples collected from four vibrocores (VC211, VC212, VC13 and VC216). Sample depths are indicated in centimetres below present sea level. Symbols for lithology are similar to those used for the core descriptions in Fig. 7. The percentages are based on the pollen sum of trees, scrubs, herbs and grasses. The types included in the sum are given to the left of the column indicating the pollen sum.

perus in the latest part of Allerød and the Younger Dryas–Preboreal transition zone.

The stratigraphically uppermost 5 samples represent sequence III in cores VC13 and VC211 (Fig. 7).

The lowermost gyttja sample (0134) in core VC13 belongs to the *Corylus* maximum (Hazel–Pine period) around the time for immigration of *Ulmus*, but before *Alnus* and *Quercus* arrives. This suggests an age of 8900–8300 yrs B.P. (Iversen, 1973). It means that between samples 0135 and 0134 in VC13 there is a major hiatus of at least 1000 ^{14}C years.

Samples 0133 (gyttja) and 0132 (peat) belong to the *Corylus* maximum after the immigration of *Ulmus* and around the time for immigration of *Alnus* and *Quercus*, which indicates an age of about 8000 yrs B.P. (Iversen, 1973). The interpreted ages are confirmed by ^{14}C date K-5533 (Table 1) sampled in VC13 at a depth of 1460 cm and by ^{14}C date K-5532 (Table 1) sampled in the same stratigraphic level in core VC211 at a depth of 1380 cm.

The stratigraphically youngest samples (0131, VC13; 2111, VC211) are characterized by decreasing values of *Corylus*, high and increasing values of *Ulmus*, *Alnus*, *Quercus* and *Tilia*, while *Fraxinus* and *Hedera* are newly introduced. This pollen

TABLE 1

^{14}C dating results

Sample ID	Core	Depth below sea level	^{14}C yrs B.P.	$\delta^{13}C$ ‰PDB
K-5531	VC211	1340 cm	7900 ± 135	−27.1
K-5532	VC211	1380 cm	8090 ± 125	−25.6
K-5533	VC13	1460 cm	8010 ± 105	−28.7
K-5648	VC216	1250 cm	9430 ± 135	−29.5

spectrum is characteristic for the beginning of the Lime period (Iversen, 1973) indicating an age of 7500–8000 yrs B.P., which is confirmed by ^{14}C date K-5531 (Table 1) in VC211 at the same depth as pollen sample 2111.

Barrier (beach) ridge and back-barrier lagoon development

Interpretation of the pollen data indicates that the "Lagoon and freshwater coastal deposits" (sequence II) date back to the later part of the Allerød and Younger Dryas Chronozones (11,500–10,000 ^{14}C yrs B.P.). This late glacial period (Late Weichselian Substage) is in the Baltic Basin characterized by the existence of the Baltic Ice Lake, as documented by isostatically raised, relict coastal deposits, that can be followed onshore along the central and northern part of the present Baltic Sea (Björck, 1979; Eronen, 1983; Svensson, 1989).

The position of the present Fakse Bay near the margin of the area covered by the Weichselian icecap, implies that the isostatic rebound has been limited, probably resulting in fossil Baltic Ice Lake coastline deposits below present sea level (Svensson, 1989, fig. 118), indicating the southwesternmost marginal deposits of the Baltic Ice Lake. The limited isostatic rebound indicates that the damming of the Baltic Ice Lake most likely caused a transgressive development in the southernmost part, resulting in typical transgressive coastal deposits.

Mainly glacigenic deposits were source areas for the coastal deposits, redeposited by beach processes in a paraglacial setting. Church and Ryder (1972) defined the term "paraglacial" with reference to fluvial systems, but the first use of the term in the context of coastal sedimentation was in Forbes and Taylor (1987).

Recent and historical transgressive, paraglacial coastal deposits have been a subject of increasing interest, and various coastal types and associated sedimentological models have been described (Orford and Carter, 1982, 1984; Carter and Orford, 1984; Boyd et al., 1987; Forbes and Taylor, 1987; Carter et al., 1989; Duffy et al., 1989; Hill, 1990). The models show that coastal deposits clearly depend on the distribution and character of the glacigenic source sediments, variability in regional basin dynamics and rate of change of relative water level in the basin. These criteria can be used to describe the local Fakse Bay Baltic Ice Lake coastal evolution.

The distribution and character of the glacigenic source sediments in the study area is evident from the mapping of the glacial surface topography (Fig. 4), showing a morphology consisting of SE–NW oriented elongated ridges cut through by narrow valleys.

At the time of the damming of the Baltic Ice Lake the glacial landscape formed a shoreline, characterized by two prominent headlands (Brunhoved Flak and Gyldenløves Flak) and an intervening embayment (Figs. 4 and 11). The embayment between the headlands was very shallow (a water depth of max. 5 m) and the distance between the two headlands about 2.5 km. The headlands are believed to have consisted of glacigenic deposits similar to the present surface of the former headlands, capable of supplying sand and gravel for longshore transport.

Because the Baltic Ice Lake was an isolated lake, the tidal influence on coastal sedimentation was limited.

The sheltered lacustrine basin indicates that the wave energy under normal wind conditions was low in the study area. On the other hand, storm events are likely to have exerted a strong influence on the coastal evolution. This applies to storms from an easterly direction with a fetch of several hundred kilometres through a free passage north of Bornholm (Figs. 1 and 2). This suggests, that wave action was responsible for reworking, transportation and initiation of a paraglacial coastal barrier probably linking the two headlands (Fig. 5)

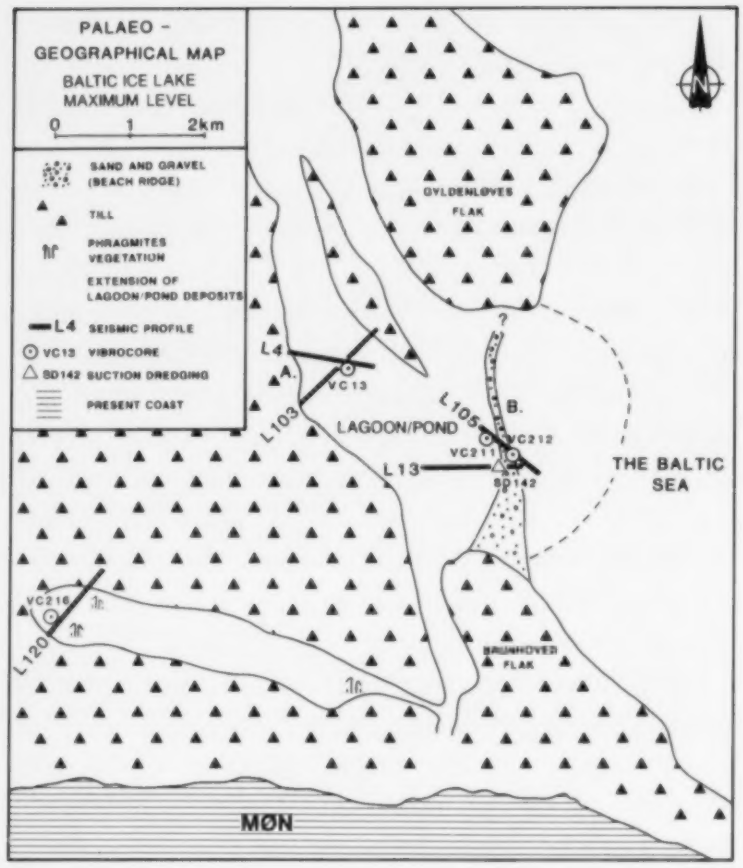

Fig. 11. Paleogeographical map of the detailed study area. The maximum transgression level of the Baltic Ice Lake is indicated by a barrier beach ridge and lagoon/pond system. The preserved fossil barrier is located on top of the coastal lagoon/pond deposits, having migrated in the order of 1.5–2 km west of the first appearance of the fine laminated lagoon/pond deposits (first appearance marked by a dash line).

and thus forming a barrier beach ridge (Fig. 12A) (see also, Carter et al., 1987; FitzGerald et al., 1987; Duffy et al., 1989).

The initial barrier beach ridge was presumably later eroded and only the finely laminated clay-silt deposits filling out the depression between the former headlands have thus been left. These preserved parts of the barrier beach ridge are located on top of the coastal pond deposits. The ridge thus must have migrated to a position of 1.5–2 km west of its initial location (Fig. 11).

The preserved sedimentological imprint is well documented by the corings (Fig. 7) showing finely laminated clayey-silt, backshore sediments, with an upward increasing interlayering of sand laminae, representing increasing proximity of overwash deposits as the barrier beach ridge moved landwards.

The proximal overwash deposits are revealed in the landward dipping seismic reflectors (Fig. 6). These records show that the preserved part of the ridge is composed exclusively of overwash deposits consisting of coarsening upward sand and gravel facies (Fig. 7).

Recent coastal research demonstrates that where sediment supply is limited, barrier stretching and landward retreat into the embayment via overwash processes results in constant landward beach ridge migration under rising or stationary sea level (Carter et al., 1987; Kelley, 1987; Forbes et al., 1991).

The rate of change of the relative basin water level can be determined by back-barrier pond investigations. Onlapping of the fine laminated sediments (Sequence II) in the pond basin (Figs. 6 and 8) indicates a pond water-level rise of minimum 4.5 m during the barrier migration period. The pond basin does not show any sign of inlet deltas and channels. From this it can be deduced that the pond basin may have established its own water level (Fig. 12B) balanced by seepage through the barrier beach ridge. The internal erosional unconformity (parasequence boundary) in the pond basin sediments (Figs. 6 and 8) implies that the water level was temporarily lowered at least once, probably due to the formation of one or more storm-induced major inlets, thus transforming the pond into a lagoon. It is tempting to conclude that the changes of the pond water level under normal circumstances closely followed those of the Baltic Basin water level. This implies that in the southwestern part of the Baltic Ice Lake there was a transgression amounting to about 4.5 m during the period 11,500–10,000 ^{14}C yrs B.P., resulting in a relative rate of water-level rise of 3 mm/yr. In the same period coastal retreat was in the order of 1.0–1.5 m/yr, values that correspond well to the present-day rates of relative sea-level rise and coastal recession along the Atlantic coast of Nova Scotia in eastern Canada (Taylor et al., 1985; Boyd et al., 1987).

The preservation potential of drowned transgressive coastal beach ridges normally is very limited due to remobilization and landward transportation of coarse beach ridge sediments. The typical sea bottom of such a transgressed paraglacial embayed headland coastal type is a smoothed glacial surface, mainly consisting of offstripped

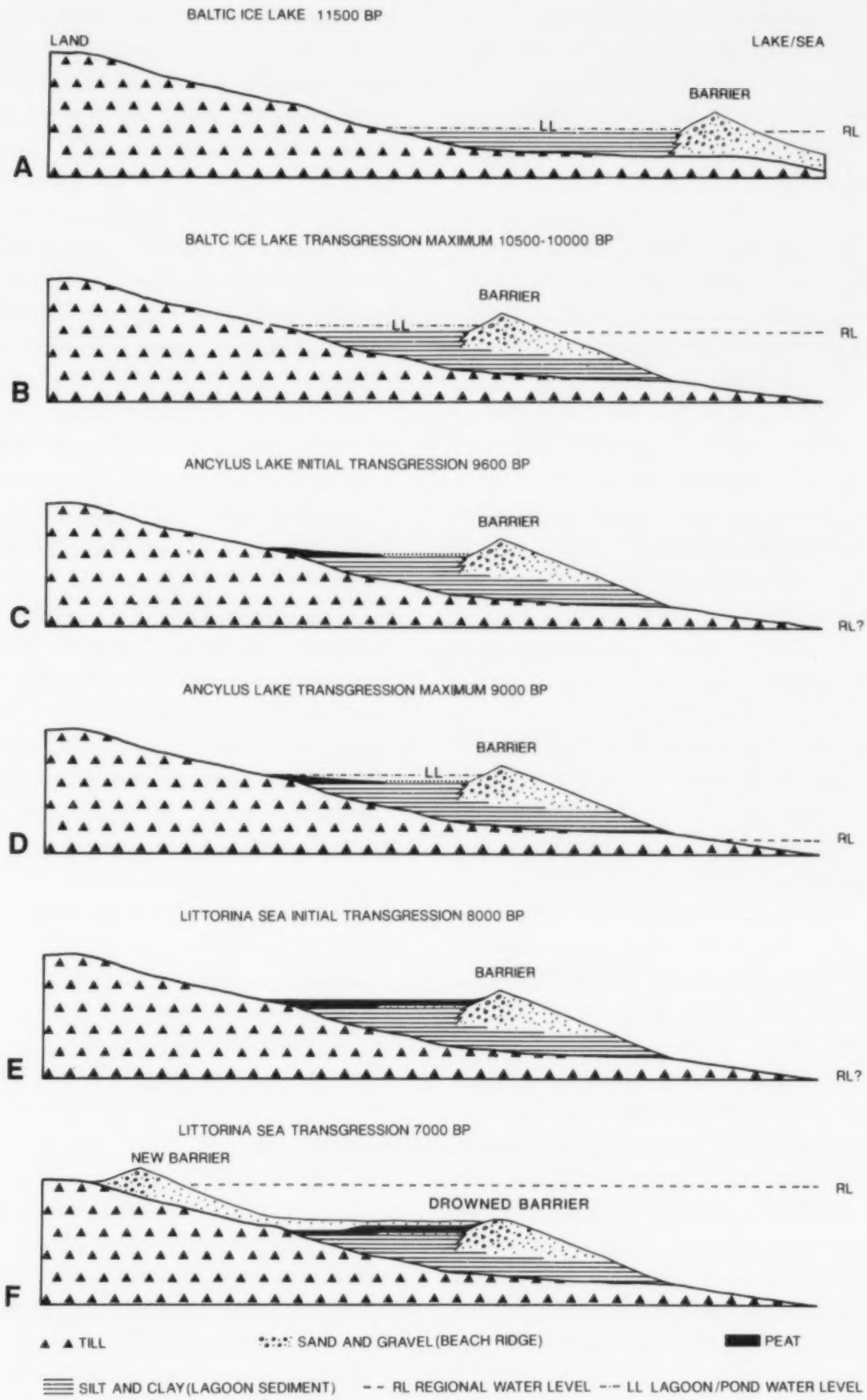

Fig. 12. A schematic model showing the late- and postglacial development in the southernmost Fakse Bay area. Successive profiles (*A–F*) show the water-level changes and deposition of sediments related to transgressive phases (Baltic Ice Lake, Ancylus Lake and Littorina Sea) and the intervening lowstands.

glacial headlands and preserved lagoon-pond infill in the former glacial valleys. Many authors, for example Oldale (1985), Carter et al. (1987), Davis and Clifton (1987), Forbes and Boyd (1989) and Forbes et al. (1991) have suggested, however, that barrier beach ridges under influence of rapid sea-level rise can be preserved by overstepping or in place "drowning" (Sanders and Kumar, 1975; Swift et al., 1985). The preservation of the drowned beach ridge in Fakse Bay is presumably due to the fact that the beach ridge represents the transgression maximum of the Baltic Ice Lake (Fig. 12B). This event has been dated by several researchers, e.g. Berglund (1966), Björck (1979), Donner (1982), Björck and Diegerfeldt (1984, 1986) and Svensson (1989). These authors have dated this event at around 10,500–10,300 yrs B.P., corresponding well with the supposed age of the youngest lagoon-pond sediments in the survey area.

Subsequent development

Further development of the barrier beach ridge stopped when the Baltic Ice Lake was finally drained (Fig. 12B and C).

The general picture in the southwestern part of the Baltic Basin is that in the Early Holocene a period of low water level followed, possibly only interrupted by the Ancylus Lake Transgression (9600–9000 yrs B.P.). Later i.e. about 8000 yrs B.P., the Littorina Sea entered the area (Kolp, 1986; Björck, 1987, 1989; Svensson, 1989).

In the survey area, the barrier beach ridge and lagoon/pond deposits are covered with gyttja–peat–gyttja deposits (Fig. 7) draping the entire coastal sequence (Figs. 6, 8 and 9). Pollen data (Fig. 10) from the distal part of the lagoon show that barrier and lagoon deposition stopped at the Younger Dryas–Preboreal transition zone, with a conformable transition to the following bog deposition (Fig. 12C). In the central and proximal part of the basin a quite prominent sand layer (Figs. 7 and 12 C) marks an erosional discordance between sequences II and III. The hiatus is at least of the order of 1000 ^{14}C years. The lowermost gyttja layer corresponds well to the Ancylus Lake transgression maximum and the initial drainage period of the Ancylus Lake, in which a high groundwater level still can be expected in the area (Fig. 12D), even in spite of the fact that the lake level apparently did not reach the level of the fossil barrier beach (Jensen and Petersen in prep.). The peat layer is well dated by ^{14}C dating and pollen samples (Fig. 10), giving ages close to 8000 yrs B.P. (Late Boreal Chronozone). This corresponds to the low water level in the Baltic Basin between the Ancylus Lake transgression and the Littorina Sea transgression (Fig. 12E) (Eronen, 1983; Björck and Dennegård, 1988). The uppermost gyttja layer shows a pollen spectrum, representing the beginning of Early Atlantic Chronozone characterized by rising ground water level, just prior to transgression of the area by the Littorina Sea.

The Littorina Sea transgressed the fossil Baltic Ice Lake coastal deposits about 7000 yrs B.P. (Jensen and Petersen, 1992), resulting in extensive erosion of the glacial deposits. The subsequent supply of paraglacial source sediments produced nearshore deposits that covered the drowned late glacial coastal deposits (Fig. 12F). In the period following 7000 yrs B.P. the continued Littorina Sea transgression overstepped (Swift et al., 1985) the early marine coastal deposits (Jensen and Petersen in prep.). A transgression maximum at about 2000 yrs B.P. was followed by a slight regression to the present water level 1 m lower (Mikkelsen, 1949; Krog, 1979).

Investigations of the overstepped Littorina Sea coastal deposits reveal spit and spit platform deposits at present water depths of 9 to 12 m (Jensen and Petersen, 1992).

Conclusions

Seismic sequence stratigraphical principles used on shallow seismic data, combined with detailed lithological and stratigraphical information, provided a powerful tool in mapping subaqueous Pleistocene and Holocene deposits. Based on these methods, the investigations in the Fakse Bay show the following evolution during the Late Pleistocene and Early Holocene (Fig. 12A–F):

(A) Baltic Ice Lake 11,500 yrs B.P. The damming of the Baltic Ice Lake caused the initial development of a barrier beach ridge. This ridge system

sheltered a pond, which in storm situations possibly was transformed into a lagoon due to formation of ephemeral inlets.

(B) Baltic Ice Lake transgression maximum 10,500–10,000 yrs B.P. Landward retreat of the barrier beach ridge stopped at the transgression maximum (relative water level of −13 to −14 m). During the preceding 1000 to 1500 years, the barrier beach ridge had apparently migrated westward over a distance of the order of 1.5–2 km.

(C) Ancylus Lake initial transgression 9600 yrs B.P. The final drainage of the Baltic Ice Lake resulted in a period of low water level likewise characterising the initial transgression period of the Ancylus Lake. In the distal semi-enclosed areas, gradual drying resulted in vegetation while the drainage resulted in erosion and non deposition in the central part of the former pond area.

(D) Ancylus Lake transgression maximum 9000 yrs B.P. The period of low water level was interrupted by the Ancylus Lake transgression. Even though the maximum water level of the Baltic Ice Lake was not reached, the transgression was capable of raising the groundwater level, transforming the former pond/lagoon area in to a freshwater lake.

(E) Littorina Sea initial transgression 8000 yrs B.P. The Ancylus Lake transgression was interrupted by the second drainage event after the deglaciation in the Baltic Basin. At the initial stage of the final Littorina Sea transgression, the low water level had resulted in a comprehensive overgrowth of the former back-barrier beach ridge areas.

(F) Littorina Sea transgression 7000 yrs B.P. The Littorina Sea transgressed the fossil Baltic Ice Lake coastal deposits about 7000 yrs B.P. Possibly due to vegetational armoring, the fossil Baltic Ice Lake coastal deposits were preserved. Continued transgression led to extensive erosion of the shallow glacial deposits, supplying material for shallow marine sedimentation that partly covered the former coastal deposits.

Acknowledgements

Financial support for the investigation was given by the National Forest and Nature Agency, the Danish Research Academy and the Geological Survey of Denmark. An early version of the manuscript was critically reviewed and editorial suggestions were provided by Antoon Kuijpers. The manuscript was further improved by the critical reading of Claus Andersen, Christian Christiansen, Holger Lykke-Andersen and Donald Forbes. Technical assistance was provided by Alice Rosenstand. I direct my best thanks to the above mentioned.

References

Aber, J.S., 1980. Kineto-stratigraphy at Hvideklint, Møn, Denmark and its regional significance. Bull. Geol. Soc. Den., 28: 81–93.

Aber, J.S., 1982. Model for glaciotectonism. Bull. Geol. Soc. Den., 30: 79–90.

Baartman, J.C. and Christensen, O.B., 1975. Contributions to the interpretation of the Fennoscandian Border Zone. Dan. Geol. Unders. Afh., Raekke 2, 1092: 1–47.

Berglund, B.E., 1966. Late-Quaternary vegetation in eastern Blekinge, southeastern Sweden. A pollenanalytical study. I. Late-Glacial time. Opera Botanica 12:1, 180 pp.

Berthelsen, A., Konradi, P. and Petersen, K.S., 1977. Kvartære lagfølger og strukturer i Vestmøns klinter. Dan. Geol. Foren., Arsskr., (1976): 93–99.

Björck, S., 1979. Late Weichselian stratigraphy of Blekinge, SE Sweden, and water level changes in the Baltic Ice Lake. Univ. Lund, Dep. Quat. Geol., Thesis 7, 248 pp.

Björck, S., 1987. An answer to the Ancylus enigma?—Presentation of a working hypothesis. Geol. Fören. Stockholm Förh., 109: 171–176.

Björck, S., 1989. The geodynamic and geologic value of a regional network of shore displacement curves: examples from southern Sweden. Geol. Fören. Stockholm Förh., 111: 292–294.

Björck, S. and Dennegård, B., 1988. Preliminary stratigraphic studies on the Late Weichselian and Holocene development of the Hanö Bay, southeastern Sweden. Geogr. Pol., 55: 51–62.

Björck, S. and Diegerfeldt, G., 1984. Climatic changes at Pleistocene/Holocene boundary in the Middle Swedish endmoraine zone, mainly inferred from stratigraphic indications. In: N.-A. Mörner and W. Karlén (Editors), Climatic Changes on a Yearly to Millennial Basis. Reidel, Dordrecht, pp. 37–56.

Björck, S. and Diegerfeldt, G., 1986. Late Weichselian–Early Holocene shore displacements west of Mt. Billing, within the Middle Swedish end-moraine zone. Boreas, 15: 1–18.

Boyd, R., Bowen, A.J. and Hall, R.K., 1987. An evolutionarymodel for transgressive sedimentation on the eastern shore of Nova Scotia. In: D.M. Fitzgerald and P.S. Rosen (Edi-

tors), Glaciated Coasts. Academic Press, San Diego, pp. 87–114.

Bowman, D., Christiansen, C. and Magaritz, M., 1989. Late-Holocene coastal evolution in the Hanstholm–Hjardemaal region, NW Denmark. Morphology, sediments and dating. Geogr. Tidsskr., 89: 49–57.

Carter, R.W.G. and Orford, J.D., 1984. Coarse clastic barrier beaches: a discussion of the distinctive dynamic and morphosedimentary characteristics. Mar. Geol., 60: 375–388.

Carter, R.W.G., Orford, J.D., Forbes, D.L. and Taylor, R.B.,1987. Gravel barriers, headlands and lagoons: an evolutionary model. In: Proc. Coastal Sediments '87 (New Orleans). Am. Soc. Civ. Eng., Washington, pp. 1776–1792.

Carter, R.W.G., Forbes, D.L., Jennings S.C., Orford, J.D., Shaw, J. and Taylor, R.B., 1989. Barrier and lagoon coast evolution under differing relative sea-level regimes: Examples from Ireland and Nova Scotia. Mar. Geol., 88: 221–242.

Church, M. and Ryder, J.M., 1972. Paraglacial sedimentation: a consideration of fluvial processes conditioned by glaciation. Geol. Soc. Am. Bull., 83: 3059–3072.

Davis, R.A., Jr. and Clifton, H.E., 1987. Sea-level change sand the preservation potential of wave-dominated and tide-dominated coastal sequences. In: D. Nummedal, O.H. Pilkey and J.D. Howard (Editors), Sea-level Fluctuations and Coastal Evolution. SEPM Spec. Publ., 41: 167–178.

Donner, J.J., 1982. Fluctuations in water level of the BalticIce Lake. In: T. Aartolahti and M. Eronen (Editors), Studies on the Baltic shorelines and sediments indicating relative sea-level changes. Ann. Acad. Sci. Fenn. Ser. A3, 134: 13–26.

Duffy, W., Belknap, D.F. and Kelly, J.T., 1989. Morphology and stratigraphy of small barrier–lagoon systems in Maine. In: L.G. Ward and G.M. Ashley (Editors), Physical Processes and Sedimentology of Siliclastic-Dominated Lagoon Systems. Mar. Geol., 88: 243–262.

Eronen, M., 1983. Late Weichselian and Holocene shore displacement in Finland. In: D.E. Smith and A.G. Dawson (Editors), Shorelines and Isostasy. Inst. Br. Geogr., Spec. Publ., 16: 183–206.

Eyles, N., Eyles, C.H. and Miall, A.D., 1983. Lithofacies types and vertical profile; an alternative approach to the description and environmental interpretation of glacial diamict and diamictite sequences. Sedimentology, 30: 393–410.

Faegri, K. and Iversen, J., 1975. Textbook of Pollen analysis. Munksgaard, Copenhagen, 295 pp.

FitzGerald, D.M., Baldwin, C.T., Ibrahim, N.A. and Sands, D.R., 1987. Development of the Northwestern Buzzards Bay Shoreline, Massachuetts. In: D.M. FitzGerald and P.S. Rosen (Editors), Glaciated Coasts. Academic Press, San Diego, pp. 327–357.

Forbes, D.L. and Boyd, R., 1989. Submersible observations of surficial sediments and seafloor morphology on the inner Scotian Shelf. In: Submersible Observations off the East Coast of Canada. Geol. Surv. Can. Pap., 88-20: 71–81.

Forbes, D.L. and Taylor, R.B., 1987. Coarse-grained beach sedimentation under paraglacial conditions, Canadian Atlantic coast. In: D.M. FitzGerald and P.S. Rosen (Editors), Glaciated Coasts. Academic Press, San Diego, pp. 51–86.

Forbes, D.L., Taylor, R.B., Orford, J.D., Carter, R.W.G. and Shaw, J., 1991. Gravel barrier migration and overstepping. Mar. Geol., 97: 305–313.

Hill, P.R., 1990. Coastal Geology of the King Point area,Yukon Territory, Canada. In: P.R. Hill (Editor), The Beaufort Sea Coastal Zone. Mar. Geol., 91: 93–111.

Hintze, V., 1937. Moens Klints Geologi. (Edited posthumously by E.L. Mertz and V.Nordmann). Reitzel, Copenhagen, 110 pp.

Houmark-Nielsen, M., 1987. Pleistocene stratigraphy and glacial history of the central part of Denmark. Bull. Geol. Soc. Den., 36: 1–189.

Hyde, G., 1986. En glacialgeologisk undersøgelse af klinternepå Nordøstmøn samt klinternes bagland. Ms. Thesis, 115 pp. (unpubl.)

Ising, J., 1989. Late Weichselian pollen stratigraphy, paleomagnetic secular variations and radiocarbon chronology at the Torreberga ancient lake, Skåne, Sweden. Geol. Fören. Stockholm Förh., 112(3): 281–292.

Iversen, J., 1973. The development of Denmark's Nature since the last Glacial. Dan. Geol. Unders., Ser. C, 7, 126 pp.

Jensen, J.B., 1992. Sequence stratigraphy of Late Pleistocene and Holocene deposits off the island of Møn, SW Baltic. In prep.

Jensen, J.B. and Petersen K.S., 1992. The Baltic Ice Lake andLittorina Transgression in the southwestern Baltic: Evidence from drowned coastal deposits in Fakse Bugt (Bay), Denmark. In prep.

Kelley, J.T., 1987. An inventory of coastal environments and classification of Main's glaciated shorelines. In: D.M. FitzGerald and P.S. Rosen (Editors), Glaciated Coasts. Academic Press, San Diego, pp. 151–177.

Kolp, O., 1986. Entwicklungsphasen des Ancylus-Sees. Petermanns Geogr. Mitt., 130(2): 79–94.

Kolstrup, E. and Buchardt, B., 1982. A pollen analyticalinvestigation supported by an ^{18}O-record of a Late Glacial lake deposit at Grænge (Denmark). Rev. Paleobot. Palynol., 36: 207–230.

Krog, H. 1979. The Quaternary history of the Baltic. Denmark.In: V. Gudelis and L.K. Königsson (Editors), The Quaternary history of the Baltic. Acta Univ. Symp., Univ. Ups. Ann. Quin. Celeb., 1: 207–217.

Lundquist, J., 1986. Late Weichselian glaciation and deglaciation in Scandinavia. Quat. Sci. Rev., 5: 269–292.

McCann, S.B. and Kostaschuk, R.A., 1987. Fjord Sedimentationin Northern British Columbia. In: D.M. FitzGerald and R.S. Rosen (Editors), Glaciated Coasts. Academic Press, San Diego, pp. 33–49.

Mikkelsen, V.M., 1949. Præstø Fjord. The Development of the postglacial vegetation and a contribution to the history of the Baltic Sea. Thesis, Copenhagen. Dan. Bot. Ar., Bd. 13, 5, 171 pp.

Nielsen, L.H., Johannesen, P.N. and Surlyk, F., 1988. A Late Pleistocene coarse-grained spit-platform sequence in northern Jylland, Denmark. Sedimentology, 35: 915–937.

Oldale, R.N., 1985. A drowned Holocene barrier spit off Cape Anne, Massachusetts. Geology, 13: 375–377.

Orford, J.D. and Carter, R.W.G., 1982. Crestal overtopping and washover sedimentation on a sandy-gravel barrier coast, Carnsore Point, southeast Ireland. J. Sediment. Petrol., 52: 265–278.

Orford, J.D. and Carter, R.W.G., 1984. Mechanisms to account

for the longshore spacing of overwash throats on a coarse clastic beach in southeast Ireland. Mar. Geol., 56: 207–226.

Petersen, K.S. and Konradi, P.B., 1974. Lithologisk og palæontologisk beskrivelse af profiler i Kvartæret på Sjælland. Dan. Geol. Foren., Arsskr., (1973): 47–56.

Posamentier, H.W. and Vail, P.R., 1988. Eustatic controls on clastic deposition II—Sequence and system tract-models. In: C.K. Wilgus, B.S. Hastings, C.G.St.C. Kendall et al. (Editors), Sea-level Changes: An Integrated Approach. SEPM Spec. Publ., 42: 125–154.

Posamentier, H.W., Jervey, M.T. and Vail, P.R., 1988. Eustatic controls on clastic deposition I—Conceptual framework. In: C.K. Wilgus, B.S. Hastings, C.G.St.C. Kendall et al. (Editors), Sea-level Changes: An Integrated Approach. SEPM Spec. Publ., 42: 109–124.

Sanders, J.E. and Kumar, N., 1975. Evidence of Shoreface Retreat and In-Place "Drowning" During Holocene Submergence of Barriers, Shelf off Fire Islands, New York. Geol. Soc. Am. Bull., 86: 65–76.

Shaw, J. and Forbes, D.L., 1987. Coastal barrier and beach-ridge sedimentation in Newfoundland. In: Proc. Can. Coastal Conf. (Quebec) Natl. Res. Counc., Ottawa, pp. 437–454.

Shaw, J. and Forbes, D.L., 1990. Barrier-platform and spillover deposits in St. Georges's Bay, southwest Newfoundland: Products of coastal sediment dispersal during the Holocene transgression. In prep.

Shaw, J., Taylor, R.B. and Forbes, D.L., 1990. Coarse clastic barriers in eastern Canada: patterns of glaciogenic sediment dispersal with rising sea levels. Geol. Surv. Can., In prep.

Surlyk, F., 1980. Geology of the European countries, vol. 1 Denmark. Dunod, Paris, pp. 42–50.

Svensson, N.O., 1989. Late Weichselian and Early Holocene shore displacement in the central baltic, based on stratigraphical and morphological records from eastern Småland and Gotland, Sweden. Lundqua Thesis, 25, 195 pp.

Swift, D.J.P., Niedaroda, A.W., Vincent, C.E. and Hopkins,T.S., 1985. Barrier island evolution, middle Atlantic shelf, U.S.A. Part I: Shoreface dynamics. Mar. Geol., 63: 331–361.

Taylor, R.B., Wittmann, S.L., Milne, M.J. and Kober, S.M., 1985. Beach morphology and coastal changes at selected sites, mainland Nova Scotia. Geol. Surv. Can. Pap., 85-12, 59 pp.

Tirant, P.L., 1979. Seabed Reconnaissance and Offshore Soil Mechanics for the Installation of Petroleum Structures. Inst. Fr. Pét. Publ., 132 pp.

Vail, P.R., 1987. Seismic stratigraphy interpretation using sequence stratigraphy. In: A.W. Bally (Editor), AAPG Atlas of Seismic Stratigraphy. Am. Assoc. Pet. Geol. Stud. Geol., 27(1): 1–10.

Vail, P.R., Mitchum, R.M., Jr., Todd, R.G.,Widmier, J.M., Thompson, S., III, Sangree, J.B., Bubb, J.N. and Hatlelid, W.G., 1977. Seismic stratigraphy and global changes of sea level. In: C.E. Clayton (Editor), Seismic Stratigraphy—Applications to Hydrocarbon Exploration. Am. Assoc. Pet. Geol. Mem., 26: 49–212.

Van Wagoner, J.C., Mitchum, R.M., Posamentier, H.W. and Vail, P.R., 1987. Seismic stratigraphy interpretation using sequence stratigraphy, Part 2: Key definitions of sequence stratigraphy. In: A.W. Bally (Editor), AAPG Atlas of Seismic Stratigraphy. Am. Assoc. Pet. Geol. Stud. Geol., 27(1): 11–14.

Van Wagoner, J.C., Posamentier, H.W., Mitchum, R.M., Vail, P.R., Sarg, J.F., Loutit, T.S. and Hardenbol, J., 1988. An overview of the fundamentals of sequence stratigraphy and key definitions. In: C.K. Wilgus, B.S. Hastings, C.G.St.C. Kendall et al. (Editors), Sea-level Changes: An Integrated Approach. SEPM Spec. Publ., 42: 39–45.

Wentworth, C.K., 1922. A scale of grade class terms forclastic sediments. J. Geol., 30: 377–392.

Marine Geology, 107 (1992) 103–137
Elsevier Science Publishers B.V., Amsterdam

Beach systems of the central Netherlands coast: Processes, morphology and structural impacts in a storm driven multi-bar system

Andrew D. Short

Coastal Studies Unit, Department of Geography, University of Sydney, Sydney, NSW 2006, Australia

(Received March 11, 1991; revision accepted November 13, 1991)

ABSTRACT

Short, A.D., 1992. Beach systems of the central Netherlands coast: Processes, morphology and structural impacts in a storm driven multi-bar system. *Mar. Geol.*, 107: 103–137.

The 124 km long central Netherlands coast consists of a sand barrier system fronted by beach and surf zone containing 2 to 3 bars. The beach and surf zone are the product of wind waves generated in the North Sea, interacting with the medium to fine shoreface sands, in a micro tidal environment. The inner bar is usually attached to the beach as a ridge and runnel cut by drains and rips, the second and third bars are highly rhythmic and are characterised respectively by transverse bars and rips and rhythmic to longshore bar and trough bar types. Structural impacts influence 48 km of shore with harbour moles inducing lower wave energy and shoreline progradation, a 4.5 km long dyke replaces part of the beach but apparently has had little impact on mesoscale bar dynamics, while 158 groynes in three groyne fields have produced more intermediate, rip driven, surf zones. Natural beach processes however dominate the entire coast with the hierarchical bar morphology related to cross-shore wave breaking. The equilibrium beach concept of Wright et al. (1987) was used to empirically predict beach/bar type. The results explain both the hierarchy of bar type and the temporal variation in beach-bar type. Finally a multi-bar "beach model" for the coast is presented which builds upon the single bar model of Wright and Short (1984).

Introduction

The Netherlands coast is 432 km long of which 82% consists of sandy beach systems. The entire coast has a west to north orientation and faces the southern North Sea. The contemporary processes affecting the coast are related to wave, tide and wind regimes of the North Sea region interacting with the Netherlands shelf, beach, barrier and estuarine systems. The nature and degree of this interaction varies considerably around the coast, in response to changing boundary conditions and processes regimes. The boundary conditions include shoreline orientation, particularly to waves and wind; the geomorphology (barrier and estuary); structural impact (dykes, surge barriers, breakwaters, groynes and nourishment); and sediment characteristics. The process regimes include the tide range, tidal and littoral currents, wave climate, wind climate and storm surges.

This paper is concerned solely with the central Netherlands coast, the provinces of North and South Holland, which contain 124 km of essentially continuous sandy shoreline (Fig. 1). The aim of this study is to determine the nature and variability of the beach system that fronts the entire central coast, and in particular, to assess the interaction of wave, sediment and shoreface gradients and in place structures that produce the multi-bar morphology, and its spatial and temporal variation.

The beach system is defined as including the subaerial beach and surf zone. Along the central coast this includes the shore parallel bar systems,

Correspondence to: A. Short, University of Sydney, Coastal Studies Unit, Department of Geography, Sydney, N.S.W. 2006, Australia.

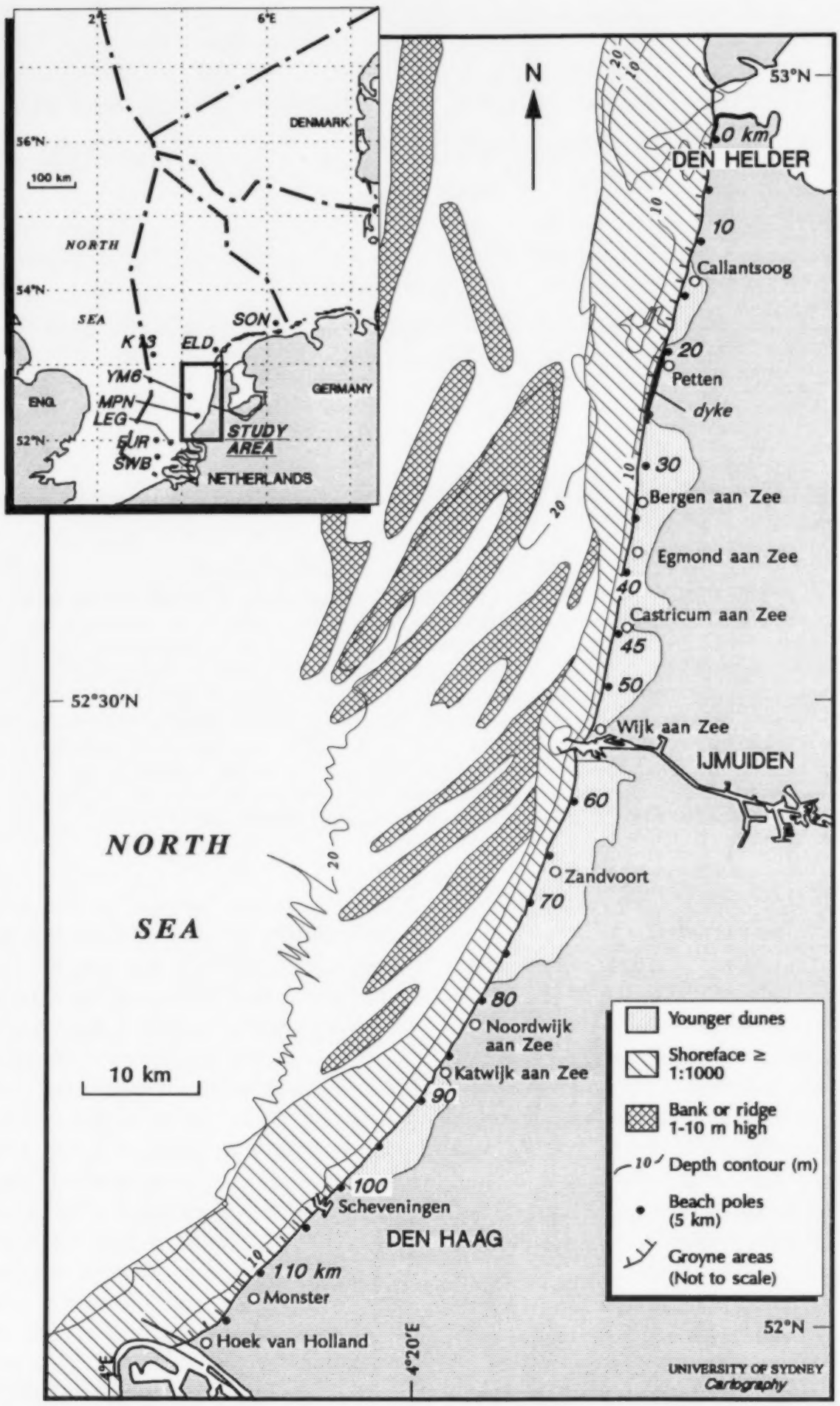

Fig. 1. The central Netherlands coast and study area, Den Helder to Hoek van Holland. Shown are the location of 5 km beach poles, all major structural features (groynes, breakwaters, dykes), the extent of the coastal slope or shoreface (from Van Alphen and Damoiseaux, 1988) 'Younger Dunes' and major towns. Insert shows location of the eight wave stations in The Netherlands sector of the North Sea (Source: Roskam, 1988).

but not the inner shelf shore connected ridges. It is essentially in the inner, steeper coastal slope (>1:1000) region of the Dutch shoreface (Fig. 1) as mapped by Van Alphen and Damoiseaux (1988).

Data base and methods

The Netherlands has probably the best studied and best monitored coast in the world. As a result a wealth of data and information exists on coastal evolution, coastal processes and change. Much of this has recently been summarised as a result of two major projects. In 1987 the "Coastal Genesis" project produced a series of reports on coastal behaviour at scales of 5000, 1000 and 100 years. This was followed in 1989 by the "Coast Defence after 1990" project which produced 20 technical reports on all aspects of Netherland's coast defence. The reports of Stolk et al. (1987), and particularly Stolk (1989), provide an excellent overview and background information on the geological evolution and physical nature of the Netherland coast. Also the report of Dillingh and Stolk (1989) for the European CORINE "Coastal erosion" project provides a good review of contemporary shoreline changes.

The study of beach morphodynamics requires information on both the morphology or beach type as well as the variables that contribute to morphological change, particularly sediments and coastal processes. For the 124 km long central coast, information is also required at a sampling interval that will permit an assessment of longshore or spatial change in beach morphodynamics, and over a sufficient period of time to permit assessment of temporal change.

The spatial and temporal sampling procedure adopted by the study was largely pre-determined by the nature and availability of data (Table 1). To account for spatial change a minimum 1 km sampling interval was chosen to coincide with the 1 km beach poles along the coast. The location of the 1 km poles are also shown on the 1:25,000 topography maps and are marked on 1:4000 aerial photographs. This interval gave 118 sample points for the central coast, extending from km 1 at Den Helder in the north and km 119 at Hoek van Holland in the south (Fig. 1). These points or beach pole numbers are used to locate and identify features throughout this paper. The remainder of this section briefly describes the data base and methodology, and is followed by sections on the major results.

The morphology of the beach and bar systems, and the location of all rips, was obtained from the 1:4000 aerial photographs taken annually by *Rijkswaterstaat* between 1982 and 1988 (Table 2). The photographs were used to continuously record beach type for the beach/bar 1, bar 2 and bar 3 (the latter when visible) by visual comparison to the beach model of Wright and Short (1984). This data was then sampled at 1 km intervals with a numeric value assigned to each beach type (Table 3).

Rip location ($\pm$10 m) was recorded for all rips visible on the 1:4000 aerial photographs. The rip type (RR, TBR, RBB or LBT, Table 3) was determined from the bar/beach morphology. In addition rip orientation (north, west/shore normal, south) was recorded, as well as longshore rip length for skewed rips.

Beach sediments, in conjunction with waves and tides, determine the beach morphodynamic type (Wright and Short, 1984). In order to assess the nature and spatial variation in sediments along the central coast, the results of three recent reports were utilised (Table 1). They provided information on 334 dune, beach and surf zone samples. The aim was to determine the mean sediment characteristics and the presence, if any, of longshore trends in grain size which could in turn contribute to spatial trends in beach morphodynamics.

Beach profiles, usually extending 1000 m seaward, are surveyed annually every 250 m by *Rijkswaterstaat*. From this data set 118 cross-shore profile envelopes (Fig. 2) were plotted by *Rijkswaterstaat* for each kilometre beach pole (km 1–118) from 1976 to 1985. Each profile envelope was used to measure the following morphometric variables: tan B slope to 1000 m; number of bars present; width of the subaerial beach; height of the beach; and area of the beach/bar 1; area and width of the sweep zone where bars are mobile; amplitude of bar 2; and mean distance to and normal migration/mobility of the shoreline (bar 1), bars 2 and 3. A summary of the results are listed in Table 4.

TABLE 1

Major data types and sources—central Netherlands coast

	DATA	SOURCE
1.	Location - features	1:25 000 Topographic maps showing all 1 km beach poles, groynes, breakwaters and dykes
2.	Sediments:	
	* Dune	Kohsiek, 1984
	* Beach	van Bemmelen, 1988
	* Surf zone	van Alphen, 1987
3.	Waves:	
	1976-1986	Rijkswaterstaat, Tidal Waters Division Roskam, 1988
	1987-1988	KNMI, Division of Oceanographic Research
4.	Beach profiles:	
	1976-1985	Rijkswaterstaat, Tidal Waters Division
	Nearshore profiles	1:10 000 sounding charts, Rijkswaterstaat
5.	Beach morphology:	
	1982-1988	Aerial photographs (1:4 000) Rijkswaterstaat, Mapping and Survey Division
	1966, 1968, 1970, 1971	Air photo mosaics Rijkswaterstaat, North Sea Directorate

Nearshore profiles extending several kilometres seaward are surveyed periodically by *Rijkswaterstaat*. They are published as individual survey lines and as bathymetric charts. Twenty-three profiles spaced at approximately 5 km intervals between km 5 and 118, and 49 profiles at 1 km intervals between km 70 and 119 were obtained from *Rijkswaterstaat*. These profiles were used to measure the nearshore gradient out to the break in slope, and the distance to and depth of the break in slope. A comparison of inner (surf zone) and outer (shoreface) slope characteristics is given in Table 5.

Wave parameters are recorded at eight deep-water stations in the Netherlands sector of the North Sea (Fig. 1). Daily, monthly and annual summaries were obtained from *Rijkswaterstaat* for the four stations closest to the coast (LEG, MPN, YM6, ELD) for the period 01.01.79 to 31.12.86. Records from 01.01.87 to 31.12.88 (usually 3 hourly and 8 per day) were obtained for MPN and YMG from the Royal Netherlands Meteorological Institute (*KNMI*), Division of Oceanographic Research. The latter data was summarized into daily averages of wave height and period. The entire data set was organized to provide two continuous daily records of wave height (H_o) and period (T_o) for MPN and YM6, the two stations closest to the central coast (Fig. 1). When daily data was missing from these stations, it was obtained from one of the other stations (LEG or ELD). The records were analyzed for two purposes. First, to provide daily wave conditions leading up to the date of 1987 and 1988 aerial photographs, and second, to permit an assessment of the monthly and annual wave climate. In addition a summary of wave directions for the LEG station was extracted from Roskam (1988).

TABLE 2

Date and coverage of vertical aerial photographs central Netherland coast

Vertical Aerial Photographs, 1:4 000[1] Date	Coverage (km)	C/B+W
04.04.82	59-82	B+W
09.04.83	26-55	B+W
15.04.83	56-118	B+W
15.05.84	0- 2	B+W
14.04.84	3-20	B+W
11.04.84	56-97	B+W
01.02.85	1- 34	B+W
24.04.85	35-118	B+W
25.05.86	26- 58	B+W
26.05.86	59- 60	B+W
30.04.86	61-115	B+W
24.05.87	2- 54	B+W
09.05.87	55- 97	B+W
24.04.88	1-25	C
22.04.88	26-55	C
07.05.88	56-118	C
Aerial Photograph Mosaics, 1:8 000[2]		
28.02.66	108 - 119	B+W
16.03.68	86 - 103	B+W
17.06.70	86 - 119	B+W
14.07.71	86 - 119	B+W

C = colour; B + W = black and white.
[1]Source: *Rijkswaterstaat*, Mapping and Survey Division.
[2]Source: *Rijkswaterstaat*, North Sea Directorate.

Tides do make an important contribution to beach morphodynamic processes and type, as recently reviewed by Short (1991b). Along the central coast the tide is micro-tidal and relatively uniform longshore ranging from 1.4 m at Den Helder to 1.7 m at Hoek van Holland. Therefore the range itself is not considered important in contributing to temporal or spatial variation in beach morphodynamics and is not considered further.

Tidal currents are prominent along the central coast. The tide floods to the north, with a maxi-

TABLE 3

Classification of beach types

Beach Type[1]	Abbreviation Used in Report	Nominal Value
Reflective	R	1 1.5
Low tide terrace/ridge and runnel	LTT/RR	2 2.5
Transverse bar and rip	TBR	3 3.5
Rhythmic bar and beach	RBB	4 4.5
Longshore bar and trough	LBT	5 5.5
Dissipative	D	6

[1]Based on Wright and Short, 1984.

mum surface flow of between 0.6 to 1.0 m/s, and ebbs to the south, with a lower velocity resulting in a northward residual of about 0.05 m/s (Wiersma and Van Alphen, 1988). Roelvink and Stive (1990) found that while tide currents dominate inner shelf transport, inside the 8 m depth contour wave induced cross-shore transport increases to ultimately dominate the surf zone. While the tide currents will imprint themselves on the surf zone current regime, and can be measured at the shoreline in calm conditions, they are considered secondary to waves in producing beach changes and are therefore not considered further in this study.

Storm surges are a major threat to all beaches and low lying sections of the North Sea coast. Coastal processes and beach change, will be most intense during the high seas and winds, that produce a storm surge. The storm surge will therefore have a temporal impact on beach type, leading to offshore suspended sediment transport (Steetzel, 1990) and more dissipative conditions during high, sea-surge conditions. Unfortunately, while storm surges can be expected to produce shoreline erosion and more dissipative beach conditions, the morphological data base (the aerial photographs) do not include the coast immediately following a storm surge. Therefore this high energy end of the wave-surge spectrum can only be inferred from models of beach behaviour and the literature rather than the existing data base.

The following sections examine in more detail the major parameters that contribute to beach morphodynamics, followed by an assessment of the beach morphology. For more details on the actual parameters see Short (1991a).

Sediments

In order to characterize the dune, beach and surf sediments this study used respectively the

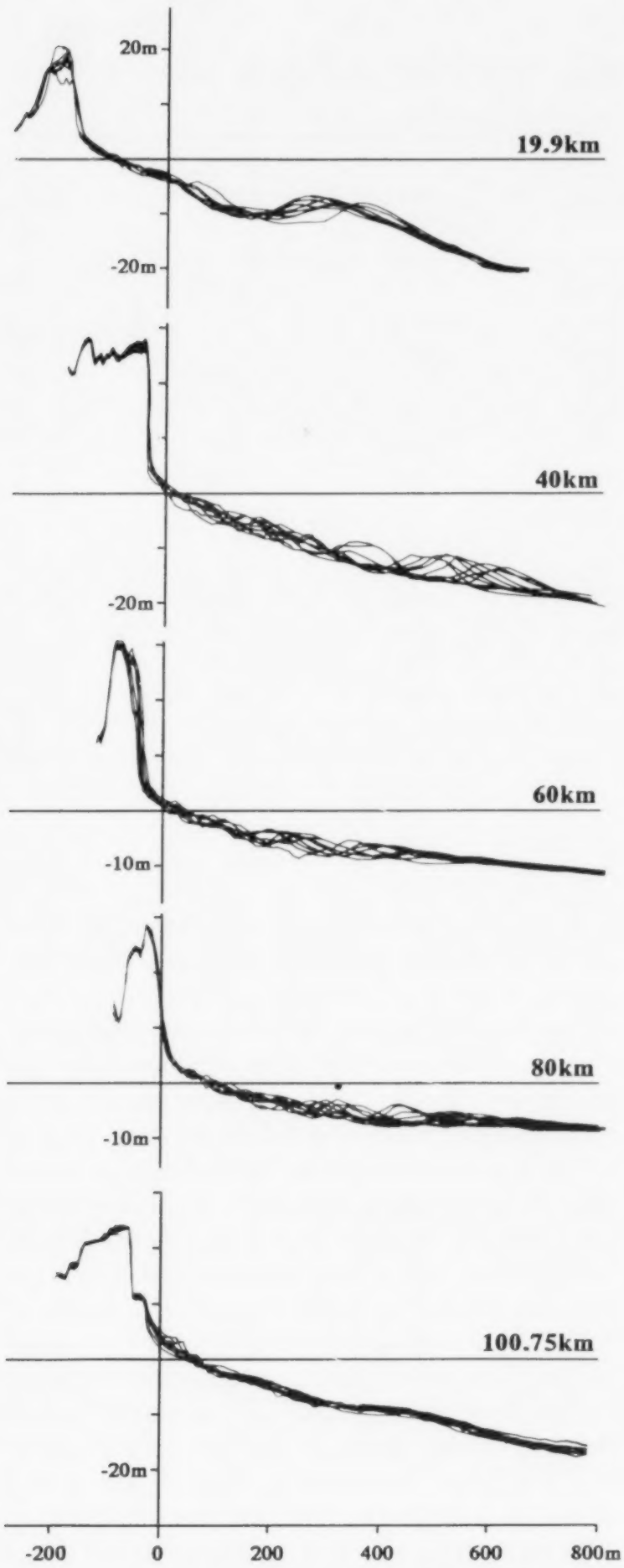

Fig. 2. An example of beach profile envelopes (1976–1985) along the coast at km 19.9, 40, 60, 80 and 100.75. Source: *Rijkswaterstaat*, Tidal Waters Division.

results of Kohsiek (1984), Van Bemmelen (1988) and Van Alphen (1987). The dune sands are relatively uniform alongshore with an overall mean of 226 μm. The slight size trends which do occur, particularly the coarsening around km 12, 18, 44 and 60 are paralleled by similar trends in the MHW beach sands (Fig. 3). The MLW beach sands are the coarsest (D_{50} = 286 μm) with a high degree of longshore variation. Comparing the three populations (dune, MHW, MLW), the dune sands remain consistently fine (< 280 μm) and uniform, while the beach sands are more variable. The MHW and MLW sands display both parallel trends (km 70–120) as well as opposing trends (km 0–70) suggesting a more uniform population in the south. The most significant trends are however related to the shoreward decrease in grain size from MLW to MHW to the dunes.

In the surf zone–nearshore sediments are coarsest at 200 m (D_{50} = 229 μm), fine seaward to 400 and 800 m (189 and 185 μm) then coarsen to 800 and 1000 m (201 and 212 μm). This trend was also observed south of Bergen (km 35) by Wiersma and Van Alphen (1988) who suggest they represent three dynamic regimes associated with: (1) high energy surf zone and beach unit; (2) seaward fining across the mid surf zone (400–600 m); and (3) coarsening beyond 800 m possibly due to increasing flood tide velocities.

Given the aims of the sediment analysis were to assess longshore trends in grain size and select representative grain size characteristics, the following conclusions were made: (1) No longshore trends were coherent across all sediment populations (dune, beach, surf zone), a conclusion reached by Wiersma and Van Alphen (1988) and Stolk (1989). The former consider subsoil inheritance to partially explain the present patterns. (2) For the purpose of this study of beach morphodynamics, the inner surf zone sediments were selected for more detailed trend assessment and for use in equations requiring grain size characteristics. The inner surf zone sands (200 to 400 m) display a weak trend with coarser sands north of IJmuiden (km 0–56) and finer sands to the south (Fig. 3). Based on these values mean grain diameters of 240 μm (sediment fall velocity w_s = 0.027 m/s) and

TABLE 4

Summary of inner slope (surf zone) morphometric characteristics, based on beach profiles between km 1-118 along the central Netherlands coast

	n	mean	SD	Max	Min
tan B	116	0.013	0.004	0.040	0.005
No. bars	118	2.6	0.7	4	0
Net beach width	117	42.7 m	29.2	240	0
Net beach amp.	112	1.4 m	0.5	3	0.5
Area bar 1	110	83 m^2	49	300	5
Area sweep zone	114	1420 m^2	576	3 200	220
Width sweep zone	117	692 m	164	850	190
Amp. bar 2	114	2.0 m	0.6	4	1
Bar 1 distance	-	80 m	-	100	0
Bar 1 migration	110	59 m	23	150	10
Bar 2 distance	-	200 m	-	300	0
Bar 2 migration	112	113 m	45	200	10
Bar distance	-	480 m	-	600	400
Bar 3 migration	82	175 m	64	300	20

Original Source: *Rijkswaterstaat*, Tidal Waters Division.

200 μm (w_s = 0.0205 m/s) were adopted for locations north and south of km 56 respectively.

Waves

Waves arriving on the Netherlands coast are generated by wind blowing over the North Sea, together with occasional low northerly swell arriving from the north Atlantic. The strongest wind and largest waves are associated with W–E tracking subpolar low pressure systems. These produce a predominantly westerly flow of air and are the major source of wave generation for the coast. The wave climate is however, highly variable, as it depends not only on the frequency and track of the cyclones, but also their regional wind direction, velocity and duration. The wave generating forces act across a sea with a variable fetch, a relatively shallow shelf, including the shoal areas of the Dogger and Bruine Banks, together with numerous ridges off the Netherlands coast. The banks produce both wave attenuation and refraction of northerly swell which further complicates the wave regime. Near the coast relatively low nearshore gradients, shoreface connected ridges and ebb tide deltas (Fig. 1) further effect breaker conditions. Finally, within the surf zone the location and elevation of the shore parallel bars, induces cross shore, breaker wave transformation.

The wave climate of the Netherlands coast was recently published by Roskam (1988) who summarized data for the eight deepwater stations for the period 1979–1986. The wave exceedence curves are reproduced in Fig. 4a and the wave directional tables reformated in Fig. 4b. Waves on the central Netherlands coast arrive from all offshore directions. They arrive at the coast between 75 and 85% of the year, with a modal wave of 1 m height and 5 s period. Most waves arrive from the W–WSW though they are spread across the SSW to NNE sectors.

Temporal variation in wave conditions, drives beach change, and is therefore essential for any assessment of beach morphodynamics. Temporal

TABLE 5

Inner slope and outer slope width, outer depth and slope characteristics

Inner Slope (Surf zone)

Variable	Width	Depth	Tan B
n	117	116	116
Mean	692 m	8 m	0.0123
Median	800	8	0.011
Mode	800	8	0.01
Standard deviation	164	2	0.004
Minimum	190	4	0.005
Maximum	850	16	0.04

Outer Slope (Shoreface)

Variable	Slope break	Depth	Tan B
n	18	18	18
Mean	3728 m	16.3 m	0.0045
Median	3575	16.3	0.00042
Mode	3750	20.5	0.0036
Standard deviation	1150	2.6	0.001
Minimum	2150	9.7	0.003
Maximum	6850	20.5	0.0075

variation for the central coast can be assessed from the daily, monthly and annual wave characteristics for YM6 and MPN stations. The high degree of variability in the wave height is illustrated in Fig. 5 which plots daily wave height for 1987 and 1988. Waves exceed 1–1.5 m approximately 5 to 6 times per month. During 1987 and 1988 waves exceeded 1.5 m on 30 and 37 occasions respectively, probably related to the passage of low pressure cyclones across the North Sea. Both year's also display the winter increase in wave height discussed below.

The monthly and annual wave height summaries for YM6 and MPN are illustrated in Fig. 6. Both stations show the same trend, which consists of the following four wave 'seasons'. Summer (April–August) is the period of lowest waves (0.93–1.08 m monthly mean height) with low variance (sd = 0.17–0.24 m). For all years (1979–1988) the highest

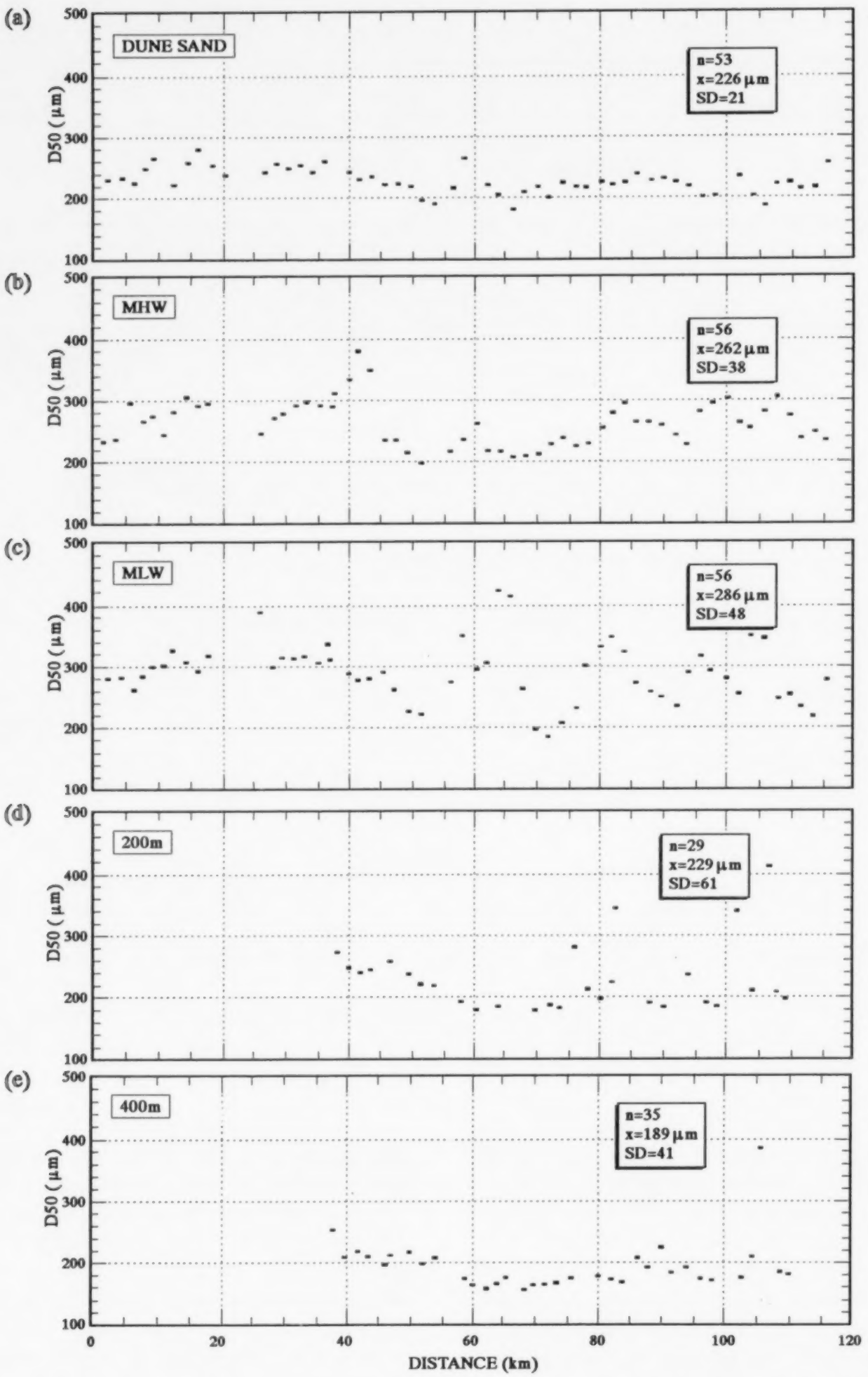

Fig. 3. Dune, beach and inner surf zone mean grain size along the central Netherlands coast. Shown are dune sands (a) from Kohsiek (1984), and beach sands (mean high water (b) and mean low water (c) from Van Bemmelen, 1988) and grain size at 200 m (d) and 400 m (e) distance from the shoreline (from Van Alphen, 1987). Box indicates sample number, mean and standard deviation. Distance refers to kilometre beach pole locations shown in Fig. 1.

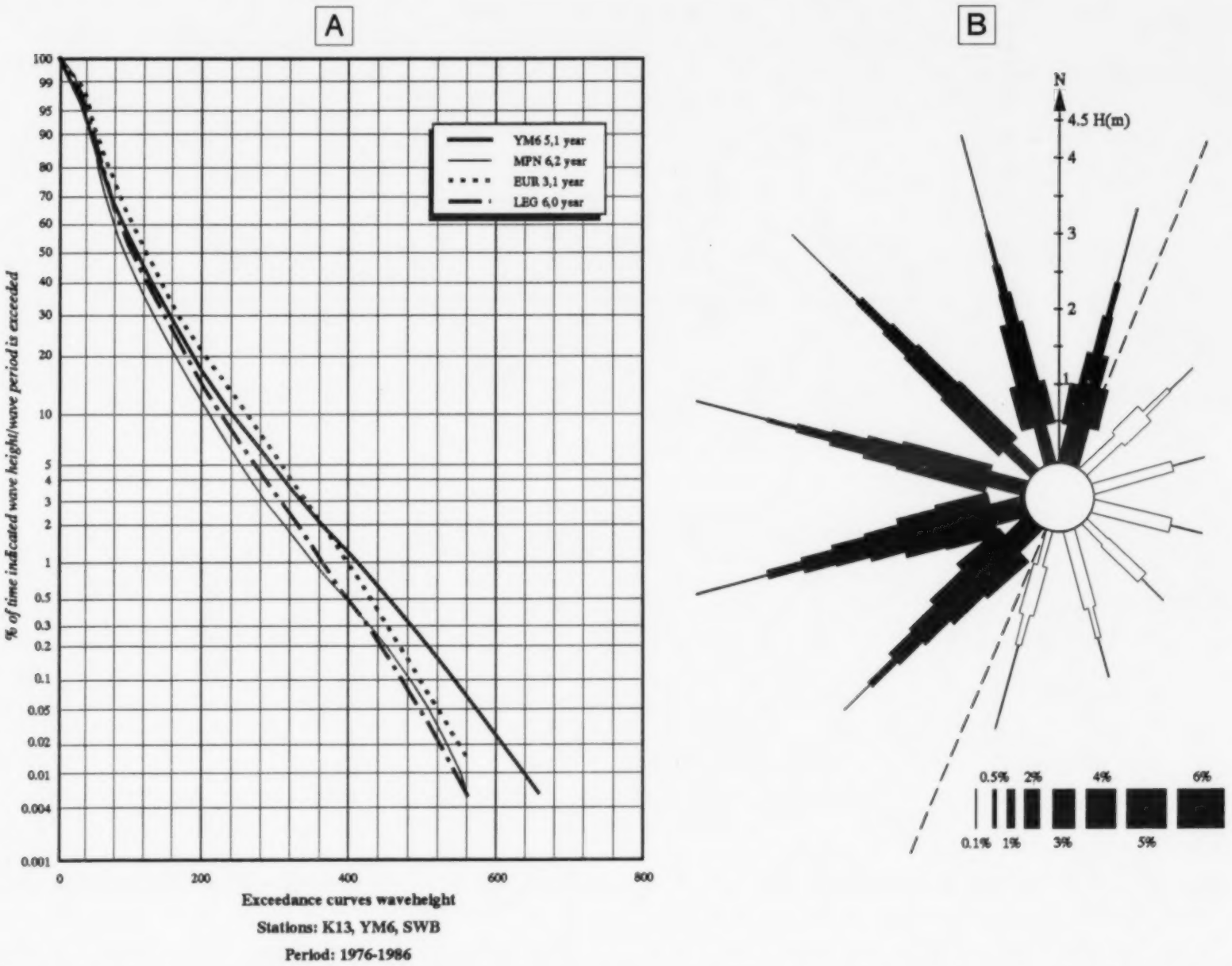

Fig. 4. (A) Wave exceedence curve from YM6, MPN, EUR and LEG wave stations. Modified from: Roskam, 1988. See Fig. 1 for locations. (B) Wave rose for LEG station based on data from Roskam, 1988. The rose includes wave direction, height and frequency of occurrence. The dashed line indicates the alignment of the central Netherlands coast. The shaded directions produce waves at the coast, while open roses should result in waves moving offshore and calms at the shoreline.

summer monthly mean (H_{mo}) was 1.57 m (period $T = 7.8$ s), the lowest 0.59 m ($T = 4.84$ s). *Summer* is a period of low and consistently low waves, with few major storms as illustrated by the lower variance in Fig. 6a and b. *Fall* (September and October) is a transition period between summer and winter. It is characterised by increasing wave height and variance the latter produced by the occurrence of higher waves.

The *winter* period (November–January) contains the highest waves increasing in size each month to peak in January ($H_{mo} = 1.86$ m). While November and December have relatively low variance (sd = 0.26 m), January has the highest variance (sd = 0.71 m) with some years of extreme storminess and high waves such as 1984 ($H_{mo} = 3.23$ m), but also occasional calm years, such as 1982 ($H_{mo} = 0.71$ m). The extreme January waves are followed by a marked drop in wave height, in the February and March *spring* period. Mean wave height drops dramatically to 1.26 m in February, and continues in March, before the next drop to the April summer conditions. The February variance is relatively high (sd = 0.41 m). Large storms can occur such as in 1988. However, usually it is a quieter month than January.

Wave period averages 4.9 s (sd = 0.3 s), with a consistent trend of slightly longer wave periods

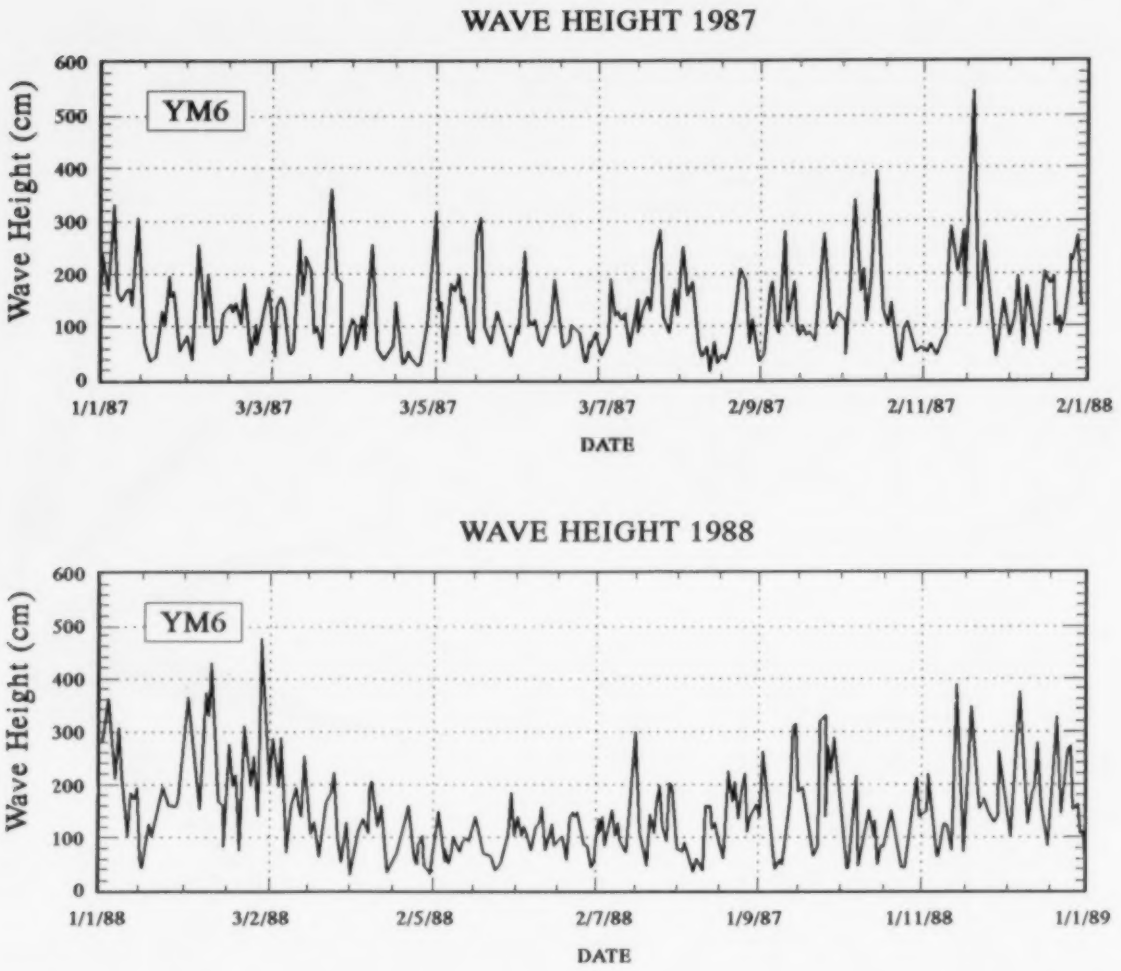

Fig. 5. Daily mean wave height for YM6 station, 1987 and 1988 (see Fig. 1 for location). Based on data supplied by the *KNMI*, Division of Oceanographic Research.

during winter compared to summer (Fig. 6c). The most important variation in wave period, however, is associated with wave height. As mean wave height increases so too does mean wave period. Modal wave period is 3–5 s. for waves less than 1.5 m, but increases to 5–7 s for waves 1.5 to 4 m, and 7–9 s for waves greater than 4 m (Roskam, 1988).

Beach morphology

An assessment of the natural beach morphology, including rip characteristics of each of the three bars, is now presented. This is followed by an empirical prediction of the hierarchical bar type, the impact of structures on beach morphology, and a tentitative 'beach model' for the multi-bar central Netherland coast.

Beach/bar 1

The subaerial beach extends from the foot of the vegetated dune out to low water. It runs the entire length of the coast, except along the Hondsbossche Dyke (km 20–26), and in the harbour moles at IJmuiden and Scheveningen. It averages 43 m in width (Table 4) only increasing substantially in width (*max.* = 240 m) adjacent to the IJmuiden breakwater where recent shoreline progradation has occurred. The beach consists of a usually dry backshore which slopes at about 1:15 and is only awash during severe storms and storm surges. This is fronted by a more active ridge and runnel system.

The modal beach state (BS) for the beach/bar 1 is a ridge and runnel (Fig. 7, mean BS = 2.08, sd = 0.39) (see Table 3 for explanation of BS values). This relatively narrow range is accounted for by the infrequent erosion as noted by Van den Berg, (1977) together with rapid ridge recovery, as noted by Doeglas (1954), both of which are a characteristic of this beach type (Short, 1979). It is also confirmed by the profile data (Fig. 8) which reveal a mean net shoreline oscillation of 59 m (sd = 23 m). This oscillation is not only greater than the mean beach width of 43 m (sd = 29 m) but is relatively uniform

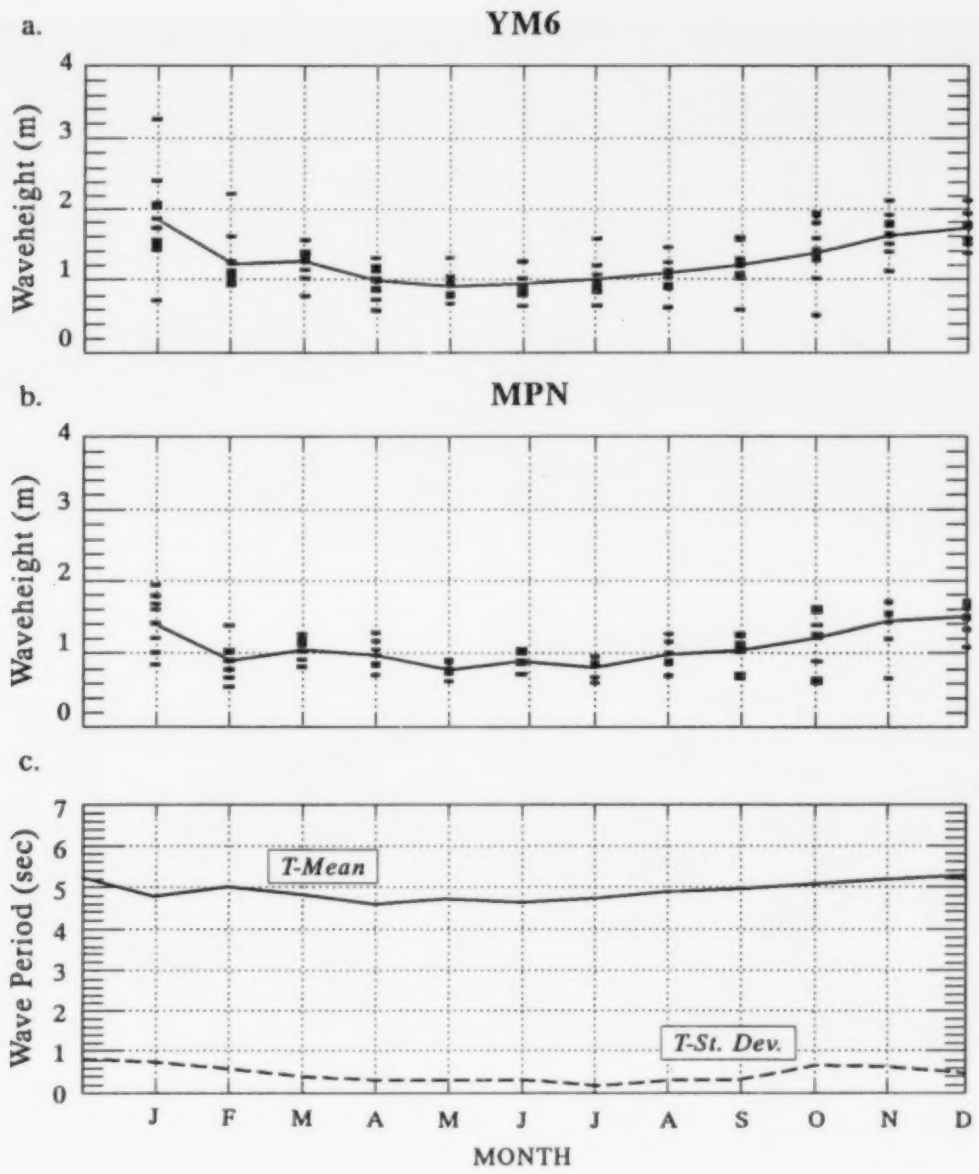

Fig. 6. Mean monthly wave height at YM6 (a) and MPN (b) stations for period 1979 to 1988. Mean for each month is given by points, while the line joins monthly mean for the 10 years. (c) Mean-monthly wave period and standard deviation for MPN station for 1979–1988.

alongshore. This mobility represents two processes. Firstly, beach erosion (LTT) and recovery (RR), which in Van den Berg's (1977) three survey lines resulted in beach change of 17, 39 and 42 m (mean = 33 m); and second, longshore (northward) migration of points of bar attachment (Fig. 9).

Bar 1 'drain' rips

Bar 1 is modally RR (53%) with LTT (29%) and TBR (6%). Two rip types were observed with bar 1. The first is the rip or 'drain' which discharges the runnel, the second the transverse rips associated with LTT, usually as a 'mini-rip' and TBR. The RR system is backed by a shore parallel runnel. Waves overtop the berm, particularly at high tide and during higher waves, and water collects in the runnel. This water is discharged back to the surf via drains, which transect the ridges (Fig. 7). Well developed drains were observed on the 1987 and 1988 photographs. Their mean spacing ranged from 407 to 683 m with an overall mean of 505 m, which as will be seen, is the same magnitude as the TBR rips.

Bar 1 transverse rips

Transverse rips consist of a relatively deep rip channel, usually fed by one or two longshore rip feeder channels, separated from adjoining rips by a transverse bar (Fig. 10). Transverse rips were most commonly observed on bar 1 as mini or small rips in the LTT, and less frequently as a

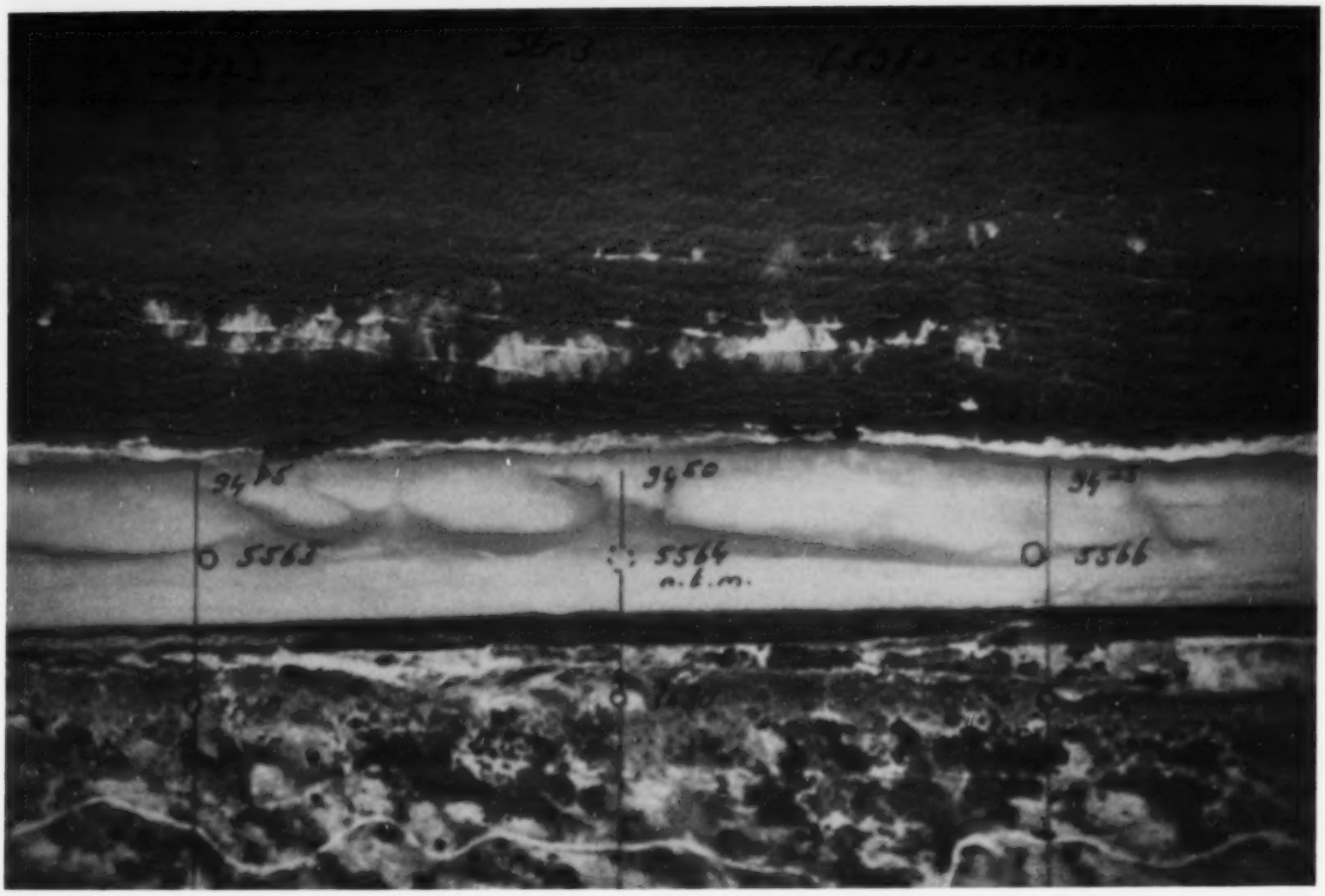

Fig. 7. Aerial photograph illustrating the beach with a single ridge and runnel with drains at km 94, 15.04.83. Source: *Rijkswaterstaat*, Mapping and Survey Division.

TBR system. Their mean spacing ranged from 341 to 984 m with an overall mean of 502 m (Fig. 11).

The rips were observed to be heavily skewed to the south on 1983, 1984 and 1987 photographs (Fig. 10a), to the north in 1986 and more shore normal in 1985 and particularly 1988 (Fig. 10b). A time series of rip observations is required to accurately assess rip orientation. In the absence of these data the wave rose (Fig. 4b) would suggest rips should be to the north about 30%, shore normal about 30% and to the south about 40%. Also, one would expect wind driven currents and tidal currents, to contribute to rip orientation and rip circulation.

Bar 2

A second bar is present along the entire coast. This bar usually begins as a shoreline attachment and gradually moves seaward to eventually become the third bar and finally merge with the nearshore zone (De Vroeg, 1987). The outer bars migrate longshore at rates ranging from 0 toward Den Helder to a maximum of 70 m/yr near IJmuiden (De Vroeg, 1987). The bar can lie between 0 and 300 m from the shoreline, averaging 250 m (Table 4).

Based on the aerial photographs the modal bar 2 state is RBB and TBR (40% and 32%, respectively). At times the bar welds to the beach as a second ridge and runnel (22%), and very rarely, may even be reflective (1%). Under higher waves however, the bar detaches and straightens to form a LBT (5%). These values are however tentative, as they are based on a limited spatial and temporal sample, indicated in Table 2. The prevalence of rips in bar 2 is a characteristic of all its beach types (RR, TBR, RBB and LBT). The common occurrence of surf zone rips along the central coast

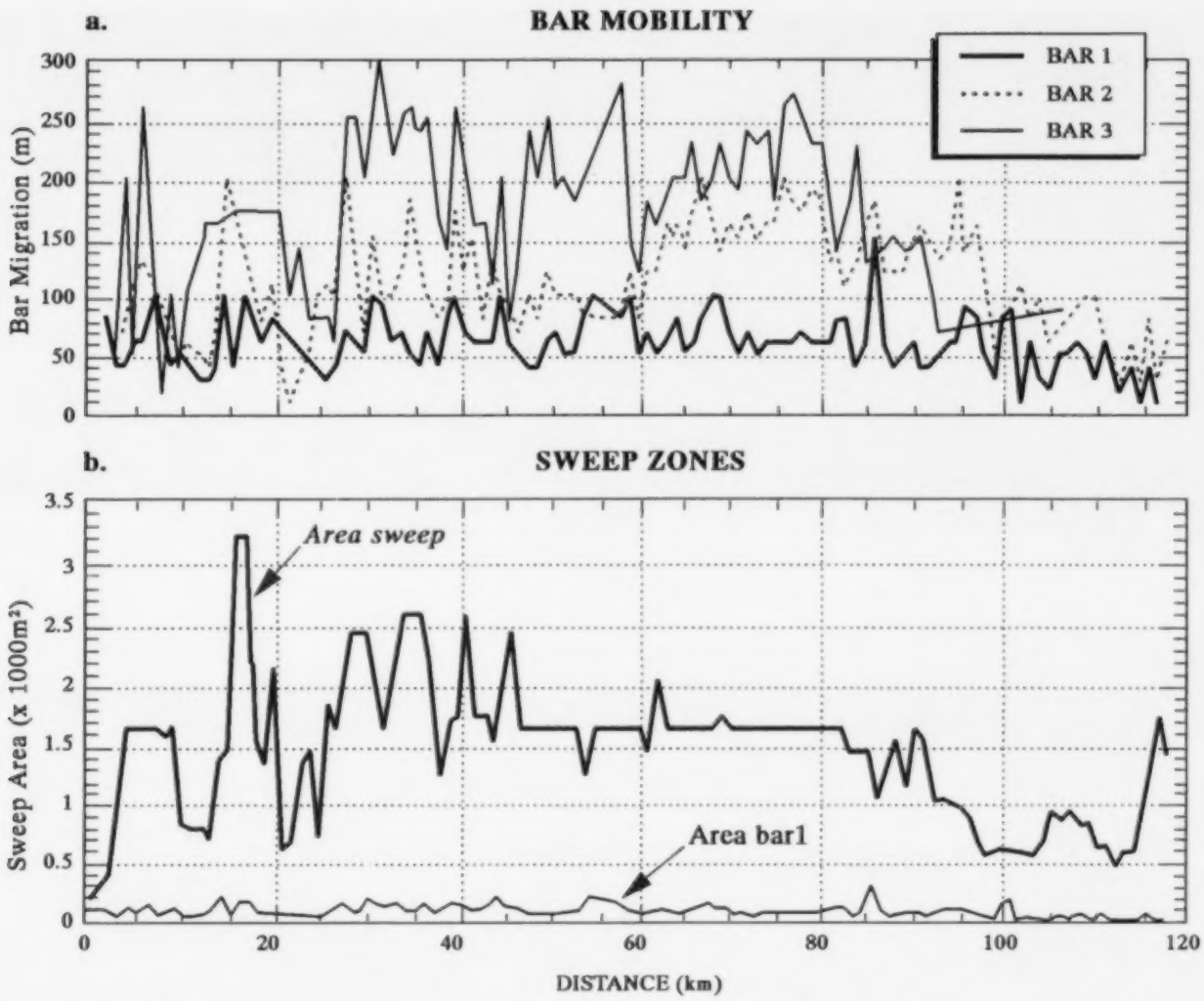

Fig. 8. (a) Plot of a longshore variation in a maximum shore normal mobility of the shoreline (bar 1) and crests of bars 2 and 3. (b) Area of shoreline change (area bar 1) and surf zone change (area sweep). Based on annual *Rijkswaterstaat* beach profile surveys 1976–1985.

has been noted by Ten Hoopen and Van Driel (1979) and Gerritsen and Van Heteren (1984).

Bar 2 is highly mobile with a mean shore normal oscillation of 113 m (Table 4). The oscillation is also highly variable longshore (Fig. 8). The oscillation in bar crest can be contributed to by two modes of bar change. First, high frequency on–offshore bar migration in response to periods of low and high waves, as reflected also in the shift in bar type from attached (RR and TBR) to detached (RBB and LBT) bar. Second, to lower frequency lateral bar migration recorded by De Vroeg (1987), which also results in net offshore bar migration.

Bar 2 rips

Bar 2 varies from RR to LBT a range of types dominated by rip topography. However, like bar 1 rip currents will only occupy the topography during higher wave conditions. The aerial photographs reveal bar 2 rips in 1983, 1985, 1986 and 1988 and in the 1968, 1970 and 1971 airphoto mosaics. Their absence in some years, and along sections of the coast, is more a function of limitations in the sampling technique than their absence alongshore. The air photo samples indicate that the rip spacing ranged from 355 to 909 m with an overall mean of 595 m, about 100 m longer than the bar 1 rips (Fig. 11). Like the bar 1 rips their orientation depends on formative wave approach. Examples of a bar 2 TBR and RBB rips are shown in Figs. 9 and 10.

Bar 3

The aerial photograph observations of bar 3 are limited owing to turbidity, lack of wave breaking and limited photo coverage. They are restricted to

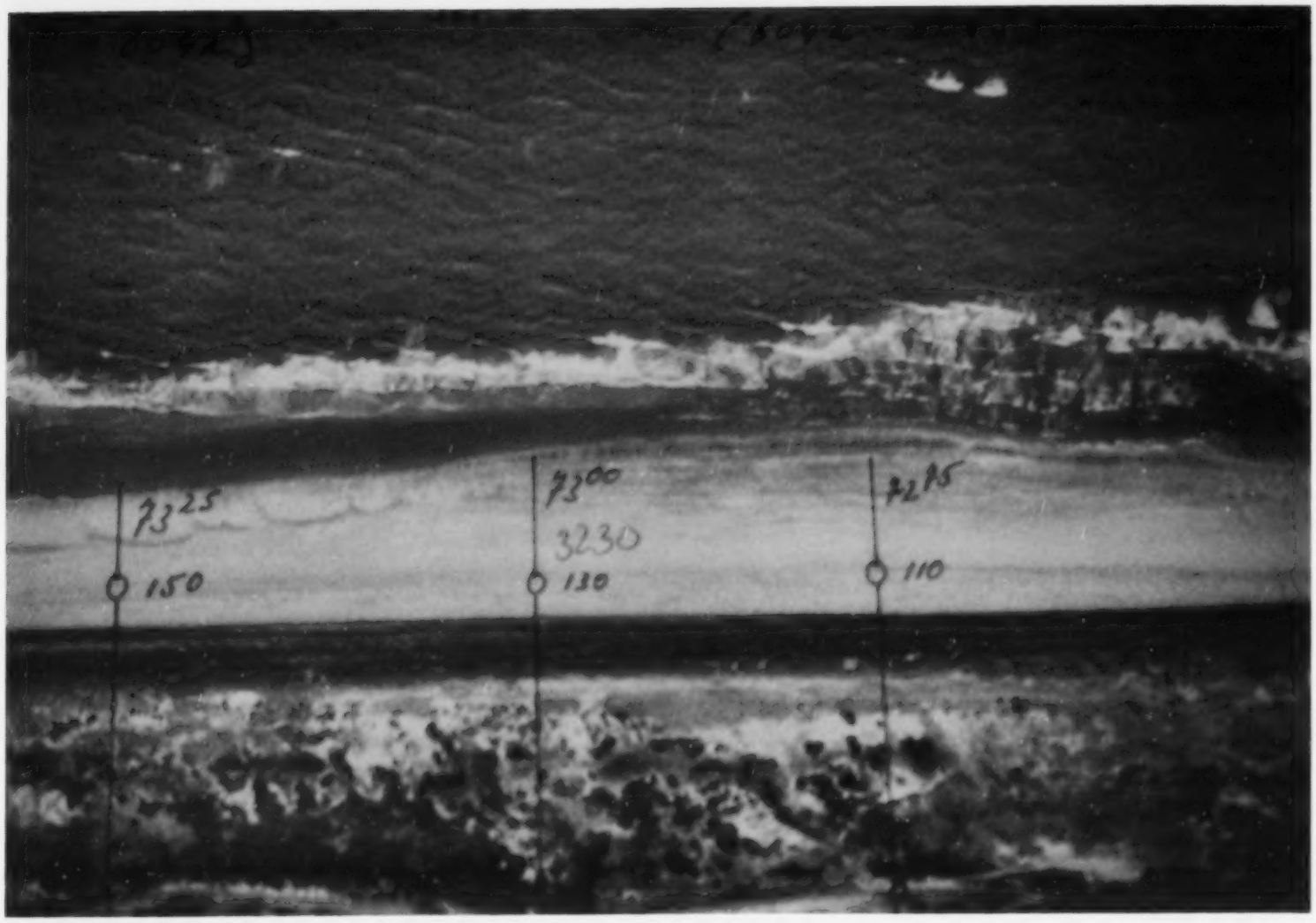

Fig. 9. Aerial photograph illustrating bar attachment and beach or shoreline protusions at km 72–73, 14.4.83. Source: *Rijkswaterstaat*, Mapping and Survey Division.

a few observations in 1983, 1985 and 1986. When observed bar 3 was modally LBT (56%) and RBB (44%). Its presence and extent is clearly verified by De Vroeg (1987) and the profile data (Fig. 2). It is present continuously between Den Helder and km 95 but not present between km 95 and 119. It is also present off the Hondsbossche dyke (km 20–25) where only two bars are present, here the missing bar is bar 1 and not bar 3.

Bar 3 is the most dynamic of the three bars experiencing predominantly offshore migration with rates similar to bar 2 (Table 6). The average on–offshore movement of the bar is 175 m over a 10 year period (Table 4) suggesting on–offshore, plus net offshore movement, contribute to bar crest mobility. This fact, like bar 2, is also supported by the decrease in bar mobility in the areas of more stable bar forms north of km 25 and south of km 85 (Fig. 8).

Bar 3 rips

Bar 3 is dominated by RBB and LBT both characterized by large rip systems. As these rips are less topographically controlled, they are only likely to be active during higher wave events. This fact combined with the sampling limitations discussed earlier resulted in the spacing of only four bar 3 rips being recorded. They gave a mean spacing of 900 m, almost twice that of bar 1. This is to be expected particularly if one assumes the rip spacing is determined by edge waves (e.g. Aagaard, 1991).

Beach/bar types

In order to examine the factors contributing to the hierarchical range in beach-bar types illustrated in Fig. 12 and summarised in Fig. 13, the dimensionless fall velocity (Short, 1986) and the concept

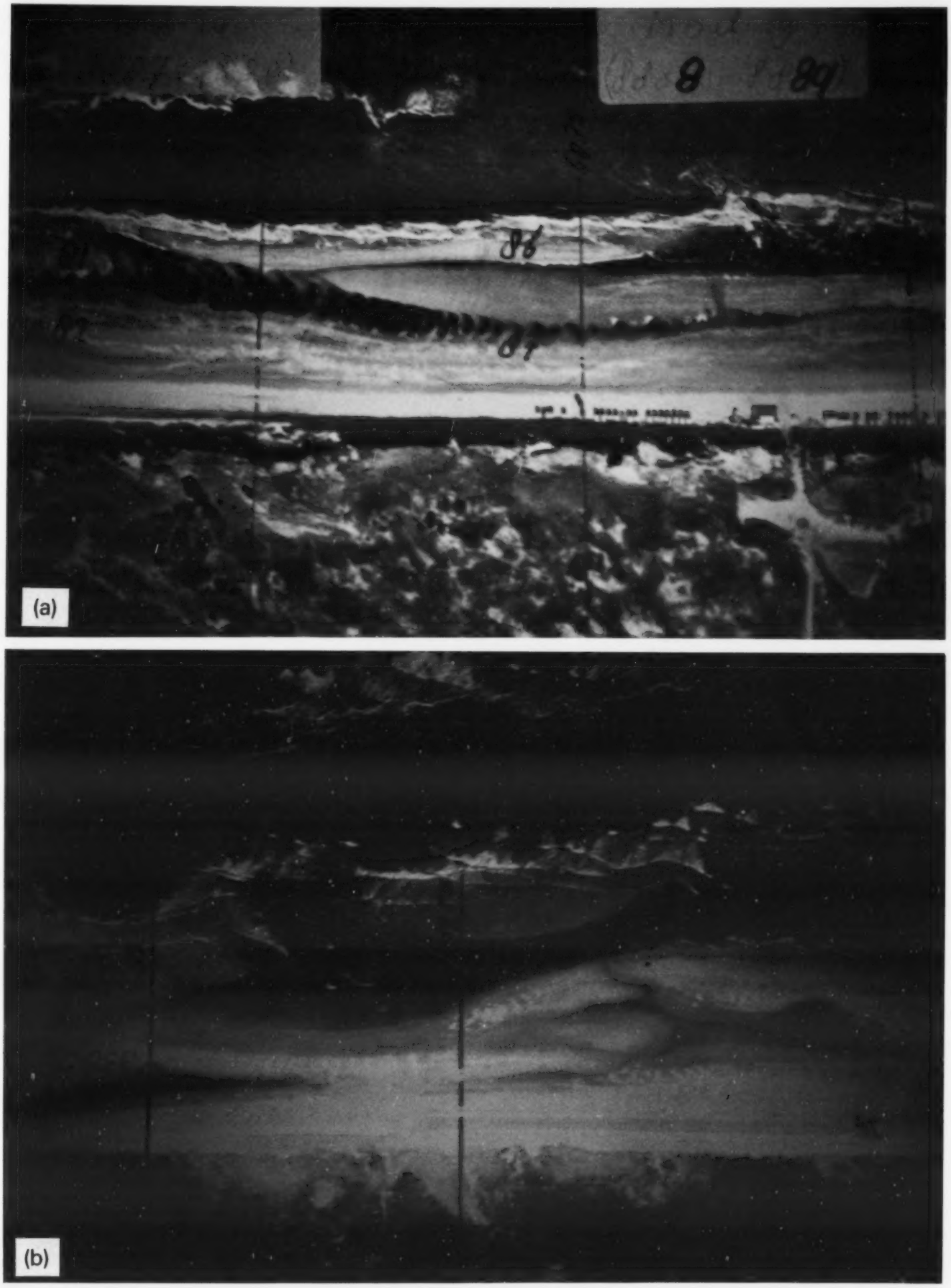

Fig. 10. Examples of rip types. (a) southerly skewed bar 1 TBR containing megaripples, with attached bar 2 TBR pulsating into trough, km 49, 24.08.87. (b) combination of bar 1 RR drain and bar 2 TBR-RBB rips, km 39, 22.04.88. Source: *Rijkswaterstaat*, Mapping and Survey Division.

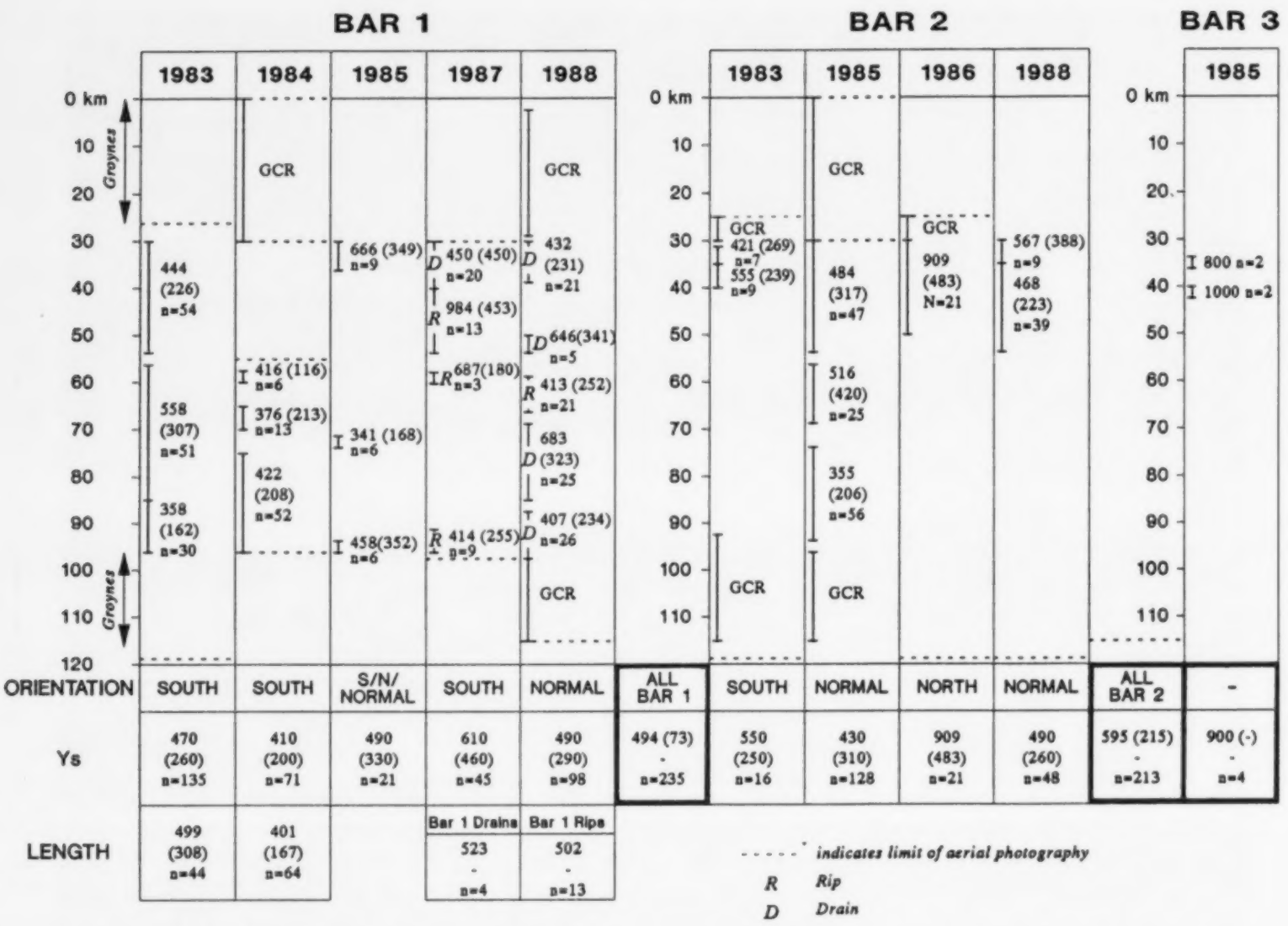

Fig. 11. Rip spacing and length based on aerial photographs 1982–1988. Numbers indicate, mean rip spacing (m), standard deviation in brackets and number of rips (n) for each sector indicated by vertical bars. GCR = groyne controlled rips. The lower columns indicate dominant rip direction (orientation) the summaries of all rip spacing for the year (Ys) and length of all bar 1 and bar 2 rips, where their length is heavily skewed.

of surf zone equilibra (Wright et al., 1987) is used to assess the role of wave height, period and sediment fall velocity in contributing to beach-bar type and change.

Wright et al. (1987) found they could achieve a reasonable prediction of a single bar type if antecedent wave conditions and sediment characteristics were known. Working in the swell dominated coast of southeast Australia they derived the following empirical equation:

$$\bar{\Omega}N = \left(\sum_{i=1}^{D} 10^{-i/\Phi}\right)^{-1} \sum_{i=1}^{D} (\Omega i\, 10^{i/\Phi}) \qquad (1)$$

where Ω is the dimensionless fall velocity $\Omega = H/T_{ws}$, and Ω is the predicted Ω value for the day in question, D is the number of antecedent days used to calculate $\bar{\Omega}$N usually 30, $i = 0$ for the day in question, and i/Φ is a decay function where $\Phi = 5$.

In order to apply this equation to the central Netherlands coast the following was required. (1) Actual beach-bar type for a given day. These were obtained from the annual air photographs taken by *Rijkswaterstaat* from 1982–1988. (2) Daily wave conditions for up to 30 days prior to each photograph. These were provided by *Rijkswaterstaat* (1982–86) and the Royal Netherlands Meteorological Institute (1987–88). (3) Representative sediment fall velocity, which were discussed earlier.

A complicating problem in a multi-bar system is the fact that breaker wave height will decrease shoreward. To estimate the decrease in wave height two empirical approaches were used.

TABLE 6

Some characteristics of the three bar system along the central Netherlands coast

	BAR 1	BAR 2	BAR 3
Location	km 0-119	km 0-119	km 0-85
Beach Type			
Modal	RR	TBR	RBB/LBT
Range	R-TBR	R-LBT	RBB-LBT
Rip Spacing[1] (m)	500	600	900
Distance to bar[2] (m)	80	250	500
Lateral bar mobility[2] (m)	60	120	180

[1]Fig. 11.
[2]Table 4.

Keady and Coleman (1980) proposed the formula:

$$H_r/H_i = 0.58(H_i/d)^{-0.8} \quad (2)$$

to predict the reformed wave height (H_r), where H_i is the initial wave height and d the water depth at wave breaking. Aagaard (1989) used this formula and found that for low waves ($H<0.6$ m) it predicts an increase in breaker height. He derived an empirical equation, based on regression analysis where:

$$H_r = 667H_i + 0.048 \quad (3)$$

In Table 7 the two equations are used to calculate H_r on bar 2 and bar 1 for a range of typical wave conditions together with the corresponding values of Ω. Using Wright and Short (1984) and Short (1986) findings beach-bars should be reflective when $\Omega<1$, intermediate when Ω is between 1 and 6, and dissipative when $\Omega>6$. The results in Table 8 suggest the following:

(1) During storm conditions ($H_b>3$ m, $T=7$ s) the entire surf zone is dissipative (i.e. $\Omega>>6$). This is in agreement with the observations of Van den Berg (1977) who observed flat post storm profiles on beach/bar 1 about 7% of the time.

(2) During moderate to high waves ($H_b=1.5$–3 m) the outer surf zone remains dissipative ($\Omega>6$) while the inner surf zone tends towards more intermediate conditions ($\Omega=4.6$–9.9).

(3) Under modal and low wave conditions ($H_b<1.5$ m) waves first break on bar 2 producing dissipative-intermediate conditions ($\Omega=3.7$–9.6) with intermediate conditions dominating at the shoreline ($\Omega=2.8$–6.7).

All the above results are likely to be conservative owing to overestimates of the H_i which is based on a wave station 18 km offshore. Consequently one would expect intermediate conditions to prevail more frequently across the inner (bar 1) and midsurf zone (bar 2) under modal and transitional waves (i.e. $H_b<2$ m).

The next step was to use the daily wave data in eqn. (1), together with a slightly modified version for the eastern Danish coast proposed by Aagaard (1988) where:

$$\bar{\Omega} = [\sum_{i=1}^{D} 10^{-i/\Phi}]^{-1} \sum_{i=1}^{D} (\Omega_i 10^{-i/\Phi}) \quad (4)$$

Fig. 12. Highly rhythmic beach and bar topography immediately south of Egmond aan Zee (km 39). Waves are just breaking on bar 3, bar 2 is highly rhythmic and attached to the beach in places, while attached bar 1 forms rhythmic ridge and runnel systems (13.07.89).

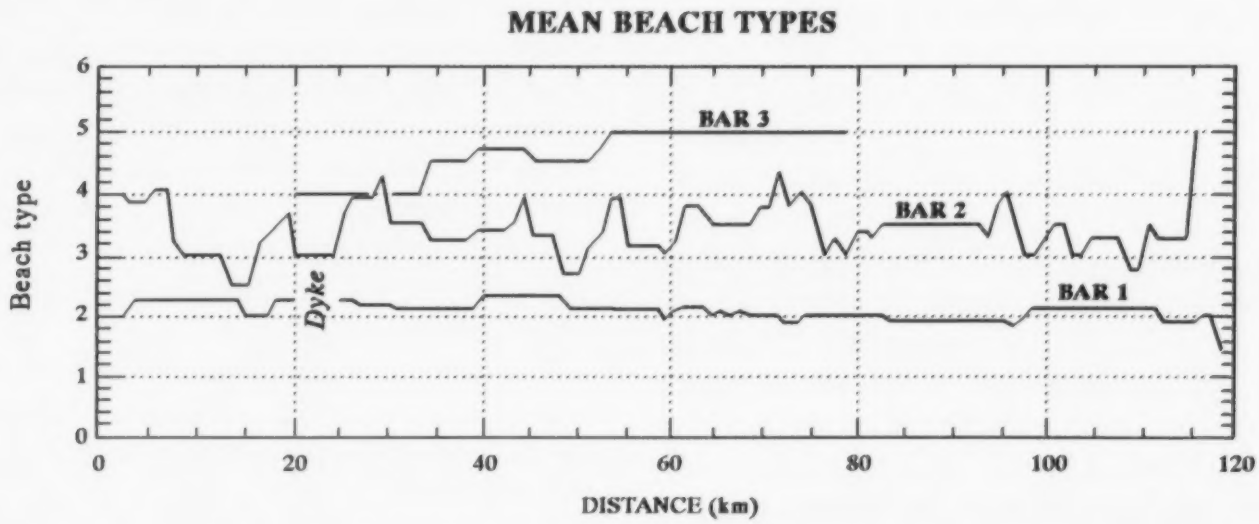

Fig. 13. Longshore variation in mean beach type for beach/bar 1, bar 2 and bar 3, based on annual aerial photographs 1982–1988. Distance refers to kilometre beach pole locations shown in Fig. 1.

TABLE 7

Incident (H_i) and reformed (H_r) breaker wave heights using eqns. (2) and (3) (italics) and predicted Ω at each bar

	Bar 3		Bar 2		Beach/Bar 1	
	Hi		Hr		Hr	
Storm[1]	5	26.4	2.9	15.3	1.7	9
	5		*3.38*	*17.9*	*2.25*	*11.9*
	4	21.1	2.76	14.6	1.7	9
	4		*2.72*	*14.4*	*1.8*	*9.8*
	3	15.9	2.61		13.8	1.7
	9					
	3		*2.05*		*1.4*	*7.2*
Transition[2]	2	12.3	1.60	9.9	1.11	6.85
	2		*1.38*	*8.5*	*0.96*	*5.9*
	1.5	9.2	1.04	6.4	0.74	4.6
Modal[3]	*		1.3	9.6	0.9	6.7
	*		1	7.4	0.7	5.2
Low[3]	*		0.5	3.7	0.4	2.8

[1] $T=7$, $w_s=0.027$, $d=4$ m (bar 3), $d=2$ m (bar 2).
[2] $T=6$, $w_s=0.027$, $d=2$ m (bar 2).
[3] $T=5$, $w_s=0.027$.
*No wave breaking.

where $D=10$, day $i=0$ is used while Φ remains 5. The lower D value implies the beach responds more rapidly to the Danish sea environment than the Australian swell environment of Wright et al. (1987).

In Table 8 the predicted Ω at initial wave breaking (bar 3) ranges from 3.7 to 12.9. On the three occasions bar 3 could be typed it was rhythmic bar and beach to longshore bar and trough, while corresponding Ω ranged from 7.1 to 8.4, above

TABLE 8

Predicted Ω values and observed beach and bar morphology along the central Netherlands coast (Source: Short, 1991a)

Year	D	Predicted				Observed mean beach types[3] (and standard deviation)		
		0-56 km[1]		56-118 km[2]				
		H	N	H	N	Bar 1	Bar 2	Bar 3
1982	10	4.95	6.22	6.52	2.19	2.06	2.3	
	30	4.95	6.21	6.52	2.17	(0.49)	(0.1)	
1983	10	8.41	9.80	11.08	12.91	2.0	3.3	4.6
	30	8.42	9.81	11.10	12.92	(0)	(0.83)	(0.39)
1984	10	3.68	4.31	4.85	5.67	1.57	2.55	
	30	3.72	4.35	4.89	5.73	(0.49)	(0.72)	
1985	10	7.09	7.56	9.34	9.95	1.95	3.57	4.90
	30	7.08	7.53	9.32	9.92	(0.27)	(0.75)	(0.21)
1986	10	8.26	9.35	10.28	12.31	2.15	4.1	4.7
	30	8.26	9.33	10.88	12.29	(0.32)	(0.47)	(0.27)
1987	10	8.01	9.11	10.55	12.00	2.0	3.24	
	30	8.02	9.12	10.57	12.01	(0)	(0.96)	
1988	10	5.58	4.94	7.35	6.50	2.55	3.61	
	30	5.58	4.94	7.35	6.51	(0.29)	(0.5)	

[1] $w_s = 0.027$ m/s.
[2] $w_s = 0.0205$ m/s.
[3] 1 = reflective; 2 = low tide terrace; 3 = transverse bar and rips; 4 = rhythmic bar and beach; 5 = longshore bar and trough; 6 = dissipative.
H = Hald eqn. (4); N = Narrabeen eqn. (1).

the intermediate-dissipative threshold and well above the $\Omega = 4.1$ for producing a longshore bar and trough at Narrabeen (Wright et al., 1987). Aagaard (1988) obtained similar results from his Danish coastal sites and suggested the dissipative to intermediate transition values be raised to 17.8. This would improve the results, but the problem remains of accounting for the decreasing H_b and across the surf zone and presumably lower beach state.

In order to obtain a more realistic measure of Ω on bars 2 and 1, the H_r from eqns. (2) and (3) was used to calculate two additional scales of Ω as wave height decreased across the surf zone. In Fig. 14 the predicted Ω for each year and the observed beach state for each bar is plotted together with the three Ω scales. The additional scales indicate the predicted Ω for bar 2 and bar 1 resulting from the reduced breaker wave height. For example when predicted Ω=9 on bar 3 it is reduced by wave breaking to 6 on bar 2 and 5 on bar 1. Consequently predicted beach type will vary accordingly. The overall result of using three scales is to leave bar 3 within the predicted dissipative range, to have bar 2 oscillating around the dissipative-intermediate boundary, and to place bar 1 below boundary and increasing in the lower intermediate regime. In general this adjustment provides reasonable results, particularly if eqn. (4) with $D=10$ is used, that is H in Table 8.

Figure 14 also shows the predicted frequency of occurrence of each beach type for each bar systems, based on calculations of Ω made using the reduced breaker wave heights, and the deepwater wave frequencies from Roskam (1988). These can then be compared with the observed beach types based on the aerial photographs in Fig. 15. As the observed values are based on a biased (spring

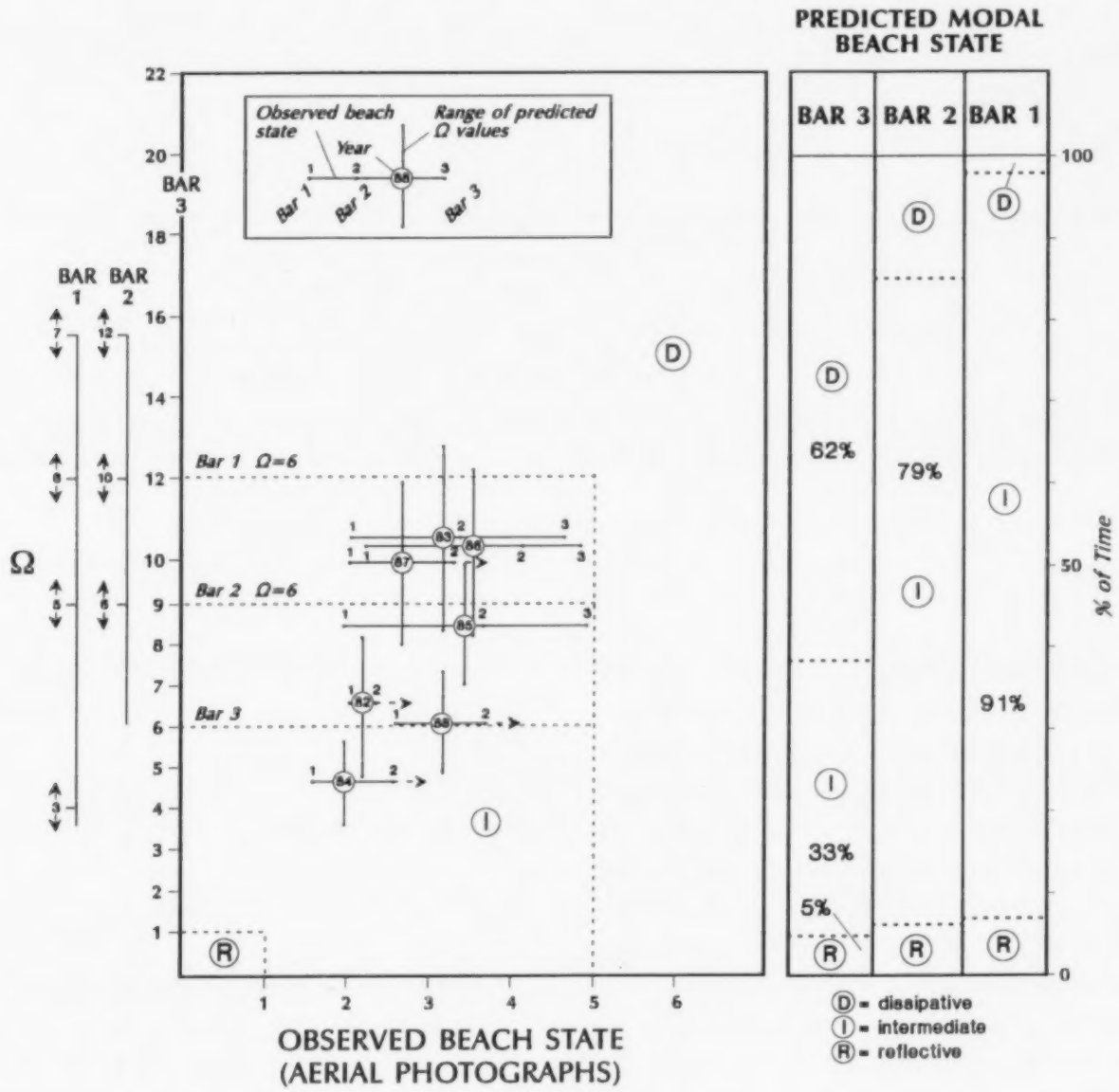

Fig. 14. The relationship between predicted and observed beach state at time of annual aerial photographs for 1982–1988. The three scales for are for each bar as a result of the decreasing wave height based on eqns. (2) and (3). The range of predicted Ω is a result of using eqns. (1) and (8). Upper range is due to ΩN, lower range to ΩH. Horizontal dashed lines provide threshold Ω values between intermediate and dissipative domains for each bar. Bar graphs at right show predicted modal beach states for bar 3 and subsequent predictions based on reduced wave heights for bars 2 and 1.

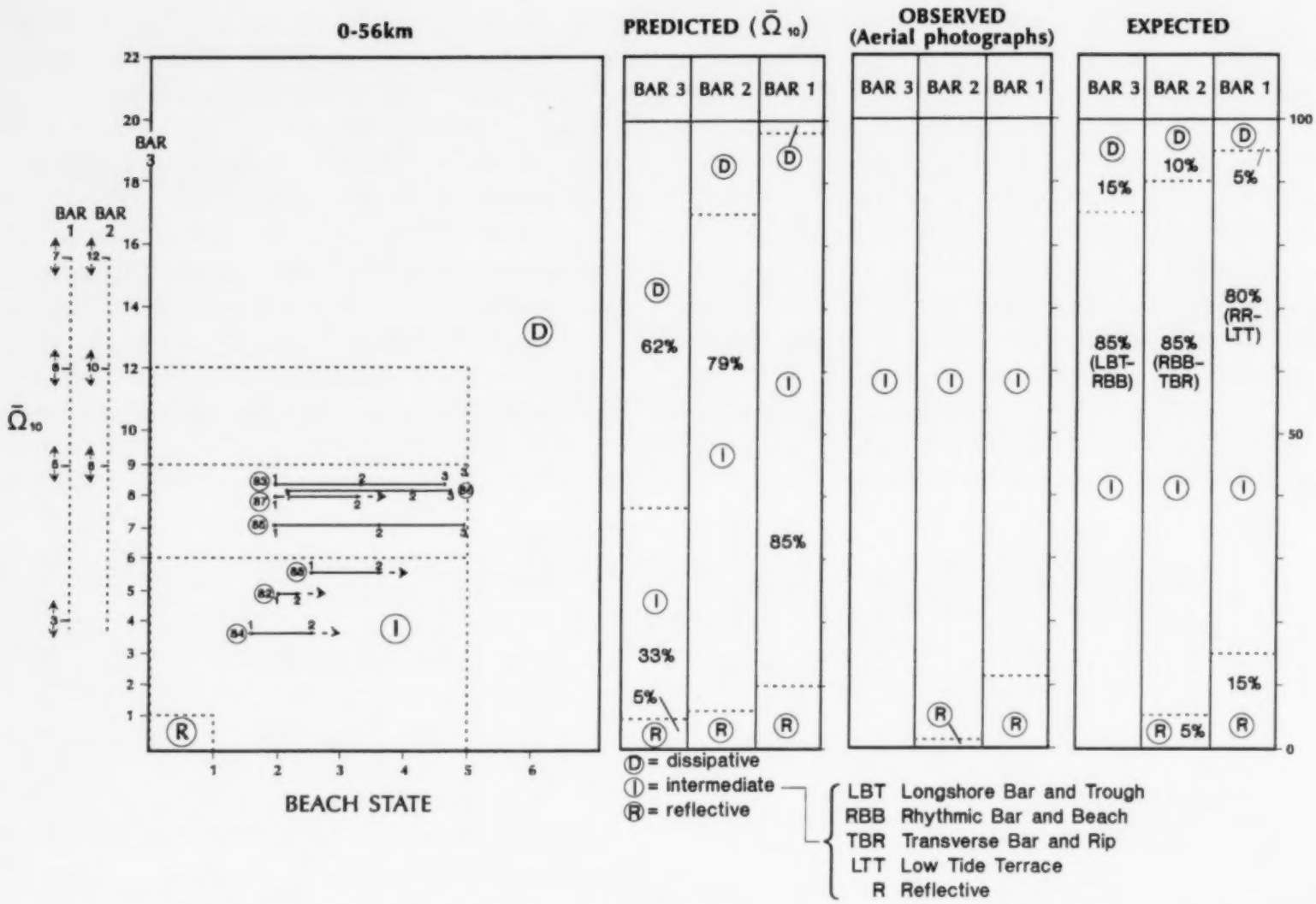

Fig. 15. The relationship shown in Fig. 14 plotted using only the ΩH values. The bar 2 and bar 1 vertical scales (on left) represent the predicted ΩH values for the corresponding bar 3 value based on H_o and T_o values from Roskam (1988). The predicted beach type for each bar is obtained from Fig. 14, the observed from aerial photographs (Short, 1991a) and the expected is an estimate which should lie between the observed and predicted frequencies.

conditions) and small sample, it is expected that the actual values would lie somewhere between. An estimate of these is given in the third 'expected' columns. These results suggest that the entire system is 'expected' to be dissipative only 5%. It is predominantly intermediate, though the modal beach type ranges from LBT–RBB (bar 3), RBB–TBR (bar 2) to RR–LTT (bar 1). The outer bar will never be reflective while the second bar will only be reflective at points of bar attachment.

Finally, in reviewing these results it must be stressed that there is much room for variation in the calculation of the values, both in the formula used and the estimates of H_i and H_r, particularly across the surf zone. The results suggest the best estimate is to use eqn. (4) and the Aagaard threshold of $D>I$ of $\Omega\sim12.5$, or to reduce H_b across the surf zone and use the adjustable scale in Fig. 15.

Structural impacts

Breakwaters

Numerous structures occupy 48 km of the central coast (Fig. 1) and influence beach morphology in two ways. First, the larger harbour breakwaters or moles at Den Helder, IJmuiden (Fig. 16) and Hoek van Holland, together with Den Helder's ebb tide delta, all induce lower nearshore gradients, and substantial reduction in breaker height toward the breakwaters. This has produced four wave shadow

Fig. 16. View of the harbour moles at IJmuiden harbour entrance (km 56–58). Note the wide low gradient beach, the result of over 200 m of recent shoreline progradation and the decrease in wave height towards the moles (13.07.89).

zones with breaker height approaching zero, particularly toward Den Helder and the IJmuiden moles. At IJmuiden it has resulted in substantial shoreline progradation, on the order of 1.2 million m^3/yr since 1963 (De Ruig and Louisse, 1991). The net result is a wide low gradient beach, surf zone and nearshore, with the adjacent bars merging with the ebb tide delta. The beach type in all cases shifts to a lower and/or inactive type, inactive here meaning remains unchanged following higher waves or storm erosion. The inactive morphology is particularly noticable in the beach-groyne field toward Den Helder. Their long term impact on beach morphology is partially illustrated by longshore variation in the mean beach type. At both Den Helder (km 0) and Hoek van Holland (km 120) there is a shift in bar 1 toward lower energy more reflective conditions (RR to R) and bar 2 toward more dissipative (Fig. 13), the latter suggesting an inactive 'storm' bar form.

Hondsbossche dyke

The Hondsbossche dyke (km 20–25) was constructed in its present location in 1823, to seal the former estuary. The dyke was built in line with the 1823 beach. Since then over 100 m of shoreline retreat, has left it seaward of the present shoreline (Fig. 17). As a result it replaces the beach along this 4.5 km section of coast. It is interesting to note however, that the outer bars 2 and 3 continue their migration past Hondsbossche apparently unaffected by the dyke (De Vroeg, 1987). Because of its location seaward of the beach line the groyne field along the dyke is usually devoid of sand, and

Fig. 17. Aerial view looking north to the Hondsbossche dyke constructed in this location in 1823. It has been stranded by continuing shoreline retreat. Note groynes and rips in the foreground (13.07.89).

therefore ineffective in directly influencing or containing sediment transport.

Groyne fields

Three groyne fields have been constructed along the coast (Fig. 1). Most groynes intersect the beach/bar 1 and bar 2. Their major impact is to induce a topographically controlled variation in nearshore topography, wave breaking and refraction, surf zone circulation, and sediment transport and accumulation. All this is superimposed on the natural shoreline processes. The groyne fields and the adjacent non-groyned beaches provide a natural laboratory in which to assess their impact.

The structural characteristics of the groyne fields are illustrated in Fig. 18. The 90 groynes between km 0–20 (Fig. 19) are usually 200 m apart, with some 300 m and others more random. The second field between km 25–30 has a range of spacings from 200 to 530 m. Likewise the southern field from km 97–115 has three modes at 200, 300 and 500 m with others ranging from 50 to 550 m in spacing. The groynes usually extend between 100 and 200 m seaward of the beach and are awash at high tide.

The more obvious impact of the groynes is to produce more rips and locate them adjacent to one or both groynes. This is illustrated in Fig. 20b–d which illustrates both natural and groyned section of coast exposed to the same wave conditions. The figure shows that (1) more rips are present in the groyne fields; (2) most rips are adjacent to groynes; (3) in more widely spaced groynes additional mid groyne rips occur; and (4) the beach/bar 1 while interupted by the groynes remains modally RR. In a recent study of a New York groyne field Bauer et al. (1991) found that with oblique wave approach longshore currents and associated eddies will dominate, with offshore flows moving along the groyne margins in rip-type currents.

Figure 21 shows well developed RBB rips existing adjacent to each groyne. On the same day decreasing wave height towards Den Helder (km 0) resulted in the beach type within the groyne field shifting between TBR (km 4–5), to RBB (km 2–3) to RR (km 1–2) and to R (km 0–1), indicating there is a wave threshold below which rips will not occur within the groynes.

In summary groynes have the following impacts:

(1) Interrupt the beach/bar 1 and bar 2 system (Fig. 19).

(2) The nature and scale of the interruption depends on the prevailing beach type and groyne spacing.

(3) Reflective beaches are uneffected (Fig. 21) apart from shoreline orientation.

(4) RR are largely uneffected, apart from orientation and groyne controlled drainage channels.

(5) Groyne controlled TBR may replace RR with increasing wave height, and in a modal TBR beach the groynes will induce more rips, both at groynes (Fig. 20b), and in more widely spaced groynes in mid groyne locations. As mean groyne spacing is 200–300 m and mean rip spacing is 400–500 m the groynes are inducing 50 to 100% more rips, as well as controlling their location.

(6) The TBR beach state is also more likely to shift into a RBB state, i.e. detached bar, in the presence of a groyne field (Fig. 21).

(7) The LBT state will however be broken up by the groynes into a lower groyne controlled RBB or TBR state.

(8) while groynes will tend to produce more rips and move the lower beaches/bar up, and the higher states down, as much as one beach state, they do not appear to determine the actual beach type or larger scale processes such as bar attachment and migration. This implies that the groynes are superimposed on the natural beach conditions and that the natural conditions will by and large prevail, with the groynes serving as an irritant rather than determinant of beach morphodynamics.

(9) Finally, the greater number of rips and the higher beach type act as if the surf zone has been translated shoreward. Given the greater sediment mobility in the surf zone compared to the shoreline (Table 4 and Bauer et al., 1991), this should result in greater sediment mobility within the groyne field, and therefore greater potential sediment transport. If this is the case, the groynes may produce the opposite of their intended effect. One might also ask what criteria was used in determining the groyne spacing (Fig. 18) and lengths, none

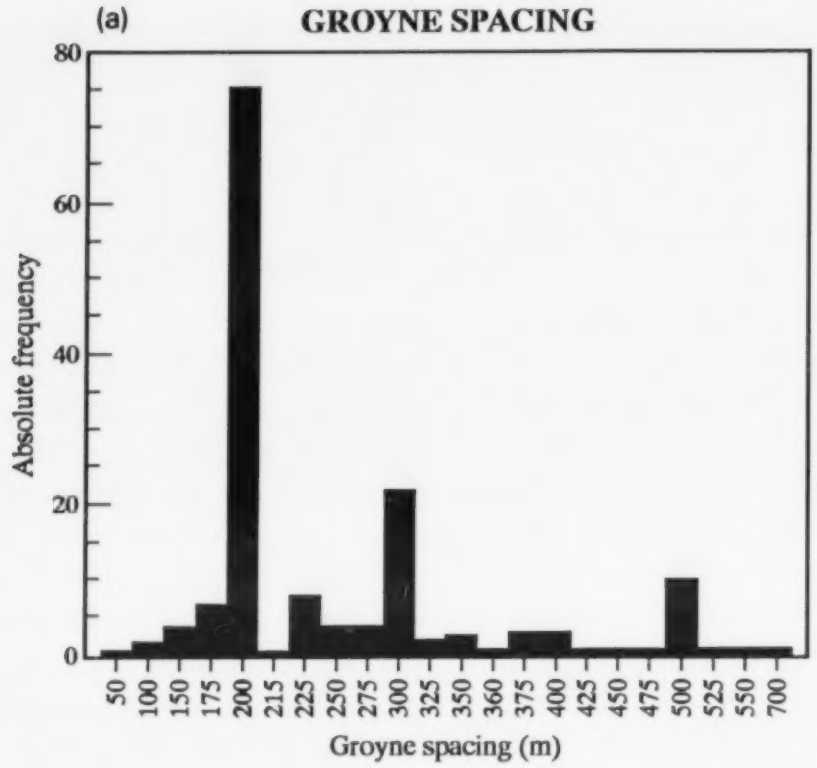

(b) **GROYNE SPACING FOR THREE GROYNE FIELDS**

LOCATION	km 0-20	km 25-30	km 97-115
Number of groynes	90	11	57
Average spacing (m)	218	370	314
Median	200	350	300
Mode	200	500	200
Standard Deviation	45	129	168
Minimum	100	200	50
Maximum	360	525	1100

Fig. 18. (a) Frequency plot of groyne spacings for the central Netherlands coast, with characteristics of the groyne fields (b).

of which are sympathetic with the natural beach rhythms (e.g. Fig. 20b–d).

"Beach model" for the central Netherlands coast

The beach system of the central Netherlands coast was classified using the beach model of Wright and Short (1984) developed for the micro-tidal swell dominated, southern Australian coast. While this model has been shown to have general application in similar wave dominated, micro-tidal environments outside Australia (e.g. Horikawa, 1988; Lippmann and Holman, 1990) it has only limited application to the multi-barred Netherlands coast. While the Australian sediments and tides range are similar to those along the central

Fig. 19. The groyned beach system fronting the village of Callantsoog (km 14). Waves are barely breaking on the outer (bar 3), bar 2 lies as a transverse bar and rip system with groyne controlled rips, while the inner bar 1 is welded to the beach. A high but narrow foredune protects Callantsoog from the North Sea (13.07.89).

Netherland coast, the wave climate is significantly different in several ways. First, the North Sea is a storm wave environment generating seas rather than swell. Modal wave period is 5.1 s and ranges from 3–9 s, compared to periods of 8–16 s in southern Australia. Wave heights are also limited in the North Sea ranging only from 0–5 m. Of equal importance is the episodic nature of the waves with storms and high waves followed by days, weeks and in summer even months of lower often ineffective wave action. Unlike beaches in the Australian swell environment that are constantly adjusting to changing wave conditions, the sea environment has short periods of high waves

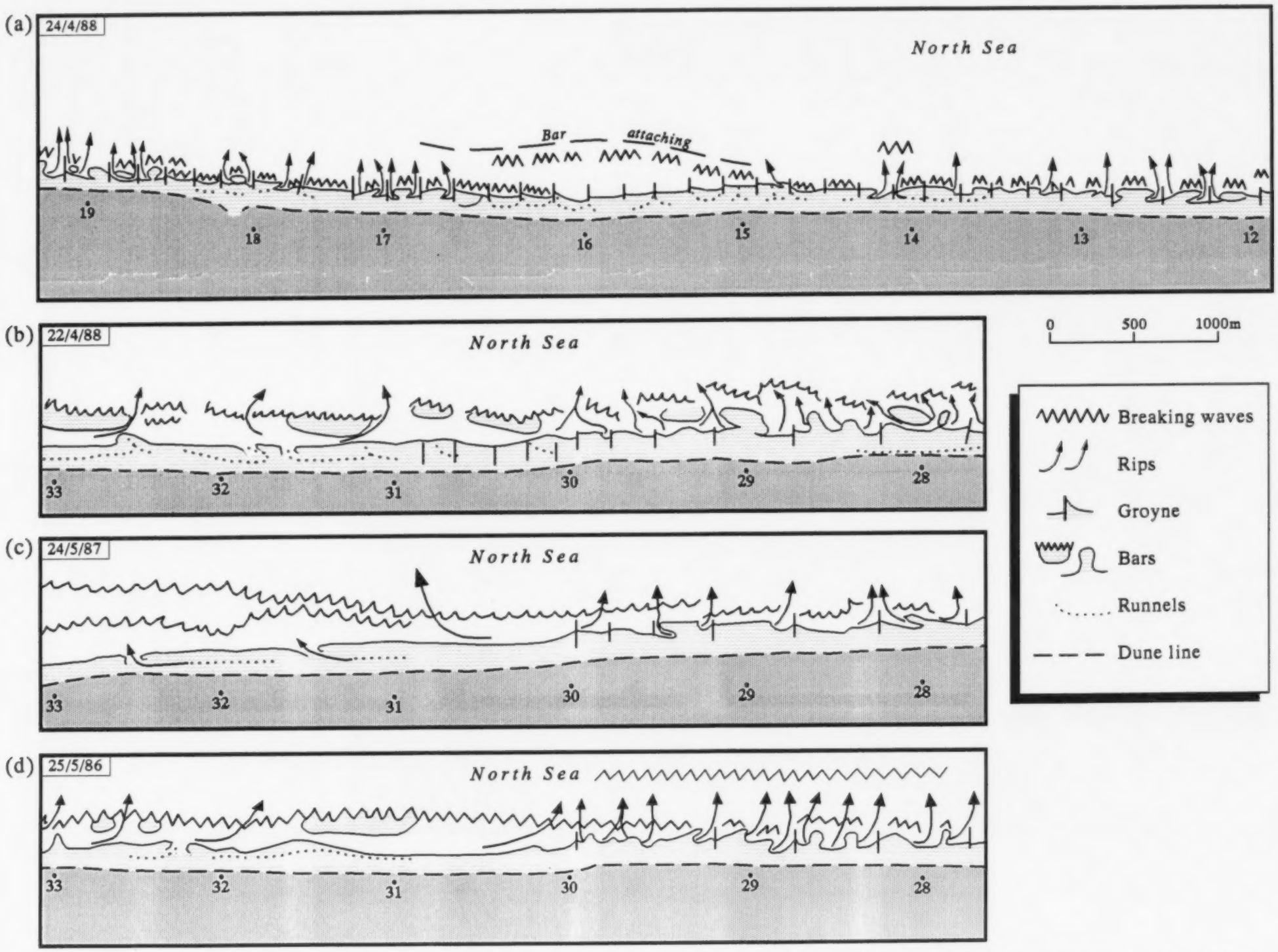

Fig. 20. Morphological sketch of beach based on aerial photographs. Numbers refer to km poles, dates indicated. Note the impact of groynes in producing more numerous groyne controlled rips. (a) In the northern groyne field (km 12–19), the groynes have induced rips in a RR topography. Note in lee of the attaching bar lower wave result in no rips. (b–d) Between km 28 and 33 rip number doubles in the groyne fields. Source: sketched from photos supplied by *Rijkswaterstaat*, Mapping and Survey Division.

Fig. 21. An example of groyne controlled rips. Ridge and runnel bar 1 with RBB bar 2 having rips skewed to north and exiting against northern groyne, km 9–8, 24.04.84. Source: *Rijkswaterstaat*, Mapping and Survey Division.

when conditions tend toward more dissipative beaches, followed by longer periods of low to no waves when the system, slowly shifts towards more intermediate-reflective conditions, or remains inactive.

Finally, the potentially high angle of wave approach and following winds on the central coast, can produce rip and bar topography heavily skewed to the north or south.

The result is first of all a three bar system, whereas the Wright and Short model has one up to two. Second, the scale of temporal change and beach "memory" is shorter in the sea opposed to swell environment, a result also reached by Aagaard (1989) on the eastern Danish coast.

These factors have been considered in constructing Fig. 22 which is a preliminary beach model for the central Netherlands coast. It is preliminary because it is based on a limited morphological data base, as indicated by the discrepancy between the observed and expected frequency of occurrence of each type (Fig. 15).

The most interesting feature of this model is the hierarchy of bar types within each beach state. Only at the full dissipative (a) and fully reflected (f) states are all bars of a similar type. In the dominant intermediate states a range of bar types is produced by two factors. First, the shoreward decrease in breaker wave height (Table 7), which produces a shoreward shift to lower energy beach types; and second, a corresponding decrease in bar and rip spacing may be attributable to the role of larger scale progressive edge waves during storms (bar 3) and smaller scale standing edges waves (bars 2 and 1) during moderate waves, as proposed by Aagaard (1989, 1990) and in his multi-bar model for the Danish coast (Aagaard, 1991).

While infragravity waves have been measured

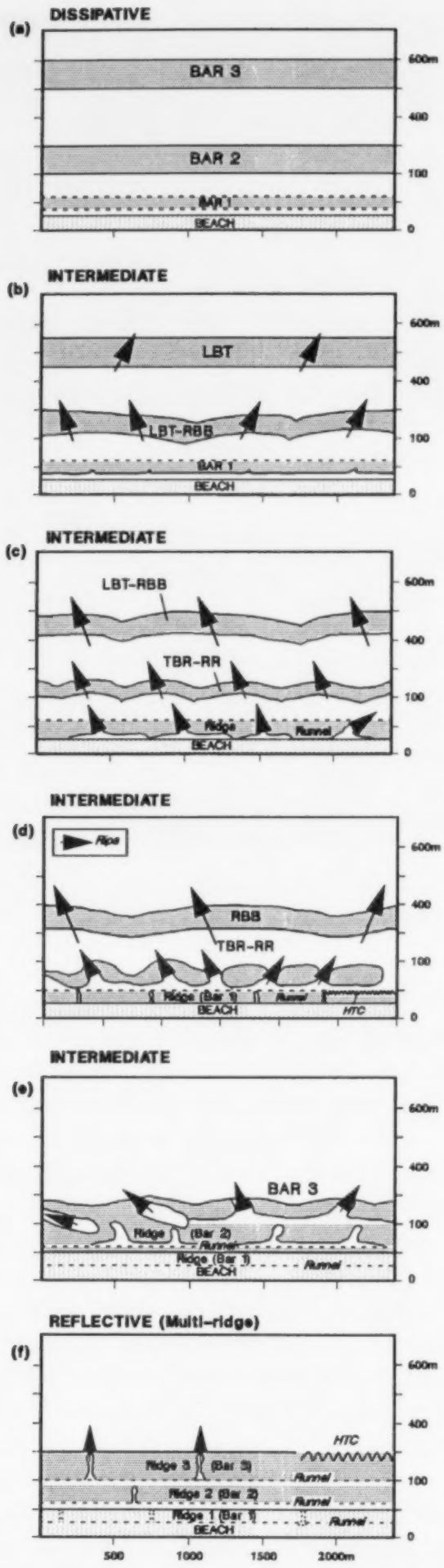

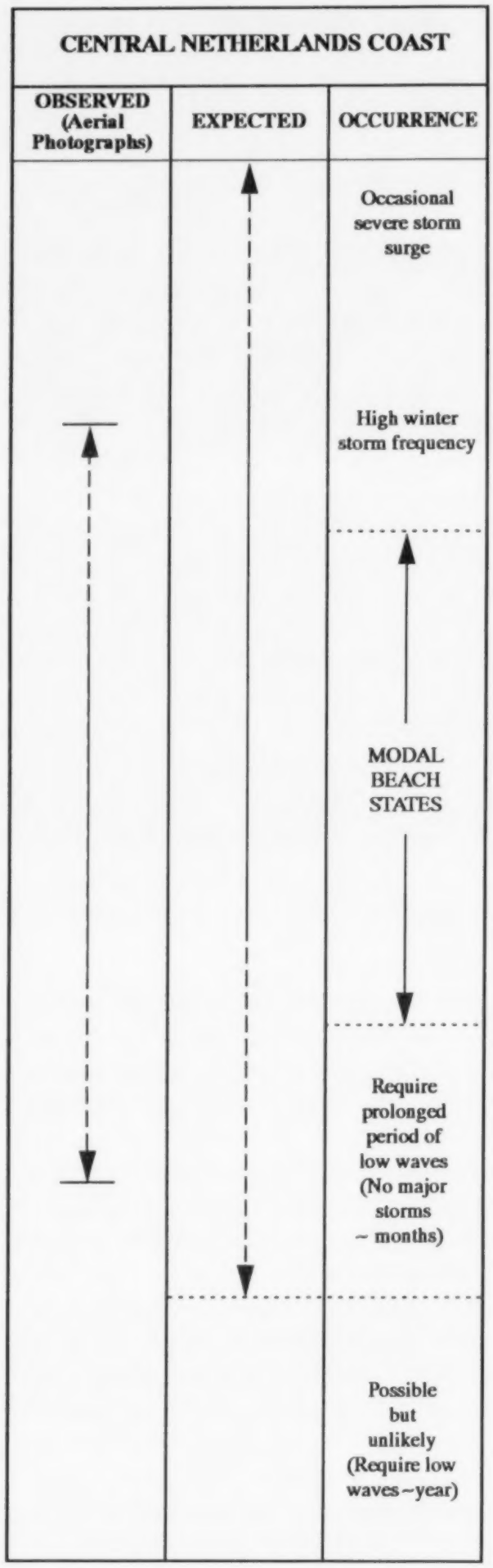

Fig. 22. Possible range of beach states on the central Netherlands coast. States (b), (c) and (d) were observed on the 1982–1988 aerial photographs. Type (a) is expected following severe storms and storm surges. Types (e) may occur following prolonged low wave periods and type (f) is only possible following extreme periods (months) of low wave conditions, and consequently is unlikely to occur on the Netherlands coast. Note arrows indicate rip location when active. Rips on bars 2 and 3 may be inactive during states (c) and (d).

in the study region (Gerritsen and Van Heteren, 1984), and may be roughly correlated with bar and rip spacing (Short, 1991a), field data is insufficient to make conclusive remarks.

In Fig. 22a, the dissipative end member, represents the shape of the beach that is expected to follow storm waves and surges of sufficient duration to permit a fully developed dissipative beach system, containing three shore parallel bars. Flow is expected to be essentially onshore at incident wave frequency switching more to infragravity frequency towards the shore, and offshore as a standing wave at infragravity frequencies (Wright and Short, 1984). Rip circulation if present is relatively weak and suppressed by the shore normal flows. Such a state would probably require a series of closely spaced major storm events and should therefore have a very low frequency of occurrence. This state was not observed on the aerial photographs and likewise an identical state predicted by Aagaard (1991) was not observed on his Danish aerial photographs, nor Lippman and Holman (1990) Duck observations. However, observations at other sites by the above authors and Wright and Short (1984) suggest such a state should exist under appropriate conditions.

More usually on the Netherlands coast, individual major storm seas or normal winter storms produce a high energy intermediate beach state (Fig. 22b or c), with a continuous outer bar either straight (LBT) or rhythmic LBT–RBB, a highly rhythmic bar 2, and bar 1. Large scale rip circulation dominates across the surf zone. As the three bars move shoreward under post-storm conditions increasing rhythmicity leads to Fig. 22c and d the modal beach states on the central coast. The outer bar 3 is continuous though broken by widely spaced rips. It is separated from bar 2 by a 100–150 m wide trough. Bar 2 is highly rhythmic and dominated by detached (RBB) or attached (TBR) bars and rip systems. The inner bar 1 attaches to the beach as TBR in Fig. 22c, and welds to the beach as a ridge and runnel by Fig. 22d.

On the lower energy Danish Baltic Sea coast ($H \sim 0.55$ m, $T = 2.5$–3.5 s) Aagaard (1991) observed a similar sequence on bar 1 in stages b, c and d, however his bar 2 and 3 while becoming highly rhythmic did not attach to bars 1 and 2 respectively. He did not observe bar 1 reaching beyond stage d in Fig. 22.

If prolonged periods of no storms and/or low waves occur, continued onshore bar migration *could* lead to an attachment of the three bars in Fig. 22e with bar 3 being RBB–TBR, bar 2 TBR–RR and bar 1 RR/R. It is possible that an unusually long period of low waves *could* produce Fig. 22f when all three bars weld as a series of ridge and runnels. However the latter (f) and possibly (e) are more likely theoretical end members, rather than actual scenarios. Only long term monitoring of beach behaviour will permit refinement of both the bar patterns and frequency of occurrence of the states illustrated in Fig. 22. These hypothetical stages were also not observed by Aagaard (1991) or Lippman and Holman (1990) though the latter have observed the reflective single bar member at other sites.

While Fig. 22 represents a major conclusion of this paper it is in fact only a starting point for a more rigorous analysis of the Netherland beach systems. Such an analysis commenced at Egmond aan Zee in 1989 with a cooperative *Rijkswaterstaat*–University of Utrecht study of the bar morphodynamics and sediment transport. No doubt when the results of this study of beach and surf zone morphodynamics is complete, it will be able to both rigorously test the conclusions reached in this study, and build a more robust model of the central Netherland beach systems.

Conclusions

The 120 km long central Netherlands coast is a sandy transgressive barrier containing a beach and two to three bar system for most of its length. The beach–bar system is exposed to a highly episodic seasonal storm wave environment with high frequency (~30 per year), short duration (2–3 days) storm waves ($H_s = > 1.5$ m, $T = 5$ s), followed by longer period of calms, particularly during summer.

The beach morphology is composed of fine to medium grained, quartz sand. It consists of an inner beach-bar 1 usually attached to the beach as a ridge and runnel. The outer bar 2 is highly rhythmic and rip dominated. It is characterised by

TBR and RBB, ranging from RR to LBT while the bar 3 is typically LBT to RBB.

All bars are characterised by rips. The bar 1 has RR or TBR rips averaging 500 m in spacing, bar 2 has TBR rips averaging 600 m while bar 3 has RBB–LBT rips averaging 900 m.

The equilibria surf zone concept of Wright et al. (1987) and Aagaard (1989) was used to predict the hierarchy of beach/bar types across the three bars, using real time wave data and actual beach/bar types. Using a decay function to reduce breaker wave height across the surf zone, the equilibrium dimensionless fall velocity provided a reasonable predictor of beach type across the three bars, which modally shift from RBB–LBT (bar 3 to TBR (bar 2) to RR (bar 1).

Structures occupy 48 km of the coast. The 4.5 km long Hondsbossche dyke, while replacing the beach-bar 1, has little apparent impact on the surf-zone-bar 2. Three groyne fields intersect the beach-bar 1 and occasionally bar 2, and result in a shift to more intermediate beach conditions, typically producing groyne controlled TBR and RBB. The rips usually exit adjacent to one or both groynes, resulting in more frequent rips occurrence and doubling of their number when they are present.

The harbour moles at IJmuiden and Hoek van Holland have resulted in shoreline progradation of up to 200 m as well as a reduction in wave height and shift in a lower energy, often inactive, beach type toward the moles.

Finally a preliminary beach model for the multi-bar central Netherlands coast is presented, with two theoretical end members of fully dissipative and reflective, connected by a descending hierarchy of intermediate bar/beach types in general agreement with the multi-bar model proposed for the Danish coast by Aagaard (1991). The most important aspect of these results and the model is that in multi-bar systems the bar and rip spacing, and beach type all decrease shoreward suggesting the influence of both progressive and standing edge waves. The surf zone equilibria approach using the dimensionless fall velocity reasonably explains the hierarchy of bar types, results also in agreement with those reached by Aagaard (1989) for the Danish Baltic coast.

Acknowledgements

This paper was researched while the author was Belle van Zuylen Visiting Professor at the Institute for Geographical Research at the University of Utrecht. The Institute's board is sincerely thanked for providing the opportunity to undertake research on the Netherlands coast. Many people and organisations in the Netherlands rendered valuable assistance in planning and acquiring the data presented here. At the University of Utrecht, Professor Joost Terwindt set me off on the right track, Piet Hoekstra shared his office, computer and thoughts, Aart Kroon got me to the beach, and Kathelijne Wijnberg assisted in all data acquisition and analysis. At *Rijkswaterstaat*, A.P. Roskam assisted with wave data, A. Kosten with aerial photographs, T. Nyland with beach profiling and Hans Wiersma provided additional aerial photography as well as showing me the coast from the air. E.D. Bouws of the Royal Netherlands Meteorological Institute provided additional wave data. Figures were drafted by Peter Johnson and the paper typed by Sandra Donnelly.

References

Aagaard, T., 1988. Nearshore bar morphology on the low-energy coast of Northern Zealand, Denmark. Geogr. Ann., 70A.

Aagaard, T., 1989. Infragravity waves and nearshore bars. Ph.D. Thesis, Inst. Geogr., Univ. Copenhagen, 234 pp.

Aagaard, T., 1990. Infragravity waves and nearshore bars in protected, storm-dominated coastal environments. Mar. Geol., 94: 181–203.

Aagaard, T., 1991. Multiple-bar morphodynamics and its relations to low-frequency edge waves. J. Coastal Res., 7: 801–813.

Bauer, B.D., Allen, J.R., Nordstrom, K.F. and Sherman, D.J., 1991. Sediment redistribution in a groin embayment under shore-normal wave approach. Z. Geomorph. N. F., 81: 135–148.

De Ruig, J.H.M. and Louisse, C.J., 1991. Sand budget trends and changes along the Holland coast. J. Coastal Res., 7: 1013–1026.

De Vroeg, J.H., 1987. Schematisering brandingsruggen met behulp van jaarlijkse kustmetingen. Vakgroep Waterbouwkunde, Tech. Univ. Delft, 37 pp. + figs. + appendices. (A schematic representation of surf zone bars based on annual coastal survey.)

Dillingh, D. and Stolk, A., 1989. A short review of the Dutch coast. Nota GWIO-89.004, Tidal Waters Division, Rijkswaterstaat, 30 pp. + 14 photos.

Doeglas, D.J., 1954. The origin and destruction of beach ridges. Leidse Geol. Meded., 20: 34–47.

Gerritsen, F. and Van Heteren, J., 1984. Low frequency oscillations on the Dutch coast. Proc. Coastal Eng. Conf., ASCE, 19th, pp. 625–641.

Horikawa, K. (Editor), 1988. Nearshore dynamics and coastal processes. Univ. Tokyo Press, 522 pp.

Keady, A. and Coleman, R., 1980. In: W.F. Tanner (Editor), Shoreline Past and Present. Coastal Res., Florida State Univ., Tallahassee, pp.149–168.

Kohsiek, L.H.M., 1984. De korrelgrootte karakteristiek van de zeereep (stuifdijk) langs de Nederlandse kust. Rijkswaterstaat, nota WWKZ-84G.007, 38 pp. + figures. (The grain size characteristic of the most seaward range of dunes along the Dutch coast.)

Lippmann, T.C. and Holman, R.A., 1990. The spatial and temporal variability of sand bar morphology. J. Geophys. Res., 95: 11575–11590.

Roelse, P. 1990. Beach and dune nouorishment in the Netherlands. Int. Conf. Coastal Eng. (Delft). ASCE, 22nd.

Roelvink, J.A. and Stive, M.J.F., 1990. Sand transport on the shoreface of the Holland coast. Int. Conf. Coastal Eng. (Delft). ASCE, 22nd.

Roskam, A.P., 1988. Golfklimaten voor de Nederlandse kust. Rijkswaterstaat, Nota GWAO-88.046, 21 pp. + figures. (Wave climate of the Dutch part of the North Sea.)

Short, A.D., 1979. Three dimensional beach stage model. J. Geol., 87: 553–571.

Short, A.D., 1986. A note on the controls of beach type and change, with examples from south east Australia. J. Coastal Res., 3: 387–395.

Short, A.D., 1991a. Beach morphodynamic systems of the central Netherlands coast. Inst. Geogr. Res., Univ. Utrecht, 106 pp.

Short, A.D., 1991b. Macro–meso tidal beach morphodynamics—an overview. J. Coastal Res., 7: 417–436.

Steetzel, H.J., 1990. Cross-shore transport during storm surges. Int. Conf. Coastal Eng. (Delft). ASCE, 22nd.

Stolk, A., 1989. Zandsysteem kust—een morfologische karakterisering. Technisch rapport 1, Kustverdediging na 1990. Rijksuniv. Utrecht, Vakgroep Fysische Geografie, Rapport GEOPRO 1989.02, 97 pp. (Sand system coast—a morphological characterization, Tech. Rep. No. 1—coastal defence after 1990.)

Stolk, A., Wiersma, J. and Zitman, T.J., 1987. Kustgenese. Grootschalige vorming en ontwikkeling van de Nederlandse kust. Rijkswaterstaat Fase 1, 1987, Deelrapport III, 120 pp. (Coastal genesis—large scale formation and development of the Dutch coast.)

Ten Hoopen, H.G.H. and Van Driel, G.B., 1979. Rapportage fotovluchten muistroomonderzoek. Rijkswaterstaat, Nota WWKZ-79G.013, 13 pp. + figures. (Report on photoflights rip current investigation.)

Van Alphen, J., 1987. De morfologie en lithologie van de brandingszone tussen Terheijde en Egmond aan Zee. Rijkswaterstaat, notitie NZN87.28, 22 pp. (The morphology and lithology of the surfzone between Terheijde and Egmond aan Zee.)

Van Alphen, J.S.L.J. and Damoiseaux, M.A., 1988. Geomorfologische kaart van de Nederlandse kustwateren, schaal 1: 250,000. K.N.A.G. Geogr. Tijdschrift, 22: 161–167. (Geomorphological map of the Dutch coastal zone.)

Van Bemmelen, C.E., 1988. De korrelgrootte-samenstelling van het strandzand langs de Nederlandse Noordzee-kust. Rijksuniversiteit Utrecht. Vakgroep Fysische Geografie Report Geopro 1988-01. Utrecht, 38 pp. +8 bijlagen. (The grain size composition of the beach sand along the Dutch North Sea coast.)

Van den Berg, J.H., 1977. Morphodynamic development and preservation of physical sedimentary structures in two prograding recent ridge and runnel beaches along the Dutch coast. Geol. Mijnbouw, 56: 185–202.

Wiersma, J. and Van Alphen, J.S.L.J., 1988. The morphology of the Dutch shoreface between Hook of Holland and Den Helder (The Netherlands). In: P.L. de Boer, A. van Gelder and S.D. Nio (Editors), Tide-influenced Sedimentary Environments and Facies. Reidel, Dordrecht, pp. 101–111.

Wright, L.D. and Short, A.D., 1984. Morphodynamic variability of surf zones and beaches: a synthesis. Mar. Geol., 56: 93–118.

Wright, L.D., Chappell, J., Thom, B.G., Bradshaw, M.P. and Cowell, P., 1979. Morphodynamics of reflective and dissipative beach and coastal systems: Southeastern Australia. Mar. Geol., 32: 105–140.

Wright, L.D., May, S.K., Short, A.D. and Green, M.O., 1987. Beach and surf zone equilibria and response times. Proc. Int. Conf. Coastal Eng. (Houston), 9th, pp. 2150–2164.

Marine Geology, 107 (1992) 139–147
Elsevier Science Publishers B.V., Amsterdam

Comparing sieve and sedimentation balance analysis of beach, lake and eolian sediments using log-hyperbolic parameters

Lars Chresten Lund-Hansen[a] and Reinhard Oehmig[b]

[a]*Institute of Geology, Marine Geological Department, Aarhus University, Ny Munkegade Bygn. 520, DK-8000 Århus, Denmark*

[b]*GEOMAR Research Center for Marine Geosciences, Wischofstraße 1–4, D-2300 Kiel, Germany*

(Received June 21, 1991; revision accepted February 17, 1992)

ABSTRACT

Lund-Hansen, L.C. and Oehmig, R., 1992. Comparing sieve and sedimentation balance analysis of beach, lake and eolian sediments using log-hyperbolic parameters. *Mar. Geol.*, 107: 139–147.

Sieving and settling analyses of 29 samples from different sedimentary environments have been compared with the use of invariant log-hyperbolic parameters. Settling velocities were not converted into millimetre size. The comparison was based on kurtosis, skewness and sorting of the distributions. The comparison of the parameter values have been evaluated by a two-tailed *t*-test. The log-hyperbolic parameters values for kurtosis between the two methods differed significantly for the beach sediments. Skewness differed significantly in all three environments and sorting only differed significantly for the beach sediments. (q–N) a measure of fit between observations and the estimated log-hyperbolic distribution differed significantly in the beach and eolian sediments. The study shows that settling velocities give a better fit to the log-hyperbolic distribution opposed to sieve analysis. The study shows that the differences in the log-hyperbolic sediment parameter values differ significantly in nearly half of the comparisons. It is concluded, that great attention must be paid to the method of grain-size analysis.

Introduction

In textural studies sieving is the most common technique and has a very long tradition in sedimentology (Blatt et al., 1980). Settling of silt and clay sized particles, based on Stoke's law, is also a common method in grain-size analysis and is often used in combination with the sieving technique (Blatt et al., 1980). Within the last 50 years settling-tube systems for size analysis of sand grains have been developed (Zeigler et al., 1960; Schlee, 1966; Taira and Scholle, 1979; Brezina, 1986, 1989).

Different researchers have compared the results of the sieve and settling-tube techniques for grain-size analysis (Sengupta and Veenstra, 1968; Sandford and Swift, 1971; Coleman and Entsminger 1977; Komar and Cui, 1984). In these studies the settling velocity was converted to grain-size (mm) using the relations between settling velocity and grain-size, as given by Schlee (1966) and Gibbs et al. (1971).

Settling velocity distributions have been used to distinguish between sedimentary environments (Reed et al., 1975; Bryant, 1986), and recently different sorting processes on a dune have been investigated by using settling velocities (Hartmann and Christiansen, 1988).

The log-hyperbolic distribution, introduced by Barndorff-Nielsen (1977), Bagnold and Barndorff-Nielsen (1980) and Barndorff-Nielsen and Blæsild (1981), has shown to be highly effective in discriminating between different sedimentary environments (Barndorff-Nielsen et al., 1980; Vincent, 1986; McArthur, 1987; Hartmann, 1991). Christiansen (1984) demonstrated that the parameters of the log-hyperbolic distribution also are a better tool

Correspondence to: L.C. Lund-Hansen, Aarhus University, Institute of Geology, Marine Geological Department, Ny Munkegade Bygn. 520, DK-8000 Århus, Denmark.

0025-3227/92/$05.00

in distinguishing different sedimentary environments, compared to the parameters of Folk and Ward (1957).

The log-hyperbolic distribution is also characterized by scale/location independent parameters (Barndorff-Nielsen and Christiansen, 1988).

The present study uses the scale/location independent parameters of the log-hyperbolic distribution to compare the distributions obtained by sieving (mm) and settling analysis (cm/s) of beach, lake and eolian sediments.

Materials and methods

Ten sediments from both beach and eolian environments, and nine sediments from lakes have been analysed. The beach sediments were collected at Skødshoved and Begtrup Vig, active spits in the Bight of Århus, Denmark. The morphology of the Begtrup Vig spit is described by Schou (1960). All beach sediments were collected in the swash zone sampling only a 0.5 cm thick top layer of sediment. The tidal range in the area is 30–40 cm (Christiansen et al., 1981) and the mean yearly wave height is estimated to be about 0.5 m (J. Jensen, pers. commun.).

The lake sediments were obtained from Skanderborg Lake and Stilling Lake, which are located south of Århus, Denmark. Both lakes each cover about 3 km^2 and the sediments were collected in the swash zone, again sampling only a 0.5 cm thick toplayer of sediment. The eolian sediments were collected from five different dune locations in the northern and western part of Jutland, Denmark. Råbjerg, Nørlund and Bindeballe are inland dune areas, whereas Hanstholm and Rubjerg are coastal dune areas. Except for the Hanstholm sediments, which were sampled from profiles in dune areas in combination with another study (Bowman et al., 1989), the sediments were obtained by sampling from the 0.5 cm thick top layer. Information on environment, sample size and sample number are summarized in Table 1.

TABLE 1

Environment, sample region, sample number

Environment	Region	Sample number
Beach	Spit 1	1, 2, 3, 4, 5, 6, 7
	Spit 2	8, 9, 10
Lake	Skanderborg	1, 2, 3, 4, 5
	Stilling	6, 7, 8, 9
	Råbjerg	1, 2, 3
	Bindeballe	4
Eolian	Hanstholm	5, 6, 7, 8
	Rubjerg	9
	Nørlund	10

All sediments were treated with 6% H_2O_2 and 1 *M* HCl to remove organic material and shell fragments, respectively. Splits for settling analysis additionally were evacuated in water for release of adhering air bubbles. Stereoscopic analysis (10–60 ×) showed that all sediments entirely consisted of quartz. Ten to fifteen grammes of each sediment were sieved with ASTM-certified sieves at intervals of 0.25 ϕ. Following sieving, ϕ-size was transformed to millimetre-size. Prior to analysis, the sieves were calibrated according to the method described by Dalsgaard et al. (1990). The samples were sieved for twenty minutes using a Ro-Tap, after which the fractions were weighed (± 0.1 mg).

The sedimentation balance system consists of a glass-tube which has an inner diameter of 20 cm and a length of 192 cm. The trade mark of the system is MACROGRANOMETER.

The data sampling device is an underwater balance placed at the bottom of the tube. Compression signals from the balance is digitized with a constant rate of 10 measurements per millisecond, providing one integrated measurement per millisecond (Brezina, 1986). Sediments are introduced into the analytical system using an underwater Venetian blind placed at the top of the tube. Simultaneously with the opening of the Venetian blind the sedimentation balance starts to register the increasing weight.

The sampling was conducted at intervals of 0.02 Psi (Ψ) ($\text{Psi} = -\log_2 v_1/v_0$; v_1 = measured settling velocity and $v_0 = 1$ cm/s; Brezina, 1986).

The settling-velocities were not converted into size (mm) (Reed et al., 1975; May, 1981; Bryant, 1986). The analyses were conducted at a temperature of about 20°C and samples had a weight of about 0.3 g and were taken from the sieved sediments using a Retsch micro-splitter.

The log-hyperbolic parameters

Figure 1 shows the geometrical meaning of the log-hyperbolic parameters. My (μ) is peak diameter and ny (ν) the typical grain size, in accordance with Bagnold (1941). In Fig. 1 the abscissa is the logarithm with base e of the grain size (mm) and the ordinate is the log-probability density. Phi (ϕ) and gamma (γ) are the slopes of the asymptotes of the fine and coarse fractions, respectively. In the log-hyperbolic distribution kurtosis (ξ) or peakedness is given by:

$$\xi = [1 + \delta(\phi\gamma)^{1/2}]^{-1/2} \quad (1)$$

Skewness (χ) or asymmetry is given by:

$$\chi = [(\phi - \gamma)/(\phi + \gamma)]\xi \quad (2)$$

Kurtosis and skewness of the log-hyperbolic distribution are analogous to the common use of these parameters in the Gaussian distribution (Barndorff-Nielsen and Christiansen, 1988).

Kurtosis and skewness are developed by ϕ, γ and delta (δ). As ϕ and γ are the dimensionless slope values of the asymptotes and δ is a scale parameter, kurtosis and skewness are independent of scale (Barndorff-Nielsen and Christiansen, 1988). Kappa (κ) is a measure of the distribution sorting given by:

$$\kappa = (\phi\gamma)^{1/2} \quad (3)$$

κ is a sorting parameter of the log-hyperbolic distribution which equals the spread of the Gaussian distribution. Tau (τ) is a measure of the sorting of the distribution near the mode point ν and is given by:

$$\tau^2 = \zeta\delta^{-2}(1 + \pi^2)^{-1} \quad (4)$$

Where $\zeta = \delta(\phi\gamma)^{1/2}$ and $\pi = \frac{1}{2}(\phi - \gamma)/(\phi\gamma)^{1/2}$.

There is no direct equivalent parameter in the Gaussian distribution. Zeta (ζ) is also a sorting parameter and π is another asymmetry parameter (Fig. 1). Quasisample size (q–N) is a complicated function, which basically measures the fit between an observed distribution and an estimated log-hyperbolic distribution (Christiansen and Hartmann, 1988). The log-hyperbolic parameters were estimated by the maximum likelihood method (Barndorff-Nielsen, 1977) using SAHARA, a PC-programme (Christiansen and Hartmann, 1988) for estimating log-hyperbolic parameters.

All sediments were sieved and sediments which on basis of the sieve analyses did not pass the log-hyperbolic maximum likelihood test were excluded (Barndorff-Nielsen and Blæsild, 1981). No smoothing of either sieve or settling data were performed. The excluded sediments showed clear bimodality. Two beach sediments and one lake sediment were thus excluded. The sediments were sieved at the Institute of Geology, Aarhus University, whereas the settling analyses were carried out with the sedimentation balance at GEOMAR.

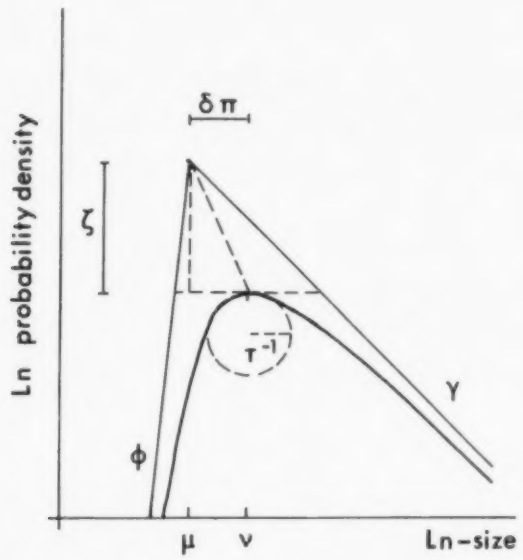

Fig. 1. Geometrical meaning of the parameters of the log-hyperbolic distribution.

Results

The sieve analyses are summarized in Table 2 which shows the grain-size range and the mean of the sediments from the three environments. Figure 2 shows the variation of the four log-hyperbolic parameter values for each environment, according to method and sample number. The

TABLE 2

Grain-size range and mean of the analysed samples by sieving

Environment	Range (mm)	Mean (mm)
Beach	0.366–0.255	0.303
Lake	1.064–0.244	0.470
Eolian	0.226–0.148	0.191

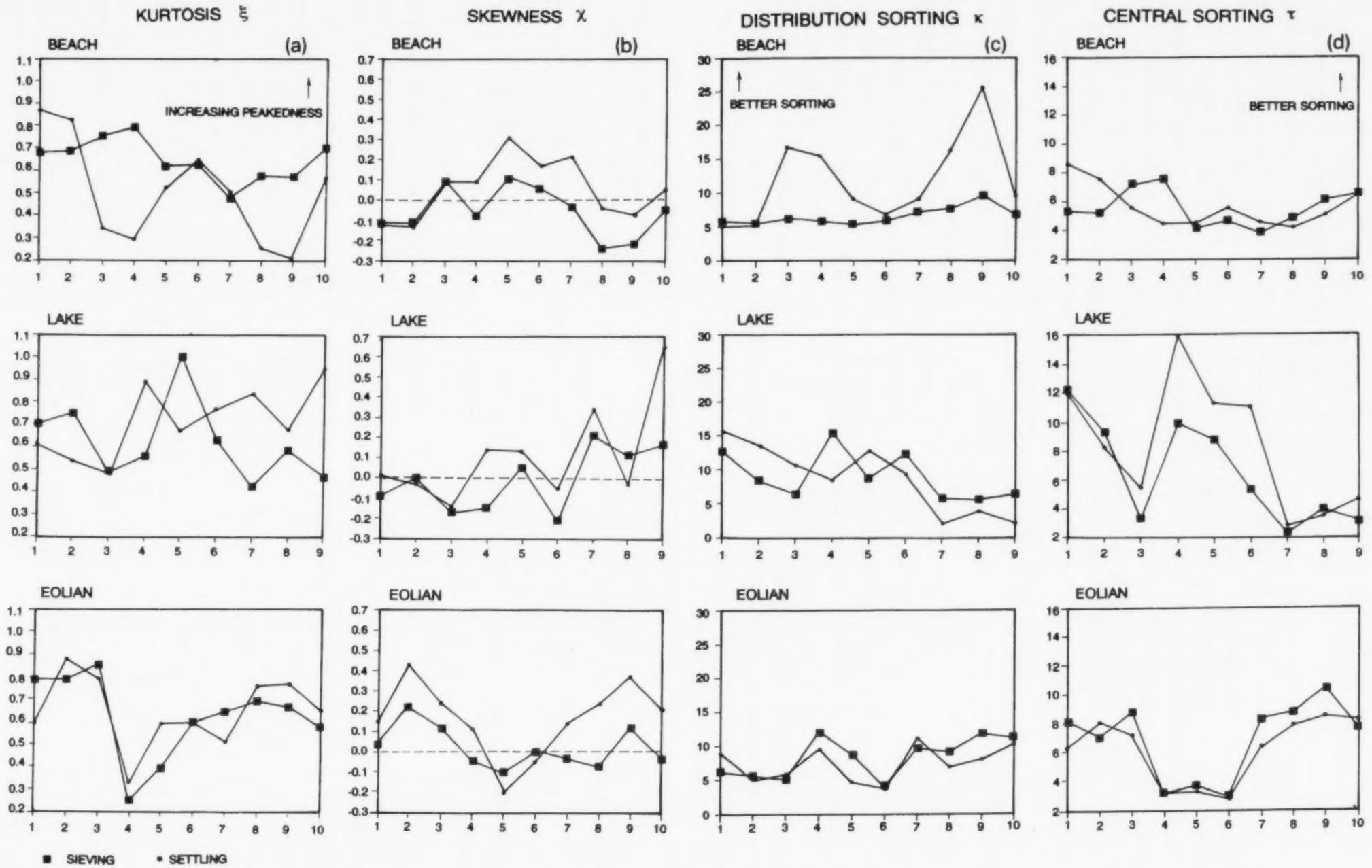

Fig. 2. Plots of Kurtosis (ξ) (A), Skewness (χ) (B), Distribution sorting (κ) (C), and Central sorting (τ) (D). Abscissa is sample number, and ordinate is parameter value.

variation of quasisample size (q–N) is seen in Fig. 3.

Kurtosis (ξ)

Figure 2A shows that the beach sediments by sieving, in general, have a higher degree of peakedness, compared to that of settling. For the lake sediments there is no systematic variances between the two methods. Only small differences and a high degree of covariance of the two methods are seen for the eolian sediments.

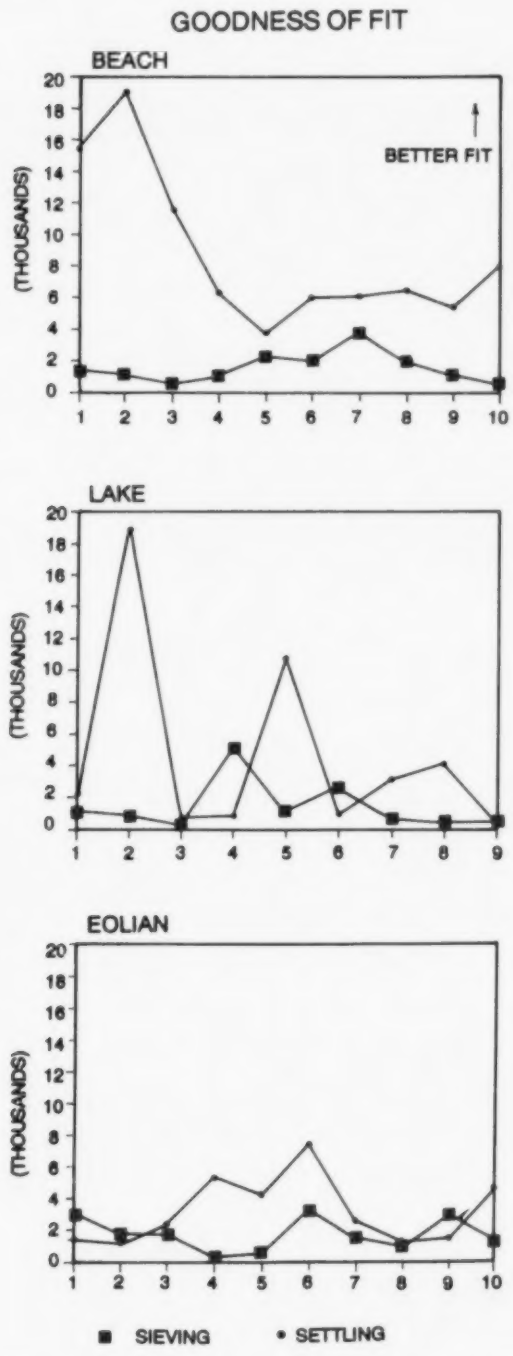

Fig. 3. Scatter plot of goodness of fit between observed and estimated log-hyperbolic distribution.

Skewness (χ)

The sediments of all three environments are, in general, more positively skewed as evaluated by the settling analyses and there is a high degree of covariance between the two methods for all three environments (Fig. 2B). More positively skewed for log-millimetre size in the log-hyperbolic distribution corresponds to more negatively skewed on the ϕ-scale, as the abscissa in the log-hyperbolic distribution is in natural logarithm to size (mm).

Distribution sorting (κ)

The beach sediments are, in general, better sorted by the settling analyses (Fig. 2C), in contrast to the lake and eolian sediments which only show small differences and a relatively high degree of covariance between the two methods.

Central sorting (τ)

There is a very high degree of covariance for all three environments, whereas only the lake sediments show some differences in the parameter values between the two methods (Fig. 2D).

Goodness of fit (q–N)

The beach sediments are clearly better fitted by the log-hyperbolic distribution resulting from settling analyses. This also holds for most of the lake and the eolian sediments.

Method, environment and parameter values

The results of the comparisons of sieving and settling analyses from sediments of the three environments are summarized in Table 3. Differences between the two methods are analysed by the use of a two-tailed t-test. A t-test was used as all parameter values, by probability plots, were seen not to deviate significantly from a Gaussian distribution. The table shows the mean parameter values of the two methods and the significance levels of the t-test, testing the hypothesis H_0: $\mu_1 = \mu_2$; H_1: $\mu 1 \neq \mu_2$, and rejecting H_0 at a certain level of significance.

The value of μ differed significantly in four beach parameters, two eolian ones and in one lake (Table 3). Table 3 also shows that skewness and (q–N) differed significantly for beach and eolian

TABLE 3

Comparison of mean distribution parameter values obtained by sieving and settling analysis

Parameter	Beach		Lake		Eolian	
	Sieve	Settl.	Sieve	Settl.	Sieve	Settl.
Kurtosis (ξ)	0.5623	0.5051[a]	0.6222	0.7122	0.6265	0.6484
Skewness (χ)	−0.0601	0.0544[a]	−0.0901	0.1124[b]	0.0280	0.1625[b]
Distrib. sort. (κ)	6.553	11.849[b]	9.061	8.703	8.353	7.393
Centr. sort. (τ)	5.584	5.674	6.504	8.368	6.865	6.158
Good. fit (q–N)	1604.1	8775.7[d]	1056.6	3199.6	1422.9	4728.8[c]

Significance levels of the two-tailed t-test is: [a]$0.1 < P < 0.05$; [b]$0.05 < P < 0.02$; [c]$0.02 < P < 0.01$; and [d]$0.002 < P < 0.001$.

environments. The degrees of freedom ($N-1$) in the t-test of the beach and eolian sediment parameters are 18, and 16 for the lake sediments. The t-test indicates a much too low level of significance for the methodical differences as the actual number of degrees of freedom are much higher (Christiansen and Hartmann, 1988) considering that a single sediment sample consists of a very high number of grains (Gibbs, 1972).

As ϕ and γ are central variables in Eqs. 1, 2, 3 and 4, which define the log-hyperbolic parameters used, it was necessary to demonstrate the effect of the slope changes of ϕ and γ using settling analysis compared to sieving.

Table 4 shows whether ϕ and γ increased or decreased by the settling analysis in comparison to the sieving analysis. It is seen that ϕ increases for most of the beach and eolian samples, whereas γ decreased for nearly all the eolian samples and for about half of the beach and lake samples.

Figure 4 shows a representative example of the log-hyperbolic distribution obtained by sieving and settling of an eolian sample (no. 10). It is seen that ϕ increases whereas γ decreases.

TABLE 4

The number of records of increasing (↗) or decreasing (↘) asymptote slopes of ϕ and γ resulting from differences using settling analysis, compared to sieving analysis

Environment	ϕ↗	ϕ↘	γ↗	γ↘
Beach	8	2	6	4
Lake	5	4	4	5
Eolian	7	3	1	9

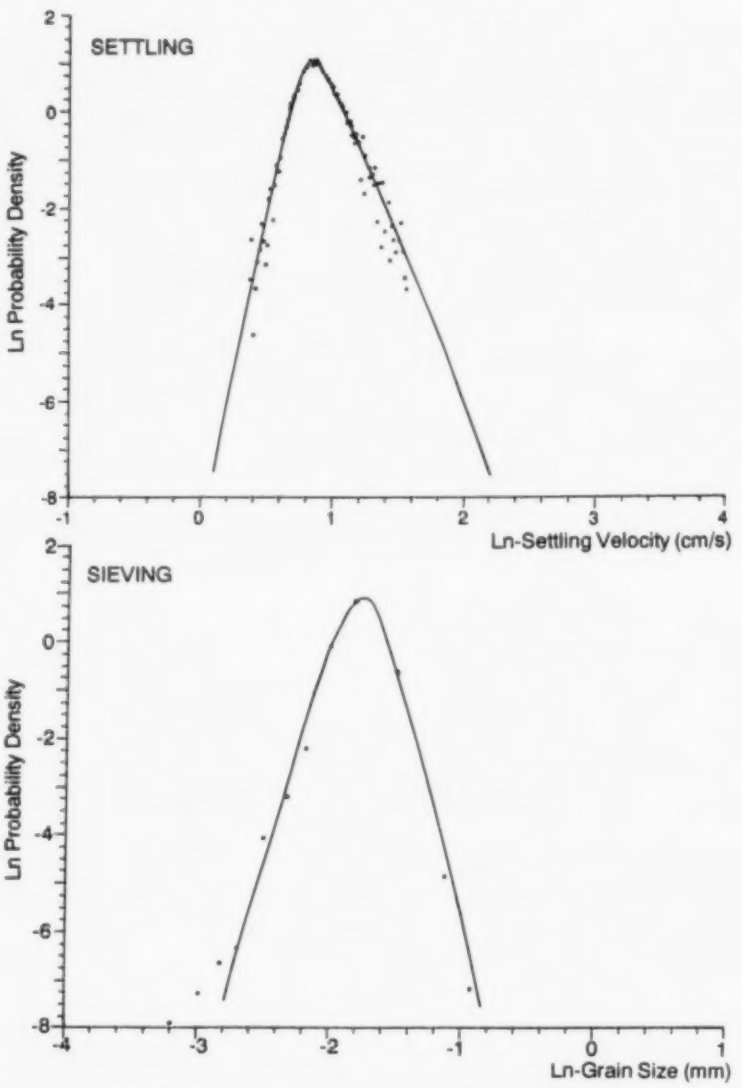

Fig. 4. Log-hyperbolic distributions obtained by sieving and settling of an eolian sample (no. 10).

Discussion

The parameters of the log-hyperbolic distribution have been used to compare the sieving and

settling techniques as the log-hyperbolic distribution utilizes parameters independent of scale in size and settling velocity. The distributions of both the grain-size and settling velocity were well described by the log-hyperbolic distribution, but considerable differences between the parameter values of the two methods were found.

Shape of the log-hyperbolic distribution

Significant differences were found for kurtosis (ξ) in the beach environment, while skewness (χ) showed significant differences in all three environments. Nearly all sediments were more positively skewed using settling analysis.

In the log-hyperbolic distribution the domain of variation of ξ and χ is referred to as the log-hyperbolic shape triangle (Barndorff-Nielsen and Christiansen, 1988). Scatter plots of ξ and χ in the shape triangle characterize a sediment as belonging to a more depositional environment for χ having a small or negative value, and a more erosional environment for χ having a large positive value. In the present study most of the sediments showed negative χ values by sieving and positive χ values by settling analysis.

The interpretation of the sediments as belonging to either depositional or erosional environments, as applied to the log-hyperbolic shape triangle, thus depends on the methods used to obtain the textural characteristics of the sediments. The plots of χ in Fig. 2B indicate a consistent difference between the distributions of the sieving and settling parameter values.

By comparing sieving and settling analyses Komar and Cui (1984) found that the sieve diameter and sedimentation diameter differed by nearly a constant of 0.40 ϕ. However, they did not observe any differences in the shape of the distribution, i.e. skewness and kurtosis between the two methods. Some researchers found by comparing sieving and settling-tube analysis that the settling data—on ϕ-scale—were more positively skewed (Coleman and Entsminger, 1977), whereas others found that they were more negatively skewed (Sanford and Swift, 1971; Jones and Cameron, 1976). However, in these studies settling velocities were converted into size (mm).

The distribution sorting (κ) differed significantly for the beach sediments, whereas the sorting near the mode point (τ), showed no significant differences in any of the environments. Sengupta and Veenstra (1968) and Jones and Cameron (1976) found that the sediments by settling-tube analysis were better sorted compared to the sieving analysis. In contrast, Coleman and Entsminger (1977) found that the settling-tube analyses were poorer sorted.

In all the beach sediments, the quasi-sample size (q–N) is higher by settling analyses, which also holds for most of the lake and eolian sediments, although the difference is not statistical significant for the lake sediments. The higher quasi-sample size for the settling analyses shows that these are much better fitted by the log-hyperbolic distribution, compared to the sieving analyses.

Settling velocity and textural characteristics

Settling velocity of sand grains depends on the size, density, shape and surface texture of the grain (Dietrich, 1982). To avoid size dependant effects of particle shape while evaluating particle size from settling velocity and in accordance with Reed et al. (1975), May (1981) and Bryant (1986) the settling velocities in the present study were not converted into size (mm). The settling velocity distributions thus represent integrations of all the above mentioned grain properties.

The slopes (ϕ) and (γ) of the asymptotes of the log-hyperbolic distribution are central variables in the parameters used. Analyses showed that ϕ increased for most of the samples by settling analysis (Table 4). This indicates that the observed differences in the parameter values between the two methods arise from changes in the fine or slow settling grain-size fraction.

The settling velocity of the grains in the fine fraction are thus higher than indicated by sieving. Sengupta and Veenstra (1968) noted that the settling of grains is controlled by the grains largest diameter, compared to sieving analysis. In sieving it is the intermediate diameter of a grain as well as its shape which controls the grains passage through the screen opening of sieves (Sahu, 1965; Ludwick and Henderson, 1968; Komar and Cui, 1984). Baba and Komar (1981) showed that non-sphericity of a grain caused its settling velocity to

be smaller than that of the mass equivalent sphere, and that this difference increases with grain diameter. No trend could be seen in γ by the beach and lake sediments, whereas γ decreased for nearly all the eolian sediments. The settling velocity of the coarse fraction of the eolian sediments are thus slower than indicated by sieving. The behavior of the eolian sediments in the sedimentation balance are thus quite different from that of the beach and lake sediments.

In this study, only grains with quartz density (2.65 g/cm^3) have been used. The different behaviour of eolian sediments according to sieving and settling-tube analysis is thus apparently caused by either the shape as the most important factor, or surface texture of the eolian sediment grains.

Distribution and environment

Sandford and Swift (1971) debated that settling-tube analyses are a more behavioristic technique compared to the sieving analyses of water-lain sediments. Although, the settling-tube is not able to recreate the hydrodynamics of the swash zone, for instance, the results of this study indicate that the observed differences between the sieving and settling method is due to behavioristic properties of the sediments in the sedimentation balance.

In studies which compare grain-size distributions of beach and dune sediments in order to differentiate the depositional environments, all sediment samples were collected from the same region, representing shore and dune areas (Mason and Folk, 1958; Friedmann, 1961; Shepard and Young, 1961; Duane, 1964; Nordstrom, 1977; Vincent, 1986). In the present study sediments were collected to compare two methods of grain-size analysis and it is shown that significant differences exist in the parameter values between the two methods in sediments from the same environment and region, for example kurtosis in the seven beach samples from the same region (Spit 1) (Table 1). This shows the significance of the method used in grain-size analysis.

Conclusions

The parameters of the log-hyperbolic distribution have been used to compare the sieving and settling techniques as the log-hyperbolic distribution utilizes parameters independent of scale. Statistical significant differences between seven of the fifteen log-hyperbolic parameters were found. The highest number of significant differences were found in the beach sediments—four of five. Skewness differed significantly for all three environments. The high number of significant differences in the beach sediments is supposed to reflect the higher level of energy transformation on the beach compared to the lake and eolian samples. For the beach and eolian sediments the study showed that the log-hyperbolic distribution was better fitted to the data obtained by settling analysis.

The present study shows that analysis using textural characteristics as kurtosis, skewness and sorting to distinguish between different sedimentary environments, must be examinated more critically, as the sediment parameter values strongly depends on the method used to obtain these values.

Acknowledgements

The present study was conducted within the GEOKAT project at Aarhus University and SFB 313 at Kiel University. We wish to thank Susanne Schultz for technical assistance. Christian Christiansen is greatly acknowledged for suggestions and critical reading of the manuscript. P. Vincent is acknowledged for helpful comments.

References

Baba, J. and Komar, P.D., 1981. Measurements and analysis of settling velocities of natural quartz sand grains. J. Sediment. Petrol., 51: 631–640.

Bagnold, R.A., 1941. The Physics of Blown Sand and Desert Dunes. Methuen, London. 265 pp. (Reprint published in 1973 by Chapman and Hall, London).

Bagnold, R.A. and Barndorff-Nielsen, O.E., 1980. The pattern of natural size distributions. Sedimentology, 27: 199–207.

Barndorff-Nielsen, O.E., 1977. Exponentially decreasing distributions for the logarithm of particle size. Proc. R. Soc. London, Ser. A, 533: 401–419.

Barndorff-Nielsen, O.E. and Blæsild, P., 1981. Hyperbolic distributions and ramifications: contributions to theory and applications. In: C. Taillie, G.P. Patil and B.A. Baldessari (Editors), Statistical Distributions in Scientific Work. Reidel, Dordrecht, 4: 19–44.

Barndorff-Nielsen, O.E. and Christiansen, C., 1988. Erosion, deposition and size distributions of sand. Proc. R. Soc. London, 417: 335–352.

Barndorff-Nielsen, O.E., Dalsgaard, K., Halgreen, C., Kuhlman, H., Møller, J.T. and Schou, G., 1980. Variation in particle size over a small dune. Sedimentology, 29: 53–65.

Blatt, H., Middelton, G.V. and Murray, R.C., 1980. Origin of Sedimentary Rocks. Prentice-Hall, Englewood Cliffs, N.J., 2nd ed., 766 pp.

Bowman, D., Christiansen, C. and Margaritz, M., 1989. Late-Holocene coastal evolution in the Hanstholm–Hjardemaal region, NW Denmark. Morphology, sediments and dating. Geogr. Tidsskr., 89: 49–57.

Brezina, J., 1986. Macrogranometer—Operation Manual. 49 pp. (Unpubl.).

Brezina, J., 1989. Sand Sedimentations-Analyse und Separation—mehr als 25 Jahre Forschung und Entwicklung. Nachr. Dtsch. Geol. Ges., 41: 149–153.

Bryant, E., 1986. Sample site variation in settling distribution subpopulations using curve dissection analysis. Sedimentology, 33: 767–775.

Christiansen, C., 1984. A comparison of sediment parameters from log-probability plots and log–log plots of the same sediments. (Geoskrifter, 20.) Geol. Inst., Aarhus Univ.

Christiansen, C. and Hartmann, D., 1988. SAHARA: A package of PC computer programs for estimating both log-hyperbolic grain-size parameters and standard moments. Comput. Geosci., 14: 557–625.

Christiansen, C., Christoffersen, H. and Schultz, E., 1981. Hydrography, sediments and sedimentation in a low energy embayment, Knebel Vig, Denmark. Geogr. Annlr., 63: 159–164.

Coleman, C.J. and Entsminger, L.D., 1977. Sieving versus settling tube: A comparison of hydrodynamic and granulometric characteristics of beach and beach ridge sands. In: W.F. Tanner (Editor), Coastal Sedimentology. Geol. Dep. Florida State Univ.

Dalsgaard, K., Jensen, L.J. and Sørensen, M., 1990. Methodology of sieving small samples and calibration of sieve sets. In: Syvitski (Editor), Principles, Methods and Applications of Grain Size Analyses. Cambridge Univ. Press.

Dietrich, W.E., 1982. Settling velocity of natural particles. Water Resour. Res., 18: 1615–1626.

Duane, D.B., 1964. Significance of skewness in recent sediments, Western Pamlico Sound, North Carolina. J. Sediment. Petrol., 34: 864–874.

Folk, R.T. and Ward, W.C., 1957. Brazos River Bar: A study in the significance of the grain size parameters. J. Sediment. Petrol., 27: 3–26.

Friedman, G.M., 1961. Distinction between dune, beach, and river sands from their textural characteristics. J. Sediment. Petrol., 31: 514–529.

Gibbs, R.J., 1972. The accuracy of particle analyses utilizing settling tubes. J. Sediment. Petrol., 42: 141–145.

Gibbs, R.J., Matthews, M.D. and Link, D.A., 1971. The relationship between sphere size and settling velocity. J. Sediment. Petrol., 44: 7–18.

Hartmann, D., 1991. Cross-shore selective sorting processes and grain size distributional shape. In: O.E. Barndorff-Nielsen and B.B. Willets (Editors). Acta Mech. Suppl., 2: 49–63.

Hartmann, D. and Christiansen, C., 1988. Settling-velocity distributions and sorting processes on a longitudinal dune: A case study. Earth Surf. Process. Landforms, 13: 649–656.

Jones, J.R. and Cameron, B., 1976. Comparison between sieving and settling-tube determinations of sand sizes by using discriminant analysis. Geology, 4: 741–744.

Komar, P.D. and Cui, B., 1984. The analysis of grain-size measurements by sieving and settling-tube techniques. J. Sediment. Petrol., 54: 603–614.

Ludwick, J.C. and Henderson, P., 1968. Particle shape and inference of size from sieving. Sedimentology, 11: 197–235.

Mason, C.C. and Folk, R.L., 1958. Differentiation of beach, dune, and aeolian flat environments by size analysis, Mustang Island, Texas. J. Sediment. Petrol., 28: 211–226.

May, J.P., 1981. Chi (χ): A proposed standard parameter for settling tube analysis of sediments. J. Sediment. Petrol., 51: 607–610.

McArthur, D.S., 1987. Distinctions between grain-size distributions of accretion and encroachment deposits in an inland dune. Sediment. Geol., 54: 147–163.

Nordstrom, K.F., 1977. The use of grain size statistics to distinguish between high- and moderate-energy beach environments. J. Sediment. Petrol., 47: 1287–1294.

Reed, W.E., Fever, L.R. and Moir, G.J., 1975. Depositional environmental interpretation from settling-velocity (Psi) distributions. Geol. Soc. Am. Bull., 86: 1321–1328.

Sahu, B.K., 1965. Theory of sieving. J. Sediment. Petrol., 35, 750–753.

Sandford, R.B. and Swift, D.J.P., 1971. Comparison of sieving and settling techniques for size analysis, using a Benthos Rapid Sediment Analyzer. Sedimentology, 17: 257–264.

Schlee, J., 1966. A modified Woods Hole rapid sediment analyzer. J. Sediment. Petrol., 36: 403–413.

Schou, A., 1960. The coastline of Djursland. Geogr. Tidsskr., 59: 10–27.

Sengupta, S. and Veenstra, H.J., 1968. On sieving and settling techniques for sand analysis. Sedimentology, 11: 83–98.

Shepard, F.P. and Young, R., 1961. Distinguishing between beach and dune sands. J. Sediment. Petrol., 31: 196–214.

Taira, A. and Scholle, P.A., 1979. Discrimination of depositional environments using settling tube data. J. Sediment. Petrol., 49: 787–800.

Vincent, P., 1986. Differentiation of modern beach and coastal dune sands—A logistic regression approach using the parameters of the hyperbolic function. Sediment. Geol., 49: 167–176.

Zeigler, J.M., Whitney, G.G. and Hayes, C.R., 1960. Woods Hole rapid sediment analyzer. J. Sediment. Petrol., 30: 490–495.

NOTES FOR ELECTRONIC TEXT PREPARATION

1. General

The word-processed text should be in single column format. Keep the layout of the text as simple as possible; in particular, do not use the word-processor's options to justify the text or to hyphenate the words.

2. Text preparation

The electronic text should be prepared in a way very similar to that of conventional manuscripts (see also Guide for Authors). The list of references, tables and figure captions should be compiled separately from the main text. Do *not* reserve space for the figures and tables in the text; instead, indicate their approximate locations, either directly in the electronic text or on the manuscript.

3. Submission

The final text should be submitted both in manuscript form and on diskette. Use standard 3.5″ or 5.25″ diskettes for this purpose. Both double density (DD) and high density (HD) diskettes are acceptable. Ensure, however, that the diskettes are formatted according to their capacity (HD or DD) before copying the files onto them.

Storage of the main text, list of references, tables and figure captions in separate text files with clearly identifiable file names (for example, with extensions .TXT, .REF, .TBL, .FIG) is required.

The format of the files depends on the wordprocessor used. Texts made with DEC WPS PLUS, DisplayWrite, First Choice, IBM Writing Assistant, Microsoft Word, Multimate, PFS:Write, Professional Writer, Samna Word, Sprint, Total Word, Volkswriter, Wang PC, WordMARC, WordPerfect, Wordstar, or files supplied in DCA/RFT format can be readily processed. In all other cases the preferred text format is ASCII.

Essential is that the name *and* the version of the wordprocessing program and the type of computer on which the text was prepared is clearly indicated on the diskette label or the accompanying checklist.

Authors are encouraged to ensure that **the disk version and the hardcopy must be identical**. Discrepancies can lead to proofs of the wrong version being made.

Illustrative material (original figures or high-quality glossy prints, or photographs showing sharp contrast) should be included separately.

ELECTRONIC TEXT CHECKLIST

Please complete this list where appropriate and include it with the diskette.

Journal : _____

Title : _____

_____

Author(s) : _____

Computer

☐ IBM compatible
☐ Macintosh[1]

Diskette

☐ formatted with MS-DOS/PC-DOS
☐ formatted with Macintosh OS

File format (if different from wordprocessor's original format)

☐ ASCII
☐ DCA/RFT
☐ DEC/DX

Wordprocessor

☐ DEC WPS PLUS[2]	version: _____
☐ DiplayWrite[3]	version: _____
☐ First Choice	version: _____
☐ IBM Writing Assistant	version: _____
☐ Microsoft Word	version: _____
☐ Multimate	version: _____
☐ PFS:Write	version: _____
☐ Professional Writer	version: _____
☐ Samna Word	version: _____
☐ Sprint	version: _____
☐ Total Word	version: _____
☐ Volkswriter	version: _____
☐ Wang PC	version: _____
☐ WordMARC	version: _____
☐ WordPerfect	version: _____
☐ Wordstar	version: _____

☐ Other (specify)[4]: _____

Diskette contents : _____

_____

_____

Remarks : _____

_____

_____

[1] In view of the further text processing on a MS-DOS compatible system submission of text files on MS-DOS formatted diskettes is recommended.
[2] Files should be submitted in DX format (option "CV" from the DEC-WPS Document Processing Menu).
[3] Files created with DisplayWrite 4 should be submitted in DCA/RFT format by means of the DisplayWrite "Convert Documents" utility.
[4] Submission of the text files in ASCII format is strongly recommended.

J. G. Baretta-Bekker, E. K. Duursma, B. R. Kuipers, NIOZ, Netherlands Institute for Sea Research, Texel, The Netherlands (Eds.)

Encyclopedia of Marine Sciences

1992. Approx. 250 pp. 127 figs.
Softcover DM 58,- ISBN 3-540-54501-8

The multidisciplinary character of marine sciences (Biology, Chemistry, Geology, Physics in Oceanography) is reflected in some 3000 up-to-date alphabetically listed keywords, and many illustrations, to give scientists, teachers, and students a helpful and time-saving aid when studying marine scientific literature. The brief explanation of the concepts, terminology and methods make this book more valuable than a pure glossary or dictionary.

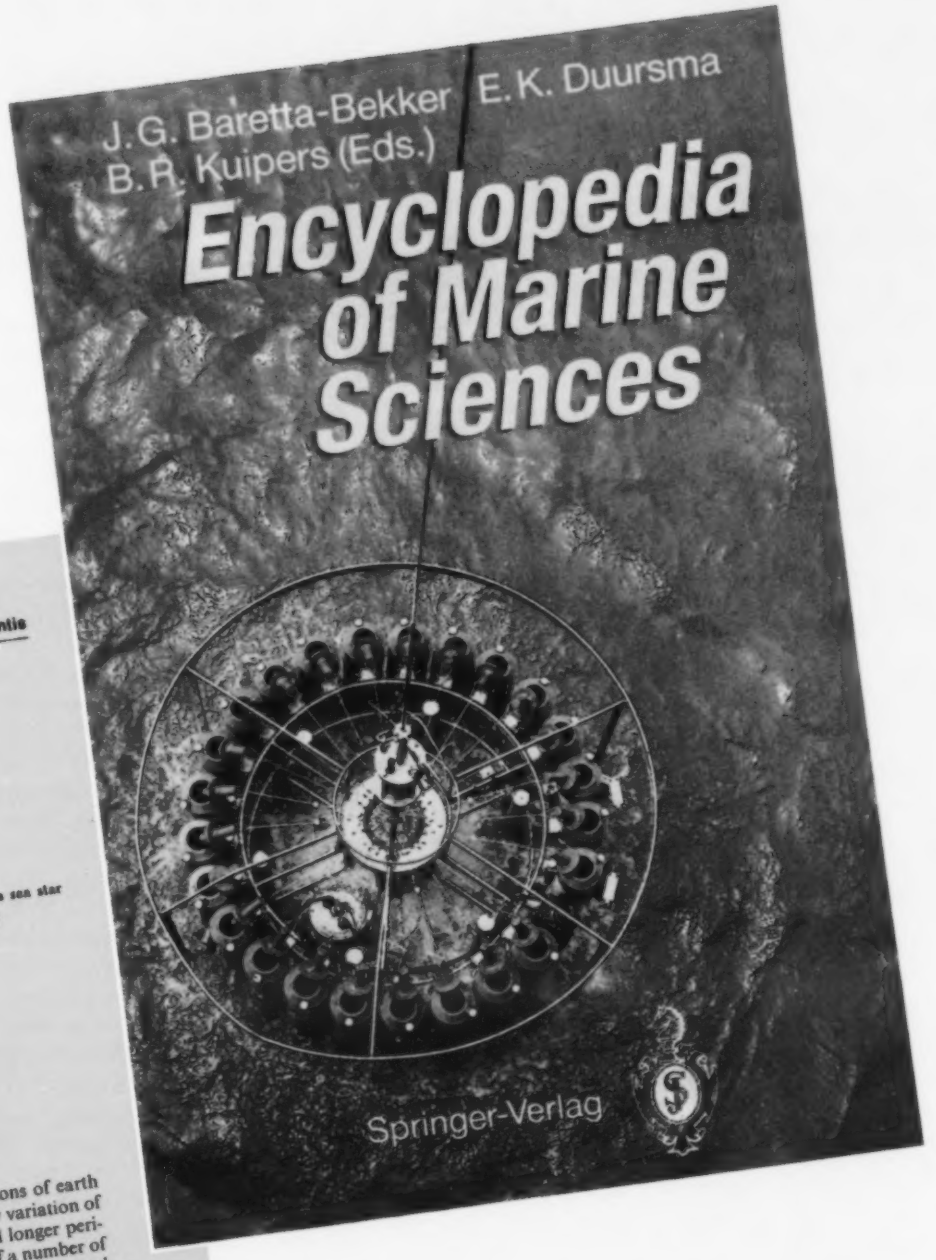

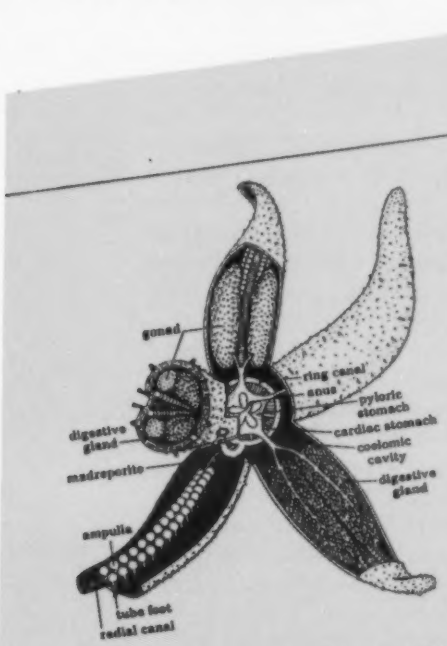

Dissection of a sea star (dorsal view)

asthenosphere see →earth's internal structure.

astronomical tides astronomical variations in the mutual positions of earth and moon and earth and sun cause variations of the →tides by variation of the tide-generating potential, at roughly monthly, annual and longer periods. As a result the tides can be considered the combination of a number of so-called astronomical tides that can be divided into a group of semi-diurnal tides (period about 12 hours), diurnal tides (period about 24 hours) and longer-period (fortnightly, monthly, semi-annual, annual and even longer period) tides. See →harmonic analysis of tides and →partial tides.

Atlantis mythical land, originally mentioned by Plato (429–348 BC) and located west of the Atlas Mountains, one of the Pillars of Hercules (the ancient name of the Strait of Gibraltar). It was an archipelago larger than North Africa and Asia Minor (present-day Turkey), together, and flooded by the sea, the present Atlantic Ocean. By some it is considered to have been a real archipelago once and various regions have been proposed as the original Atlantis, in western Europe (north Sweden, Holland, Heligoland) as well as in the Mediterranean, in the Sahara and in Nigeria. Recently it was shown that the present island of Thira in the Aegean Sea was in antiquity a much larger (volcanic) island that may have been Atlantis. The 'lost land' of Atlantis for many centuries has appealed to fantasy, and most probably it was only that.

Springer-Verlag

☐ Heidelberger Platz 3, W-1000 Berlin 33, F.R. Germany ☐ 175 Fifth Ave., New York, NY 10010, USA ☐ 8 Alexandra Rd., London SW19 7JZ, England
☐ 26, rue des Carmes, F-75005 Paris, France ☐ 37-3, Hongo 3-chome, Bunkyo-ku, Tokyo 113, Japan ☐ Room 701, Mirror Tower, 61 Mody Road, Tsimshatsui, Kowloon, Hong Kong ☐ Avinguda Diagonal, 468-4°C, E-08006 Barcelona, Spain ☐ Wesselényi u. 28, H-1075 Budapest, Hungary

tm.30.429/SF

Global Climatic Changes in Water and Heat Transfer - Accumulation Processes

by **S.G. Dobrovolski**

Developments in Atmospheric Science Volume 21

In this book global heat circulation is studied in connection with changes in large scale water transfer and accumulation processes. Special attention is given to stochastic regularities of the analyzed processes. Some deterministic approaches are also considered, whereby dynamic-stochastic models are used.
This study in global heat and moisture circulation is based upon the following main aspects:

- substantiation of the hypothesis of a two-scale separation of weather and climatic variables, which forms the basis of the stochastic theory of the climate system;
- analysis of the probabilistic structure of changes in the characteristics of heat and moisture circulation in the intermediate and larger (more than 1 month) time scales;
- study of regularities of anomalies in the characteristics of heat and moisture circulation in the atmosphere and hydrosphere for large regions through spatial statistic analysis and two-dimensional dynamic-stochastic models;
- changes in the structure of temporal variations in stochastic models, under the conditions of modified spatial scales of the processes;
- analysis of globally averaged characteristics, such as temperature of the atmosphere and oceans, and ocean level.

The work does not claim to be an exhaustive study, but will be of considerable interest to researchers and students in the fields of atmospheric science, oceanography, global change and climate impact assessment.

Contents: **Introduction. 1. Models of Large-Scale Processes in the Ocean-Atmosphere-Continents System.** Deterministic and Stochastic Properties of the System. Analogies with Simple Nonlinear Models. General Circulation Models. Basic Principles of the Dynamic-Stochastic Models Theory of the Atmosphere and Hydrosphere. Stochastic Analysis of Series of Monthly and Annual Hydrometeorological Characteristics. Maximum Entropy Method. **2. Anomalies of Global Heat and Water Exchange Between the Atmosphere and Upper Oceanic Layer.** Data on Characteristics of Heat and Moisture Circulation at the Ocean-Atmosphere Interface. Stochastic Models of Sea Surface Temperature Anomalies. Changes in the Near-Surface Air Temperature, Contact Turbulent Heat Exchange with the Ocean, and Evaporation. Dynamic-Stochastic Model of the Interaction Between the Atmosphere and Upper Oceanic Layer. **3. Variations of the Atmospheric Water Exchange.** Changes in the Moisture Content and Moisture Transport in the Atmosphere. Structure of Series of Monthly and Yearly Precipitation Values. On Statistic Regularities of Isotope Concentration Variations in Atmospheric Moisture. **4. Changes in the Atmosphere-Land Surface Moisture Fluxes. River Runoff.** Anomalies of Land Surface Water Balance Components in Different Natural Zones. A Simple Dynamic-Stochastic Model of the River Runoff in the Intermediate Time Scale. On a Globally-Averaged Stochastic Model of Annual Runoff. Variability of the Runoff, Summarized Within Large Regions. Trends in the Runoff. **5. Variations of the Water Balance Components of the Continents and the World Water Balance.** Changes in the Components of Water Balance of Continents Free from Ice. Connection with Thermal Regime. Variability of Global Water Balance Components. **6. Eustatic Fluctuations of the Global Mean Sea Level, Changes in the Mass of Ice Sheets and Global Temperature.** Recent Changes in the Global Mean Sea Level. Stochastic Models of Changes in the Global Mean Sea Level. Global Temperature Fluctuations. **7. Moisture Redistribution and Thermal Regime Variations in Paleo- and Historic Times. Stochastic Models.** Paleoreconstructions of the Global Mean Sea Level and Its Stochastic Model. Reconstruction of Thermal Regime and Moisture Circulation Processes. **Conclusion. References. Index.**

1992 280 pages
Price: US $ 108.50 / Dfl. 190.00
ISBN 0-444-88914-0

ELSEVIER SCIENCE PUBLISHERS
P.O. Box 1930, 1000 BX Amsterdam, The Netherlands
P.O. Box 882, Madison Square Station, New York, NY 10159, USA
The Dutch Guilder (Dfl) price is definitive. US $ prices are subject to exchange rate fluctuations.

(continued from inside front cover)

Publication of abstracts and contents lists
Abstracts and/or contents lists of this journal are published in the following journals: *Geoscience Contents, Geo Abstracts, Current Contents, Bulletin Signalétique, Chemical Abstracts, Marine Science Contents Tables, A.G.I.'s Bibliography and Index of Geology, Aquatic Sciences and Fisheries Abstracts, PASCAL/CNRS, Curr. Awareness. Biol. Sci. (CABS) and Oceanic Abstracts.*

Note to contributors
A detailed *Guide for Authors* is available upon your request, and will also be printed in the first volume to appear each year. You are kindly asked to consult this guide. Please pay special attention to the following notes:

Language
The official language of the journal is English, but occasional articles in French and German will be considered for publication. Such articles should start with an abstract in English, headed by an English translation of the title. An abstract in the language of the paper should follow the English abstract. English translations of the figure captions should also be given.

Preparation of the text
a) The manuscript should be typewritten with double spacing and wide margins and include at the beginning of the paper an abstract of not more than 500 words. Words to be printed in italics should be underlined. The metric system should be used throughout.
b) The title page should include, the name(s) of the author(s) and their affiliations.

Abstract
The abstract must be an informative statement of the content of the paper, explaining what the problem is, the methods used (when appropriate), a statement of the results, and the main conclusions. Constructions using phrases such as "this paper discusses", "are described" and "is reported" have no place in an abstract: by reading the abstract, the reader should be able to understand the essential qualities of the paper without referring to the paper itself. See K.K. Landes (Bull. Am. Assoc. Pet. Geol., 1951, Vol. 35, p. 1660) for a concise statement on how to write a good abstract.

References
a) References in the text start with the name of the author(s), followed by the publication date in parentheses.
b) The reference list should be in alphabetical order and on sheets separate from the text.

Tables
Tables should be compiled on separate sheets. A title should be provided for each table and they should be referred to in the text.

Illustrations
a) All illustrations should be numbered consecutively and referred to in the text.
b) Drawings should be completely lettered, the size of the lettering being appropriate to that of the drawings, but taking into account the possible need for reduction in size (preferably not more than 50%). The page format of *Marine Geology* should be considered in designing the drawings.
c) Photographs must be of good quality, printed on glossy paper.
d) Figure captions should be supplied on a separate sheet.
e) If contributors wish to have their original figures returned this should be requested in proof stage at the latest.
f) **Colour figures** cannot normally be accepted unless the reproduction costs are to be met by the author. As a rough guide, the reproduction costs for a one-page figure are ca. Dfl. 2150 (inc. tax). Please consult the publisher for further information.

Proofs
One set of proofs will be sent to the author, to be checked for printer's errors. In case of two or more authors please indicate to whom the proofs should be sent.

Reprints
Fifty reprints of each article published are supplied free of charge. Additional reprints can be ordered on a reprint order form, which is included with the proofs.

Submission of manuscripts
a) Manuscripts originating in the Americas and Far East should be submitted in triplicate to Dr. D.A. McManus, Department of Oceanography, University of Washington, Seattle, Washington 98105, U.S.A. All other manuscripts should be sent in triplicate to the Editorial Office *Marine Geology,* P.O. Box 1930, 1000 BX Amsterdam, The Netherlands.
b) Illustrations should also be submitted in triplicate. One set should be in a form ready for reproduction: the other two may be of lower quality.
c) Authors are requested to submit the names and addresses of four potential referees with their manuscripts.
d) Letter-type contributions should be submitted in triplicate to the Editorial Office *Marine Geology, Letter Section,* P.O. Box 1930, 1000 BX Amsterdam, The Netherlands. Contributions for this section should not exceed 8 printed pages and should be complete in themselves. No foldout illustrations can be accepted. The manuscripts received will be published ca. *three months* after acceptance. In order to achieve rapid publication, no proofs will be sent to the authors. Manuscripts should therefore be prepared with the greatest possible care.
e) **The indication of a FAX number on submission of the manuscript could assist in speeding communications. The FAX number for the Amsterdam office is: 020-5862696.**
f) In order to enable publication as quickly as possible after acceptance, authors are encouraged to submit the final text also on a 3.5" or 5.25" diskette. Both double density (DD) and high density (HD) diskettes are acceptable. Make sure, however, that the diskettes are formatted according to their capacity (HD or DD) before copying the files onto them. As with the requirements for manuscript submission, the main text, list of references, tables and figure captions should be stored in separate text files with clearly identifiable file names. The format of these files depends on the wordprocessor used. Texts written with DisplayWrite, MultiMate, Microsoft Word, Samna Word, Sprint, Volkswriter, Wang PC, WordMARC, WordPerfect and Wordstar or supplied in DCA/RFT or DEC/DX format can be readily processed. In all other cases the preferred format is DOS text or ASCII. Essential is that the name and version of the wordprocessing program, the type of computer on which the text was prepared, and the format of the text files are clearly indicated. **Authors are requested to ensure that the contents of the diskette correspond exactly to the contents of the hardcopy manuscript. Discrepancies can lead to proofs of the wrong version being made.**

Submission of an article is understood to imply that the article is original and unpublished and is not being considered for publication elsewhere.
Upon acceptance of an article by the journal the author(s) will be asked to transfer the copyright of the article to the publishers. This transfer will ensure the widest possible dissemination of information under the U.S. Copyright Law.

MARINE GEOLOGY
International Journal of Marine Geology, Geochemistry and Geophysics

(Abstracted/Indexed in: Geoscience Contents, Geo Abstracts, Current Contents, Bulletin Signalétique, Chemical Abstracts, Marine Science Contents Tables, A.G.I.'s Bibliography and Index of Geology, Aquatic Science and Fisheries Abstracts, PASCAL/CNRS, Curr. Awareness. Biol. Sci. (CABS) and Oceanic Abstracts)

VOL. 107 No. 1/2 CONTENTS JUNE 1992

Research Papers

Announcement

Authors may now accompany their manuscripts with floppy disks

Please see the notes on the inside back cover and the guide at the back of this issue. Authors are requested to submit a completed checklist with each diskette. Additional copies of the guide and the checklist are available from the publisher.